Microstructural Quantitative Analysis of Polymer amended Fluid Fine Tailings Using Digital Image Processing Techniques

By

MUHAMMAD HISSAN KHATTAK

A thesis submitted to the Faculty of Graduate and Postdoctoral Affairs in partial fulfillment of the requirements for the degree of

Master of Applied Science

in

Civil and Environmental Engineering

Carleton University
Ottawa, Ontario

Abstract

Understanding long-term dewatering behavior of oil sands tailings is significant to the success and optimization of tailings reclamation plans. Long-term dewatering of tailings is somewhat complex due to mechanical creep, structuration drove by electrochemical forces between clay particle and other potential mechanisms such as cementation. To modernize conceptual models of tailings dewatering, the fabric evolution of tailings over months has been studied using low vacuum SEM as well as optical microscopy methods.

Morphological information is extracted from different images using a sequence of image processing techniques, designed by trial and error to produce repeatable information for the studied material, flocculated fluid fine tailings (FFT). The designed image processing method produces binary images defining pore-space and solid particles (solid grains or flocs). The binary images are then analyzed using a software, primarily "Fiji-Image J" for quantitative analysis of the image for tends in pore and particle size distributions. The samples that were imaged were obtained from amended FFT dewatering experiments, comprising many replicates of 0.10 m high columns that were sampled over months. The tailings were dosed with a high molecular anionic polymer at two doses (600 and 800 ppm polymer per dry tailings). Columns either had one way or two-way drainage. Repeatable trends were found for all samples for both image processing techniques. The most dramatic observation was the increase in floc size over 48 hours using optical microscopy.

Dedication

The thesis is dedicated to my wonderful parents, Retd. Prof. Mian Jehanzeb, Baseerat Khattak, and my siblings, Dr. Kamran khattak and Engr. Salman Khattak.

To my uncle and mentor Dr. Haneef Mian, you will always be my hero.

Acknowledgments

I would like to take this special opportunity to thank my supervisor, Dr. Paul H. Simms, for his valuable guidance, technical and financial support, patience, and availability at each step of this study and providing me with the chance to work on this project. The best Professor I ever had in my entire school life.

I would like to thank Drs. Paul Van Geel, Siva Sivathayalan and Ning Guo for their time and for their help. I offer many thanks to Ph.D. candidate Muhammad Asif Salam for helping me on every step and supplying me all the research data. I would like to thank Carleton University oil sands tailings research group, Ph.D. candidate Yagmur, Dr. Shunchao qi, Chris, Oswaldo for their help.

I would like to express my sincere gratitude to Canada Oil Sands Innovation Alliance (COSIA), and the Carleton University for supplying financial support throughout this research program.

I would take this opportunity to thank Muhammad Haseeb Arshad for helping me in my starting days in Canada and treating me as a younger brother. My thanks are extended to all my colleagues and friends, special; Ph.D. candidate Young, Sania khan, all GCES (Graduate Civil Engineering Society) (Muslim student Association) members and some others here at Carleton University, Ottawa, and abroad.

I love you so much, my uncle Engr. Sajjad Ali Shah, dear Cousins, Muhammad Umair, Muhammad Sanan Khattak, and Muhammad Saddan Khattak. We will always remember you, Rehan Muhammad

Table of Contents

List of Tables

List of Figures

List of Appendices

This page lists all the appendices.

List of Abbreviations

- **FFT** Fluid fine tailings
- **DIP** Digital image processing
- **OM** Optical Microscope
- **SEM** Scanning Electron Microscopy
- **TWS** Trainable weka Segmentation
- **AER** Alberta Energy Regulator
- **CAPP** Canadian association of petroleum producers
- **ERCB** Energy resource conservation board
- **COSIA** Canadian oil sands alliance
- **CPT** Cone penetration test
- **SFR** Sand to fine ratio
- **K** Hydraulic conductivity
- **AOSD** Athabasca oil sands deposits
- **BSED** Backscattered Electron detectors
- **CT** Composite Tailings
- **CT** Computed Tomography
- **GSD** Grain size distribution

1 Chapter: **Introduction**

1.1 Background

Canada has the third largest oil reserves in the world having 171 billion barrels of Oil that can be recovered with today's technologies. As proven reserves, 165 billion barrels, or 97 % of these reserves are in the oil sands. (Alberta Energy and Utilities Board 2005). Bitumen is more expensive to recover and process than conventional oil and gas. However, due to the high consumption and increasing demand for crude oil in the world, technological advances in bitumen production have activated rapid growth in the industry. Production of oil from oil sands have touched the mark of 3.98 million per day and predicted to increase more in recent years (Canada Association of Petroleum Production) (www.capp.ca/publications-and-statistics/crude-oil-forecast).

One of the major impacts of Oil Sands development is the creation of large impoundments of fluid fine tails (FFT), which have highly dispersed clays at very high-water contents (Geotechnical gravimetric water content, or w, > 200%). These deposits do not appreciably dewater even over decades, their water content still being more than twice their liquid limit. Hence, they trap very large volumes of water and have no effective strength to support reclamation. The clays in the oil sands tailings originate in the oil sands deposits and are rendered dispersed through the bitumen extraction process. As an example of the volume of FFT that is produced a plant producing 15 900 m^3/day (100000 barrels/day) of synthetic crude consumes 10,0000 m^3/day of ore, which results in a tailings stream consisting of 10,0000 m^3 of loose sand, and 20,000 m^3 of fine tails, having 30% solids content (mass of

solids over total mass) (Morgenstern, et, al.1988). As a rule of thumb two barrels of fine tailings are generated for one barrel of crude oil production (Dawson. et, al 1999).

Tailings are stored in facilities known as tailings storage facilities TSF. The estimated area of these TSFs was 220 km^2 calculated in 2013, which makes these structures even visible from the space through satellite due to their enormous size. (http://www.energy.alberta.ca/oilsands/791.asp). The oil sands tailings transported hydraulically to TSF initially have a solid content (Cs) of 7 ~ 8 percent by mass. The sand particles greater than 44 microns settle down at the bottom of the beach after some time, while the fine particles which are less than 44 microns remain suspended. The settlement process of these particles is relatively slower over the decade reaching Cs of 30-40%, which is known as Fluid Fine Tailing (FFT). Due to the presence of 84 % water by volume, the gravimetric water content of these FFT is approximately 185% with the bearing capacity of less than 1 kPa.

AER's (the Alberta Energy Regulator) Directive 85 specifies industry responsibility with respect to reduction in FFT volumes and reclamation of tailings impoundments. These regulations were released in 2017 and superseded earlier Directive 74, Directive 85 needs operators to achieve "ready to reclaim" status for all their tailings within 10 years after the end of mine life. This is thought by many to imply the tailings must achieve enough strength to be formed into stable landforms that mimic the topography of the pre-existing boreal forest (Mckenna et al. 2016). Such strength is thought to require at least a solids content of 70%, or w~ 40%, close to the plastic limit of the tailings. Others suggest some

tailings can be reclaimed by the formation of end-pit lakes, where the tailings are deposited subaqueously in the mined-out pits, which has more complex requirements (Omotoso et al. 2018).

Oil sands mining operators have been investigating various technologies to accelerate dewater and reclamation, such as composite tailings (CT), in-line flocculation, centrifuge cake, and thickened tailings. These technologies will be discussed in Chapter 2. Many of these can progress the tailings to solids contents of at least 50% (w=100%) quickly after deposition (days to weeks). However, to reach 70% solids needs more dewatering.

Optimization of tailings deposition involves consideration of several phenomena that can enhance or impede dewatering post-deposition. The phenomena can include desiccation (by evaporation or freeze/thaw), consolidation, or time-dependent processes such as creep and thixotropy. However, fundamental understanding of how polymer application, which occurs in most of the proposed dewatering technologies, affects the long-term dewatering processes is not well understood.

1.2 Focus, and aims of this study:

Understanding the long-term dewatering behavior of oil sands tailings is important to the success and optimization of tailings reclamation plans. Long-term dewatering of these tailings is complex due to (a) mechanical creep, and (b) structuration driven by electrochemical forces between particles. Both phenomena have been shown to influence dewatering in FFT (Jeerivipoolvarn 2009, Miller 2010) and in polymer amended FFT (Salam et al. 2017). In structuration, it is implied that the fabric of the tailing's changes over time independently of density or effective stress, which causes changes in the compressibility of the tailings. This research investigates changes in fabric in polymer amended FFT, to improve conceptual models of tailing dewatering. This is carried out by quantitatively measuring fabric evolution of a specific polymer amended tailings over months. Images generated through low vacuum SEM (Scanning Electron Microscopy) and high-powered optical microscopy were specifically investigated. Morphological information, as well as the microstructural behavior of polymer amended tailings, were extracted from different images using a combination of image processing techniques developed specifically for this work.

This research complements the investigations of Salam et al (2017, 2018) and Qi et al (2017). who are studying creep and structuration by bench scale testing and through numerical simulation, respectively, by visualizing physical changes in the fabric of tailings as the fabric progress through different stages of dewatering over the span of hours to months.

In this research study, the experimental setup for polymer mixing, sample collection, and production of images are all done by a Ph.D. lab colleague Muhammad Asif Salam. The Images used in this study are generated by the author for qualitative analysis (Salam et al 2018). However, the same images were used in this research for quantitative analysis.

The end use of this research work, through improving visual and conceptual models about tailings dewatering, will allow for further optimization of polymer dose, type, and application in commercial tailings technologies.

1.3 Novelty of this research work.

Previously, there has been some analysis done regarding the qualitative analysis using SEM images for polymer amended tailings (Salam et al 2017, Bajwa 2015, Mizani 2016). Until now no research has been reported using Digital image processing techniques for optical microscope images and scanning electron microscope images for quantitative fabric analysis of polymer amended tailings. No work has been reported to the knowledge of the author in public domain working on using DIP techniques for fundamental investigation of dewatering in fluid fine tailings.

1.4 Outline of thesis:

The organization of the thesis is presented as.

Chapter 2: Literature review: This chapter forms of research on the following topics

- An overview of the production process of tailings from Athabasca oil sands deposits (AOSD), the main issues for fluid fine tailings after their production.
- This chapter also discusses the management of the tailings, and various technologies adopted in the industry for speeding up the dewaterability of tailings.
- Fundamental Engineering science on consolidation, a microstructure of soils.
- Interpretation and application of image processing for microstructural investigation of oil sands FFT.

Chapter 3: Material preparation: This chapter is focused on the material preparation of the polymer amended tailings for SEM and Optical Microscopy. The chapter includes sections as below.

Phase 2. No drainage boundary condition, Sample preparation for SEM images, dozed with a 600 ppm A3338 polymer.

- Phase 3. Double drainage boundary condition, Sample preparation for SEM imaging, when dozed with 600 ppm polymer A3338.
- Phase 3.5. No drainage boundary condition, Sample preparation for SEM images, dozed with 800ppm A3338 polymer

- Phase 4. Optical Microscopic sample preparations and sample imaging dozed with 600 ppm and 800 ppm polymer, on the hourly basis for single drainage.

Chapter 4: Digital Image processing and Methods for the SEM, Optical microscope images, produced from the chapter 3 for different days sample.

Chapter 5: Result and discussion section about the chapter 4 their implementation and differences.

Chapter 6: Summarizes the research findings, reports and present recommendation for further research on tailings dewaterability and management.

2 Chapter: **Literature review:**

2.1 Alberta oil sands deposits:

Oil sands are found everywhere in the world; however, Alberta sits atop the largest known deposits known as Athabasca River, Peace River and Cold Lake (Masliya et al. 2004) shown in Figure 1.

The Alberta oil sands are a major oil producing reserve. The Athabasca, Cold Lake and Peace River deposits cover an area of almost 142,200 km², comprising almost 2 trillion barrels of oil. Less than 10% (166 billion barrels) of this is recoverable through current technologies used in the industry. The average composition of Alberta oil sands reserves contains 5 % water, 10 % bitumen and 85 % solids. These oil sands consist of soils and clays 10-30 percent by weight (Chalaturnyk et al 2002).

About 20 % (1462 km²) out of total oil reserves (142,200km²) are suitable for surface mining while rest 80 percent oil is potentially recoverable through In-situ techniques. Two tons of Tar sands (Oil sands) are required to produce 1 barrel of crude oil using surface mining method (Alberta energy regulatory, BGC Engg.2010).

Figure 1: Location Map of oil sands reserves in Canada, http://www.titaniumcorporation.com/s/OilSands.asp

2.2 Production of oil sands Fluid fine tailings:

The Clark Hot Water process (originally developed Dr Karl Clark) is employed for the extraction of oil from mined ore as in Figure 2. The process starts with the (1) conditioning, following to (2) separation and finally (3) scavenging. (Clark et al 1944),

Conditioning: This is the first step of process. Oil sands ore minded are extracted by a truck and shovel method. The ore is transported in very large haul trucks almost having 400 tons capacity (https://www.syncrude.ca) to the bitumen extraction plant. At the plant, large lumps of the ore are broken, and the coarser particles are removed. Subsequently, the ore is conditioned in a pipe line, through the addition of hot water. The hot water

lowers the viscosity of the bitumen, and contribute to change in surface properties, as well as caustic soda which increases the pH, and increases water solubility of the natural surfactants within the bitumen. Residence time in the pipeline and the associated mixing due to turbulent flow allows for changes in the slurry chemistry that ease bitumen separation.

Separation: The slurry is transported through a series of vessels. In this section the temperature is kept at 40 degrees C. In the primary separation process bitumen is segregated through froth flotation to the top of the vessel, sand settles to the bottom, and mixture of bitumen, clay and water remain in the middle. Furthermore, a rake at the bottom pulls the sand component down and out of the vessel, which becomes part of tailings stream.

Scavenging: Additional bitumen is recovered from the slurry. Air is injected into the slurry in flotation tanks to create bitumen forth. An additional 2-4% bitumen is recovered during this step. To allow efficient operations of pumps the bitumen forth is heated to almost 80-degree C, and aerator is also used to remove access of the air.

In this whole process 3 m^3 of water is used for processing 1 m^3 of mined oil sands. Approximately 4 m^3 of tailings is generated from this process (Mikula et al 2012, Morgenstern and Scott 1995) for each 1 m^3 of ore after extraction, the tailings are transported hydraulically in pipelines to dammed impoundments as a slurry with solid contents (mass of solids / mass total) of 7 to 8 %. During deposition, the coarser sands

settle quickly and lock a substantial fraction of the fines (silts and clay particles) with itself forming a beach. The rest of the fines (<44 um) remain in suspension forming fluid fine tailings (FFT). FFT settles and release some water but reaches a constant Cs (30 to 40%) within 5 years.

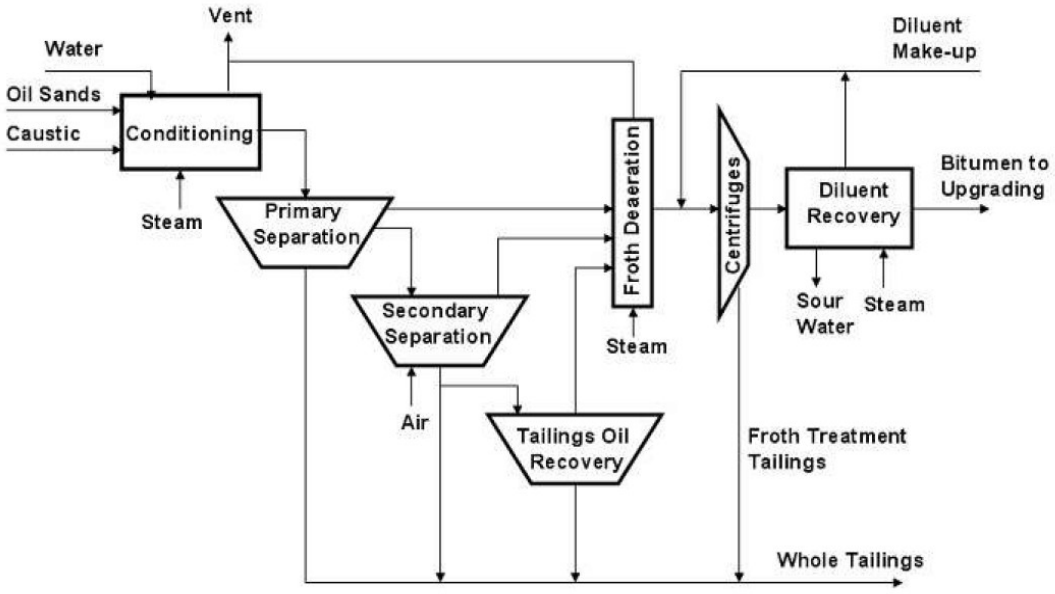

Figure 2: Clark Hot Water Representation of Process Bitumen Extraction (Chalaturnyak et al 2002)

2.3 Geotechnical behavior and properties of Fluid fine tailings:

Fluid fine tailings have properties that lead to slow consolidation, including low hydraulic conductivity and development of pre-consolidation pressure due to thixotropy (Scott et al

2013). Thixotropy is a specific mechanism in which the particles rearrange due to the electrochemical forces, which may induce a volume change, but also may manifest an increase in strength or stiffness at constant water content and volume (Mitchell 1960). Some of the geotechnical properties of FFT are summarized in Table 1(FTFC,1995; Sobkowicz, 2012). Figure 4, shows the hydraulic conductivity measured in several FFT samples. The hydraulic conductivity at a void ratio of about 4 is like that exhibited by a landfill liner, which may give an idea to geotechnical engineers about the slow consolidation rate. Very roughly the rate of consolidation can be estimated knowing the void ratio and corresponding hydraulic conductivity at the surface. At the surface, the gradient varies from about 0.22-0.25 to 0 the initial gradient can be predicted using the approaches of Been (1980) and Pane and Schiffman (1997) and takes a value of $(G_s-1)/(1+e)$. For example, for an initial void ratio of 4 and a specific gravity of 2.2, this would give a value of 0.2. For example, consider an MFT at a solids content of 35% and assuming no sedimentation, if we take a typical value of 1×10^{-3} m/day from Figure 4 and assume a gradient of 0.1, this gives a flux of 0.1 mm /day or less than 4 cm a year. Considering a 50 m deposit, at a void ratio of 4, to achieve reclamation status might take reduction to a void ratio or a reduction to 20 m in height. This 20 m would give a solids content of roughly 70%, or a gravimetric water content of about 40%, which would be enough for tailings to be re-engineered into a stable landform (Mckenna 2017) very roughly, at the flux given, this would take 750 years.

Influencing the dewatering of time-dependent processes such as thixotropy and creep (Jeerrivapoolvarn 2009, Millar 2010). Creep initially adds volume change but slows down

the rate of flow due to the lowering of void ratio near the surface. Thixotropy, which is measured in terms of density-independent strength recovery after remolding, also seems to increase the pre-consolidation pressure independent of density in certain types of FFT (Miller 2010, Salam et al. 2017). Examples of change in the compressibility of an FFT are shown by Miller in Figure 3.

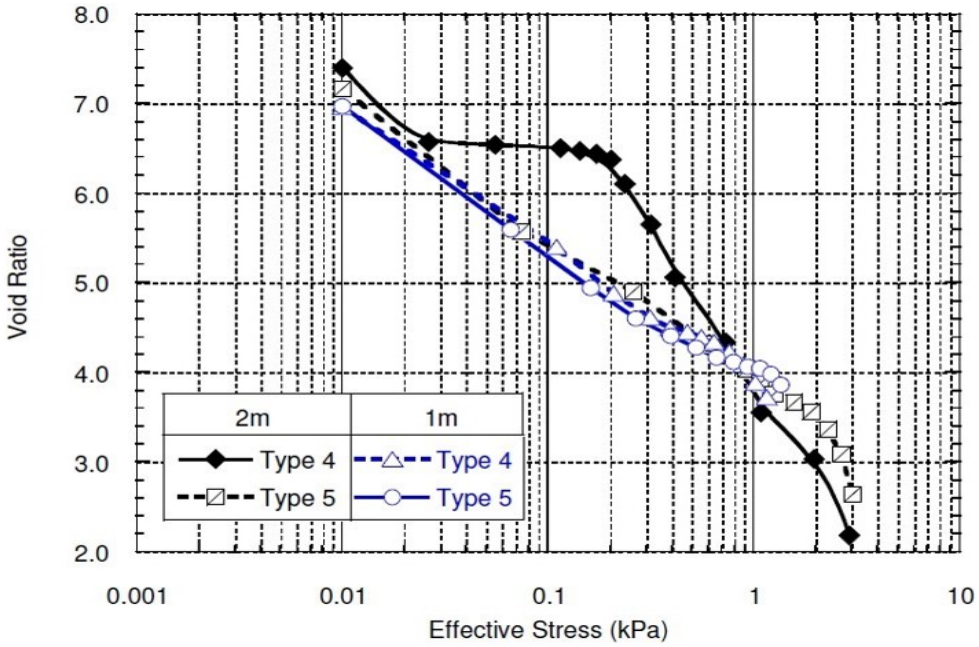

Figure 3: Apparent compressibility change in FFT depending on consolidation Time (Miller 2010)

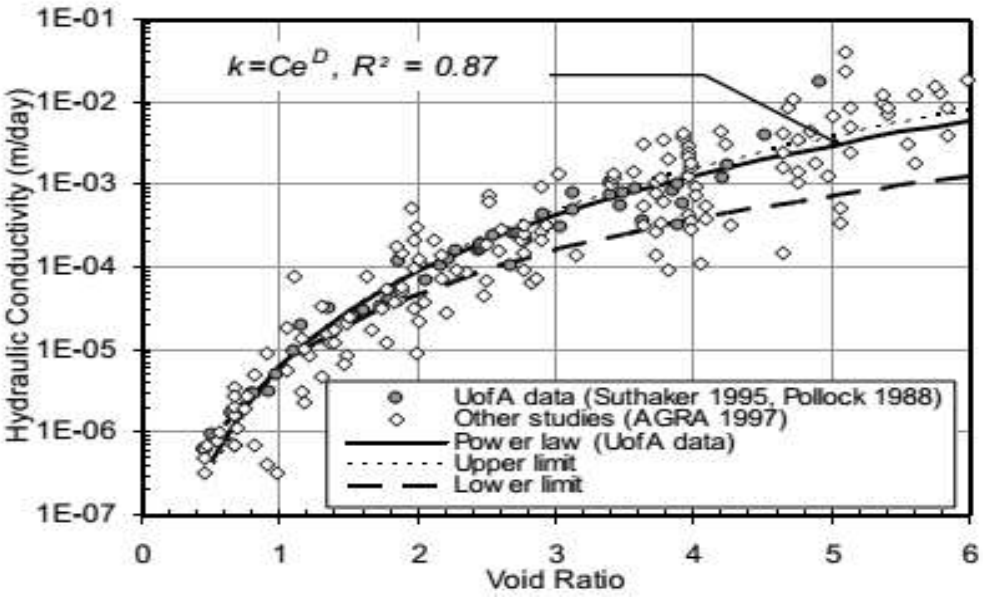

Figure 4: Hydraulic conductivity of mature fine tailings (Jeeravipoolvarn,2010)

Table 1: Properties of Fluid Fine tailings modified from BGC Engineering 2010

Fluid Find Tailings	Value
Liquid Limit (%)	40-75 (%)
Plastic Limit (%)	10-20 (%)
MBI	30%

2.4 Implications of poor dewaterability of FFT:

2.4.1 Challenges.

Storing large volumes of FFT for hundreds or thousands of years that cannot be reclaimed is unacceptable to the industry as well as most stakeholders in Northern Alberta. The liability associated with wildlife intrusion into these facilities, loss of water to the tailings, and liability of dam failure for hundreds of years are probably the key issues of concern to most stakeholders. Secondary issues include issues associated with water and water quality. Stored water released from the tailings is required to be contained in tailings dams, as the industry operates under a no water release policy. Contaminants of concern tailings water include naphthenic acids, polycyclic aromatic hydrocarbons, phenol compounds, ammonia, mercury, and other trace metals (Price 2011, Rogers et al. 2002, Mackinnon et al. 2001; Nix and Martin 1992; Mackinnon). Due to the low rate of consolidation seepage rates are small; however, due to the large scale of the tailings ponds, it is possible that seepage may still influence groundwater quality.

Approximately (80-95) % of water is reclaimed from the tailing's ponds, treated, and re-used in the bitumen extraction process (Canadian association of petroleum producers-CAPP'S). To alleviate and to take care of these tailings ponds issues, different policies have been introduced by the Government of Canada, called Alberta Energy Regulator (AER) Directives.

2.5 Government of Alberta Regulations for management of oil sands tailings:

The Alberta Energy Regulator of Canada (AER) regulates tailings management under Directive 085: Fluid Tailings Management for Oil Sands Mining (https://www.aer.ca) Directive 085 specifies that all FFT deposits be converted to "Ready to Reclaim" status within 10 years after the end of mine life. Furthermore, the directive needs ongoing efforts to reduce FFT volumes and commence and accelerate reclamation activities throughout the life of the mine.

2.6 Tailings Technologies to accelerate dewatering of FFT:

Several different industrial processes have been developed to reduce the volume of FFT over the past few decades. The focus on the treatment of tailings is to increase the solid settling rate/consolidation rate and shorten the time for liquid solid separation. For the better understanding of the oil sand dewatering, technologies that are implemented in the industry are discussed in this section. Over 34 kinds of technologies have been found in various reviews of candidate tailings technologies (BGC Engineering 2010). However,

this thesis will review only those technologies that have been successfully developed to large demonstration scale.

2.6.1 In-line Flocculation

In this method, polymer and /or an inorganic coagulant is added to fluid fine tailings in the transfer pipeline, before they are deposited into a new DDA (Dedicated disposal Areas) (Beier et al., 2013). The function of the polymer or coagulants is to facilitate floc formation. Flocculated fluid fine tailings (FFT) have also been used in conjunction with thin lift deposition or deep deposit-deposition. Thin lift deposition attempts to take advantage of evaporative drying and freeze-thaw post deposition, while deposition in deep deposits relies primarily on the initial dewatering and settling that occurs due to flocculation and subsequent consolidation.

FFT improves dewatering in at least two ways. Floc formation results in an increase in sedimentation, resulting in consequent water release within 24 hours. Additionally, FFT appears to improve the consolidation properties compared to FFT (Jereivapoolvarn 2010, Qi et al. 2017). FFT has been implemented by Suncor (Wells et al,.2011) and Shell (Matthews et al 2011) at the commercial scale. Mathews et al. (2011) reported that there was an increase in the solid content of tailings using In-line flocculation from 35 % to 45-55 % in 24 hours and 65 % solid content within two months using the thin lift deposition of tailings 0.60 m. Wells et al., (2011) reported solid concentrations increasing to 80 % by deposition of tailings in thin lift, i.e. (0.2- 0.3m) within 10 days. However,

the footprint demands, and the costs associated with in-line flocculation and controlling the impoundment geometry are relatively high. In-line flocculation is also currently being trialed in deep (>10 m) deposits, where dewatering primarily relies upon the improved consolidation properties.

Figure 5: Example of In-line flocculation of FFT in the field (Mizani et al.2013)

2.6.2 Improved CT (Composite Tailings) / NST (Non-segregating Tailings) Technologies.

Remixing sand with treated tailings is the oldest alternative tailings technology trialed at large scale. The idea was tailings in which the degree of flocculation was improved and would not segregate as easily as in the original tailings. Putting sand back into FFT provides substantial increases in geotechnical performance. For example, Hamza and Kessick (1996) used slacked lime and high molecular weight anionic polyacrylamide polymer for the flocculation in oil sands tailings. Their findings showed an increase in

the settling rates by addition of sands and low polymer dosage. Figure 6 shows the settling rates of the flocculated tailings with or without the sand incorporation. Results showed clay and sands particles settle fast and dewater rapidly. When the samples were taken in hands and squeezed, it further dewatered resulted in a stackable material showing 40-83 % wt. solids. At the full scale, however, retaining the sand in the flocculated tailings has proven to be challenging, as shearing during transport and during beaching induces segregation. Nevertheless, increasing the capture of fines within sands matrices is possible to some degree and many mines incorporate this technology into their tailings management plans (COSIA 2015).

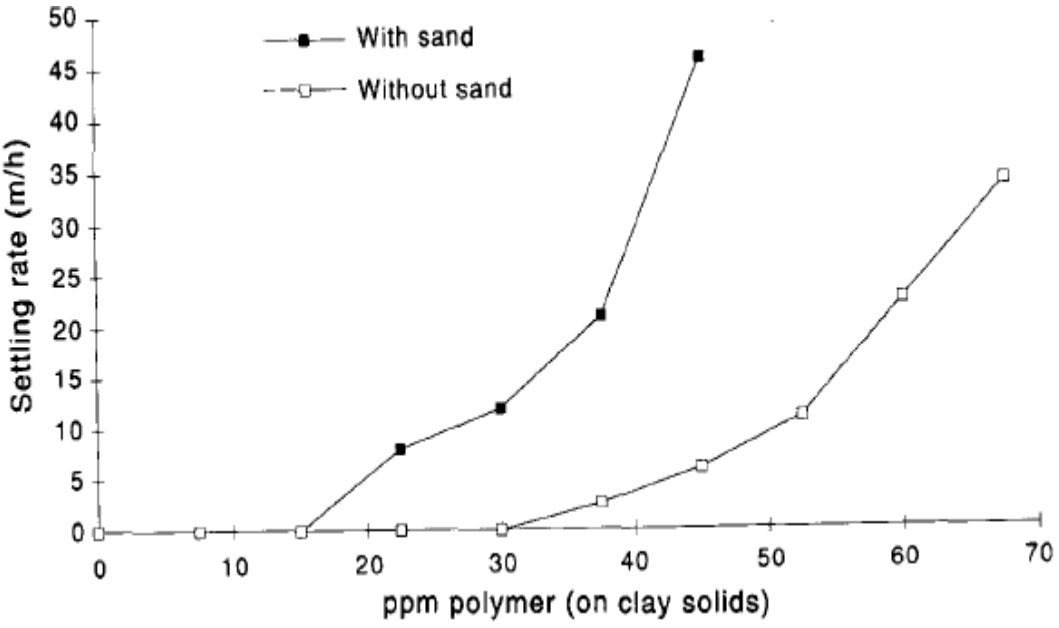

Figure 6: Settling rates of flocculated tailings with and without sand combination. (Hamza & kessick)

2.6.3 Dewatering by Centrifugation:

In this method, tailings are first mixed with a polymer and /or coagulant, then added into a large centrifuge. A Force greater than the gravity force separates fluid (consisting of the water, bitumen, and fines). Pilot scale trials were able to produce tailings up to 60 % solid content and reliably more than 50% (Devenny.2009, Owolagba and Azam 2013, Xu and, Umme 2014). In 2010 Syncrude did its deposition of cake using belts and trucks. According to Syncrude 2011 after a period of 12 months, the deposited cake had achieved enough strength, due to the process of freeze-thaw and evaporation. Syncrude did not comment on the thickness of cake obtained from such processes. Figure 7 and Figure 8 below obtained through the Syncrude website, shows tests process and the appearance of centrifuge sample cake obtained in the Syncrude 2010 campaign.

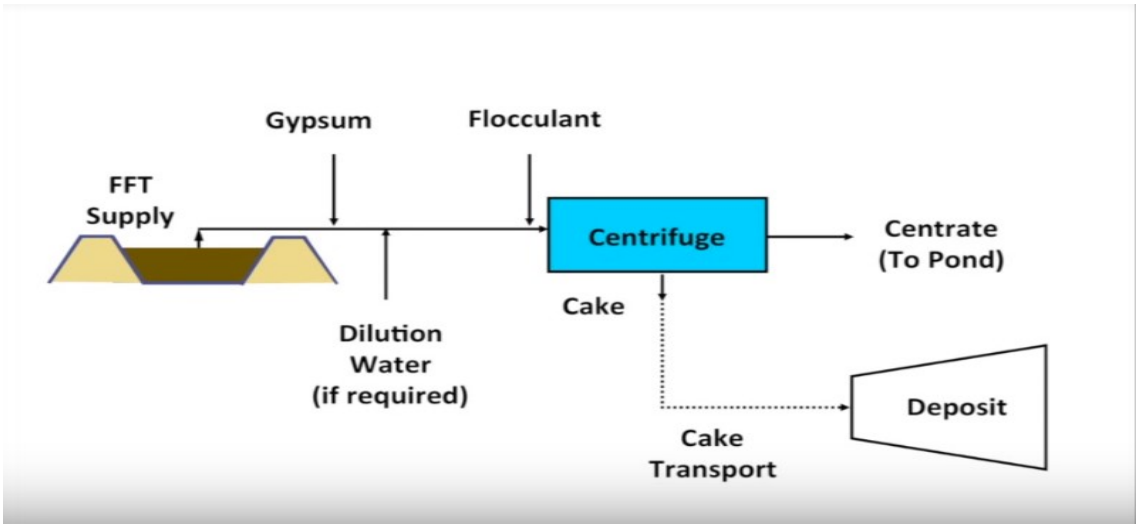

Figure 7: Process chart for cake production using centrifuge pump. (Snap shot taken from video on Syncrude website 2011)

Figure 8: Centrifuge cake sample resulted obtained, after processing tailings by centrifuge from Syncrude 2010 campaign, (Snap shot taken from video on Syncrude website 2011)

2.7 Dewatering mechanisms in FFT

2.7.1 Flocculation and sedimentation:

Both processes are used to separate the suspended solid portion from the water, the suspended particles may vary in composition charge or particle size etc. Flocculation is a process where colloids come out of the suspension in the form of the flocs or flake due to the addition of the clarifying agent. This method stabilizes the suspended particle allowing particle collision and growth of the floc and results in sedimentation as illustrated in Figure 9. Flocculation process the mixing stage, increases the particle size from submicroscopic microflows to visible suspended particles. Flocculation requires a careful attention to the mixing velocity and the amount of the mix energy. Once the floc is torn apart it is difficult to get them to reform to their optimum size and strength (Lyn et al 1992).

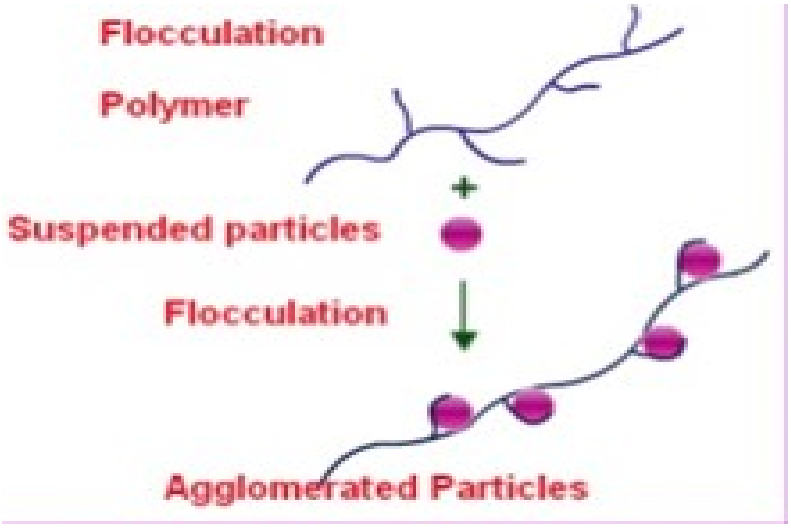

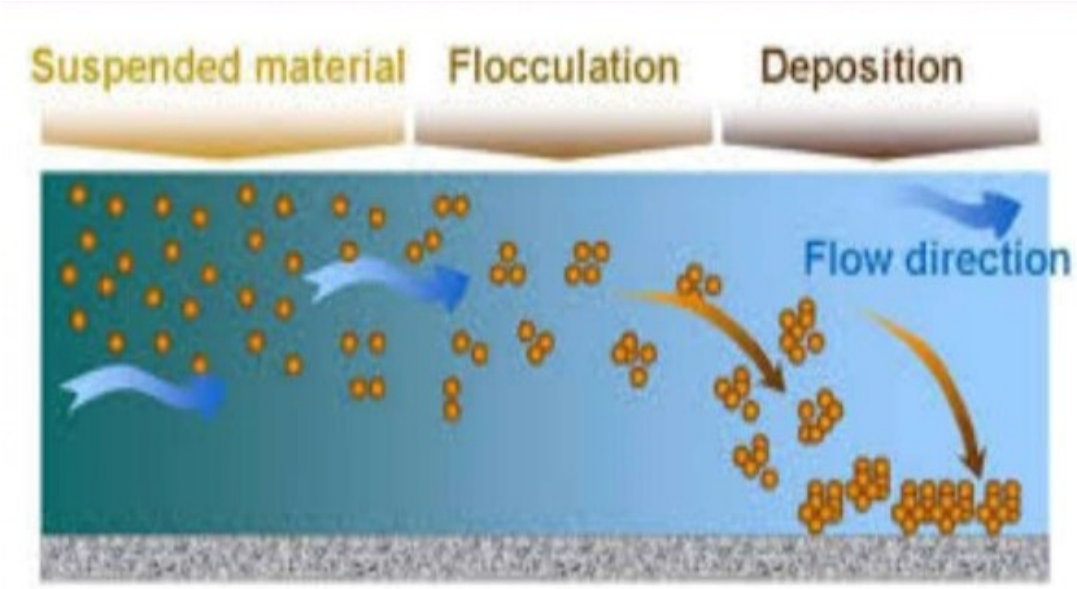

Figure 9:Flocculation process leading to sedimentation after addition of Polymer (general demonstration) (https://www.safewater.org/)

2.7.2 Consolidation in oil sands tailings:

The theory of consolidation was developed by Terzaghi in 1923 (Schiffman et al., 1969). Consolidation for saturated soils is defined as a process in which with time there is reduction in the volume of soil, and dissipation of excess pore water pressures under

applied stress. Due to change in the effective stress there is a substantial change in the volume of the soil. Soil particles are packed more tightly during the process of consolidation, resulting in the change of volume. During consolidation, the effective stresses induced in the soil controls the soil structure deformation. To explain the consolidation in detail, small and finite strain consolidation theory is explained.

2.7.3 Classical theory:

Small strain consolidation:

This theory combines the principals of effective stresses, continuity equation, and fluid flow relationship. The mathematical form of the equation is as follows in the equation (1).

$$Cv = \frac{\partial^2 u}{\partial z^2} = \frac{\partial u}{\partial t} \quad \text{..... (1)}$$

Where,

Cv= coefficient of consolidation

u =excess pore water pressure.

t= Time

z= One dimensional vertical coordinate.

This theory was based on the following assumptions (Qui, 2000)

. The soil is fully saturated with water.

1. The soil particles and pore water are incompressible.
2. A Linear time-dependent relation between void ratio and effective Stress controls the strains of soil skeleton.

3. Darcy law is valid
4. Small strains
5. During consolidation, the permeability and compressibility under an increase of load remain constant in the soil.
6. The soil is considered homogeneous.

Equation 1 can be derived from first principles considering flow into and out of a small representative volume of soils that do not change in volume. However, the consolidation process in soft soils and in similar materials such as tailings is generally associated with large strains and volume change, and large changes of hydraulic conductivity as well as compressibility (Jeeravipolvaram,2010). Different researchers (Carrier et al 1983, Schiffman et al 1988) have showed that conventional consolidation theory would provide inaccurate results in the calculation of the degree of consolidation in mineral waste slurries.

2.7.4 Finite strain consolidation theory

Gibson et al. (1967), developed a one-dimensional finite strain theory for homogenous layers of saturated clays. Considering deformation and the variable properties of

compressibility and hydraulic conductivity, Gibson et al. (1967) Derived the following Equation 2.

$$\pm\left(\frac{\rho s}{\rho f}-1\right)\frac{d}{de}\left[\frac{k\,(e)}{1+e}\right]\frac{\partial e}{\partial z}+\frac{\partial}{\partial z}\left[\frac{k(e)}{\rho f(1+e)}\frac{d\sigma`}{de}\frac{\partial e}{\partial z}\right]+\frac{\partial e}{\partial t}=0 \qquad (2)$$

In this equation ρs, ρf are the fluid and solid density, so e is the void ratio, k is hydraulic conductivity expressed as a function of e, $\sigma`$ is the vertical effective stresses which controls the void ratio, and Z is a reduced or material coordinate.

This theory is based on the Darcy law and no time-dependent effect in the soil skeleton. As the above equation does not depend on the strain, this theory can be used in the thick clay layers, when they are subjected to large settlements. Gibson in (1967) neglected the small strains limitation and considered the changes in soil permeability and compressibility during consolidation. By setting the effective stresses to zero, the theory of hindered sedimentation (Kynch, 1952) can be presumed from large stain consolidation (Been, 1980; Pane and Schiffman, 1985). Fox and Berles (1997) showed that finite strain consolidation can also be calculated using a piece-wise linear approach, where changes in volume can be neglected over sufficiently small discretization's in space and time. This allows for use of Equation 1, as long hydraulic conductivity and compressibility are updated time step to time step. The equivalence of numerical solutions of Equation 2 with the piece-wise linear approach has been demonstrated repeatedly (Fox and Berles 1997), (Qi et al. 2017).

The important difference between finite strain and consolidation is the variation in the hydraulic conductivity and stiffness with the void ratio. These relationships are presented for fluid fine tailings in Figure 10 and Figure 11 below.

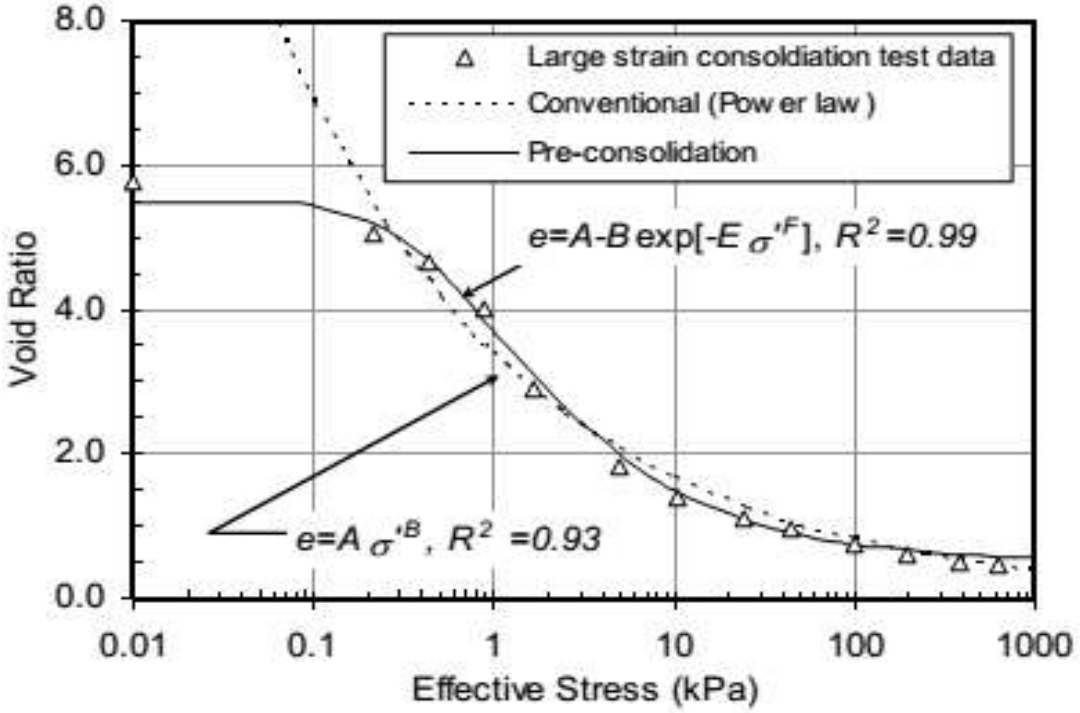

Figure 10: (Jeeravipoolvarn ,2010) Compressibility of mature fine tailings.

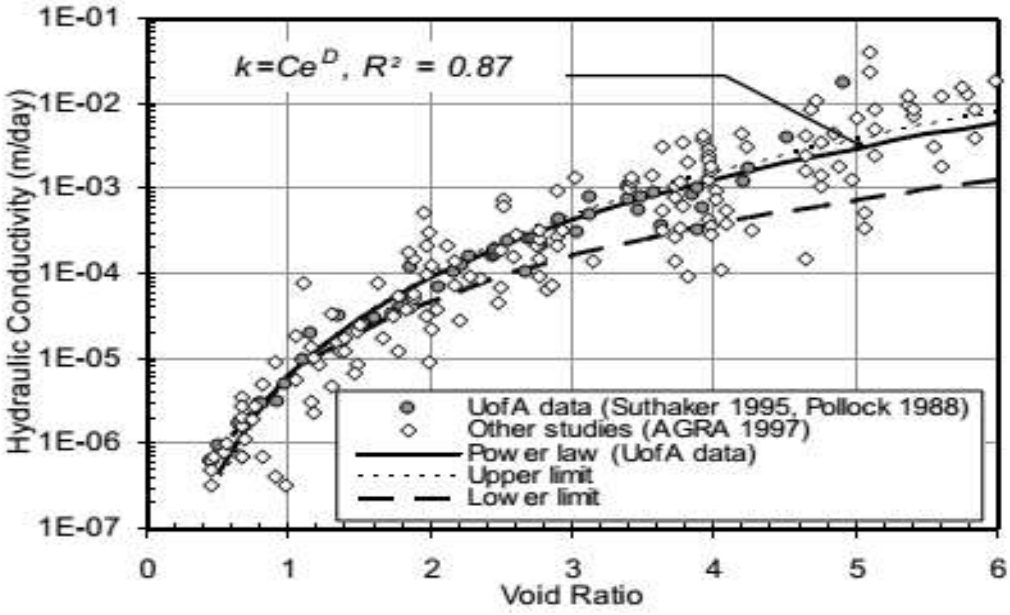

Figure 11:Hydraulic conductivity of mature fine tailings (Jeeravipoolvarn,2010)

2.8 Imaging and quantitative analysis of soil microstructure.

In the past, different techniques have been used to quantify the microstructure of geomaterials. Microstructural techniques such as computed tomography (CT), Scanning electron microscopy, X- ray computed tomography, optical microscopy, and mercury intrusion Porosmetry has successfully used to study microstructural behavior of materials. (Romero and Simms 2008).

2.8.1 Scanning Electron microscopy.

The scanning electron microscope is a device that uses a beam of high energy electrons to generate a variety of signals at the surface of the solid specimen. The signals reveal information about the sample morphology (texture), crystalline structure, and orientation.

Generally, the data is obtained from the samples in the form of the 2D images, which displays a spatial variation in sample morphology (Goldstien.J.2003, Reimer, L 1998,). There are two different methods for SEM techniques (1) Regular SEM (2) Environmental ESEM. In regular SEM high vacuum is used on samples so that only dehydrated and electrically conductive samples can be seen, while ESEM allows moisture inside the sample under various temperatures and pressures.

2.8.2 Application of Scanning electron microscopy (SEM) Tests.

SEM is extensively used in the world for identification of phases based on qualitative chemical analysis and crystalline structure. Using SEM, precise measurement of a sample smaller than 50 nm in size can be successfully accomplished. Diffracted backscattered electron detectors equipped SEM devices, can be used to examine the microfabric orientation in many materials (Egerton al. 2005, Clarke et al 2002). Table 2 shows some of the recent studies which successfully used SEM device for investigation various material properties.

Table 2: Summary of SEM device used in literature for Material property Investigation.

Type	Application used	Material property investigated	Reference
London Clay, boreholes	ESEM, (Natural moisture content)	Qualitative analysis, Pore size distribution.	Monoroy (2010)
Mine tailings	SEM/ automatic image analysis, X-ray spectrometry	Environmental characteristics	Mermillod Blondin et al 2011)
Five different soil Including gravel, medium sand, Concrete sands	SEM, X-ray, CT Image analysis	Microstructure evolution	Nielson 2004
Oil sands tailings, glacial till, compacted silt	SEM device	Qualitative macroscopic behavior	Jeeravipoolvarn 2005
RAW FFT	ESEM	Qualitative macroscopic behavior	Fard 2011
Tailings	SEM	Fabric changes,	Liang et al 2015
Mature fine tailings Dried	SEM	Qualitative analysis	Roshani et al., 2017
Mature fine tailings	SEM	Investigation of fabric	Tang et al., (1997)

2.8.3 Operation of SEM Tests:

The scanning electron microscope uses a beam of strong electrons to produce high resolution 2d or 3d images. An electron gun (electron source) in the SEM device generates electrons which are accelerated down the columns that is under vacuum, which help to prevent an interaction of atom or molecule with electron to ensure quality resolution of images and to control the path of the electrons lenses are used in SEM (Goldstein et al, 2003).

An amount of kinetic energy is carried by the accelerated electrons in the SEM. Energy is dissipated when the incident electrons interact with the solid sample under consideration. A back scattered electron detector is placed on the top of the sample. Backscattered electrons (BSE), are used for showing the contrasts and composition in samples. BSE images can also be converted to false color, which often helps the human eye distinguish subtle variations. A Secondary Electron (SE) detector is placed at the side of the electron chamber, at an angle, to increase the efficiency of detecting secondary electrons which can supply more detailed surface information. Danilaos (1993) explained and favored (BSE) for better quality images.

SEM is a nondestructive test, as the x rays generated by electron interaction, does not lead to losses or change in the volume of the material. Therefore, it is possible to use the device for analysis of same material repeatedly. The SEM device has the ability to adjust the vacuum for a wide range, it has the potential to generate a difference in the pressure with a successive reduction in the pressure and work under controlled environmental condition. (Bajwa 2015).

Under low vacuum, SEM can possibly abstract the microstructural behavior of the materials when they are fully hydrated. However, this does not work well due to the problem in resolution, therefore SEM is mostly performed on the dehydrated or on flash frozen samples. If the dehydration of sample is not done in controlled mannered, it will result in the induction of matric suction in the sample, which will alter the microstructure behavior.

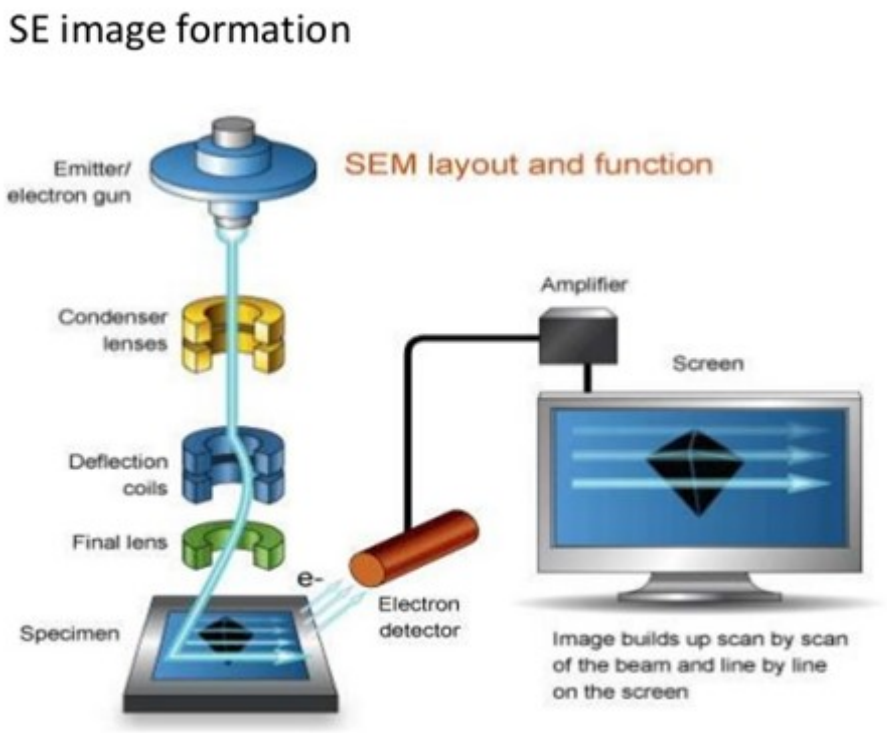

Figure 12: Working schematic of Scanning Electron Device.

2.8.4 Optical Microscopy:

Optical microscopy was first introduced in the late 17 century as the simple design of microscope to gain and understand the microstructure or nanostructure of chemicals materials or other products.

In the past, there has been enormous growth in the application of optical microscopy for micron and submicron level investigation (Herman et al 1993). Advances in digital

imaging and analysis have also enabled macroscope to acquire quantitative measurements quickly and efficiently on specimens ranging from superconductors to real-time fluorescence microscopy of living cells in their natural habitat.

The optical microscope has improved substantially with time. Images are now displayed directly on the screen of CCD camera to examine sample without the use of eyepiece. Presently, an optical microscope is used extensively in microelectronics, nanophysics biotechnology.

The only disadvantage of an optical microscope is low resolution, usually down to only sub-micron or a few hundreds of nanometers, due to the light diffraction limit. A positive feature of the optical microscope is its speed and adaptability to all kind of sample systems i.e. from gas to liquids, and to a solid sample system. (Herman et al 1998). (Binet et al 1962) used Optical microscope for the study of the plasma cell. (Novoselov et al 2005) Used optical microscope to investigate the electrical conductivity and assess the microscopic quality and macroscopic continuity of 2-d atomic crystals.

High powered optical microscopes are now cable of capturing features to almost micron resolution by using a system of lenses and backlighting. An example of this kind of microscope is the Nikon model NIS Elements AR3.2 .Figure 13 and Figure 14 illustrates the schematic diagram of this optical microscope, which is the same type used in this research.

Figure 13: Carleton University Optical Microscope used in this Study "Nikon model Ellipse TE" (WWW.Nikoninstruments.com)

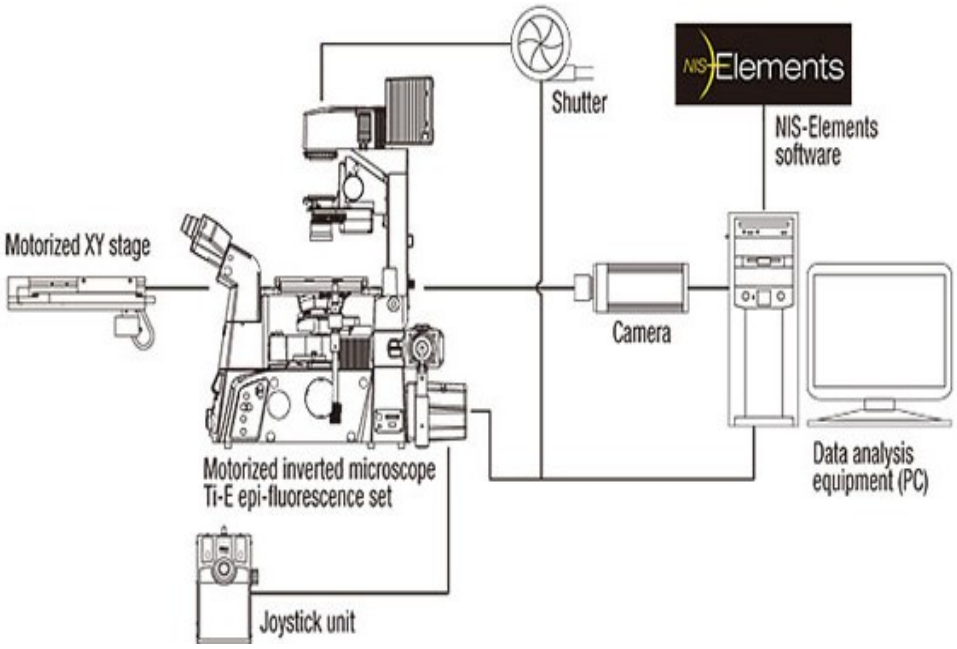

Figure 14: Schematic Diagram of the Nikon Model Ellipse TI (www.Nikoninstrument.com)

2.9 Image processing its interpretation and applications in Geotechnical field and oil sands.

2.9.1 Introduction:

DIP (Digital image processing) is a new technology introduced in the late 1980s. With the increase in digital image capture technology digital image processing also had a rapid development in the field of medicine, geography, geological engineering, and other fields. In Geotechnical Engineering the use of DIP was pioneered by (Macedo et al. 1999) and Moore et al. (1993). Macedo using first generation X-ray tomography with micrometric resolution was successful in studying the quantitative analysis of local soil sample. While Moore et al in (1993) used image processing techniques to extract the fractal characters of the soil samples through DIP.

DIP is also used in other similar fields: in Mining i.e. for crack propagation studies cartography, ergometry (characterization of fine particles using diffraction pattern generated by laser beams), Granulometry (Distribution and size calculation of particles from images), Environmental Engineering (Dispersion of smoke plumes study) etc. (Kaye 1989 and Russ 1994, Jahne 1991, Gonzales and Woods 1992).

2.9.2 Application in soil fabric characterization:

The physical property of the soil is specified with the quality of the porous medium. The structure of the soil is depended on its shape, size, placement, arrangement of the aggregates and particles as well as its voids. (Jury et al 1991, Lipiec, et al. 2007). The conductivity of air and water as well as the retention in the soil particles is all depended on the porosity of the soil. To better understanding and to understand the dynamics of water in the soil sample, it's important to educate our self with the grain and pore size distribution as well as the total porosity trend. (Ringrose et al 1984, Cássaro et al. 2011).

For characterization of soils, the soil micromorphological analysis is widely used, which includes a calculation for the soil porosity, pore size, and grains size, with the help of Digital image processing software's. Analysis of soil particles can be done using the 2-dimensional (2-D) images or 3D images. Due to low cost and easy to access, 2D images and 3D images obtained from soil samples are frequently analyzed in the industry for soil porosity investigation, and Grain size calculation (Pires et al., 2008, 2009; Passoni et al., 2014).

Heck and Elliot (2007) used software naming "Image J" on samples obtained from Ontario, for calculating the voids in the soil. Images were compared on the bases of resolution differences, and they concluded by recommending "Image J "complementary for studying and acquiring the physical properties of soil, such as "porosity" and "pore distribution. Cui et al (2011) used the digital image processing techniques on images generated using charged coupled device (CCD) camera, and long-distance microscope to study the microstructural behavior of the different geotechnical material.

Miguel et al (2015) Passoni et al (2013) used 2D images obtained from the soil of south east brazil region using the 2D Image Acquisition CCR camera coupled with the optical microscope. Through 2-dimensional images, soil pore distribution was studied. Soil structure analysis was done using public domain software Image J. It was concluded, from their research that Image "J" software can be complimentary for the calculation of porosity, pore size distribution, and total number of pores calculations.

Marcelino et al. (2007) for calculating the micro porosity of two different instruments generated images used BSE scanning electron microscope in back scattered mode and fluorescent microscope. The porosity of images was changed with sample preparation method significantly for both techniques. when compared, BSE images were much better for calculation then Fluorescent Microscope images. The image segmentation was done using UTHSCSA image tool software for each image, automatic thresholding based on the intensity histogram was done using Image Pro. Their research findings concluded that porosity measurements carried out on images attained using different methods cannot be compared. In addition, they reported that the Image Porosity measurements for comparative studies are best to be carried out by the same observer to get good results.

Table 3: Summary of different type of Soil and Techniques used in literature for Successful Quantitative analysis.

Sample type	Imaging technique	Software used	Property examined	Reference
Ontario soil	Optical microscope	Image j	Pores distribution, Grains, Porosity	Heck and Elliot 2007

Fontaine bleu sandstone	CT Imaging technique	CTAn, Fiji Image j	Visualization of 2d, 3d pores, grains	Latief 2016
Voids of soil sample south east brazil	CCD camera, optical microscope	Noesis Visolog,	Pore size distribution, quantifying total porosity	Passoni et., al 2014
Undisturbed soil samples Portugal	Back scattered SEM images (tiff format)	UTHSCSA, Image pro, µCT analysis	Soil Microporosity	Marcelino et al 2007
20cm depth soil sample ground china	12.2 DSLR camera, fluorescent light	Image pro, Matlab, Adobe photoshop	Calculation of shape factor of soil sample. Area, perimeter	Yiediboe 2015

3 Chapter: **Materials and Methods used:**

3.1 General:

This chapter describes the material parameters, sample preparation, and the experimental methodology. The experimental methods for the 10 cm columns, SEM and Optical microscope imaging used in this study was devised and carried by the PhD student Muhammad Asif Salam.

The chapter includes:

1. Properties of fluid fine tailings
2. Methods describing the preparation of the polymer amended tailings, such as preparation of polymer stock solution and the tailings- polymer solution mixing process.
3. Description of 10 cm tall columns, their instrumentation, and boundary conditions used for them, from which samples for microstructural analysis were obtained.
4. Discussion on the production of SEM and Optical microscopic images from the tailing's samples

The image analysis methodology devised by the author is described in Chapter 4.

3.2 OIL SANDS FLUID FINE TAILINGS:

The FFT used in this study were obtained from the Muskeg River Mine (MRM). Samples from the tailing's ponds were transported to Carleton University. The initial solid content of the fluid fine tailings was 33 to 35%. Tailings were remixed with bleed water (water

that was released during transportation) to bring them into their initial condition. The geotechnical properties of fluid fine tailings used in this study were compared to other authors tailings used as shown in Table 4.

Table 4: Geotechnical properties of RAW FFT from various sources

Property	Values of MRM tailings tested at Carleton by Mizani (2016)	Standards used	Jeeravipoolvarn et al. 2014 (Tailings)	Beier thesis 2015 (Tailings)	Yao thesis 2016 (Tailings)	Miller 2010 (Tailings)
Specific Gravity	2.20	ASTM D854	2.48	2.44	2.3	2.55
D10, D50, D60 (micron)	0.8, 6.4, 11.1	ASTM D422-63				
Hydraulic conductivity (cm/s) at e=4	4.3×10^{-6}	ASTM D5084-10				
Liquid limit	62.4	ASTM D4318-10	52.1-58.3	50	55	49.5
Plastic limit	26.7	ASTM D4318-10	26.9-28.2	29	28	25.8
Fine content (<4µm, %)	78.7%			96 %	91%	
MBI	30%					
Clay mineralogy	70% illite, 30% kaolinite					

3.3 Anionic Polymer A3338 stock solution preparation:

Two different dosages of macropolymer commercial flocculants (PAM) A3338 were used. PAM (A3338) is branched polymer with the average weight of 18 x 10^6 g/mol. Figure 15 illustrates the structure of anionic PAM. Experiments were performed using either 600 ppm PAM A3338 or 800 ppm PAM A3338.

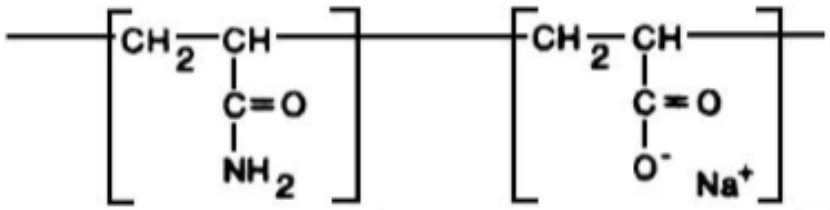

Figure 15: Structure of anionic PAM (http: www.snfcanda.com-product-literature.php)

.

3.3.1 Procedure for Preparation of stock solution:

General approach to prepare sample like those generated in a field application of in-line flocculation

To create field representative samples, a similar procedure used for the preparation of stock solution were optimized from a baseline procedure developed by Shell Canada in 2010, to prepare laboratory generated FFT similar in field properties to field generated FFT. The procedure was optimized by Bajwa (2015) and Mizani (2016) based on yield stress, capillary suction time, and 48-hour dewatering potential.

Figure 16 shows yield stress measured on samples obtained from field trials and those measured on laboratory prepared samples. Both measurements were conducted using stress growth method with shear rate of $0.1s^{-1}$. In field sample optimum flocculant dose was kept around 770 to 950 g/ton. The MFT was first mixed with the polymer stock solution in 17ft pipe and then deposited at a speed of 900 $m^{3/}$hr., Samples were taken from field as they were deposited from pipe.

Figure 16 shows that the yield stresses obtained in the field which overlaps well with the yield stresses data points obtained in the Carleton laboratory, using same polymer dosage. Therefore, the mixing time and intensity used to prepare the flocculated MFT in the laboratory was considered as representative of field mixing conditions. This method was adopted for preparation of stock solution.

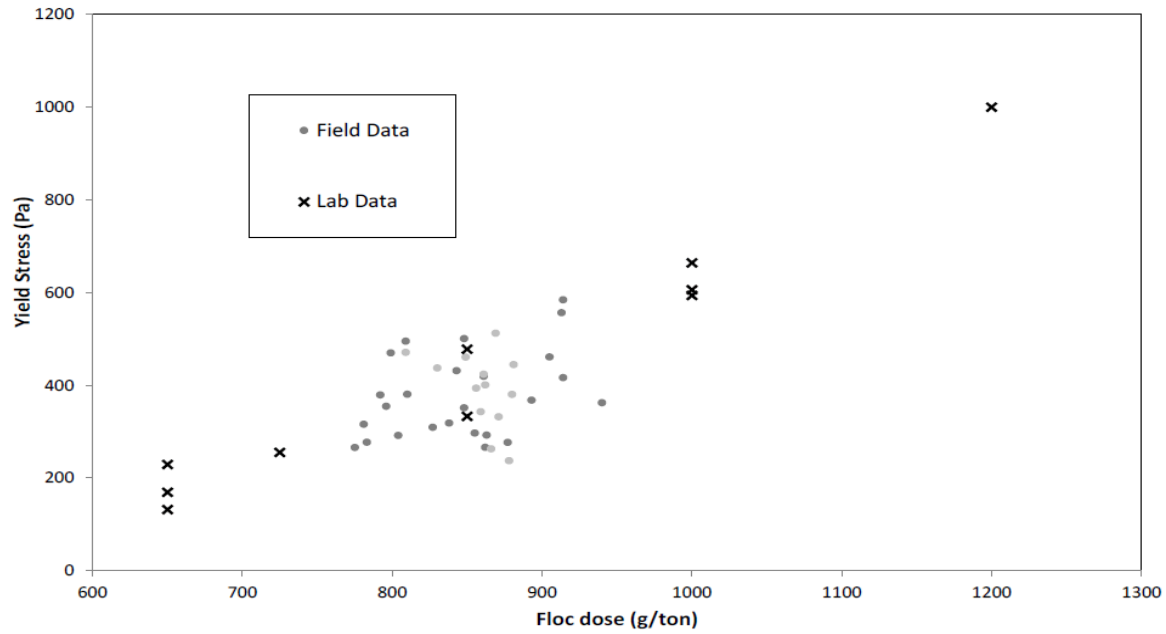

Figure 16: Comparison between yield stress values measured in laboratory and deposition in Muskeg River Mines tailings site during Aug-Oct 2012 (Mizani 2016).

3.3.2 Details of the tailing's preparation procedure

2g of A3338 (SNF) polymer (for the preparation of 0.4 % stock solution) was weighed using an analytical balance (Fisher scientific, Sartorius AG Germany, LE225D) and decanted into a 500 mL glass beaker and completed to 500 mL with deionized water (Salam et, al. 2017). Mixing of this was done using a Jar tester (Phipps and Bird, PB 700 Jar Tester) as shown in Figure 17. Mixing was done using a specific speed of the stirrer at 200 RPM for 5 minutes, and for 125 RPM for 55 mins (Mizani 2016), (Salam et, al. 2017). Finally, the stock solution was then mixed with the RAW FFT. Mixing was executed using Ika Eurostar 60 control mixer as shown in Figure 18 for 10 seconds at 250 RPM. In this

study polymer dosage 600 ppm and 800 ppm g/ton were used and its effects on FFT were examined with time.

Mizani (2016) reported for mixing times above 10 secs (15sec and 20secs) resulted in an observable irreversible collapse of flocs. Therefore 10 secs were chosen to be the optimal mixing time.

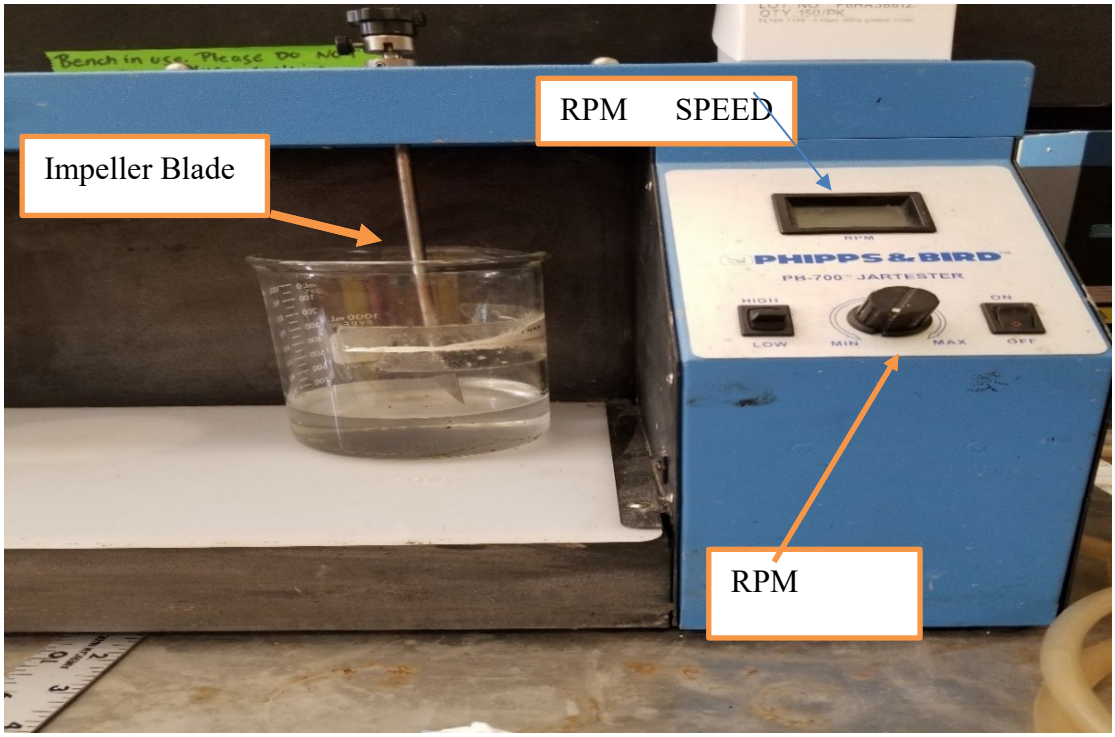

Figure 17: Phipps and bird stock solution mixer Pb 700 jar tester

Figure 18 : Mixing of Polymer with MFT for 10 Sec using IKA Eurostar

3.4 Placing of Amended tailings into duplicate columns:

The experiment was conducted in different phases, Phase 2, Phase 3, Phase 3.5 and Phase 4, Identical tests were conducted for each Phase. Each phase was dosed for 600 ppm, and 800 ppm A3338 polymer. Each polymer amended FFT were deposited into PVC columns. The boundary conditions for individual polymer dosed columns were kept as

(1)Single Drainage -The top and bottom was closed, and bleed water could only flow to the top of the tailings due to flocculation leading to settlement inside columns. Both PVC columns were covered at the top and the airspace above the bleed water was minimized (Salam et al 2017).

(2) Double Drainage: bottom was open, and tailings could drain through filter paper into a tray. 5 mm of water was kept in the tray to prevent drying from the bottom the process of bleed water moving to the top was doubled in this process due to double drainage.

Combinations of boundary conditions and polymer doses were used to generated different Phases of the experiments. This research is on samples obtained from Phase 2, Phase 3, Phase 3.5 conducted in 5 months from April 2017 till August 2017. Phase 4 was conducted parallel with phase 2 and took only 48 hours straight to produce images. The detailed procedure for the different phases is given below.

3.4.1 Phase 2

3.4.2 Single drainage dosed with 600 ppm polymer SEM Images:

Polymer amended FFT dosed with 600ppm anionic polymer were deposited in multiple replicates (10) of 15 cm diameter transparent acrylic columns to a material height of 10 cm, shown in Figure 19. Reason for use of 10 cm column was to quantify the consolidation, and non-consolidation behavior under saturated condition. The short height of the column was used as it was thought to maximize the influence of creep (Salam et al 2017). Two tensiometer were also inserted into two columns to measure pore-water pressure. The

acrylic columns were closed from the top by placing crock on it (to avoid evaporation) as well as closed from the underneath (not to allow any drainage) as shown in Figure 20. For testing and sampling, five different days labeled duplicate columns i.e. (7,14,28,56,72) covered from underneath were designed as illustrated in Figure 21. 600 ppm polymer amended tailings were deposited inside it. Samples were taken from 1 cm top of each column using spatula illustrated in Figure 24. Samples obtained were used for performing several geotechnical tests.

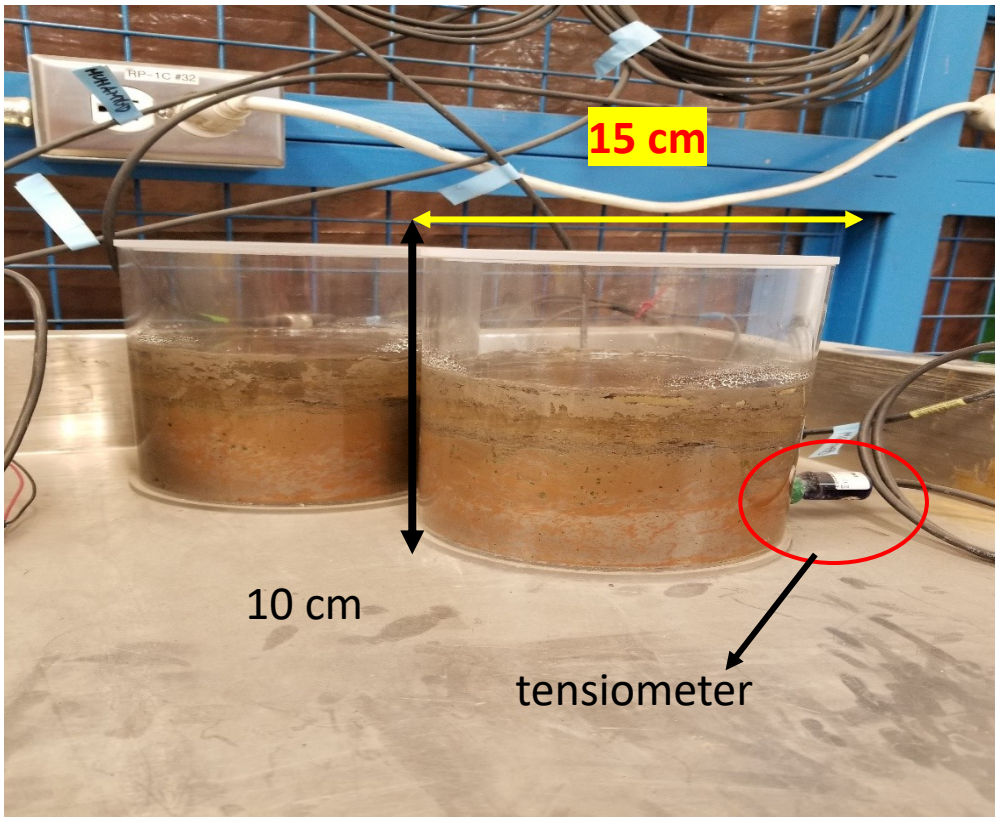

Figure 19: 10 cm column for quantification of consolidation (Salam et, al. 2017)

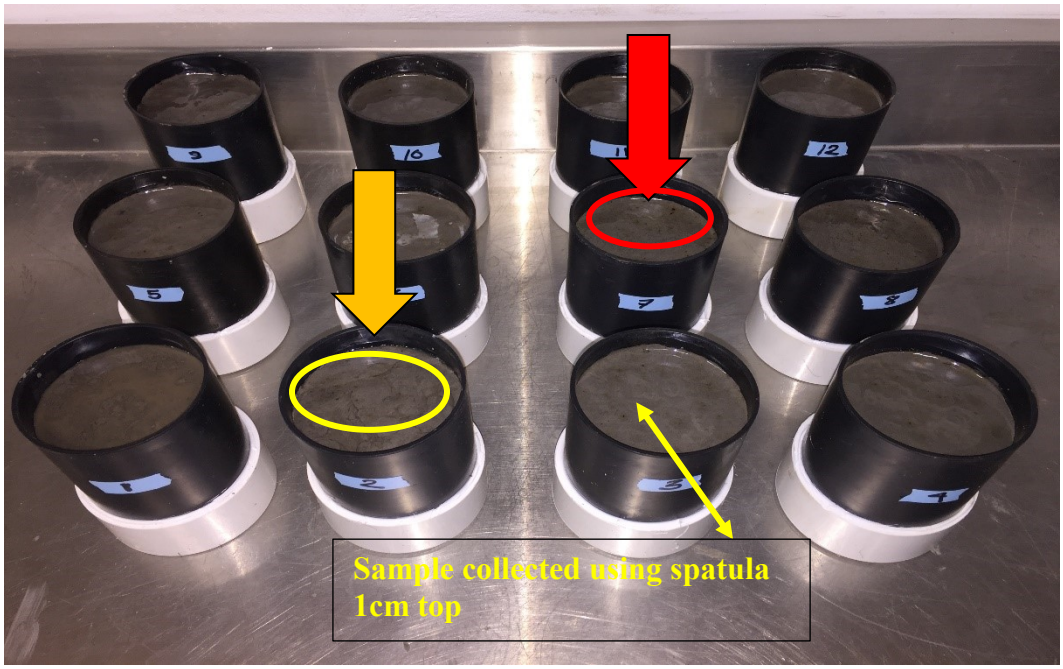

Figure 20: Single Drainage Duplicate columns for sample collection and testing (Salam et al 2018)

Figure 21: Closed bottom of duplicate labeled columns used for testing and sampling.

3.4.3 Phase 3

3.4.4 Double Drainage dozed with 600 ppm polymer.

The material preparation is as described in section 3.4.1 for 600 ppm g/ton . However, drainage was allowed out the bottom of the columns through filter paper. The replciae columns were place in a tray. Always about 0.5 cm of water was placed in the tray to impose a constant boundary condition at the bottom.

Two tensiometers was also inserted into 2 of the columns to measure pore-water pressure with time. For testing and sampling five different days labeled (covered from the top and uncovered from the bottom) duplicate columns were designed. Samples taken out from

1cm top those columns using spatula looked as illustrated in Figure 24 and these were used for performing several Geotechnical tests discussed in the coming sections.

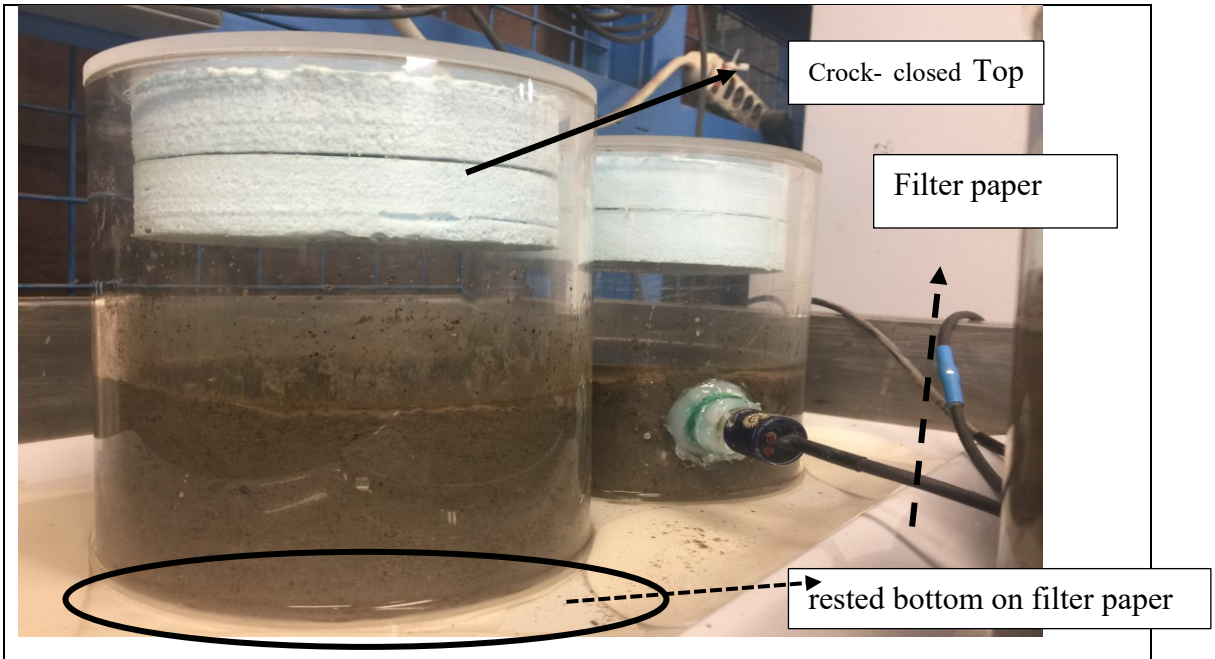

Figure 22 : Phase 3, 10 cm Double drainage column, with attached tensiometer for pore water calculation rested on filter paper for allowable drainage of water, Modified (Salam et al 2018)

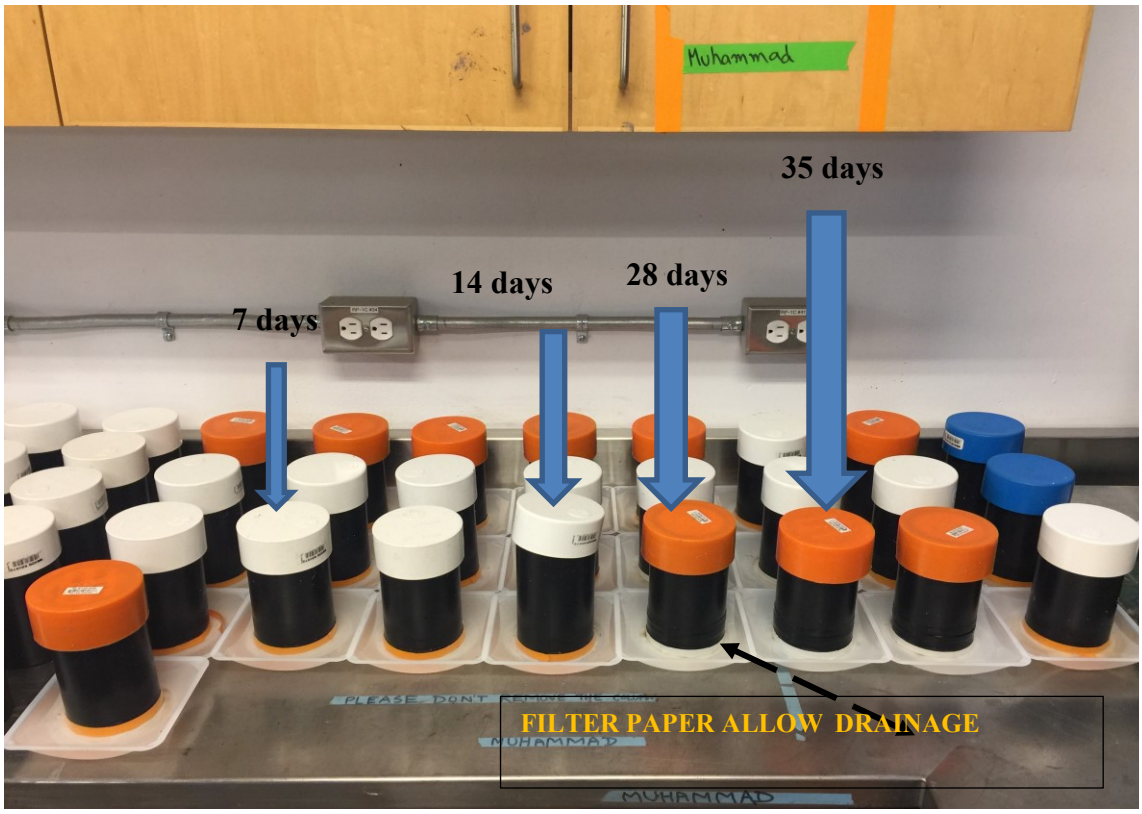

Figure 23 : Double Drainage Duplicate columns labeled for fluid fine tailings dozed with 800 ppm Anionic polymer. (Salam et al 2018)

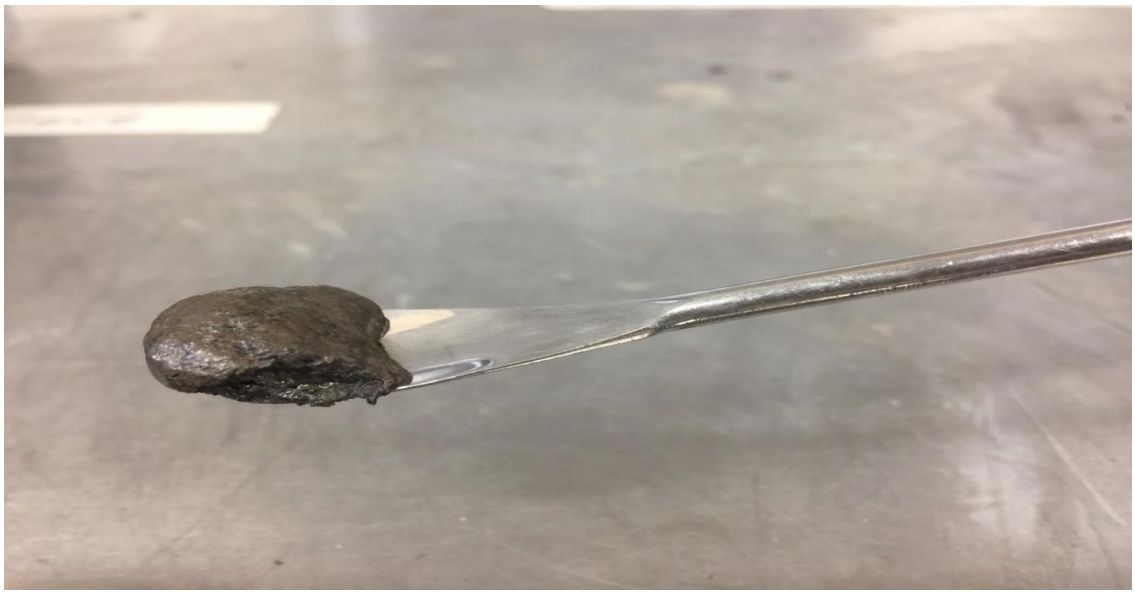

Figure 24: Sample collected using spatula from duplicate columns

3.5 Phase 3.5, 800 ppm Single drainage:

In phase 3.5 the material preparation and columns design were kept the same, however, this time tailings were dosed with 800 ppm of A3338 polymer and boundary condition for it was kept same as mentioned in Phase 2 section (Not allowing drainage).

3.6 Microstructure of polymer amend fluid fine tailings:

Samples were taken from both Phase 2, Phase 3, Phase 3.5 as well as Phase 4 duplicate columns, dozed with 600ppm and 800 ppm of anionic polyamide A3338 polymer respectively as mentioned in the above sections the samples were obtained from columns top using a spatula. Several tests were conducted on the samples obtained from these duplicate columns to track the microstructure, morphological behavior of fluid fine tailings.

3.6.1 Scanning Electron microscopy tests:

As discussed in Section 2.8.1 in detail, scanning electron device (SEM) can be used to magnify the sample from, “20 to 30,000x” with the spatial resolution of “50 to 100 nm”. This device can image an area from “1 cm to 5 microns” in width. Accordingly, to examine the structuration as well as to track the morphological behavior of FFT during long-term dewatering, Carleton university’s A Tescan Vega-11 XMU) SEM device was used. Samples, from 7 days to 72 days, were collected from top 1 cm from replicate columns mentioned in Section 3.4 transported to the SEM lab. The sample was obtained using a spatula and directly placed in the SEM device. The face of samples was kept upward in the SEM chamber, and an electronic gun was always kept perpendicular to the sample while imaging it i.e. 90 degrees.

Note: 7, 14 ,28 days means the sample were dosed with polymer and kept in columns for 7,14, or 28 days after polymer mixing, before samples were obtained for SEM or Optical microscope imaging

A rapid freezing stage of -50 ºc was applied to hydrated samples in the vacuum chamber and the samples were tested at a low vacuum of 10^{-3} Pa. Figure 25 shows a schematic cross-section of an SEM. In our study, SEM images of magnification of 200X with a view field of 750.0 µm by 750 µm were investigated for quantitative microstructure analysis.

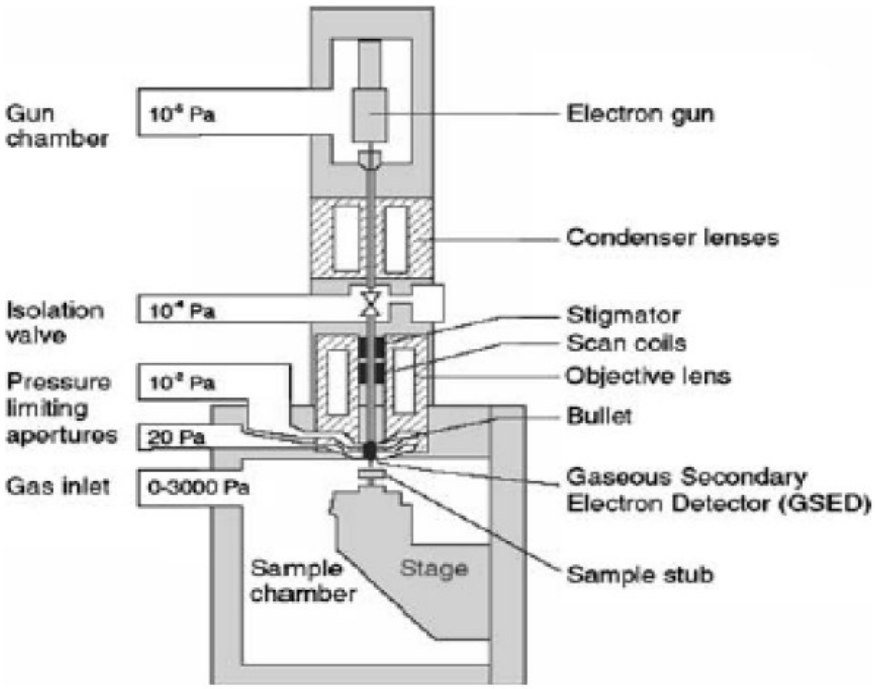

Figure 25: ESEM schematic cross section (Romero and Simms 2008)

3.6.2 Examples of Raw SEM images

Figure 26 Figure 28 were some of the examples of the Scanning electron micrograph produced for 600ppm dosage at respective days, i.e. from 1 day and 72 days. All images were originated by SEM with a same magnification of 200x and a view field of 750.0 µm by 750 µsamples were produced from columns with boundary condition described in section 3.4.1.

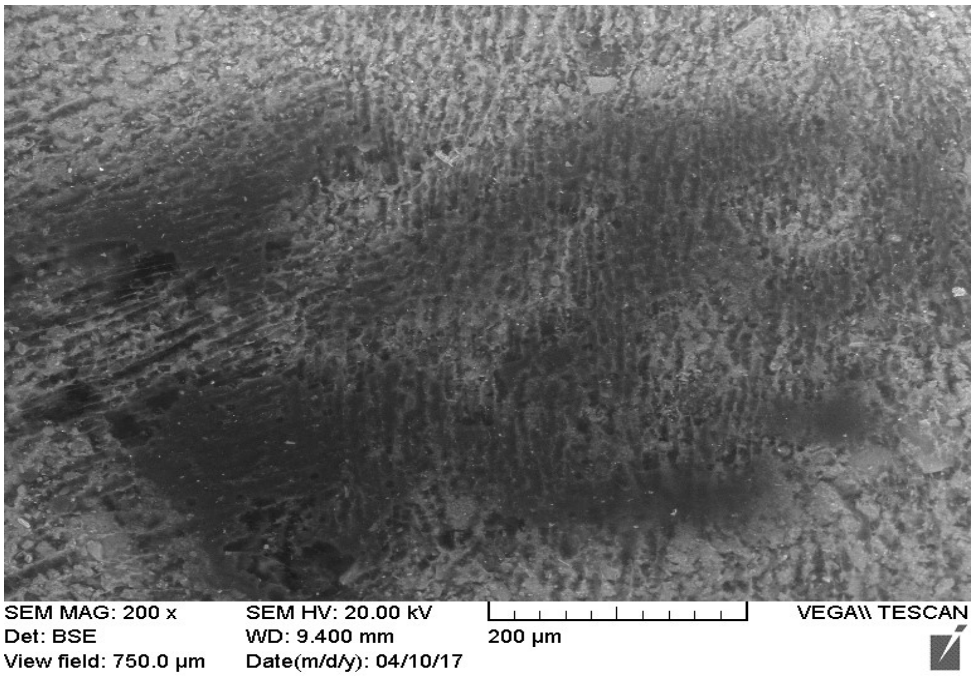

Figure 26: Scanning Electron Micrograph of polymer amended Oil sands tailings for dose of 600ppm, (After 7 day – of Polymer Mixing, Boundary Condition "Single Drainage (not allowing drainage") Magnification 200x, view field 750

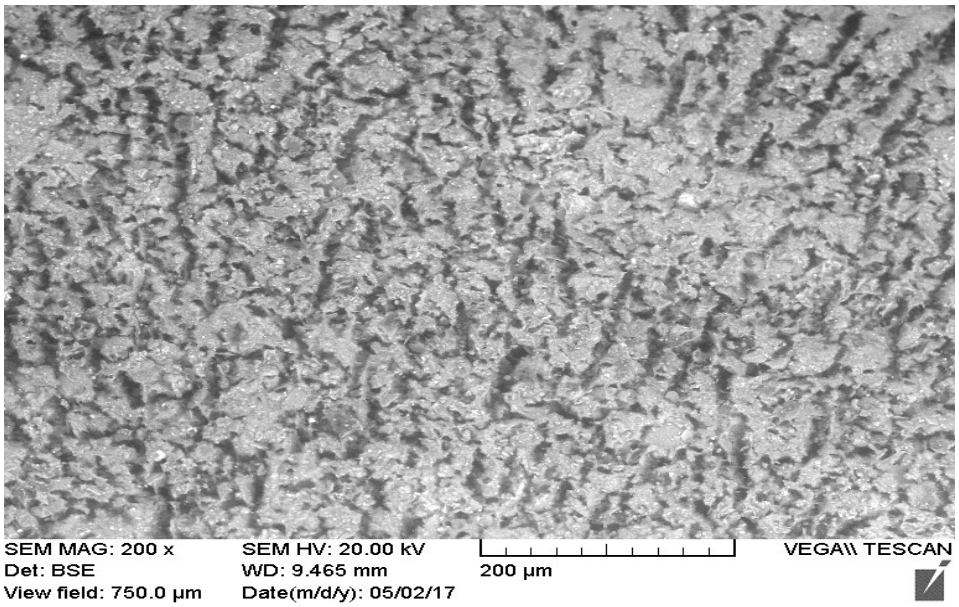

Figure 27: Scanning Electron Micrograph of polymer amended Oil sands tailings for dose of 600ppm, (After 28 day – of Polymer Mixing, Boundary Condition "Single drainage") Magnification 200x, view field 750

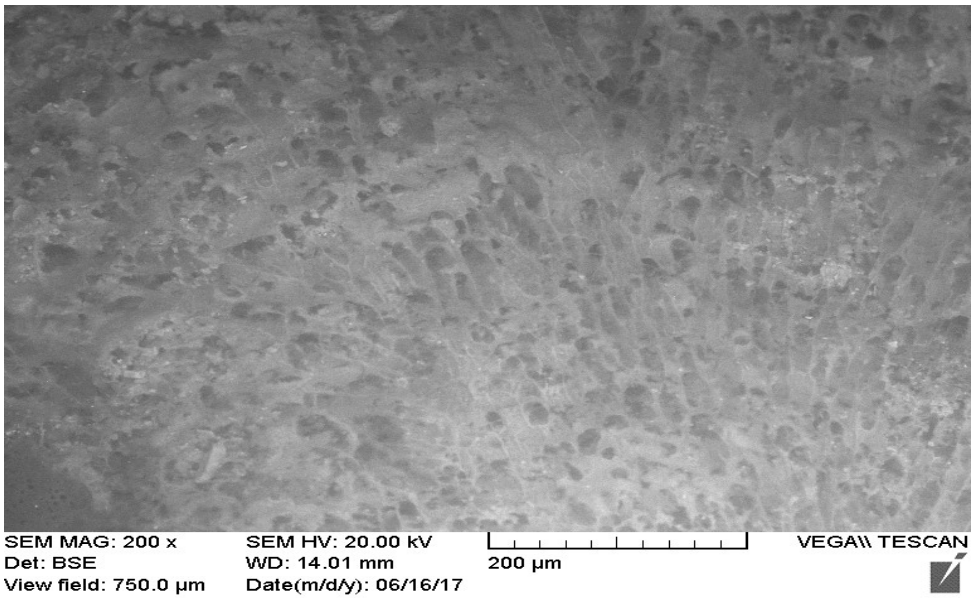

Figure 28: Scanning Electron Micrograph of polymer amended Oil sands tailings for dose of 600ppm, (After 72 day – of Polymer Mixing, Boundary Condition "Single drainage") Magnification 200x, view field 750

3.6.3 SEM Imaging of Phase 3, Double Drainage, 600 ppm dosage:

In this section, the boundary condition for polymer dosage and column were changed (allowing drainage) the bottom of the columns could drain water. Sample collection and imaging technique were same as mentioned in the section 3.6.2. However, to see the modification in microstructural behavior and effects of change in boundary condition on structuration behavior samples from duplicate columns were imaged, using same magnification field kept for Phase 2 experiment. Figure 29 till Figure 30, Shows the examples of SEM micrographs obtained for double drainage column dosed with 600 ppm dosage.

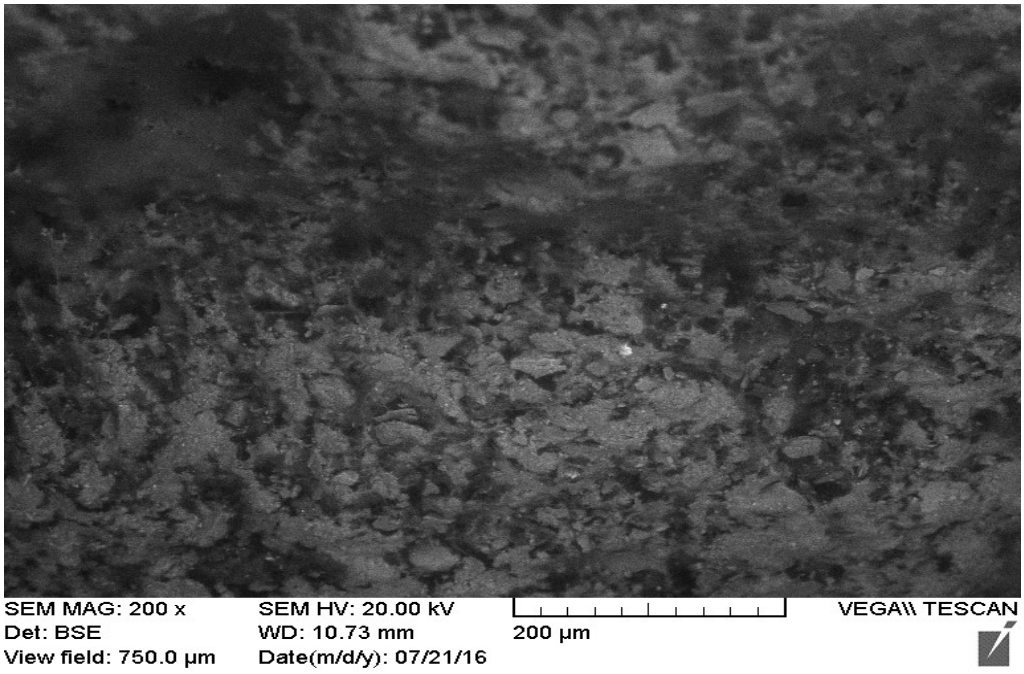

Figure 29:Scanning Electron Micrograph of polymer amended Oil sands tailings for dose of 600ppm, (After 1 day – of Polymer Mixing, Boundary Condition "Double drainage (allowing drainage") Magnification 200x, view field 750

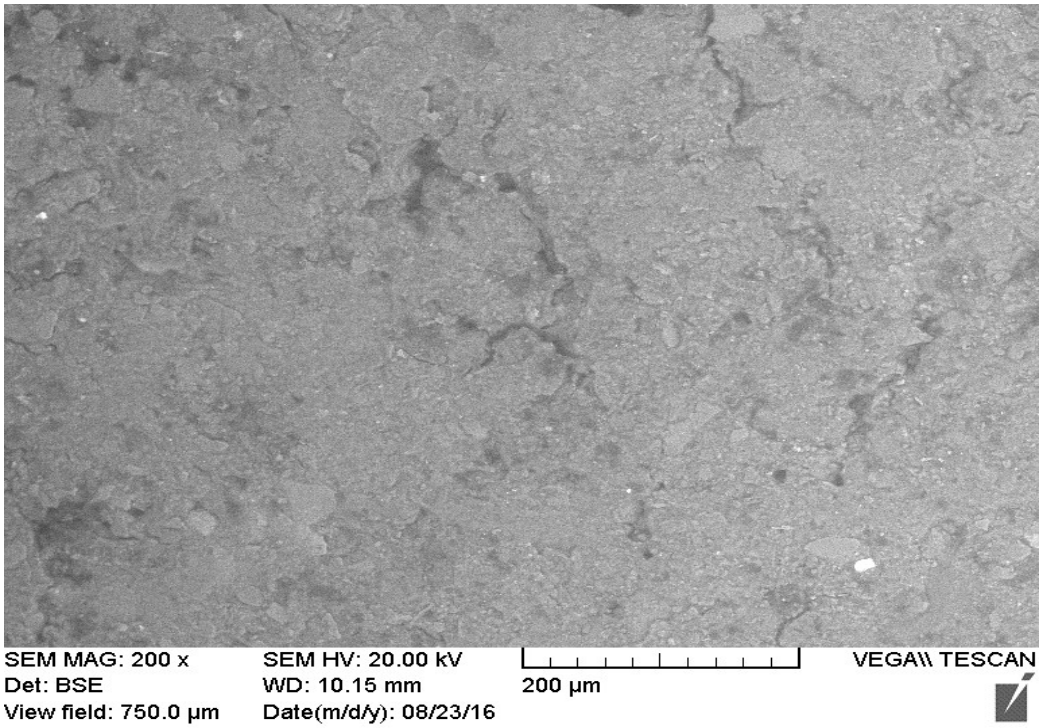

Figure 30: Scanning Electron Micrograph of polymer amended Oil sands tailings for dose of 800ppm, (After 35 day – of Polymer Mixing, Boundary Condition "Double drainage") Magnification 200x, view field 750/

3.7 Phase 3.5 SEM Imaging for 800ppm Single Drainage columns:

Figure 31 till Figure 32 illustrates examples of the SEM images obtained for quantitative analysis.

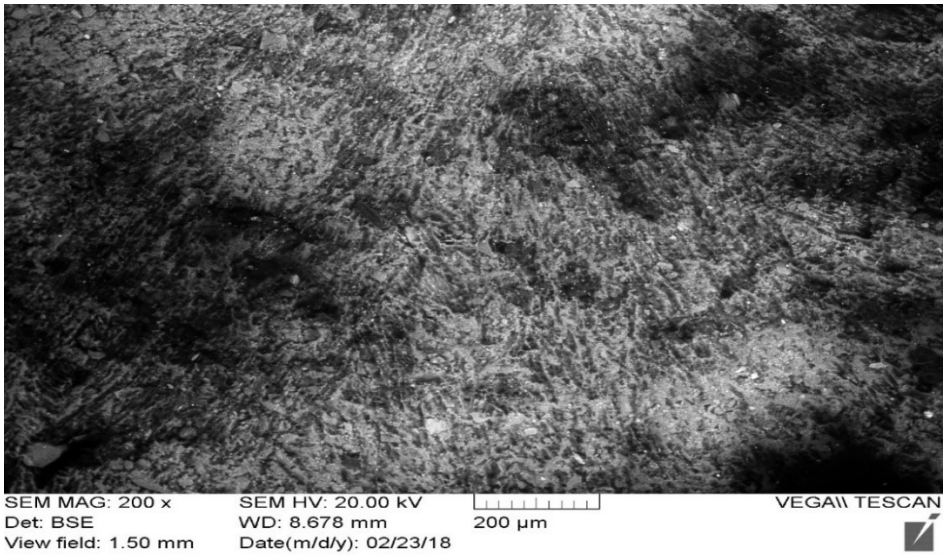

Figure 31: 1-day Single Drainage (not allowing) Image for 800 ppm dosage

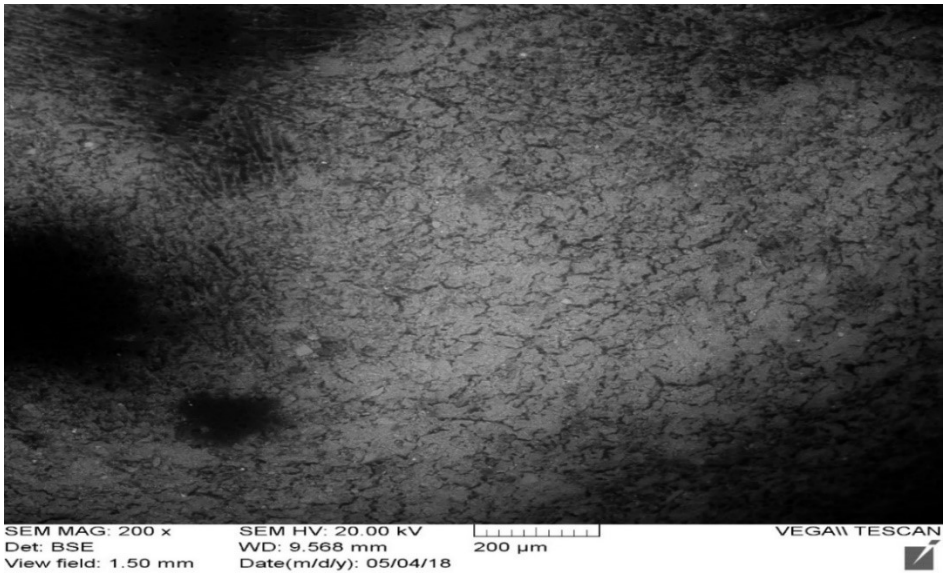

Figure 32: 72-day Single Drainage Image for 800 ppm dosage

3.8 Phase 4, Optical Microscope:

Unlike SEM, where hydrated samples were frozen before they were imaged in the SEM chamber, samples are imaged in their original state. In this method, samples were taken from duplicate columns specially designed for this analysis. Samples collected were imaged in their wet state on an hourly basis i.e. (1,2,4,8,24 and 48 hours). Carleton university Nikon Eclipse Ti Optical microscope, at a magnification of 200x view field 650 μm across width was used to study floc development.

The amended tailings were sampled from the surface of replicate columns after each hour of mixing using a needle as shown in the Figure 34 and placed onto the slides as illustrated in Figure 33. The position of the slide was changed to obtain 5 different images, on average. Due to increase in the density of tailings it was impossible to imaged samples beyond 48 hours as light source used by optical microscope could not pass through the samples. Hence tailings, were imaged till 48 hours only, for both 600-ppm dosage and 800 ppm dosage. Time between sampling and completion of imaging always took less than 15 minutes. For reference 1 hour and 48-hour images are illustrated in Figure 35 and Figure 36 and a schematic diagram of overall chapter 3 material preparation, column test methodology, sampling for image analysis, and subsequent digital image processing, is illustrated in Figure 37.

.

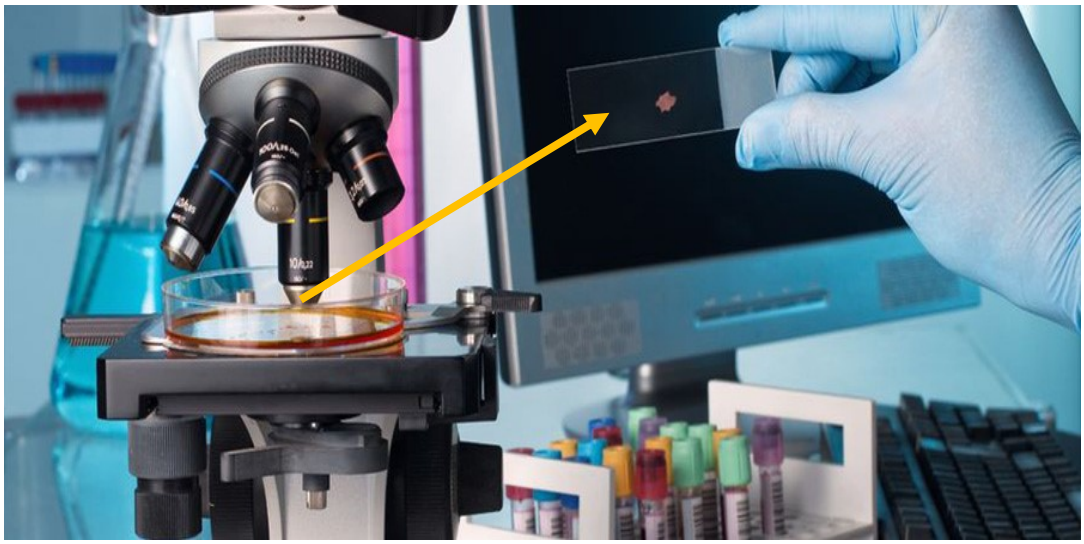

Figure 33: Optical microscope slide used for sampling of tailings, taken from replicate columns.

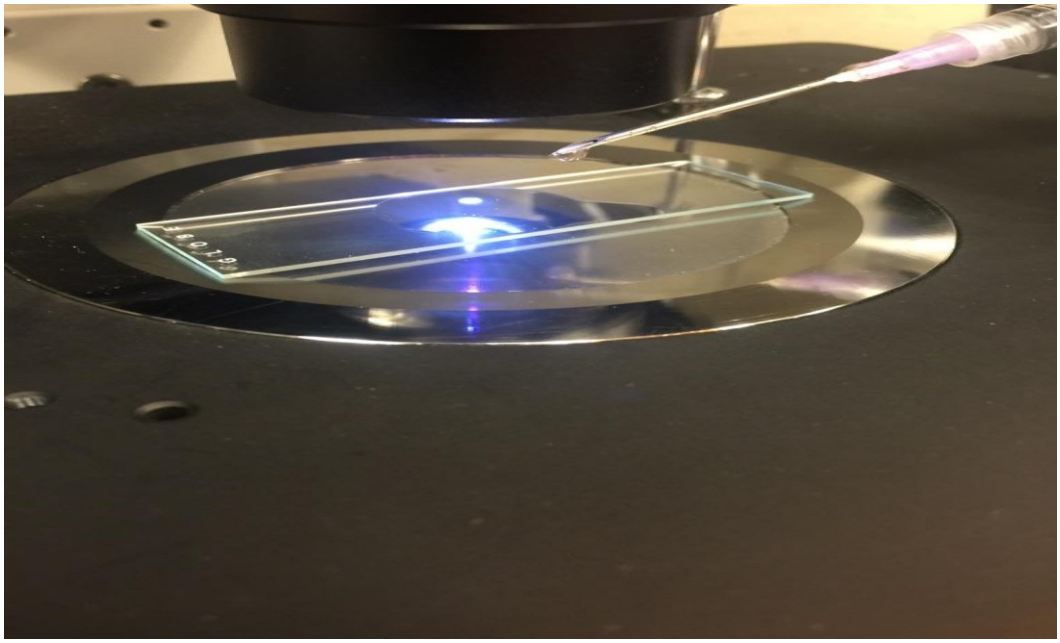

Figure 34: Sample Collection for Optical Microscope using needle (Salam et al 2018)

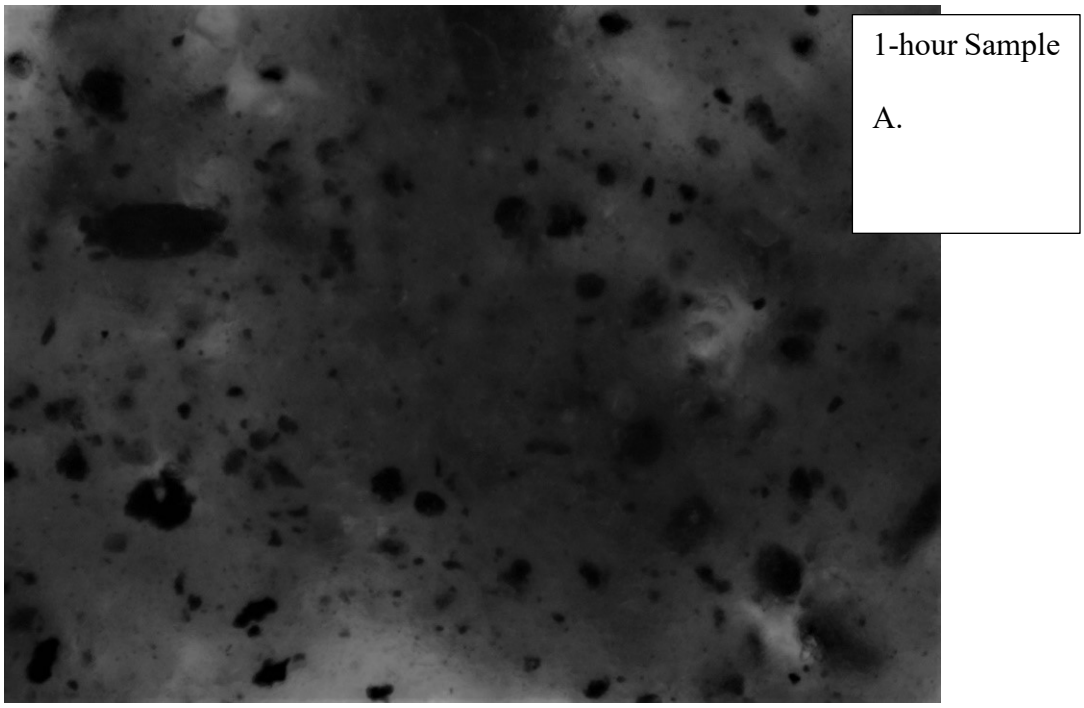

Figure 35: **Optical microscopy of polymer amended Oil sands tailings for dose of 600ppm, (A-1hour of Polymer Mixing, Boundary Condition "Single drainage") Magnification 200x, view field 650/ micron wide.**

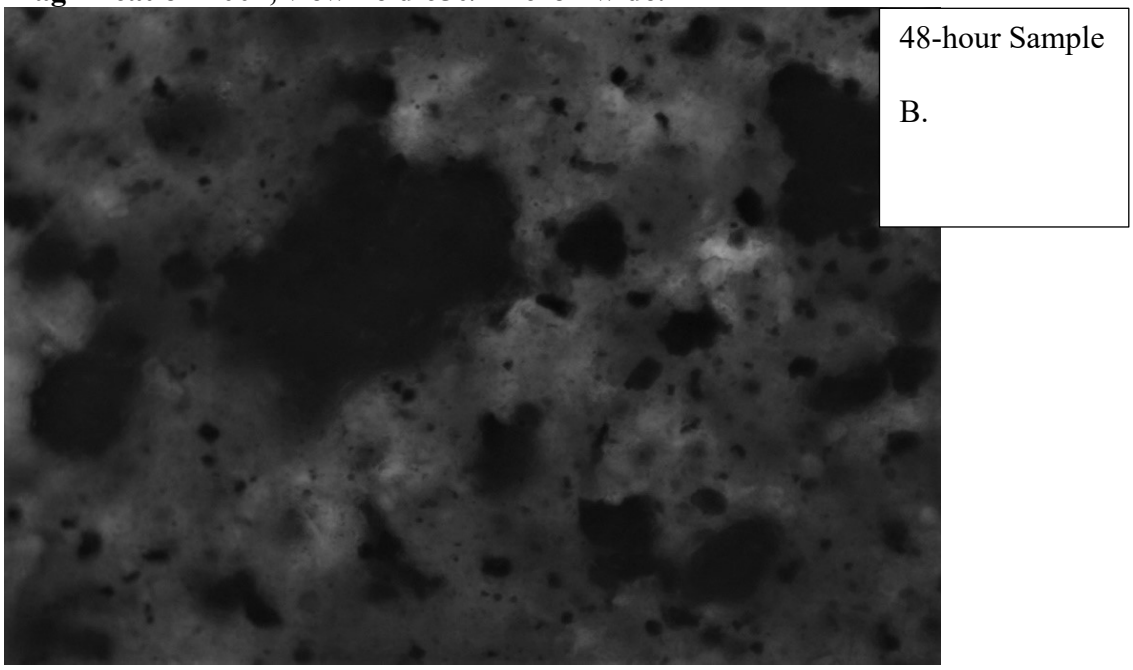

Figure 36: Optical microscopy of polymer amended Oil sands tailings for dose of 600ppm, 48 hour – of Polymer Mixing, Boundary Condition "Single drainage") Magnification 200x, view field 650/ micron wide)

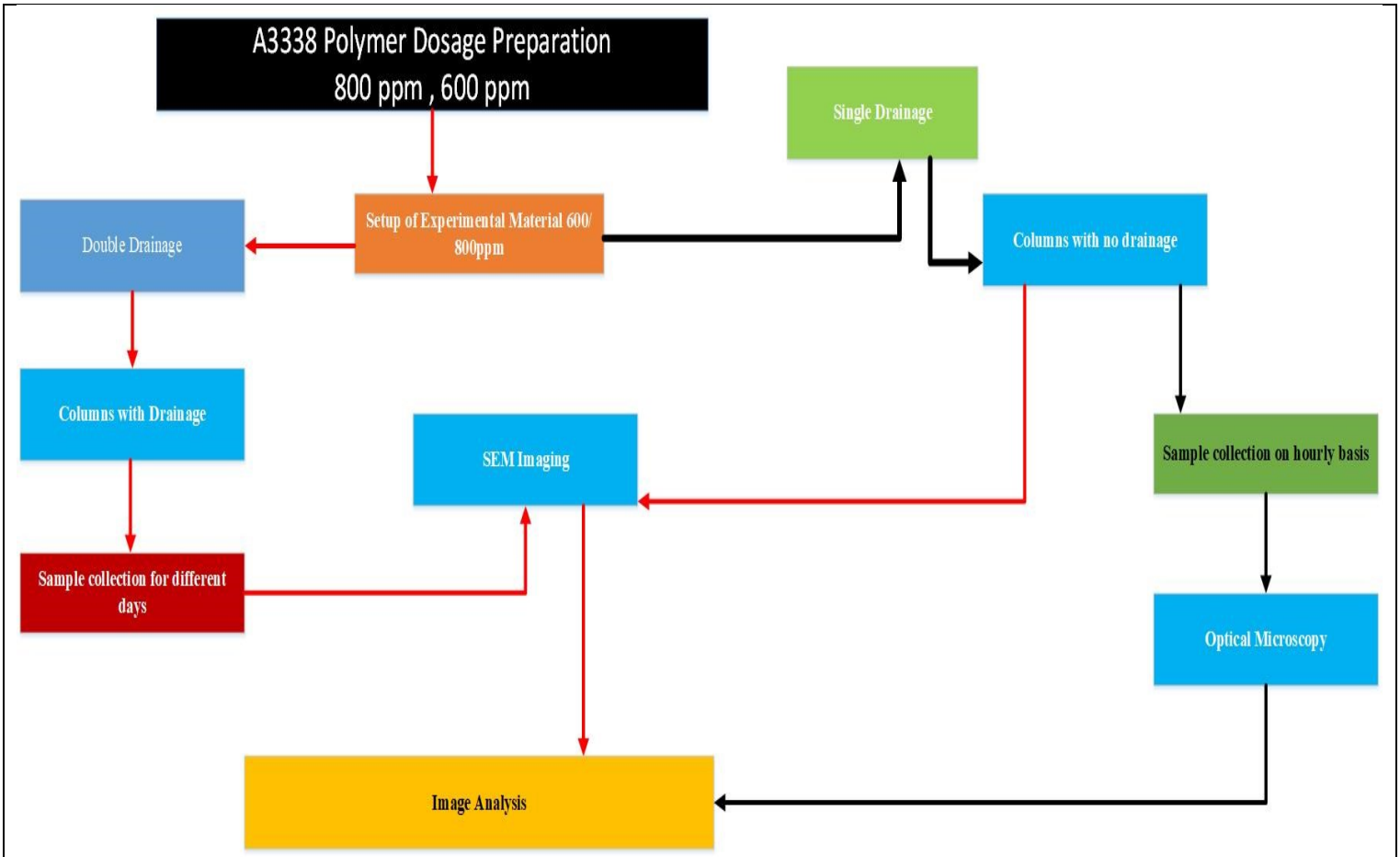

Figure 37: Schematic of material preparation, column test methodology, sampling for image analysis

4 Chapter: **Digital Image Processing Methods**

4.1 Introduction:

Greyscale images are a rectangular tiling of fundamental elements called pixels. Every raster image contains pixels and every pixel contains bits. The number of bits contained in each pixel is called image bit depth (number of bits per pixel). A pixel is the smallest element of the image that stores value proportional to light intensity, as shown in Figure 40 (Young et al 1998). For most images, pixels values are integers that range from 0 black -255 white. Examples of pixels and their intensity values are shown in Figure 38 and Figure 39.

Figure 38 :The range of intensity values from 0 (black) to 255 (white).

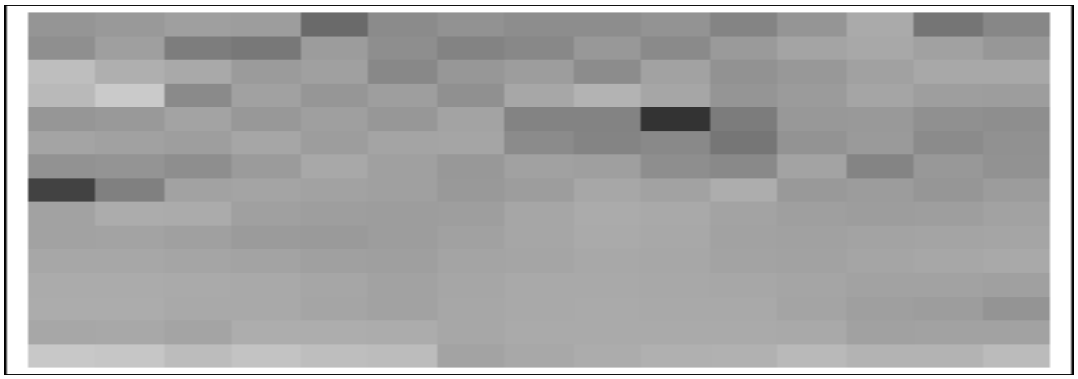

50	154	160	157	106	140	147	142	141	147	132	150	171	117	136
144	159	125	121	157	143	132	136	153	138	155	164	169	162	152
190	175	169	155	161	136	152	158	141	162	147	153	161	168	169
185	203	139	161	151	159	145	167	179	167	150	155	165	159	158

Figure 39: Pixel portion of the SEM image with pixel intensity values. (as an example)

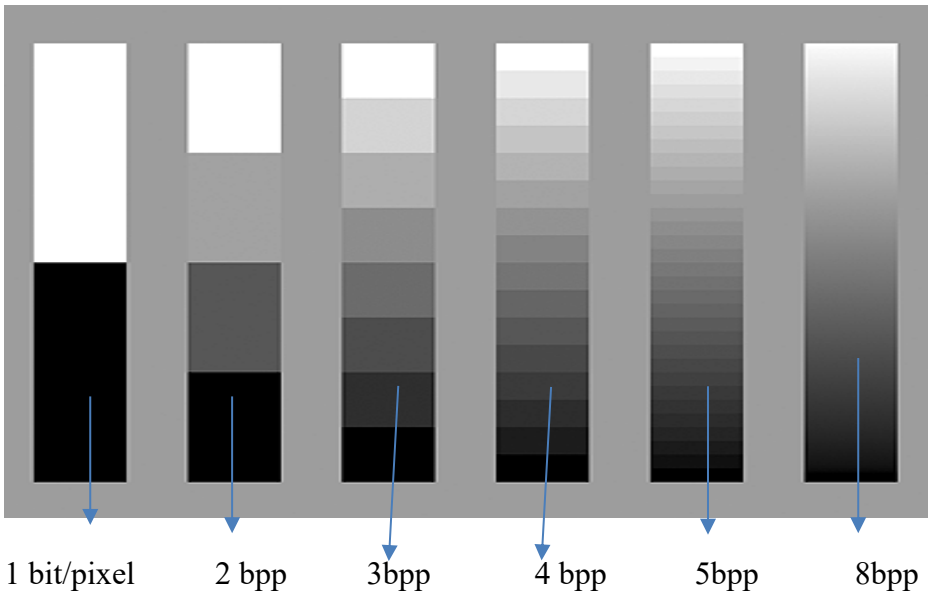

2 colours	4 colours	8 colours	16 colours	32colours	256 colors
2^1	2^2	2^3	2^4	2^5	2^8

Figure 40: Classification of bits per pixel from 1-pixel image to 8 pixels

There are many approaches and techniques used for processing images. After considerable trial and error, certain techniques were adopted in this study that allowed for the repeatable extraction of information from FFT images.

For each sample, at least 8 images were taken but at different magnifications (200x, 500x, 1000x 2000x) as shown in Figure 41 (a to c). It appeared that the 200x images provided the most representative information, showing a wide distribution of discernable flocs or particles sizes as illustrated in chapter 3 for each phase. Therefore, three "good quality" images were obtained for each sample from SEM at 200x. An example of "good quality" and "bad quality" are shown in Figure 42. The same scale was employed for optical microscope images to compare SEM and OM images.

After obtaining the SEM or OM Images, the widely used image processing software Fiji-Image J, was used for fabric investigation and quantitative analysis of the amended FFT images. Statistics on grain and pore size distribution were obtained from the image analysis.

Image treatment is necessary before images can be analyzed by any software, such as ImageJ, due to poor delineation between pores and particles in the raw images. Through trial and error, a methodology has been developed to render suitable images for grey pixel analysis. While image treatment and filtering operations to be used on any image are

application specific and generally subjective, this work attempts to develop a repeatable image processing method for this material (FFT).

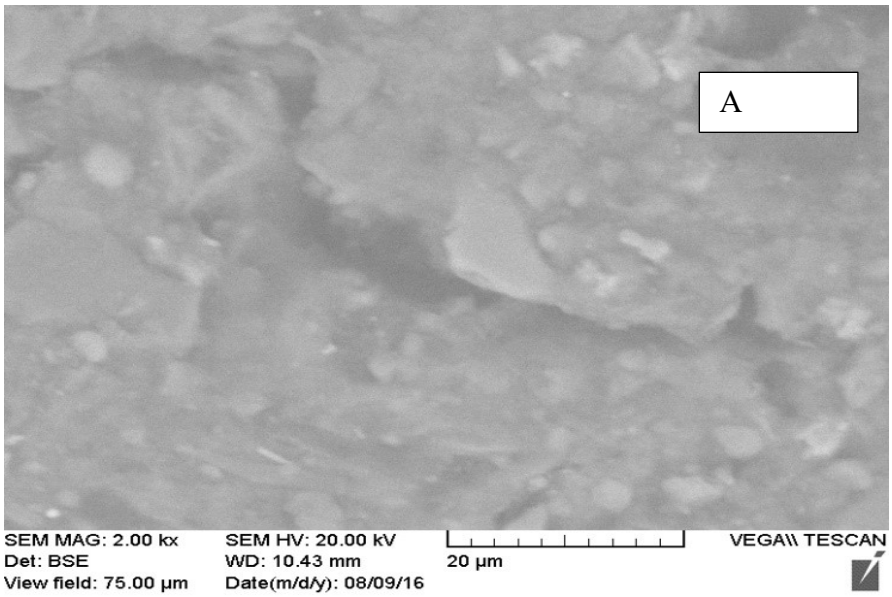

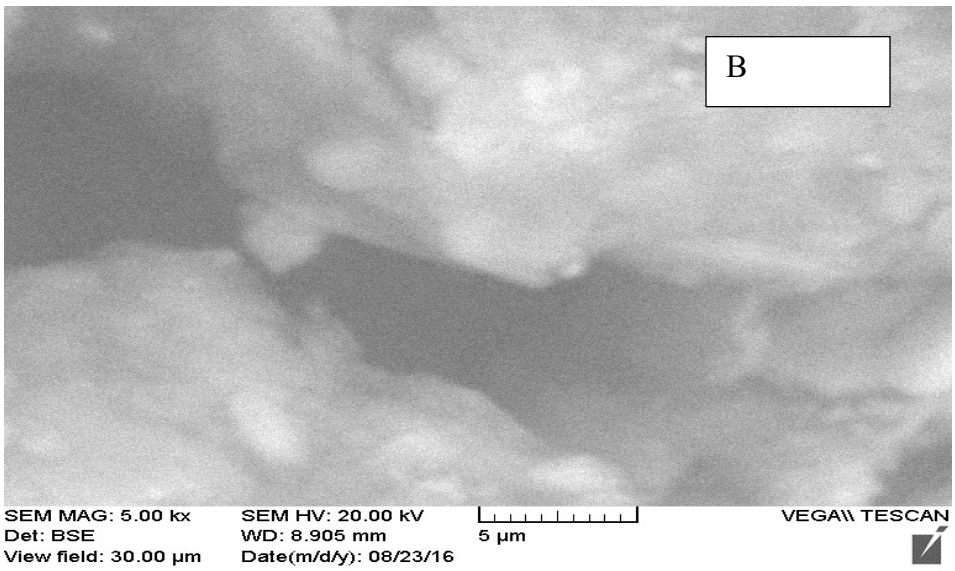

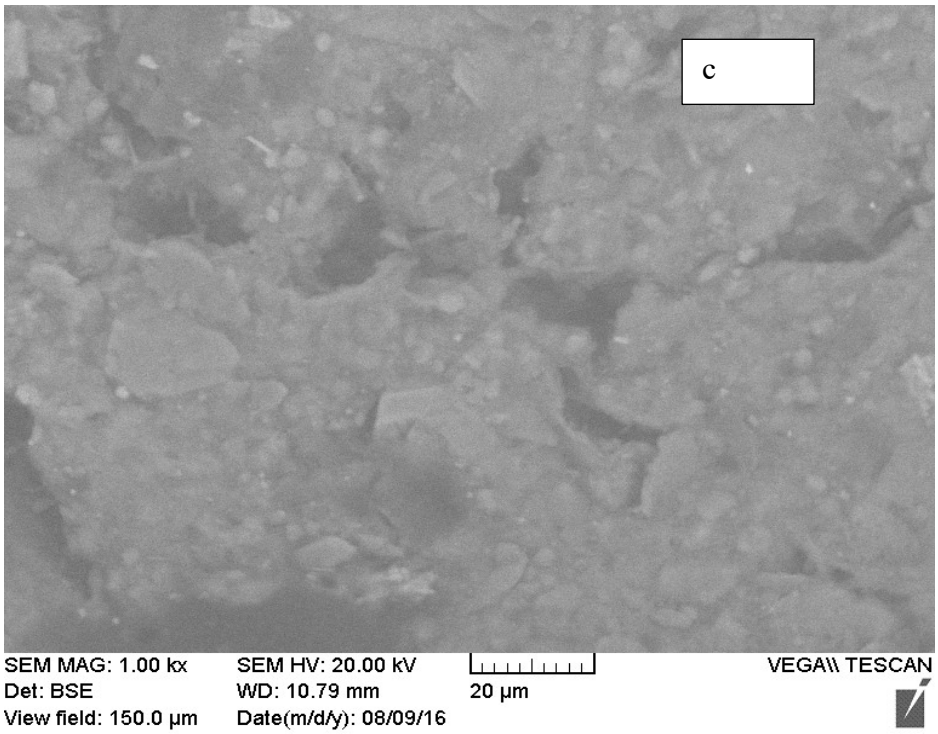

Figure 41: Different magnification SEM images generated images. (a)2000 magnification. (b)5000 (c) 1000 magnification

(a) (b)

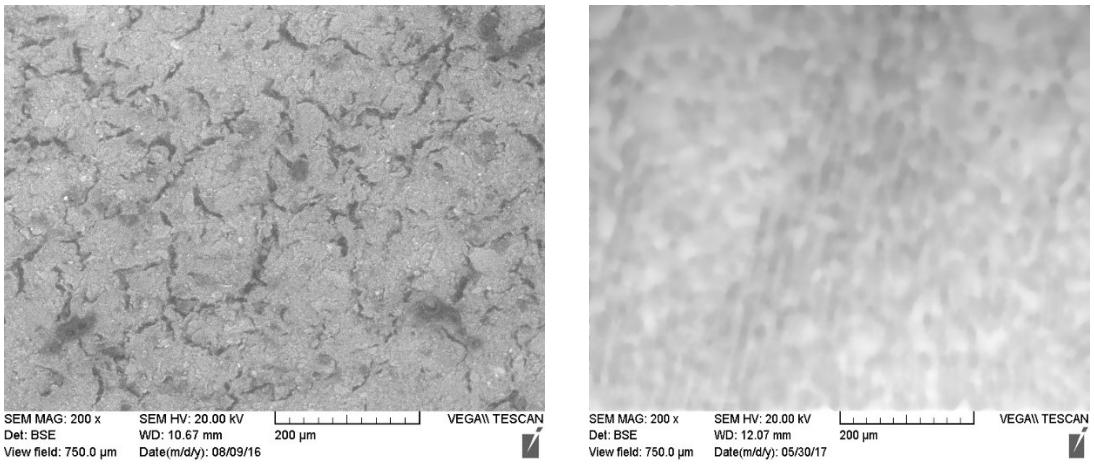

Figure 42 : Difference between good image (A) for analysis and bad image (B) (low resolution)

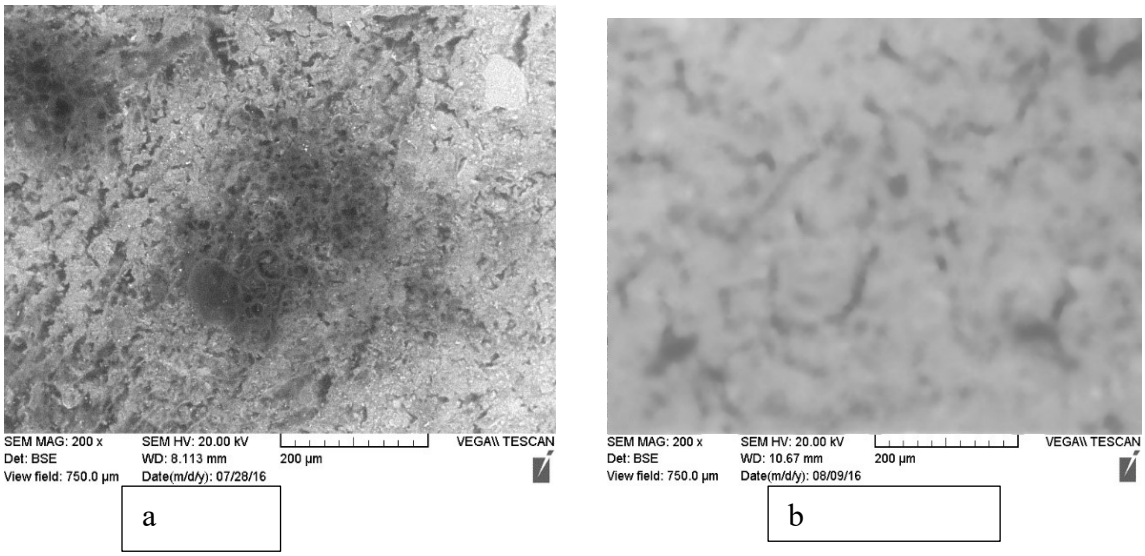

Figure 43: Difference among (a) good quality image, AND (b) bad quality image (low resolution)

4.2 Scaling the Images:

Images obtained from SEM and optical were in 8 bits (2^8 = 256 grey scale colors)' resolution and comprise 768 x 648 pixels (This means a total number of 768 x 648 = 497664 pixels are displayed at the screen in one image). The following procedure discussed below was adopted from Ferreira and Rasband (2012) for scaling images,

Using ImageJ software, freehand straight line was selected from toolbox and scale bar already displayed on SEM image was measured, *through analyze>set scale*. The scale bar Figure 44(c) measured by line tool gave us values which are shown in Figure 44(a). The

known distance for images was kept 200 as already posted on image. Furthermore, the unit of length was changed to µm. The resolution of an image after scaling was noted to be 1.0267 pixels per µm and image was converted into a 768 µm x 648µm image as Illustrated in Figure 44 (b). This scaling procedure was kept same for all sample images. Subsequently, non-image parts of the picture (E.g. the scale portion) were removed by cropping.

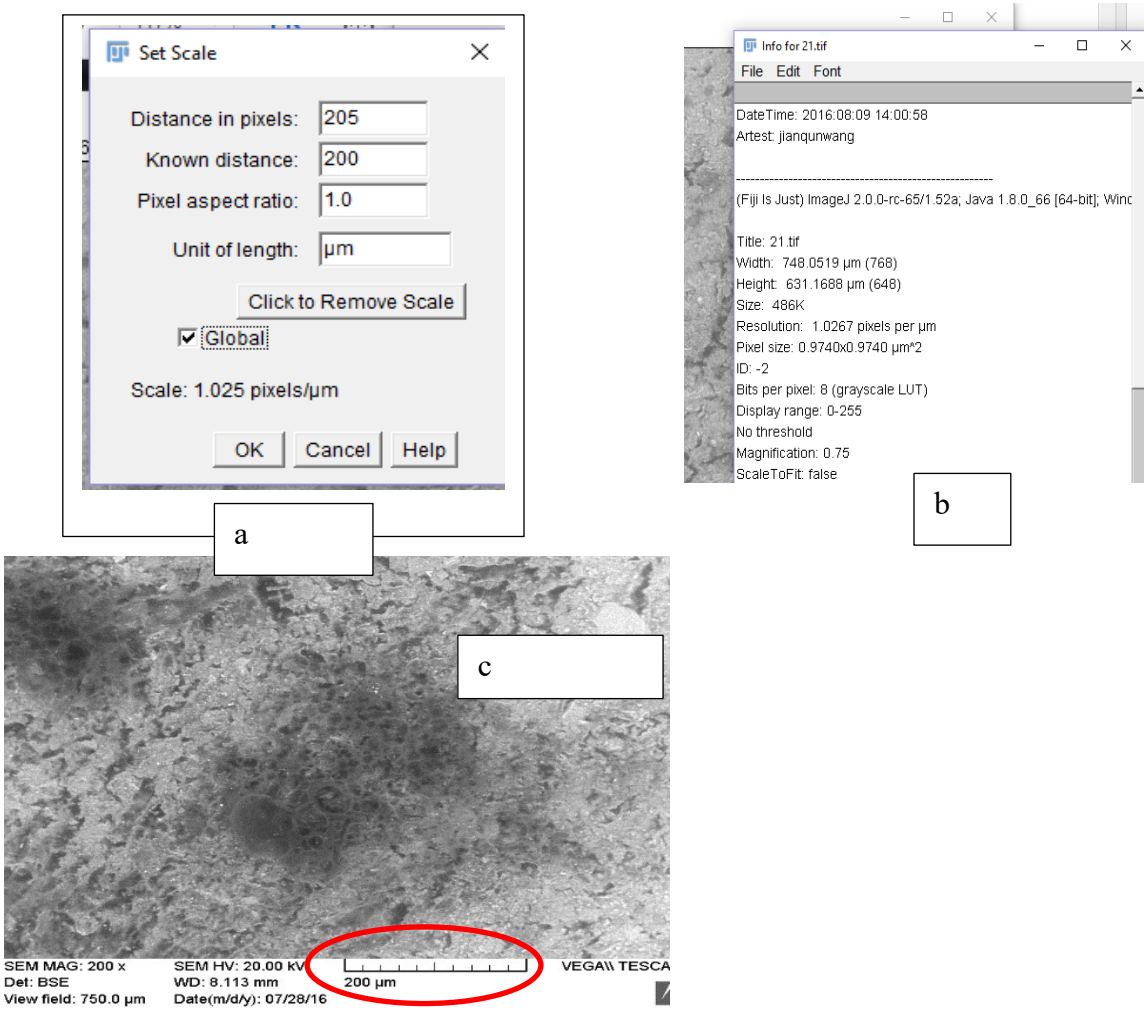

Figure 44: Image Set Scale and Updated Information (Using Image J)

4.3 Image Enhancement operations:

Image enhancement was done in “Image J” and “Adobe Photoshop”. Pixel treatment starts with noise subtraction. Noise is defined as any undesirable signal, disturbance, which camouflages the desirable information in images (Naphade 1999).

4.3.1 Filters:

There are many kinds of filters in ‘Image J”, such a linear Khuwahara, Gassien blar and many others. In this study, a median filter was applied to all images. The median filter reduces noise in images by replacing each pixel with the median of neighboring pixel value so that all image pixel has the same value of noise (Ferrier and Rasband 2012). On a per image basis, use of the median filter gave a clearer distinction between particle and pore space and was applied on images as shown in Figure 45. The default neighborhood Radius of 2.0 was used most of the time while using this tool. These filters were only applied to SEM images and not OM images.

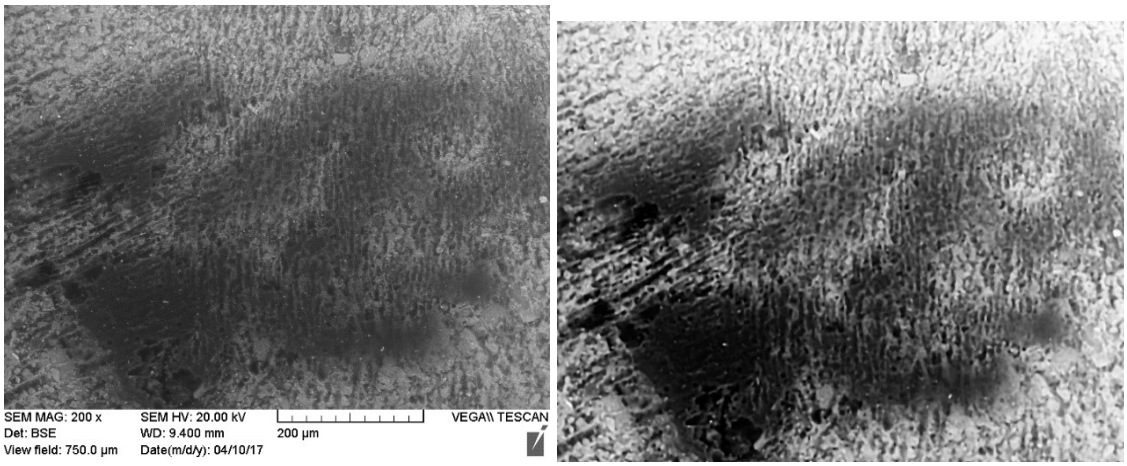

(a) **(B)**

Figure 45:Median filter (a) before and (b) after applied results

4.3.2 Enhancing Contrast:

Image contrast level was enhanced to a level that it gave a better visual distinction between particles a pore-space. This was done using *Image j> process>enhanced contrast> Saturated pixel*. This tool changes contrast compared to set a maximum number of pixels that can become saturated (having the highest possible brightness value) (Latief 2016). This technique usually generates a visually balance image; however, it was noted that a visually agreeable picture may not be the best goal for image analysis. For example, during trial and error, it was noted that increasing contrast above a certain level, generated images that over-weighted some small features. In this study, the saturation level for images was kept between 0.5-2%.

In addition, image pixel intensities were modified through normalization and histogram equalization. Histogram equalization distributes the intensity of each pixel equally throughout the image, this allows areas of lower contrast to gain higher contrast making the image intensity balance throughout the image. For example, the histogram values for our RAW image, in Figure 48 were mostly between 100 to 150 grey scale. After applying histogram equalization, the pixel values became distributed over the entire grey scale range. Each pixel value is lowered or increased by a common factor depending if it less or greater than the original mean pixel value.

Normalization distributes pixel intensities more evenly across an image, to distribute a broad histogram of image intensity (As in Figure 49). The normalize tool is quite simple, it looks for the maximum intensity of pixel and a minimum intensity of the Pixel, and then will determine a factor that scales the min intensity to black and max intensity to white. The equalize tool attempt to produce a histogram with an equal number of pixels in each intensity level. This can produce unrealistic images since the intensities can be radically distorted but can also produce images very similar to normalization.

In our case we wanted our images to be realistic as well as even distribution of intensities we used both normalization and histogram equalization tools in Figure 49. These tools enhanced the images pixels' values using histogram equalization, a modified built-in algorithm in "Image J". Furthermore, processed images were smoothed and then passed through brightness and contrast adjustments again. This was completed by following image >adjustment >brightness and contrast in "Image J". To minimize bias adjustments

in the brightness and contrast auto tool as shown in Figure 47 was used which uses default settings.

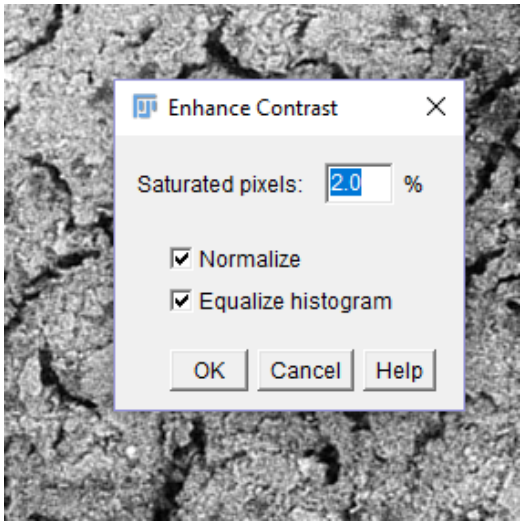

Figure 46: Contrast Enhancing and histogram Equalization followed by adjustment in brightness and contrast using image.

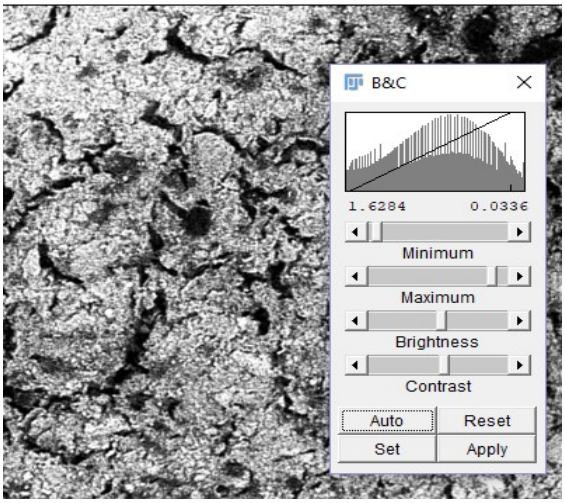

Figure 47 : Image adjustment through brightness and contrast

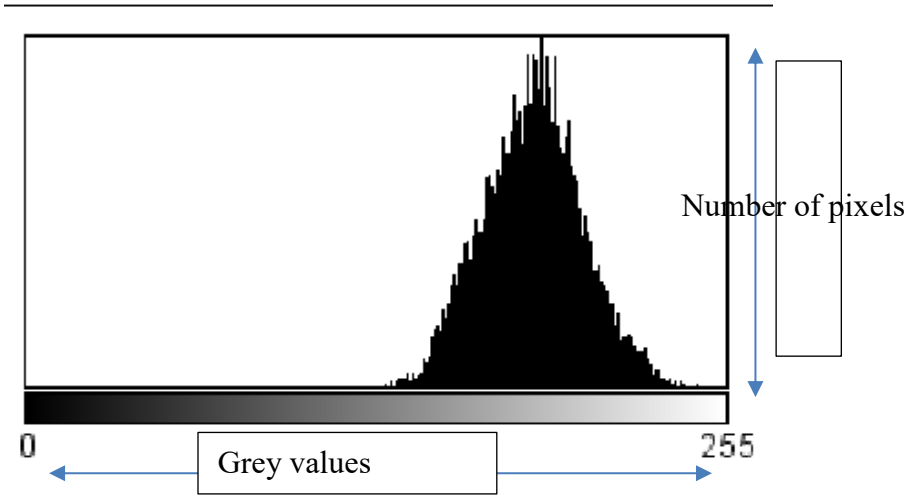

Figure 48 : Histogram values for RAW Images before image treatment.

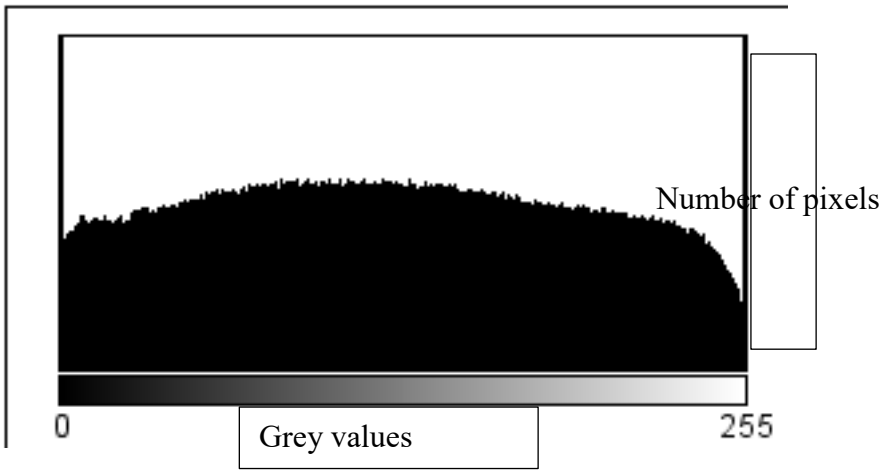

Figure 49: Histogram Equalization for images after treatment.

4.4 Filters for optical microscope:

Image treatment, scaling and enhancement operations were repeated the same as for the SEM images discussed above in section 4.1 till 4.3. However, for optical microscope images a "shadow filter" was applied.

Optical microscope generates images using a backlit light source. A shadow filter produces a virtual shadow effect upon the images by making the light to appear from different directions as illustrated in Figure 56 and Figure 58. The shadow effect makes it easy for the naked eye to distinguish between flocs and background of the image. After applying and trying different virtual effects of this tool "Northeast side" shadow effect gave us satisfying results in optical microscopy image treatment. Using other than northeast gave us more noise in the image and not a sound output as in Figure 50 result Northeast was selected for analysis as illustrated in Figure 56 and Figure 60.

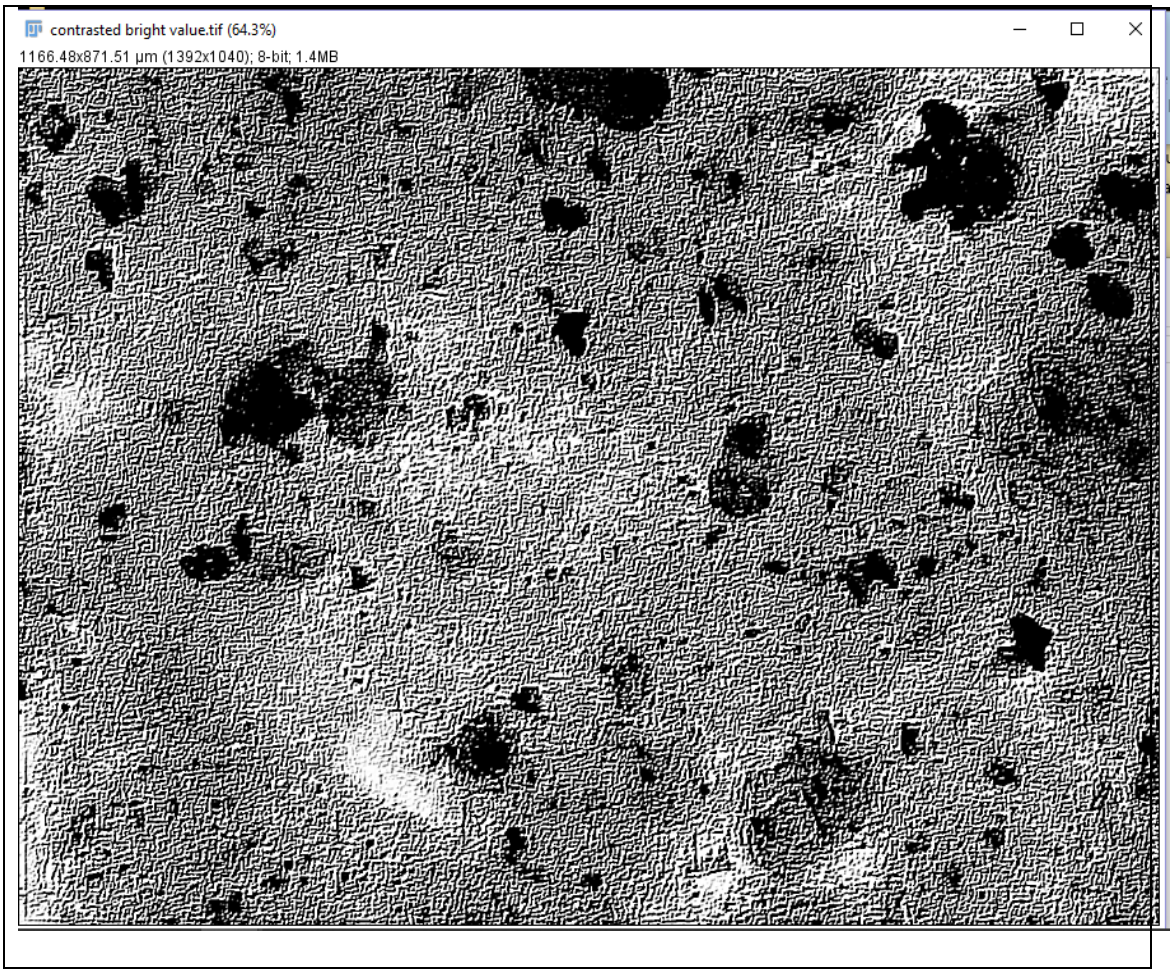

Figure 50: Results obtained while using North west filter on O.M Images.

4.5 Results of Image Enhancement operations:

Examples of results of image enhancement are illustrated in Figure 51 and Figure 52. The Same procedure was applied to all other images, readers interested in details of enhancement operations results for other images can go to appendices (A) where Results obtained after each treatment are illustrated.

4.5.1 Phase 2, SEM Images Enhancement results:

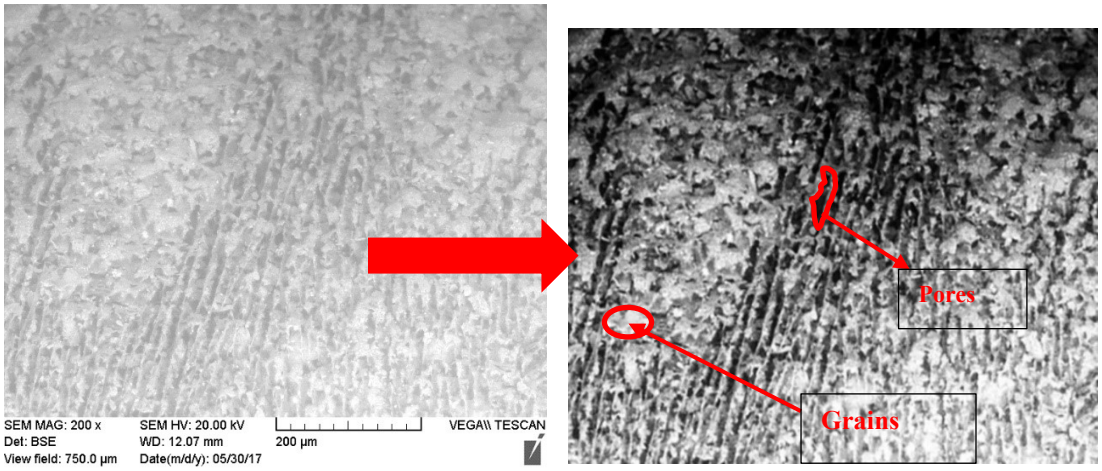

(a) **(b)**

Figure 51: Image treatment result for Phase 2, 14 days SEM Images (a) Image obtained from SEM lab before. (b) Pixel Intensity Improved image after using above procedure black sections pores white section Grains.

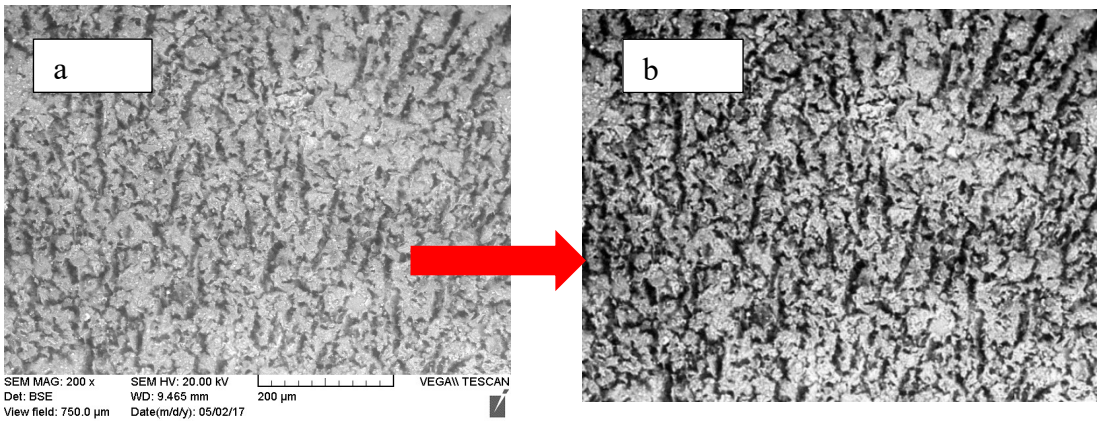

Figure 52: Image treatment result for Phase 2, 28 days SEM Images (a) Image obtained from SEM lab before. (b) Pixel Intensity Improved image after using above procedure black sections pores white section Grains.

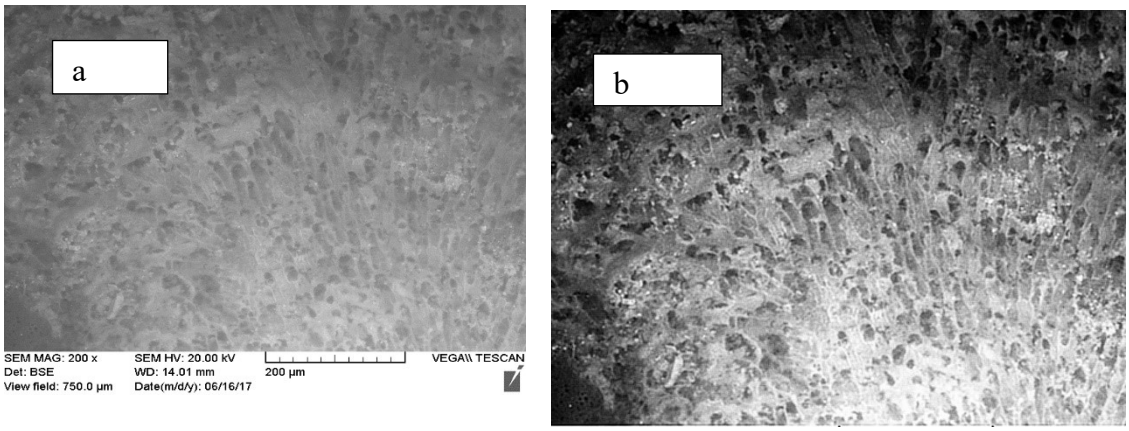

Figure 53: Image treatment result for Phase 2, 72 days SEM Images (a) before and (b) after treatment black sections pores white section Grains

4.5.2 Phase 3 image treatment results:

During analysis, it was noted that keeping same dosage 600ppm and allowing water to drain from columns gave better and understandable pixels than the phase 2 images because of the dryness of sample before frizzed in SEM chamber.

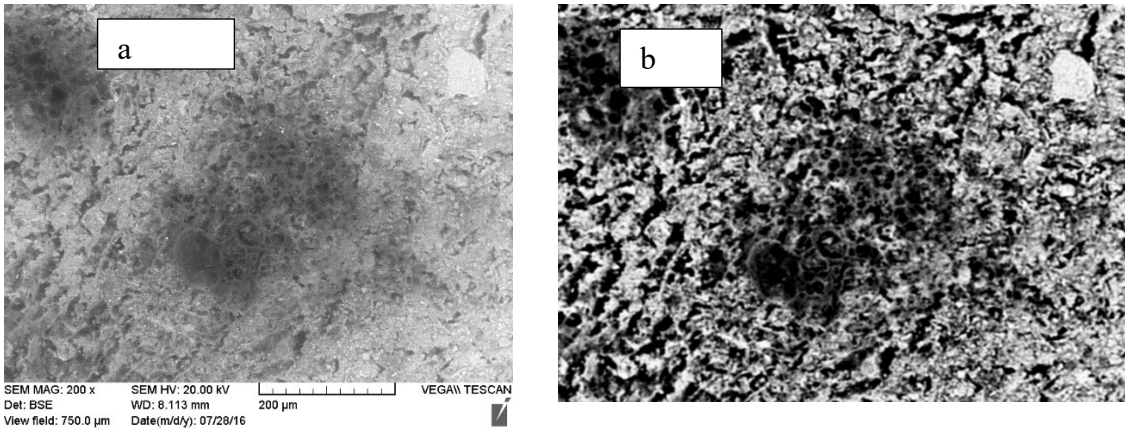

Figure 54 :Image treatment result for Phase 3, 7 days SEM Images (a) before and (b) after treatment black sections pores white section Grains.

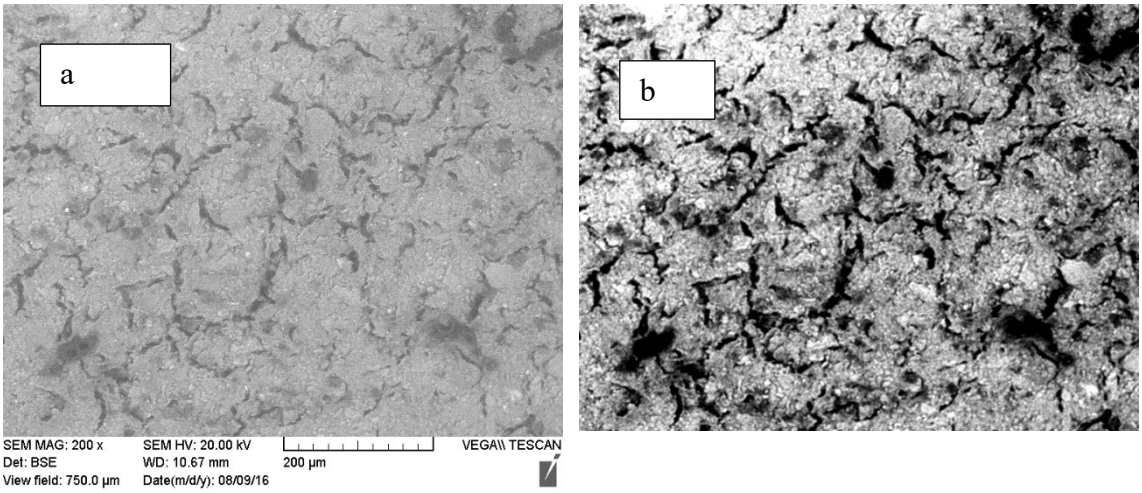

Figure 55: Image treatment result for Phase 3, 21 days SEM Images (a) before and (b) after treatment black sections pores white section Grains.

4.5.3 Phase 4 optical microscope image treatment results:

4.5.3.1 600 ppm Results;

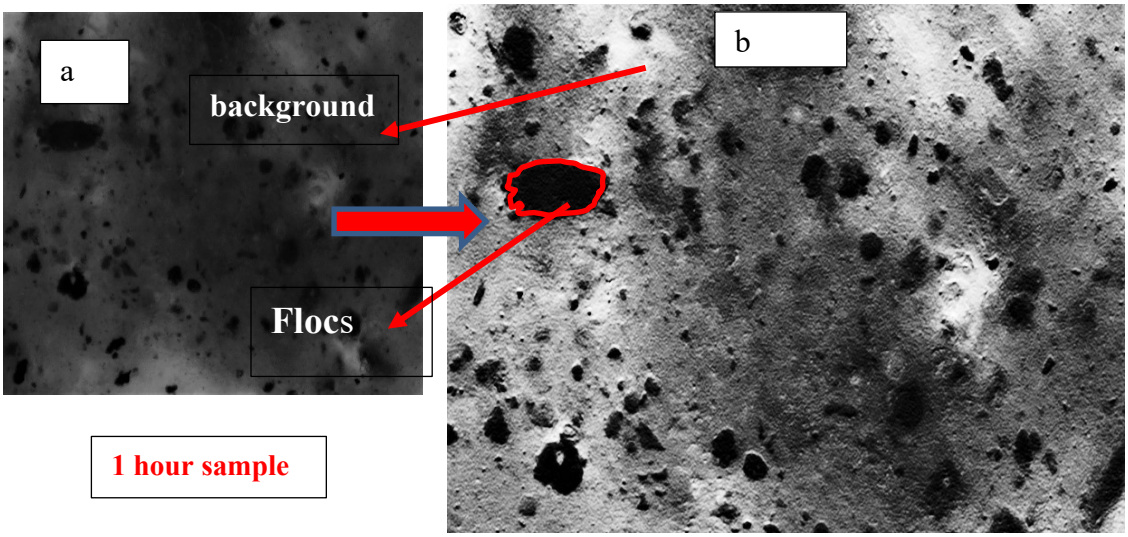

Figure 56: Image treatment result for Phase 4, 1 Hour Optical microscope Images (a) before and (b) after treatment black sections Flocs white section background light source.

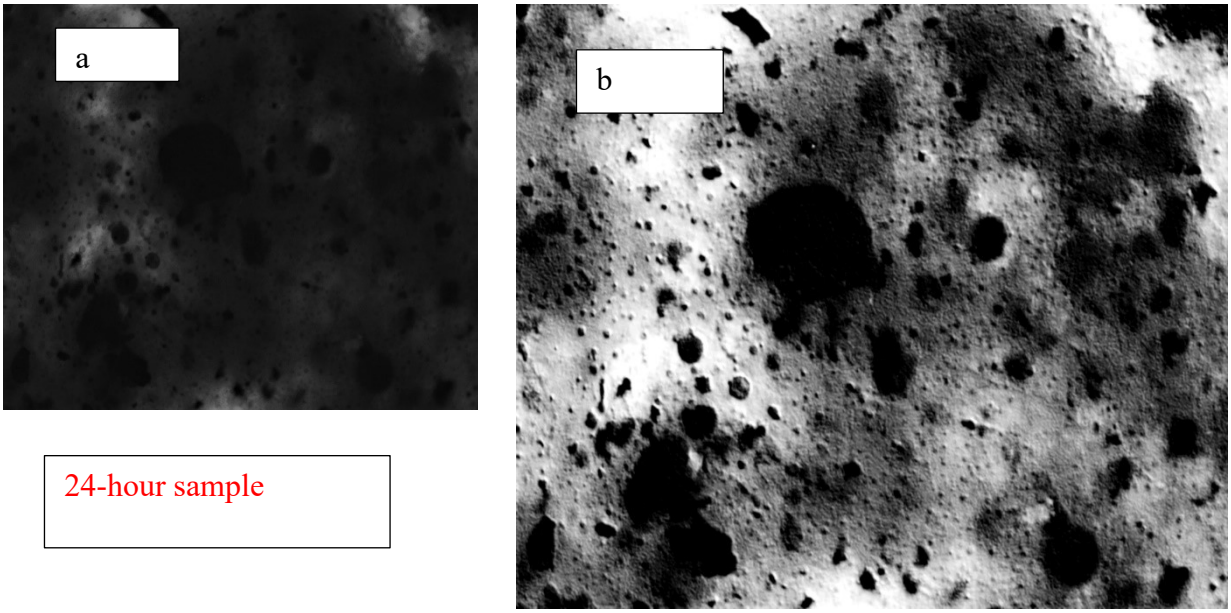

Figure 57: Image treatment result for Phase 4, 24 Hour Optical microscope Images (a) before and (b) after treatment black sections Flocs, White section background light source.

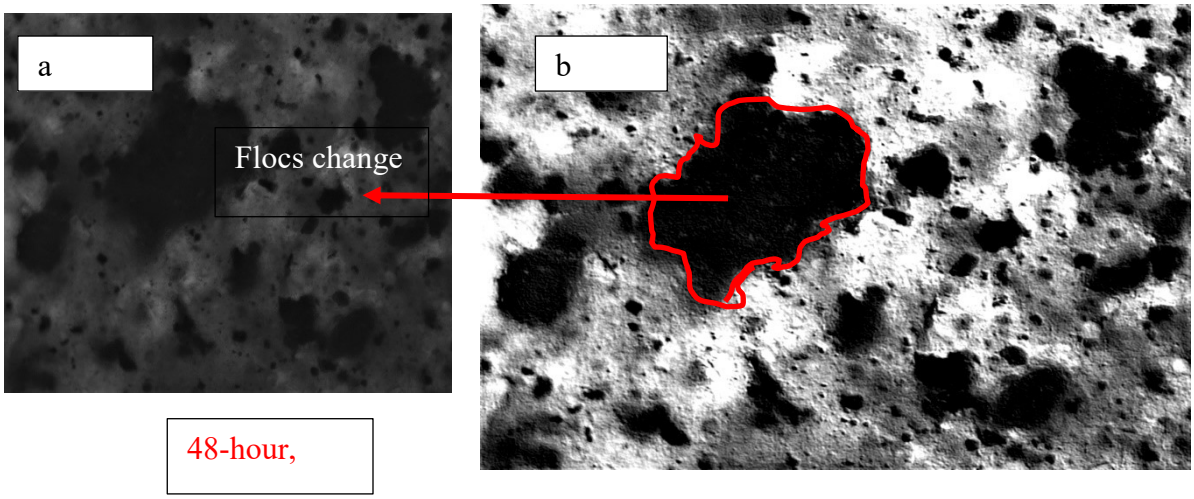

Figure 58: Image treatment result for Phase 4, 48 Hour Optical microscope Images (a) before and (b) after treatment black sections Flocs, White section background light source.

4.5.3.2 800 ppm results:

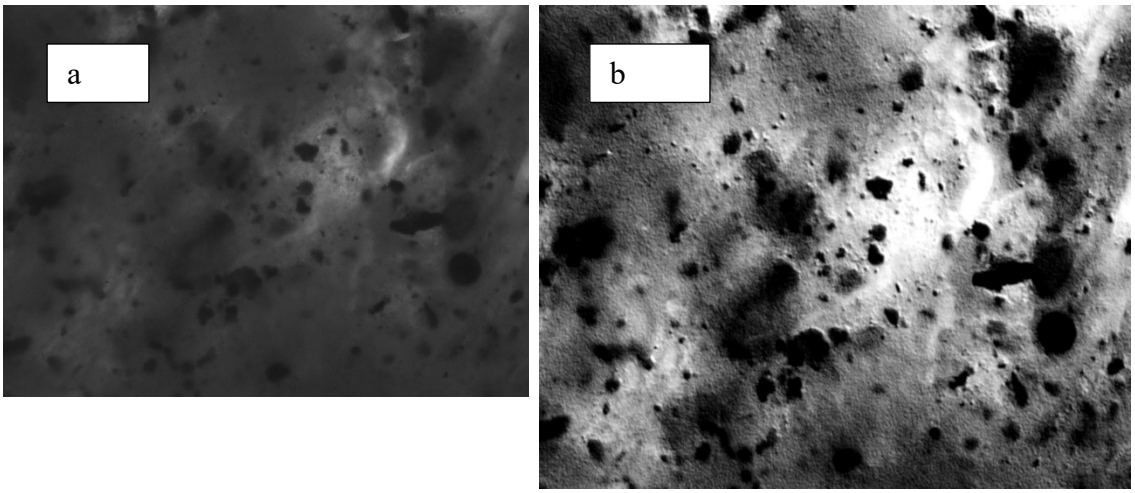

Figure 59: Image treatment result for Phase 4 dosed with 800 ppm polymer, 1 Hour Optical microscope Images (a) before and (b) after treatment black sections Flocs, White section background light source.

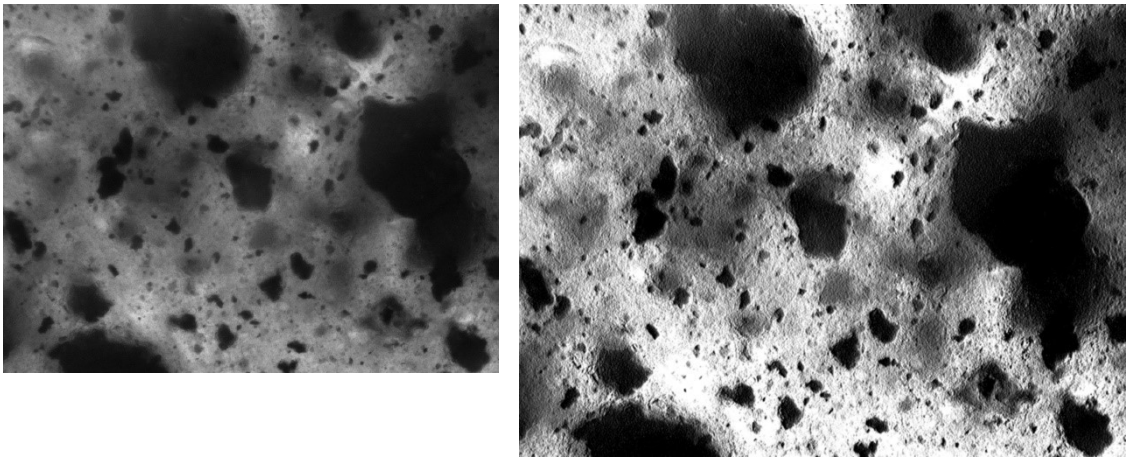

Figure 60: Image treatment result for Phase 4 dosed with 800 ppm polymer, 48 Hour Optical microscope Images (a) before and (b) after treatment black sections Flocs, White section background light source.

4.6 Segmentation

4.6.1 Introduction

Image segmentation is any operation that highlights or in some way separates two items from each other and therefore partitions the image into non-intersecting regions (Kaur et al 2014). The goal of segmentation is to simplify the image for quantitative analysis. These regions or segments consists of pixels that share a definite visual characteristic. Different ways of splitting or segmenting the images can be considered correct. Hundreds of automatic and semiautomatic algorithms have developed since digital image processing came into being. However, no method can be considered best for the all type of images (Carreras et. al, 2014). Most of the techniques are based only on the intensity information of pixel (Naphade 1999). In our study intensity, pixel-based segmentation was done to delineate pore space and solid particles.

4.6.2 Weka segmentation tool:

In this study, both SEM and OM images were segmented using the trainable weka segmentation tool available in ImageJ. This tool runs for both 2D and 3D images, to use it for 2D select the menu command *Plugins* ▶ *Segmentation* ▶ *Weka Segmentation*. For 3D features, call the plugin under *Plugins* ▶ *Segmentation* ▶ *Weka Segmentation 3D*. Both commands will use the same graphical user interface but offer different feature options in their settings (Ferreira and Rasband 2012). Images that had been processed for pixel improvement were opened in the weka segmentation tool.

The trainable weka segmentation developed by Arganda-Carreras et al., (2014) was used for analysis. The word “Trainable” means the plugin can be trained to learn from the user input and perform later the same task in unknown test data. The word “Weka” means that this tool is constantly updated by the community of users of the ImageJ software. This tool in “Fiji Image J” changes the segmentation process into pixel classification problem (Carrera’s et.al, 2014).

In this study, two different classifiers were made pores and grains as shown in Figure 61. Then each pixel in some subsection of the image was manually classified using tools for pixel selection that includes rectangular, oval, elliptical, brush polygon and freehand selection. This manual selection trains the automatic segmentation tool, which is then applied to the rest of the image. Figure 62 and Figure 63. give examples of SEM and OM images after segmentation, where each pixel in the image was classified into pore or grains. The classifier algorithm was trained according to the desire of author. The strength of this tool is that it allows the user to re-train as well as tests the classifier and change the pixel classification using toggle overlay tool in Image J until a satisfactory result is achieved.

Moreover, to avoid prejudice in segmentation for other images, the classifier trained for one set of Phase 2 SEM images single drainage was saved and reused for another SEM images phase 3 and phase 3.5. TWS (trainable weka segmentation) pipeline overview is shown as in Figure 65. After satisfactory training of classifier is done, get the probability, built-in in Weka segmentation was clicked.

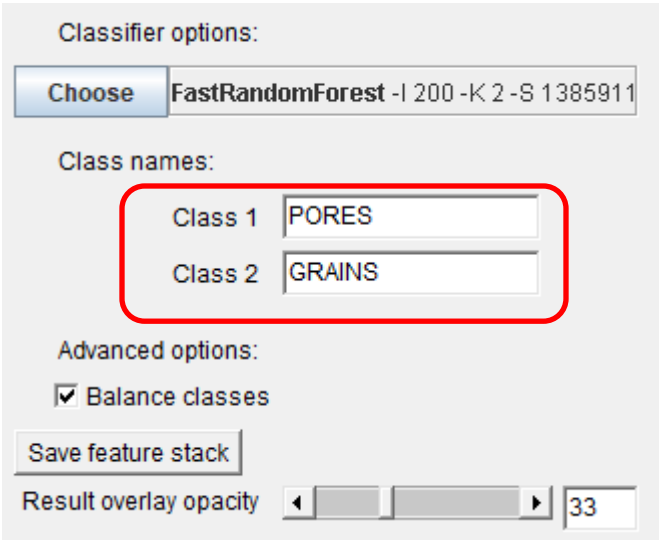

Figure 61: Adding of classifier before Training Segmentation.

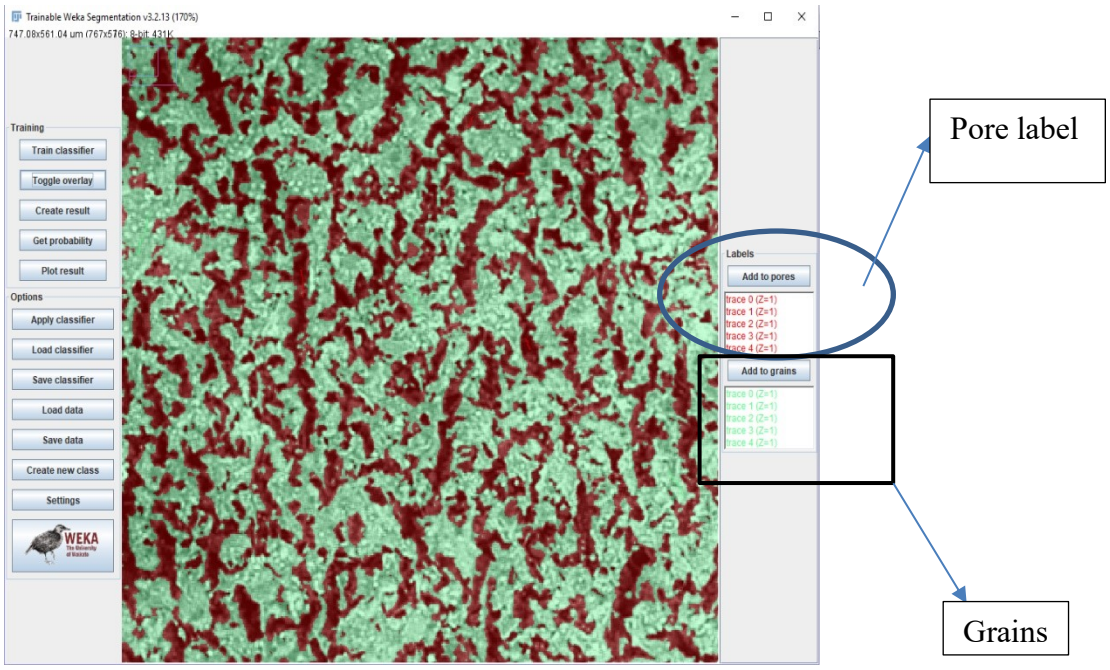

Figure 62: Trainable Segmentation tool for segmentation of images into pores and grains

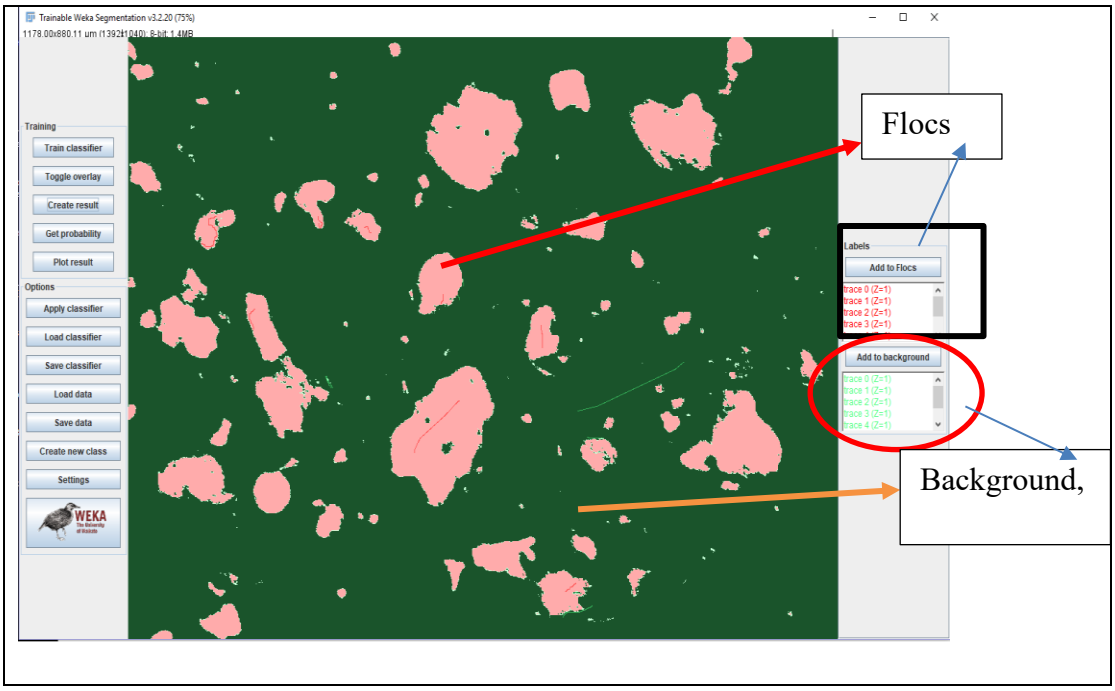

Figure 63: Optical Microscope Segmentation, (Pink shade) Flocs segmented from (green) background for further analysis.

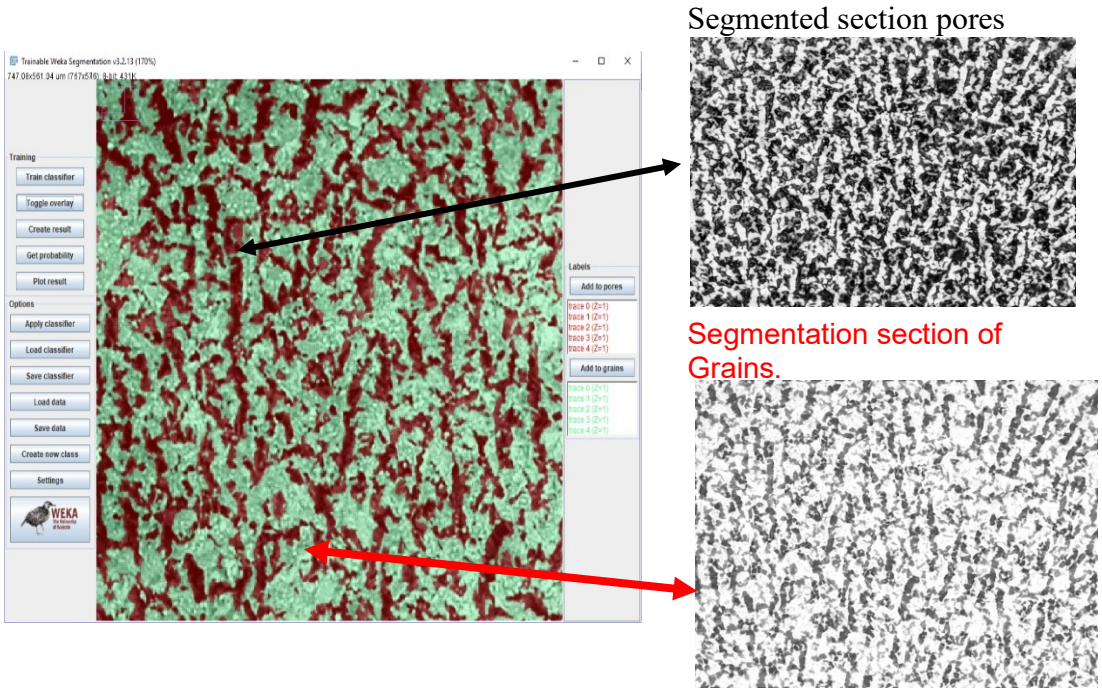

Figure 64 : Example of resulting probability map of pores and grains based on classifier

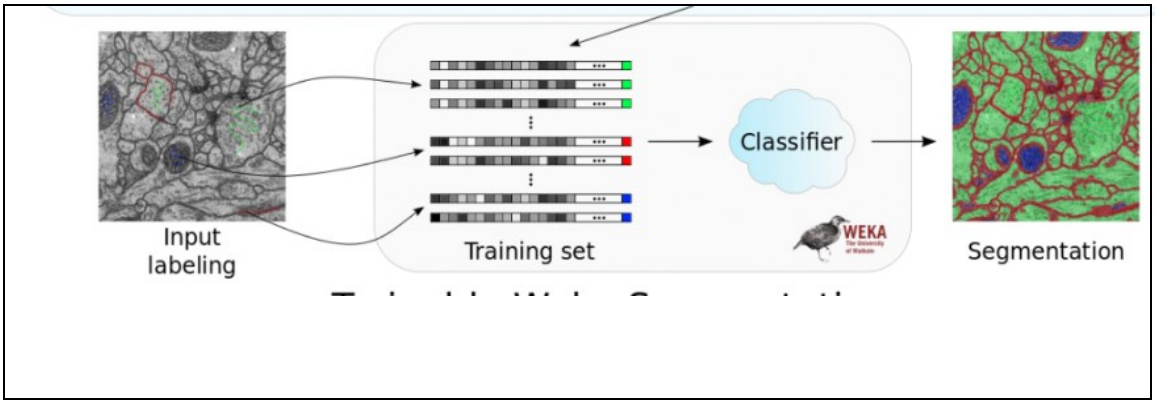

Figure 65 : Summarized TWS pipe line overview (Modified from Ferreira and Rasband 2012)

This process was repeated for phase 2, phase 3 and phase 4 images, each phase segmented images were thresholded in next step.

4.7 Image Thresholding:

Before binarization thresholding was performed as a final step to remove further unwanted (blurry regions) low frequencies, left after segmentation. Following the procedure developed in Mizani (2016), thresholding can be guided in an unbiased way by analyzing the rate of change of particle mass capture versus threshold. Mizani (2016) found that identifying a minimum in the rate of mass change function could be used to threshold in an unbiased way.

After thresholding each pixel, images were converted into perfect black and white by binarizing it. The segmented images were opened *in image j>adjust>threshold* or *CTRL + shift +t.* Increasing or decreasing the slide can do changes in image shape. By keeping the histogram value i.e. from 44% to 48.61% for thresholding gave us a better-segmented

image as low special frequency were converted Nan values (not a number) and removed later in binarization step. In this study, thresholding was specifically used to remove special frequencies left in the image by converting it into NaN.

Figure 68 and Figure 69 shows examples of thresholded images for different phase images, the same technique was applied to all other sample segmented SEM images and optical microscopic images. These images were forwarded into binarization section where each image pixel was converted into perfect black 0 or white 255 making them 1-bit Image ($2^1 = 2$). Thresholded images examples for other samples can be found in appendices B.

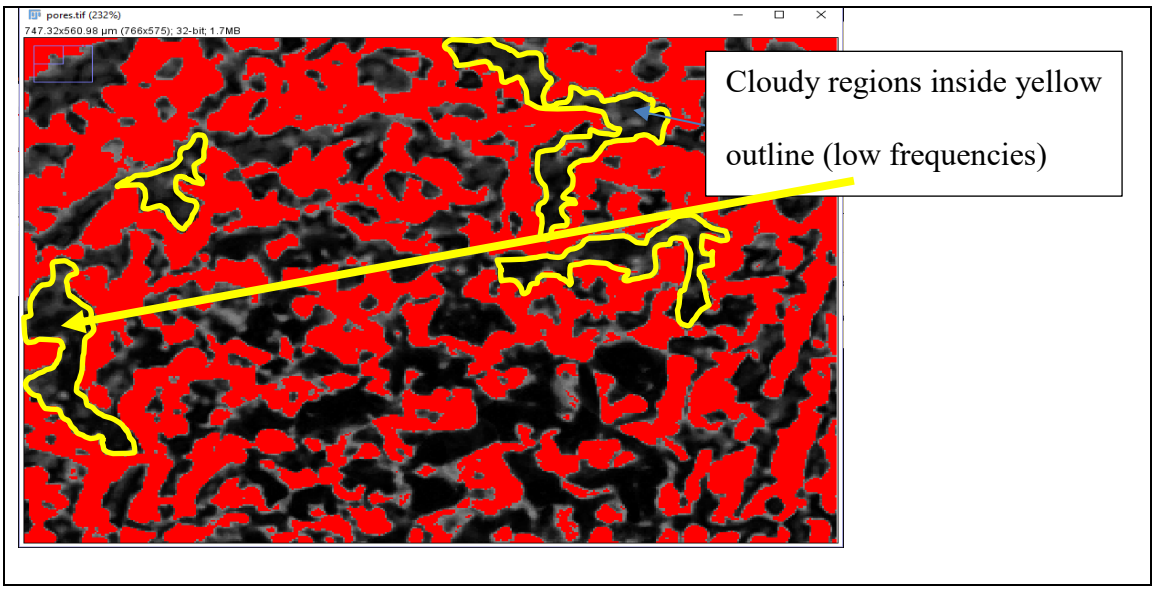

Figure 66: Blur or low frequencies in Probability image after segmentation

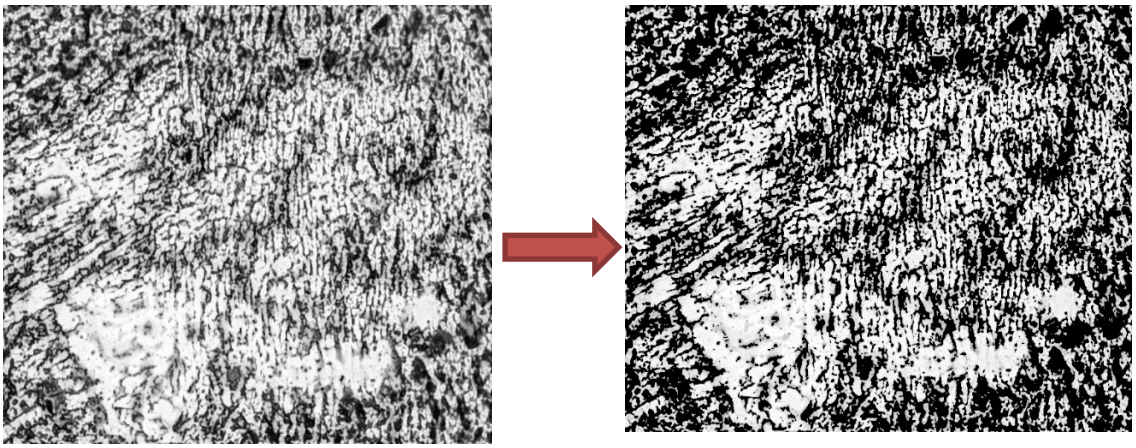

Probability Image (Image pixel values)

Thresholded (Image pixel values)

0.147032	0.175796	0.185146	0.165201
0.128614	0.173515	0.151014	0.155686
0.159424	0.176031	0.133176	0.135083
0.196453	0.172348	0.129531	0.143032
0.187663	0.142803	0.135000	0.120209
0.156388	0.150046	0.142482	0.115905
0.154561	0.137445	0.122854	0.099214

0.915585	0.926726	0.926820	0.789256	0.509846	NaN
0.905032	0.899155	0.823264	0.748429	0.574437	NaN
0.653652	0.716563	0.732304	0.691645	0.613298	0.468164
NaN	NaN	0.559365	0.661209	0.699223	0.736907
NaN	NaN	NaN	0.611052	0.765957	0.837567
NaN	NaN	NaN	0.550753	0.794940	0.913496
NaN	NaN	NaN	0.597402	0.834623	0.918346

Figure 67: Conversion of (a) Probability image before thresholding and (b) after successful operation of thresholding (removal of blurry regions) and converting background to (not a number) NaN in phase 2, 7 day (Segmented Image of pores) dosed with 600 ppm polymer.

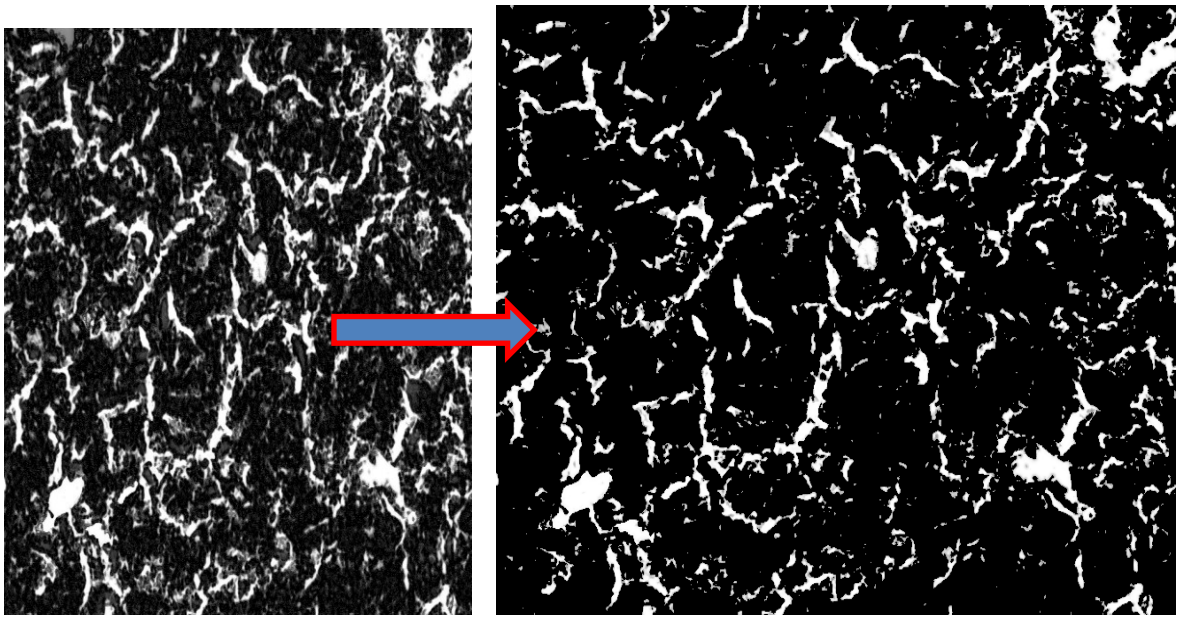

(a) (b)

Figure 68 Conversion of (a) Probability image before thresholding and (b) after successful operation of thresholding (removal of blurry regions) to phase 3, 21 day (Segmented Image of pores) dosed with 800 ppm polymer.

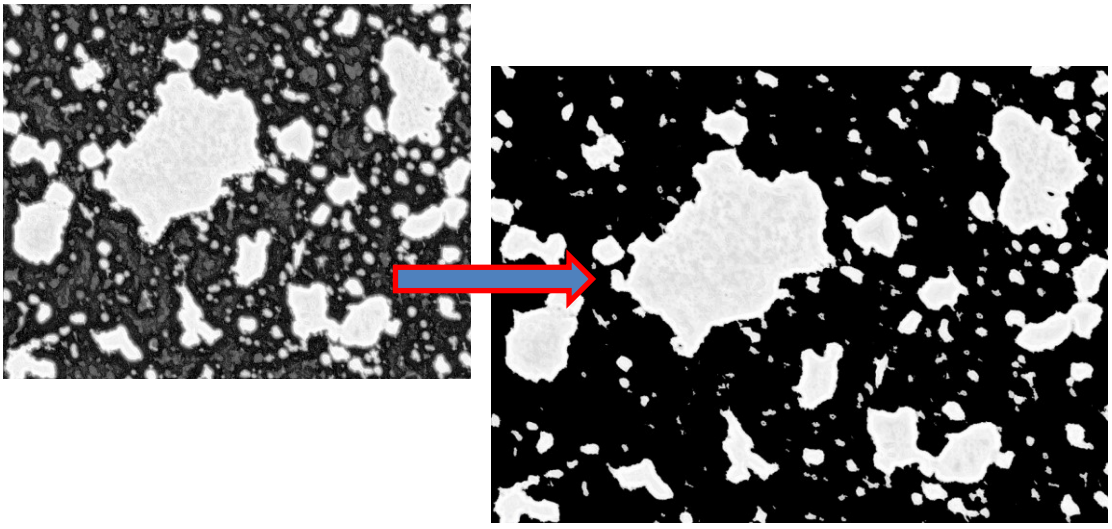

Figure 69: Optical Microscope Conversion Results, (a) Probability image before, and (b) after successful operation of thresholding (removal of blurry regions) to Phase 4, 48-day Flocs dosed with 600 ppm polymer.

4.8 Binarization step.

The final step in the process was to convert our segmented and thresholded image into a 1-bit image so that each of the pixels in the image gets a specific value which can later be used to analyze an image. By applying this tool our thresholded images were divided into foreground white, and background as black. This tool must be used when the *images>adjust>threshold (means when an image is thresholded)* tool is active. Images were converted into 1-bit binary by clicking *process>binary>make binary in* image j software.

Simple images obtained from SEM, optical microscope for different boundary conditions illustrated in Chapter 3 were finally binarized. Above procedure from section 4.5 till 4.6 were practiced on each day sample to get the 1-bit image.

After binarization, the segmented sections of pores and grains were used for quantitative analysis. The corresponding ImageJ path is *Analyze> analyze particles in* Figure 70 till Figure 77 show examples of the binary results obtained after image processing.

4.9 Phase 2 binarized Images:

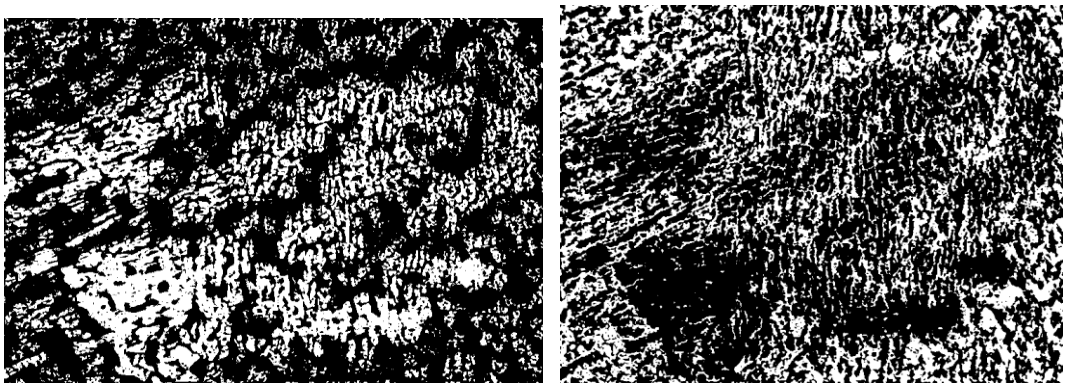

(a) (b

Figure 70 Final Binarized (a) Pore Structure Image of 7-day SEM Image (600ppm dosed Phase 2). (b) binarized Image of Grains.

Pixel Values

Prefs	465	466	467	468	469	470	471
280	255	255	255	255	255	255	255
281	255	255	255	255	255	255	255
282	0	0	0	255	255	255	255
283	0	0	0	0	255	255	255
284	0	0	0	0	0	255	255
285	0	0	0	0	0	0	0
286	0	0	0	0	0	0	0

Pixel Values

Prefs	459	460	461	462	463	464	465
274	255	255	255	255	255	255	255
275	255	255	255	255	255	255	255
276	0	255	255	255	255	255	255
277	0	0	255	255	255	255	255
278	0	0	255	255	255	255	255
279	0	0	0	255	255	255	255
280	0	0	0	0	255	255	255

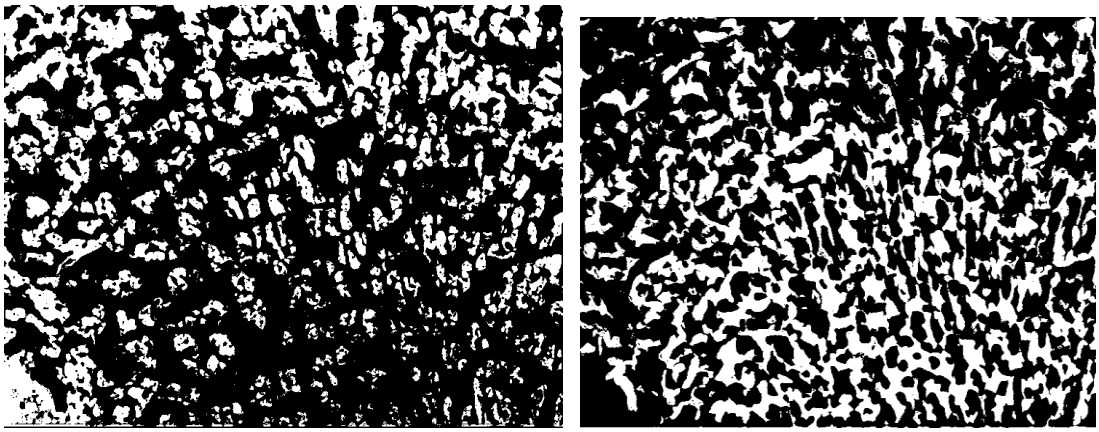

(a) **(b)**

Figure 71 Final Binarized Pore Structure Image After 72-day SEM Image (600ppm dosed Phase 2) (b) binarized Grains Image

4.10 Phase 3 binarized images

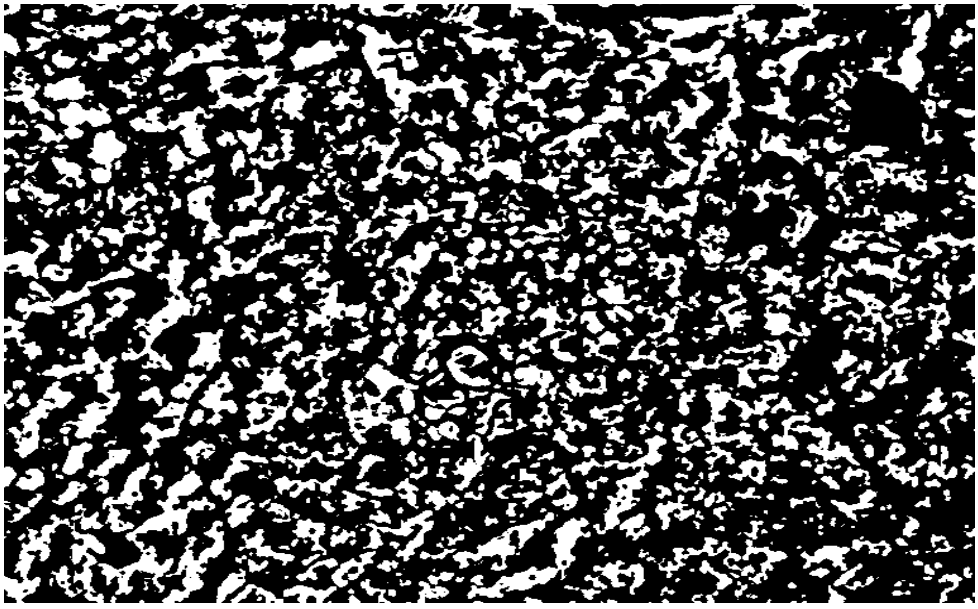

Figure 72:Final Binarized Pore Structure Image After 7-day, SEM Image (800ppm dosed).

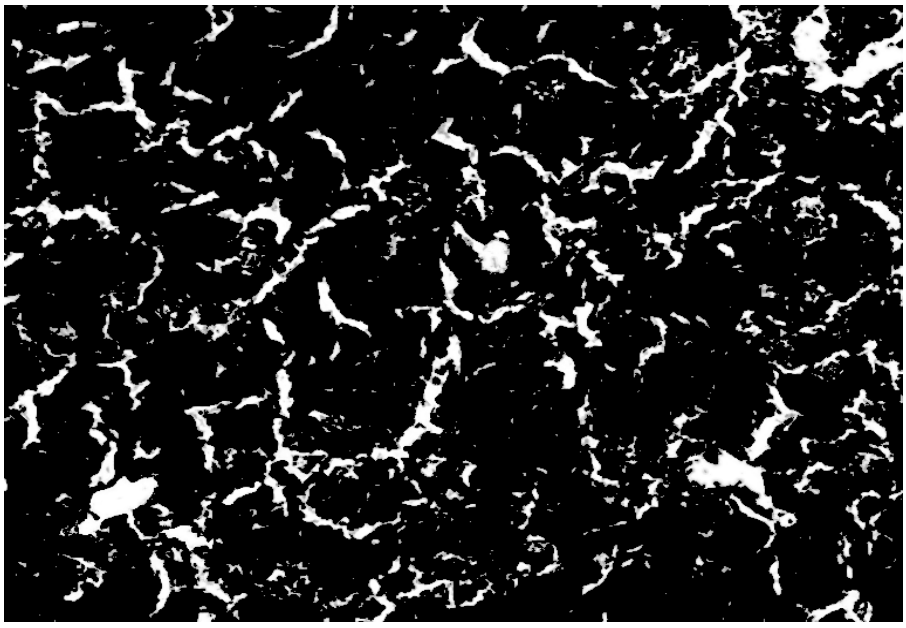

Figure 73 :Final Binarized Pore Structure Image After 21-day, SEM Image (800ppm dosed).

4.11 Phase 4 Optical microscope binarized images Results:

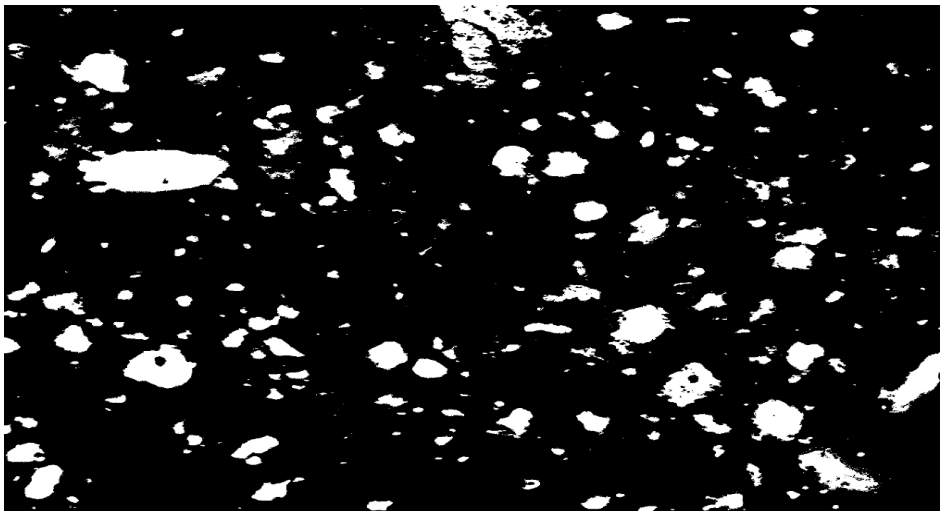

Figure 74 :O.M Final Binarized flocs Structure Image After 1-hour mixing (600ppm dosed).

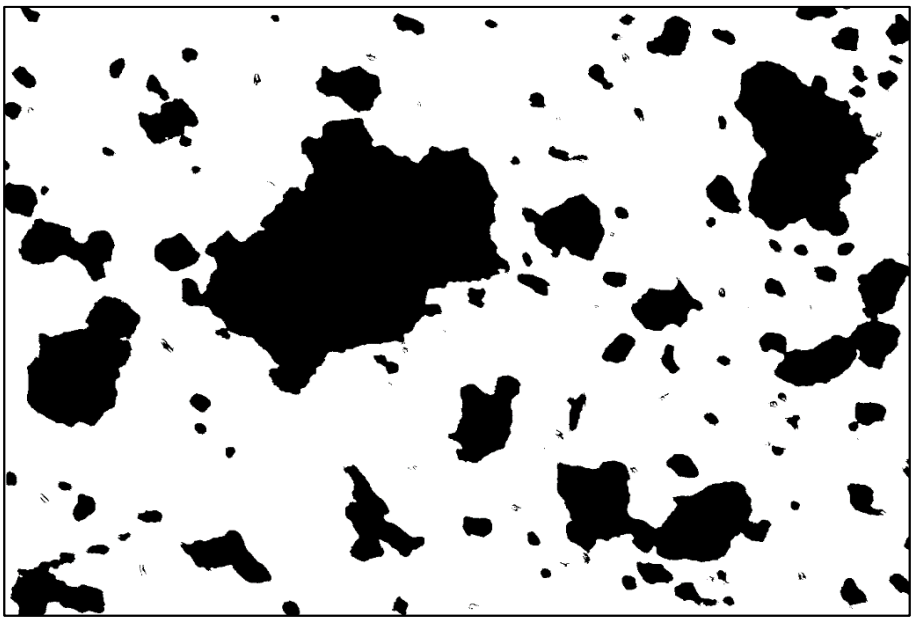

Figure 75:O.M Final Binarized flocs Structure Image After 48-hour mixing (600ppm dosed)

Figure 76; O.M Final Binarized flocs Structure Image After1 hour mixing (800ppm dosed).

Figure 77 :; O.M Final Binarized flocs Structure Image After 48-hour mixing (800ppm dosed)

4.12 Use of particle (Pore/Grain) analyzer in ImageJ:

Binarized Images were analyzed using the particle analyzer section built into the Image J software. The analysis was performed on the entire image, not on the specific area selected in Image as reported in (Bajwa 2015) and (Mizani 2016). This tool scans the entire selected image or choice until it finds the edge of objects. This command counts and measures the objects in a binary image, outline the objects using wand tool (creates a selection by tracing objects of uniform color or thresholded objects) (Ferreira and Rasband, 2012), and measures all entries in the images.

The particle analyzer extracts the features by size range and by shape (circularity). While circularity values of 1 correspond to a perfect circle, the circularity of zero stands for the infinitely elongated polygon in the image J. The software also summarized the particle analysis reporting particle count, total particle area, average particle size and area of the simulated pores. The pore diameter was then calculated based on the area and frequency of the pores in certain bin ranges. The porosity was calculated for each image on classified bins and pore diameters.

4.13 Conclusion:

The goal of this process was to convert our images from 8 bit (256 colors per pixel) throughout to 1-bit, perfect black 0 or perfect white 255 images so that software can examine the binary data.

During analysis first images pixel intensity was increased and then equalized by applying tools mentioned above. Afterward, through pixel analysis tool it can be noted clearly with each step the pixel values were changing from a contrasted image, till thresholding. And in thresholded image background was converted into NAN and finally only selected region for analysis were binarized by creating the 1-bit image (perfect back and perfect white). The steps applied above were successful in first optimizing the SEM images and optical microscope images pixel intensities for pixel classification analysis and converting images into perfect binary images without affecting shape or size of pores or grains. It was also noted that thresholding can be useful in removing blurry regions in images and was kept

between 45 to 50% for rest of analysis. The whole chapter methodology process is also concluded in the workflow diagram illustrated in Figure 78: Workflow diagram for the Image Processing and Quantitative Analysis. This flow diagram procedure designed by the author was helpful in abstracting the image features using digital image processing software Image J.

Figure 78: Workflow diagram for the Image Processing and Quantitative Analysis.

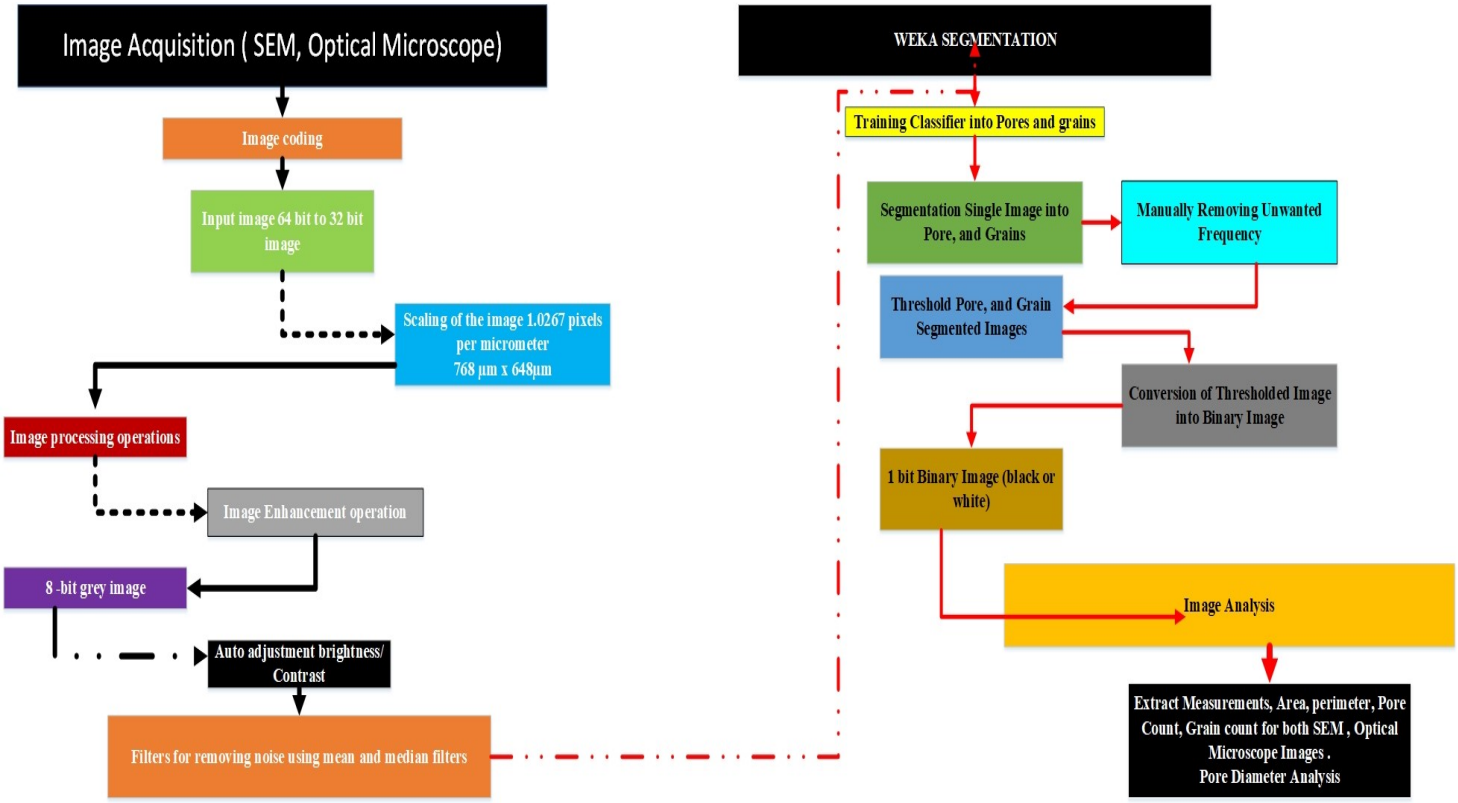

5 Chapter: **Results and Discussion:**

This chapter reports on the quantitative data analysis performed on the processed SEM and OM images. The image processing methodology is presented in Chapter 4. Each image was analyzed using built-in algorithms in the "FIJI Image J" software to obtain the following parameters:

(1) Total number of pores and grains with time.

(2) Total image porosity with time

(3) Pore diameter histogram.

(4) Change in the cumulative average grain or floc size change.

Results are initially reported for the different experimental conditions and then compared at the end of the section corresponding to the different imaging methods (SEM or OM).

5.1 SEM results

5.1.2 Phase 2: Columns with single drainage and 600 ppm polymer dose

SEM images were obtained from 7 to 72-days old samples as illustrated in Figure 79 to Figure 80. The calculated image porosity is shown in Figure 82 for 3 replicate images at each time. The image porosity showed a declining trend from about 28-34% to 22-23%, whereas the laboratory (real) porosity of the samples changed from (0.83 to 0.70) 83% to 70% over the same time frame as illustrated in Figure 83. The average pore area was also

calculated from each image and it showed a decreasing trend up to 56 days, however, the average pore area increased after 72 days in Figure 84. Note that the porosity of any image of granular media is always substantially reduced compared to the 3D porosity (Marcelino. et al. 2007). These all results show a decreasing number but increasing average size of pores and grains with time. This decline in pore number can be attributed to the growth of flocs during flocculation and or -squishing of the flocs together. Figure 86 and Figure 87 shows a more detailed analysis of pore sizes distribution and illustrated that most changes are dominated by changes in the lowest of sizes (<10 microns). Figure 79 shows examples of SEM images at 7 and 28 days that seem to reflect the observed trend of decreasing the frequency of the smallest pores and grains as suggested by the quantitative analysis of the binary images produced.

In Figure 85, the grain analysis showed a decrease in the total number of grains, though most of the change occurred before 14 days. This more closely follows the trends in the smallest pores Figure 87.

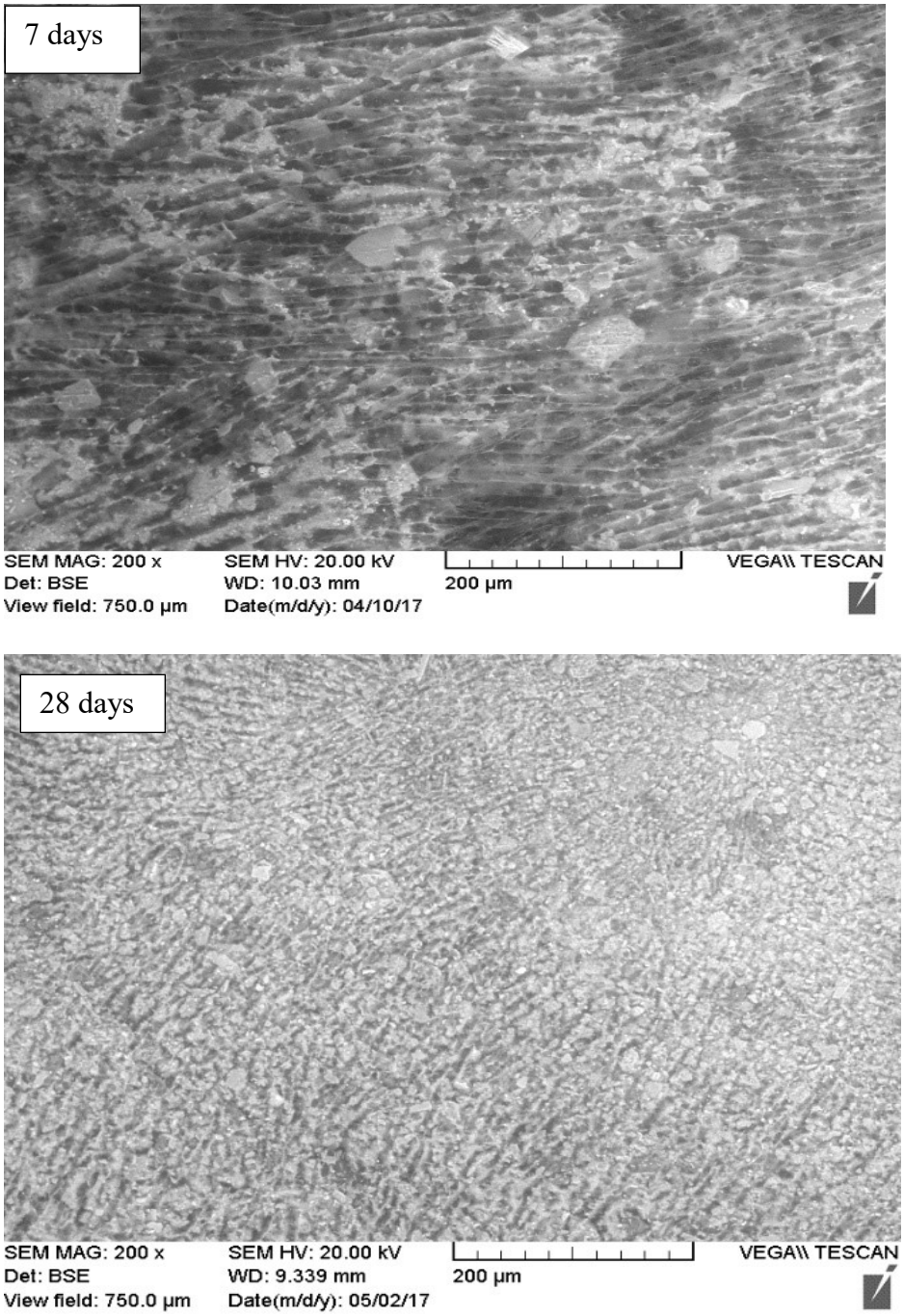

Figure 79: 2nd set of images used for Quantitative image analysis

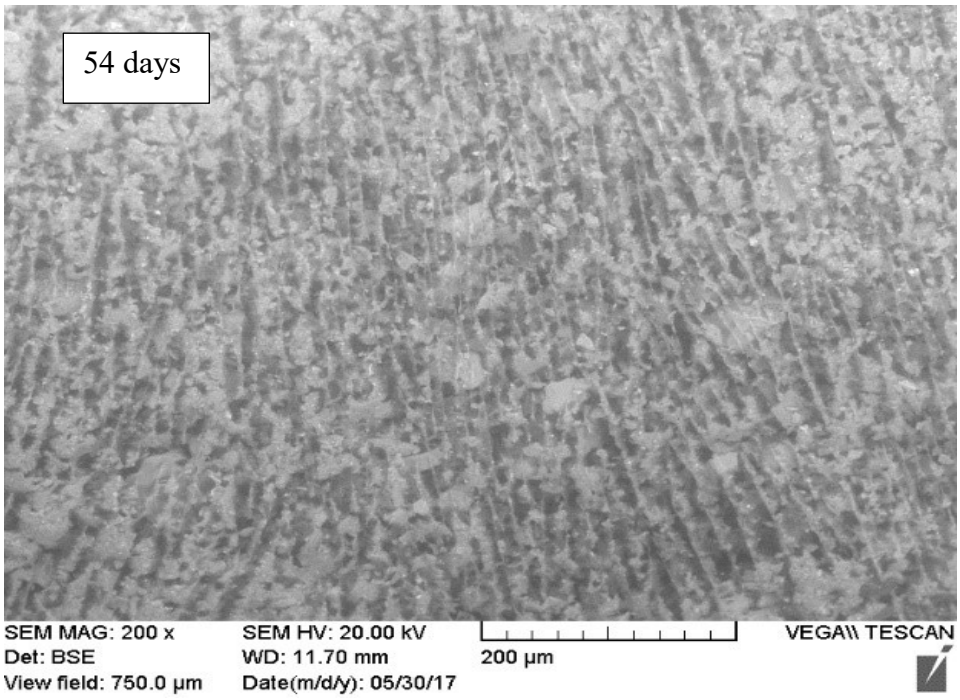

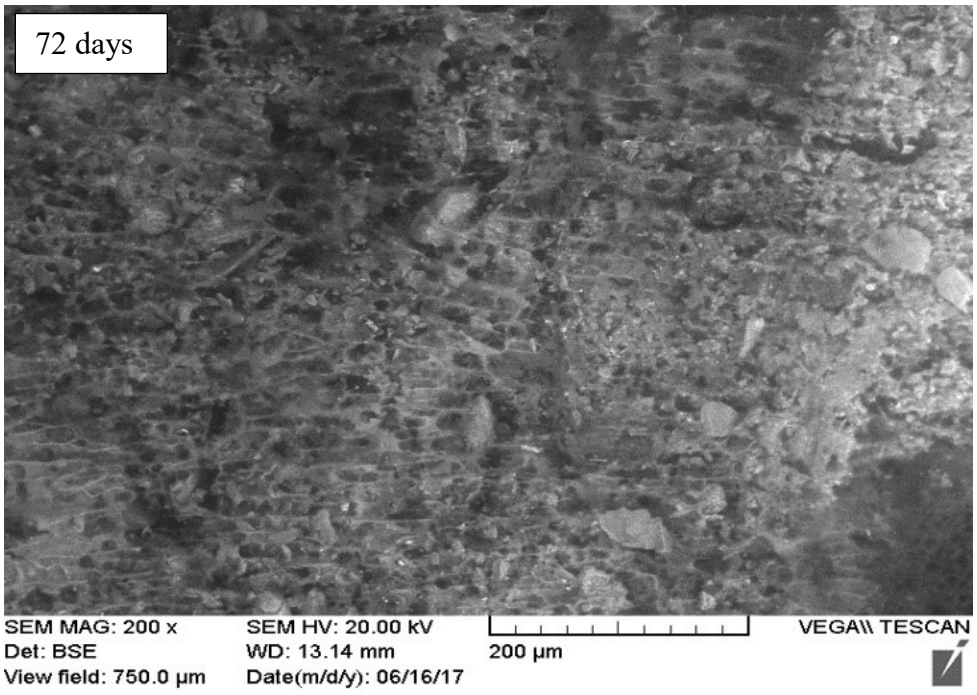

Figure 80: 2nd set of phases 2 images used for quantitative analysis of 600 ppm single drainage

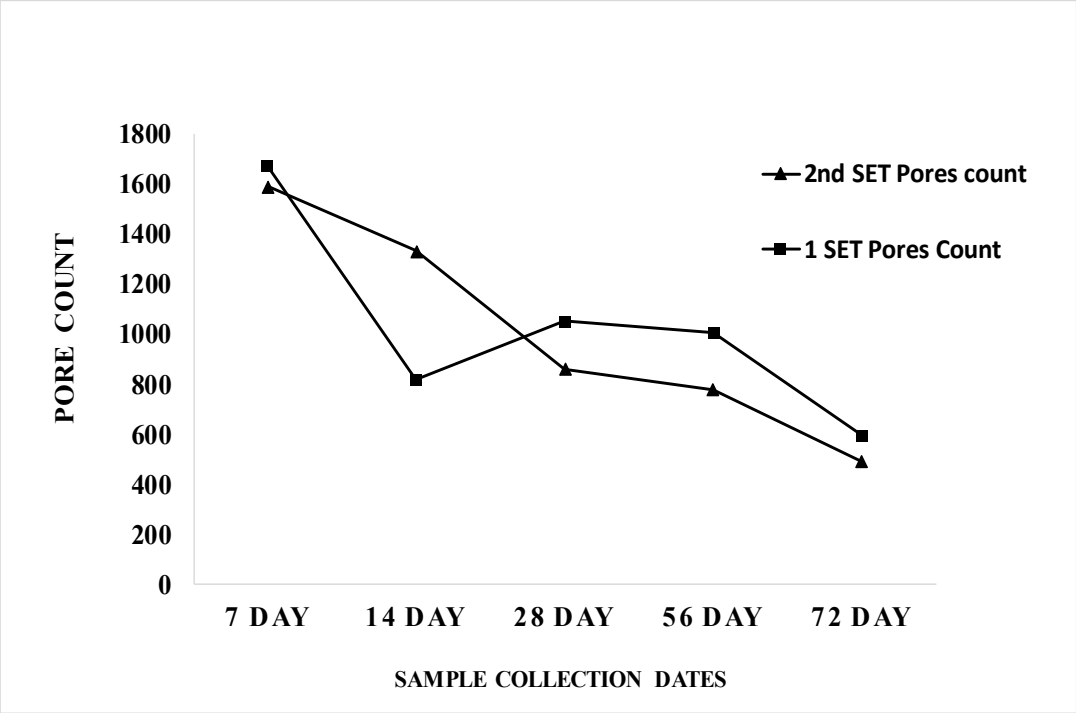

Figure 81:: Total Number of Pore Count for 600 ppm single drainage images

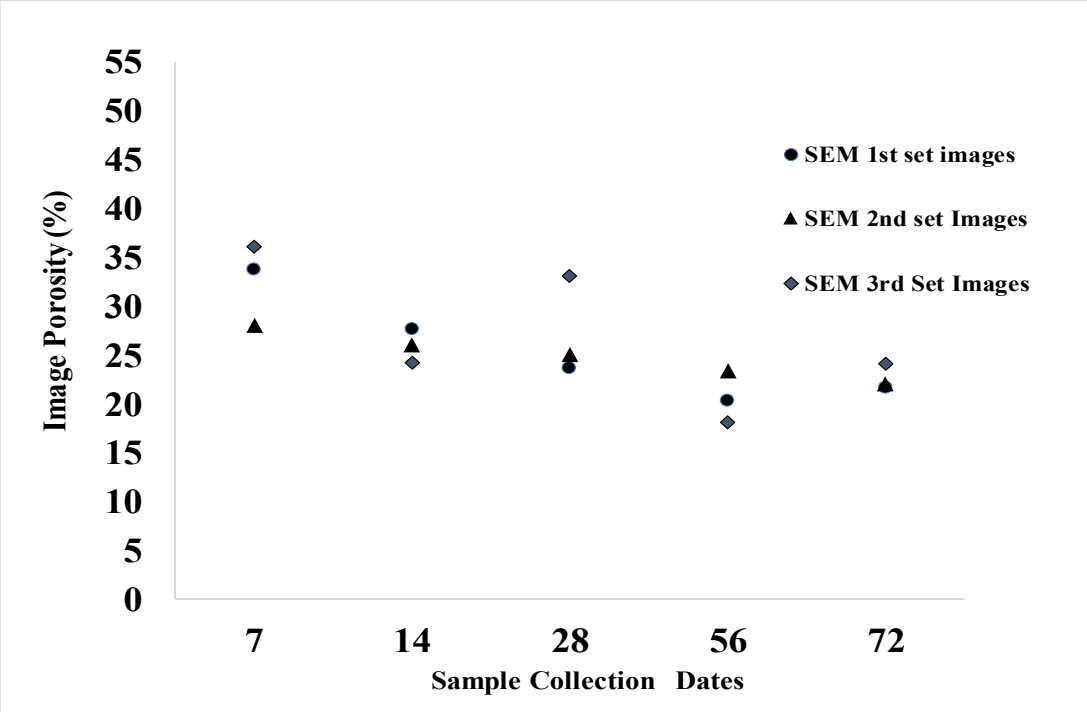

Figure 82: Image porosity trends in SEM 600 ppm single drainage for 3 different set of images

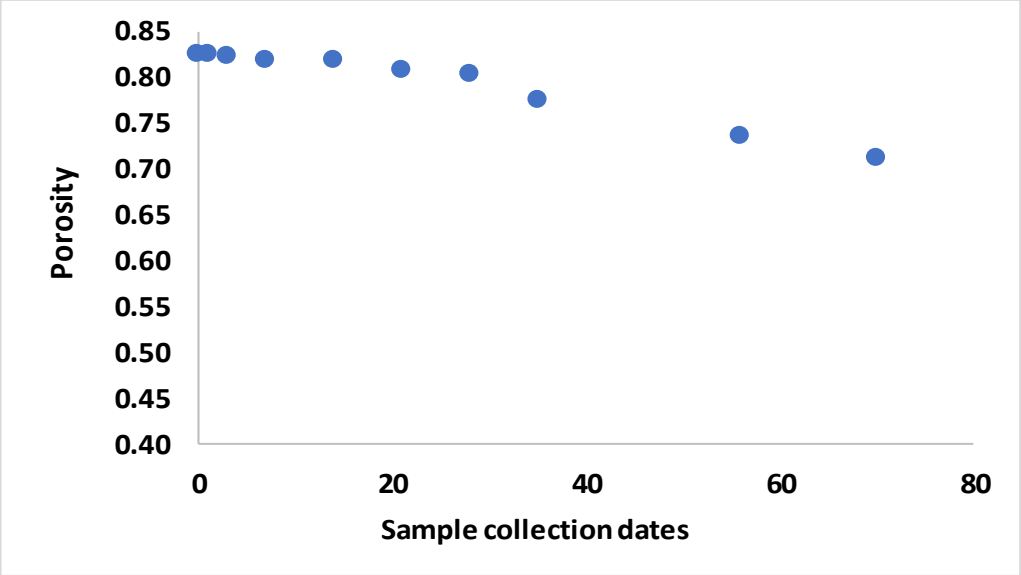

Figure 83:Laboratory Sample Porosity calculations using sample void ratio from top 1 cm of each column, 600 ppm single drainage (Salam 2018)

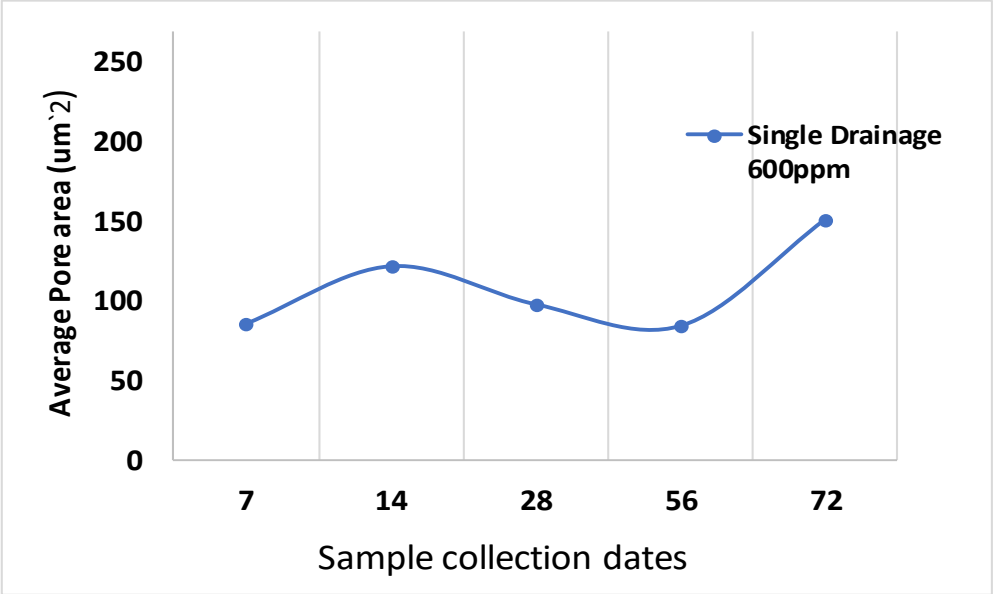

Figure 84: Average Area of pores in the single drainage 600 ppm images

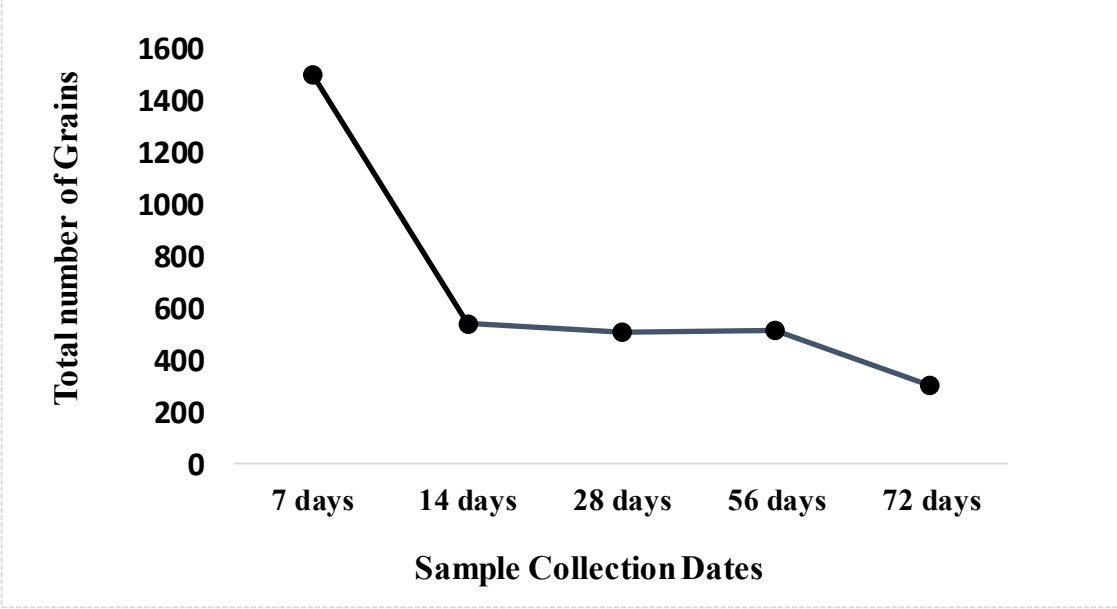

Figure 85: Total number of Grains calculations for 600ppm SEM single drainage images.

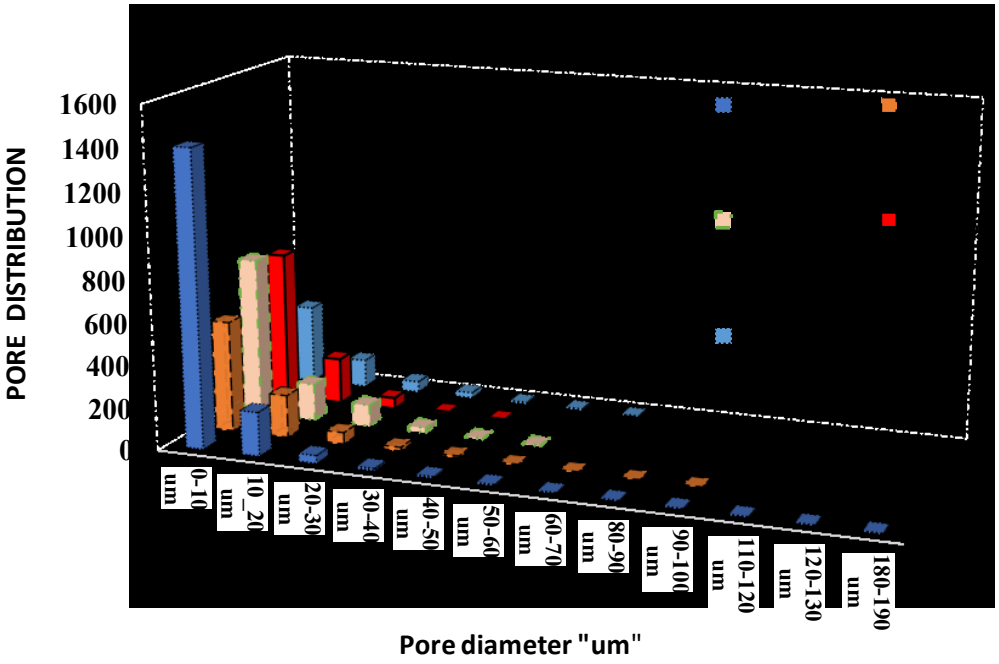

Figure 86:Pore diameter histogram from SEM 600 ppm single drainage

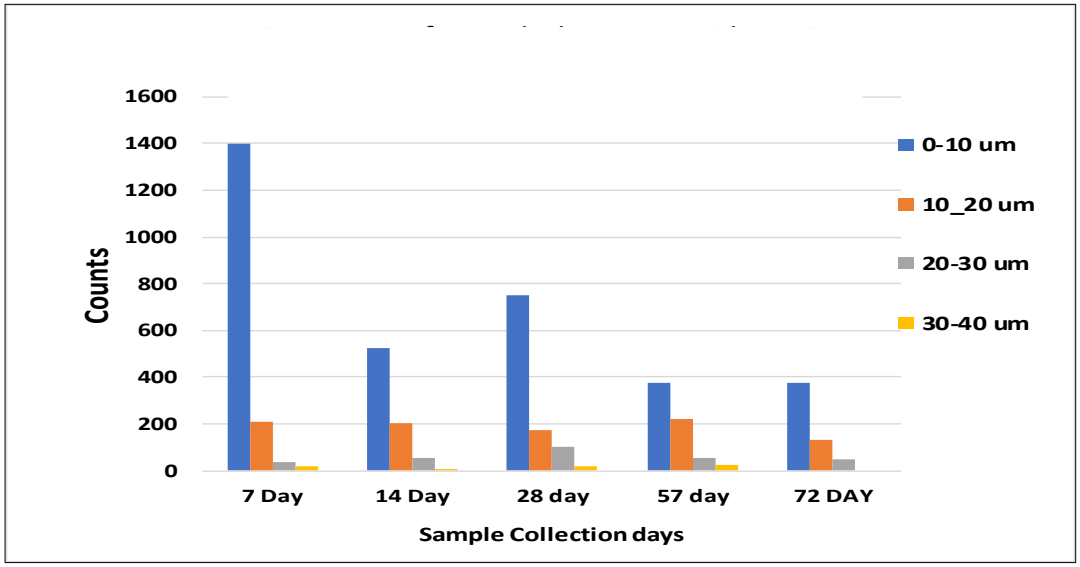

Figure 87 :Pore count from 0-40 um SEM for 600 ppm single drainage

5.2 Phase 3, Double Drainage with 600 ppm dose

SEM images for this case from 7 to 35 days are shown from Figure 88 to Figure 91. The total number of pores are shown in Figure 93. The porosity of the images was rapidly reduced compared to the single drainage cases, as shown in Figure 92. The Phase 3, 1day SEM images porosity was 29-32 %, which was nearly equal to that of the 7-day phase 2 image porosity. However, after 35 days, the porosity of the images decreased to almost 4%.

As shown in Figure 94, the average area of pores for a 1-day image was found to be between 118 to 121 μm^2. By 35 days it gradually decreased to almost 26-30 μm^2. Another set of images result was showing the same trend as in the first set of images. The real lab sample porosity was also calculated using void ratio, the porosity was changed from (0.82) 82% to (0.51)51% in only 35 days as illustrated in Figure 95.

Total Grain count was done for each set of images as illustrated in Figure 96. Interestingly, for double drainage, the total number of grains showed an increasing trend. To confirm this trend, two methods of grain count built-in in the software were used (1) Watershed tool and (2) Simple particle analysis tool both were employed.

The watershed tool uses the gradient in pixel intensity to separate particles, like how the change in gradients in topography are used to define real watersheds. The watershed tool was used with the default parameters in Image J and was only used to check the trend

shown by the simple particle analysis for grains was true or not. Even though both tools use different methods to count grains, however, both showed an increasing trend in grain frequency with time. This total Grain count trend was noted opposite to what was observed for the 600-ppm single drainage case for total grain count.

In addition, the average grain area(size) in image was also calculated for both methods and average area (size) values were different for both procedures, however, after increasing till 21 days there was unexpected fall in the average grain area (size), reason for this is discussed in comparison section 5.1 both watershed and without watershed tool used showed decreasing trend as shown in Figure 97. .

More detailed PSD histogram of Phase 3 (double drainage) was compared with Phase 2 (no drainage) histogram. The double drainage histogram illustrated in Figure 98 reported that pore size between 0-10µm showed a decreasing trend in pore count from 1 day to 35 days. The overall trend in pore count was the same for both phases (decrease from 1400 to 1600 on Day 1 down to about 600 by the end of the test) however, reaching this number took only 35 days in double drainage while 72 days in single drainage Phase 2 test.

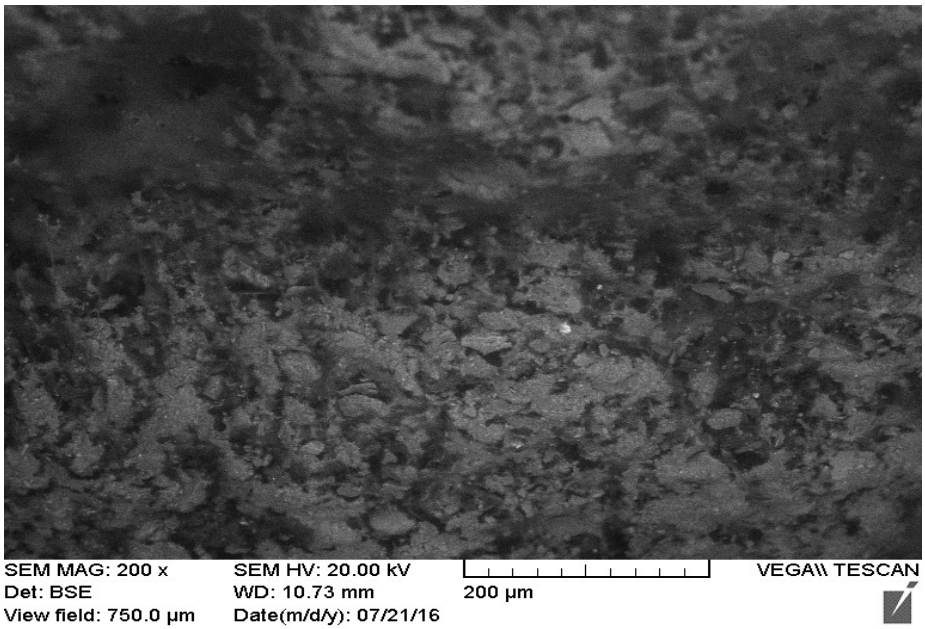

Figure 88: Scanning Electron Micrograph of polymer amended Oil sands tailings for dose of 600ppm, (After 1 day – of Polymer Mixing, Boundary Condition "Double drainage") Magnification 200x, view field 750

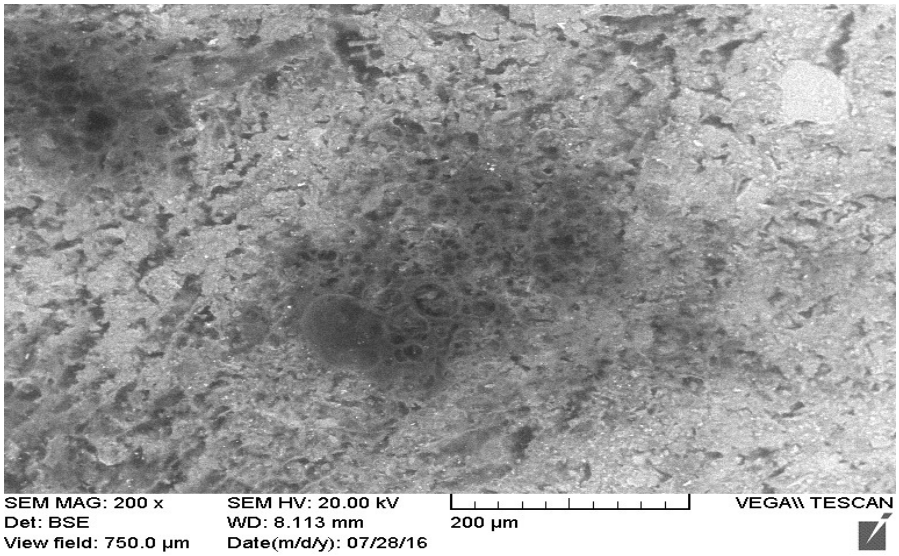

Figure 89: Scanning Electron Micrograph of polymer amended Oil sands tailings for dose of 600ppm, (After 7 day – of Polymer Mixing, Boundary Condition "Double drainage") Magnification 200x, view field 750.

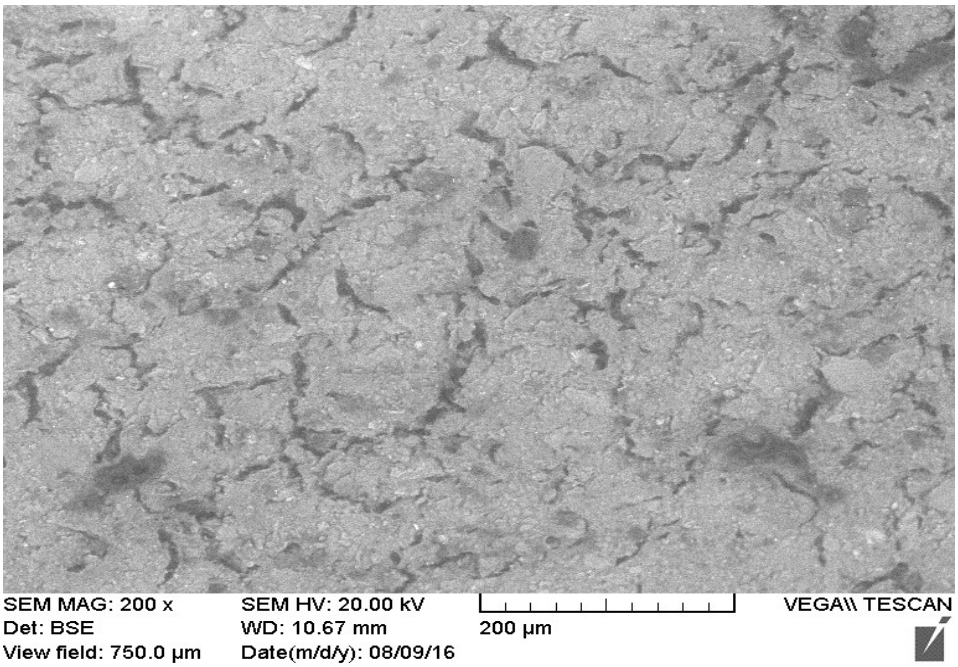

Figure 90 :Scanning Electron Micrograph of polymer amended Oil sands tailings for dose of 600ppm, (After 21 day – of Polymer Mixing, Boundary Condition "Double drainage") Magnification 200x, view field 750

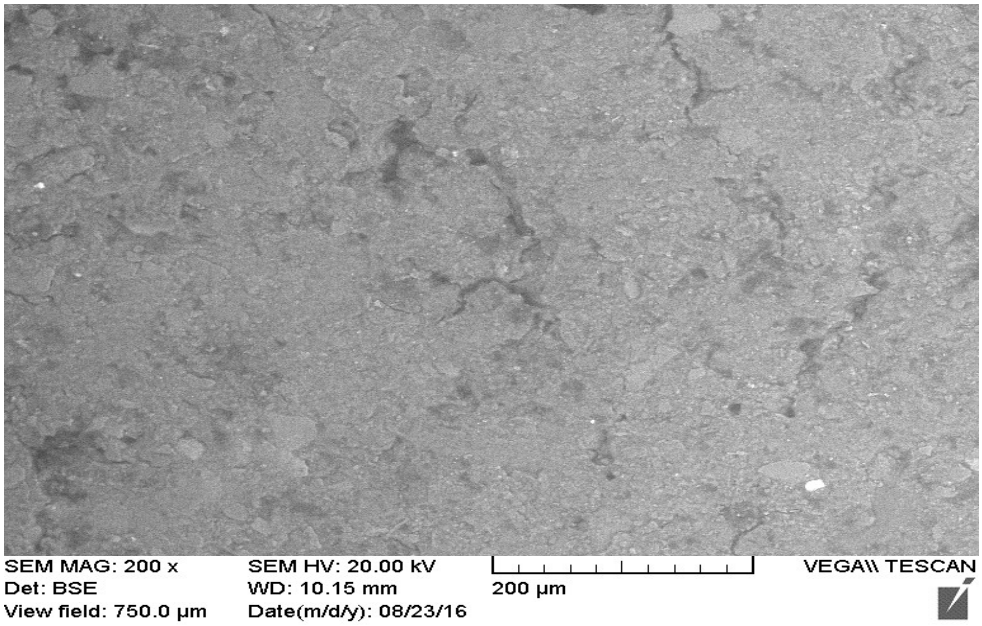

Figure 91: Scanning Electron Micrograph of polymer amended Oil sands tailings for dose of 600ppm, (After 35 day – of Polymer Mixing, Boundary Condition "Double drainage") Magnification 200x, view field 750/

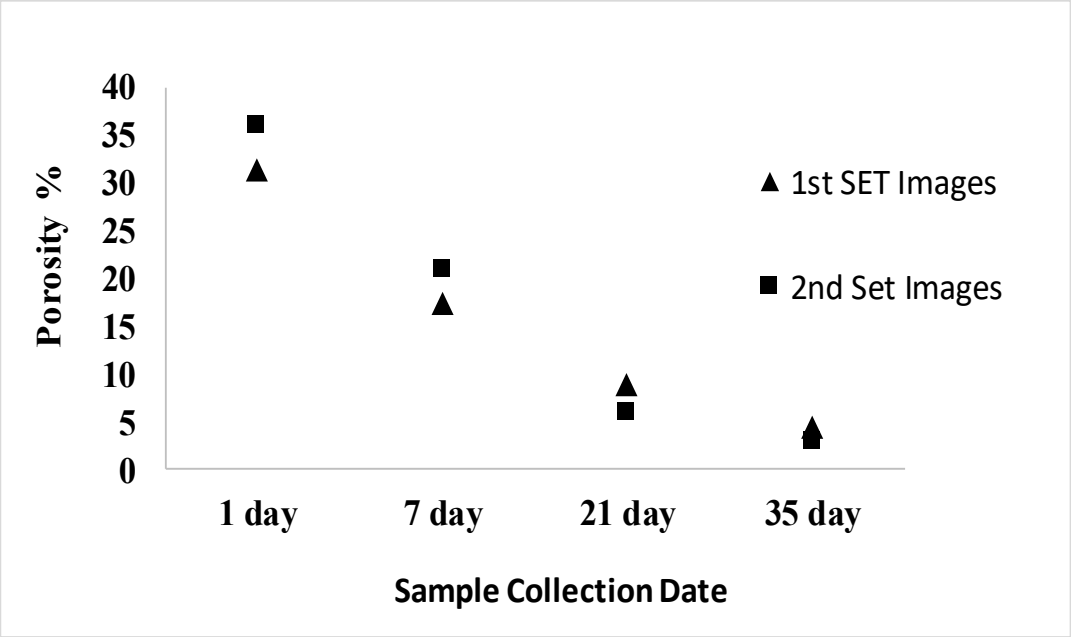

Figure 92: Porosity calculation for SEM Images dosed 600 ppm (double drainage)

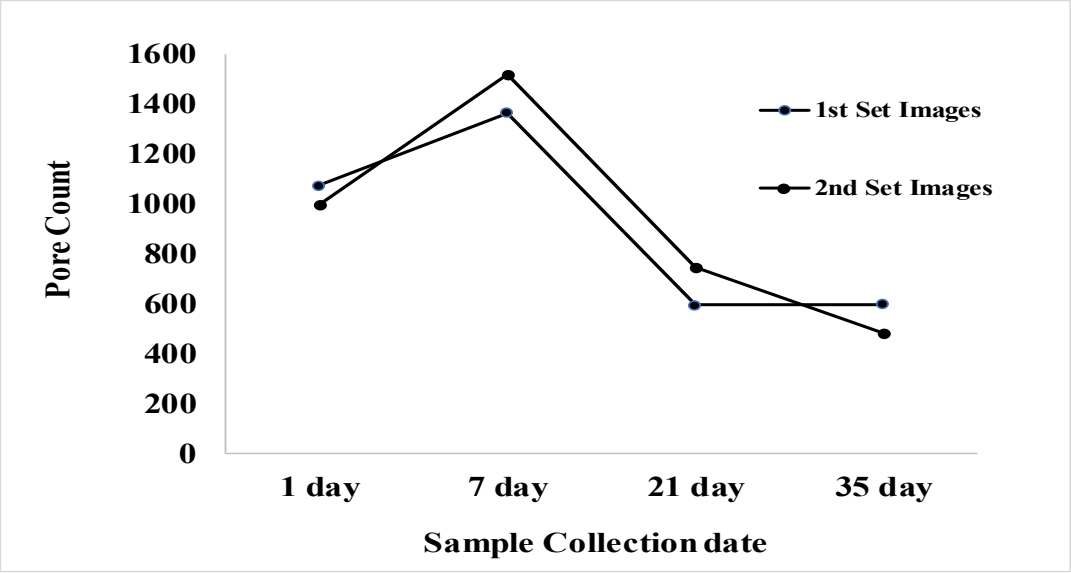

Figure 93: Total Pore number for double drainage columns (600ppm dose)

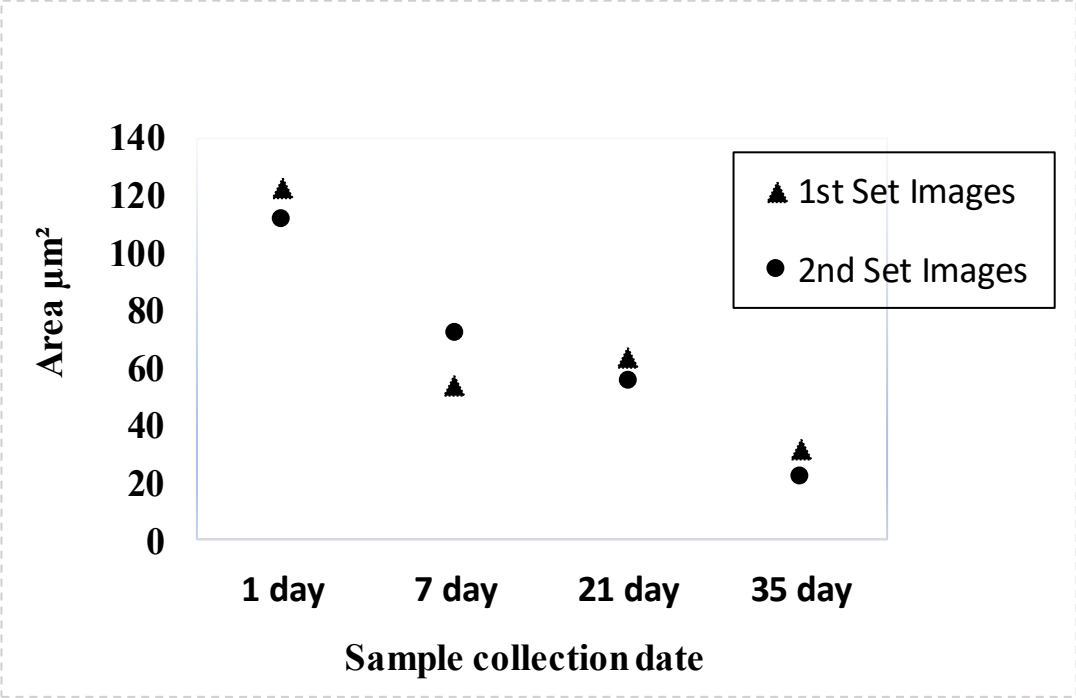

Figure 94: Calculated, Average Pore area in SEM images (dosed 600ppm, double drainage)

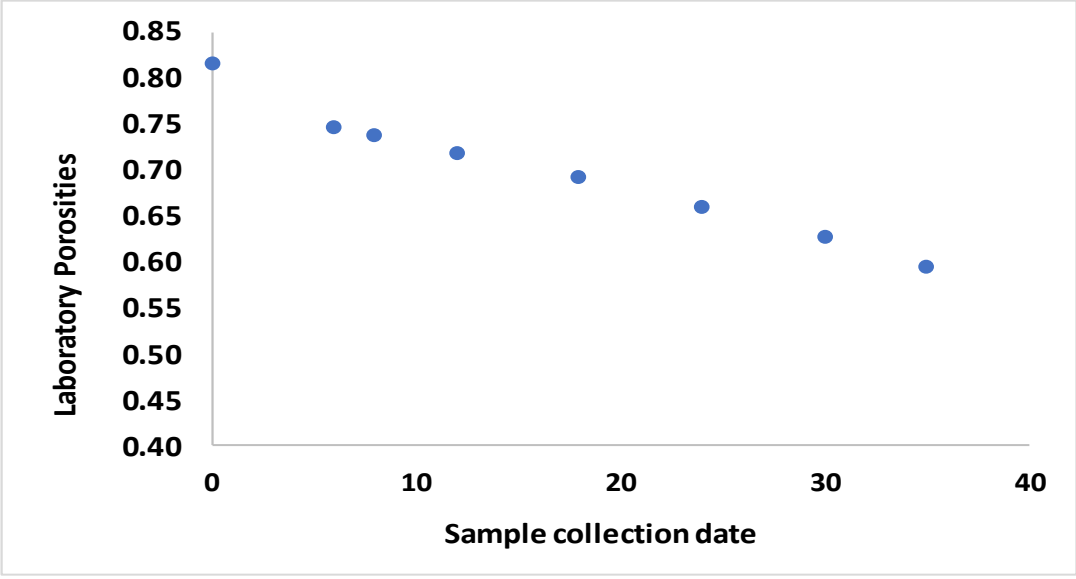

Figure 95: Laboratory Porosities Calculations for double drainage samples dosed 600 ppm (Salam 2018).

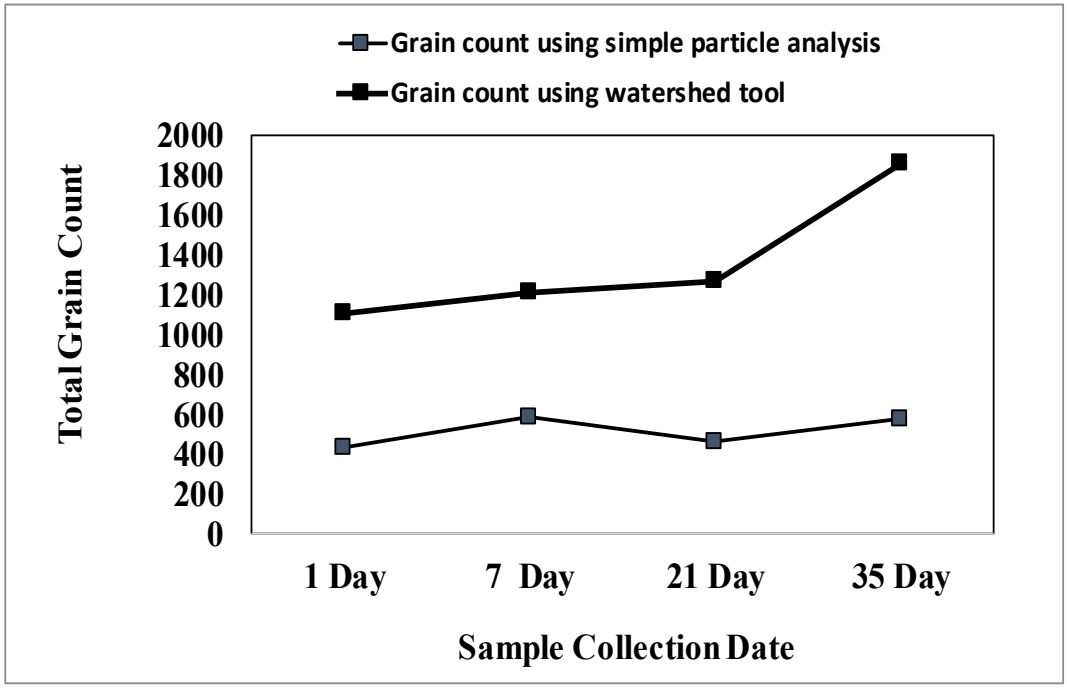

Figure 96:Grain count trend using Simple particle analysis and Particle analysis after watershed (Phase 3 Double Drainage 600ppm).

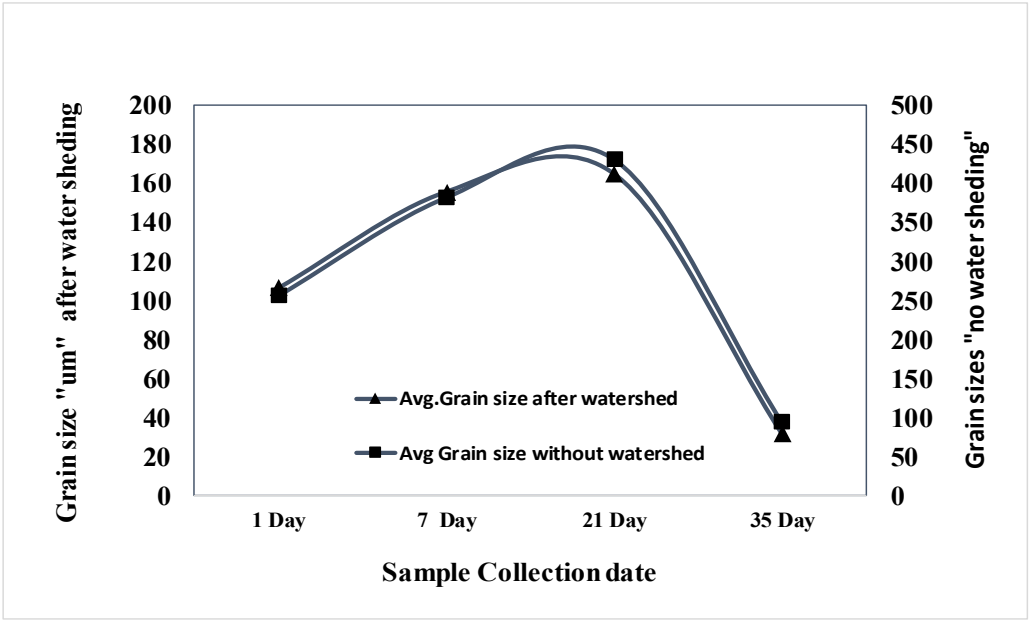

Figure 97: Average Grain Area calculated using watershed tool and without Watershed tool.

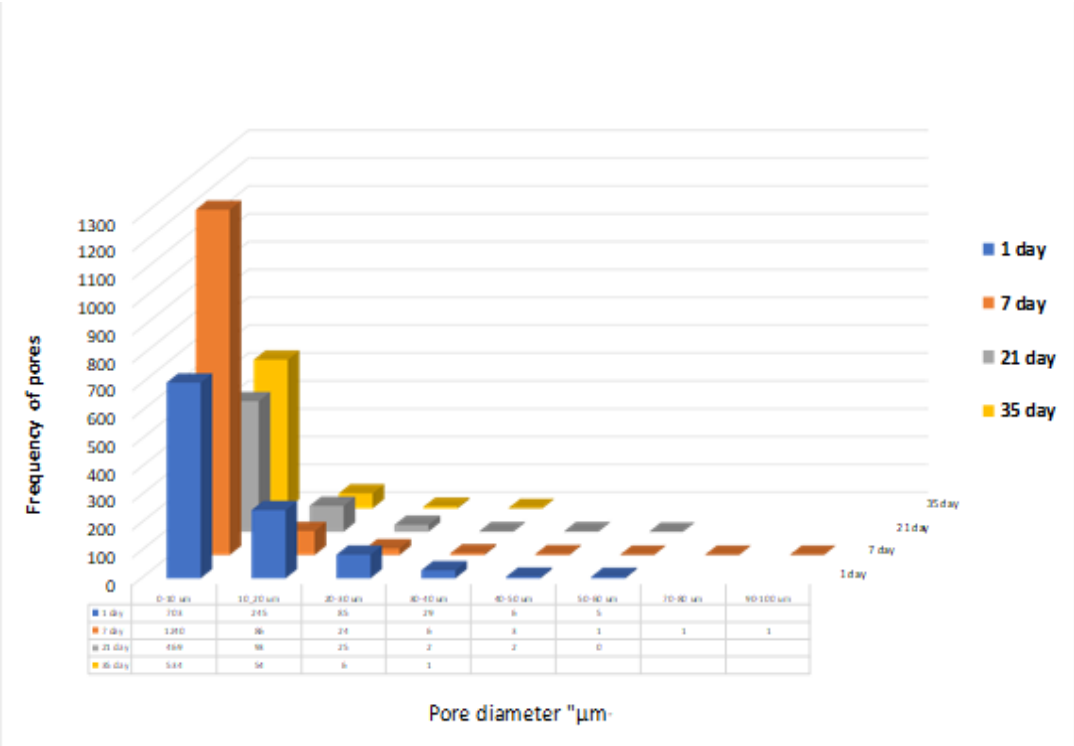

Figure 98: Double drainage Pore Diameter histogram distribution for each day sample Image

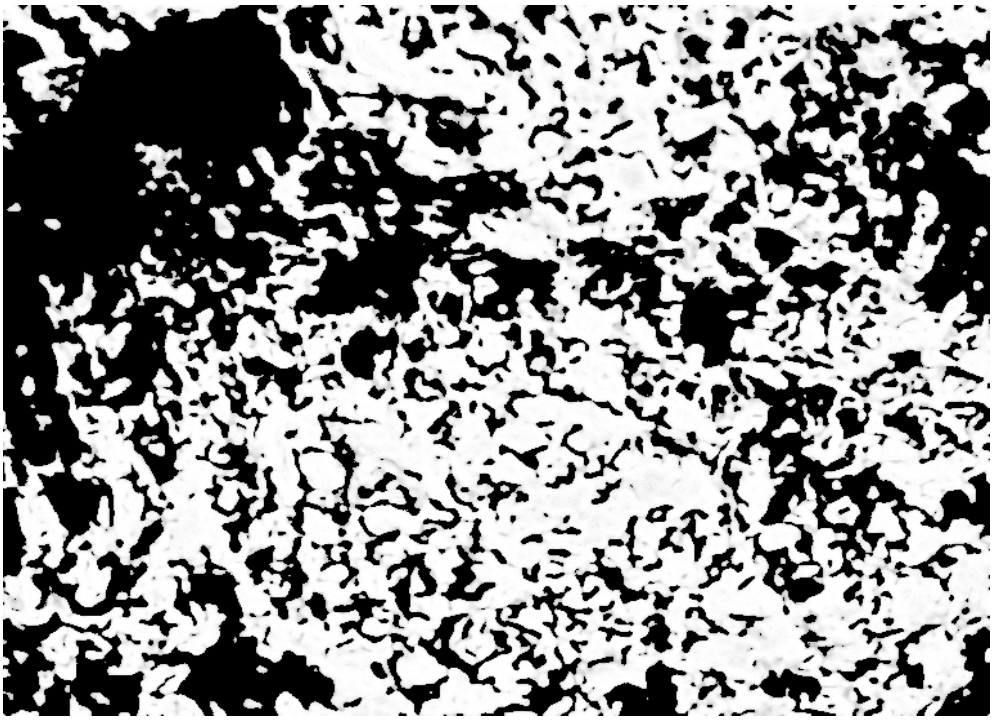

(A)

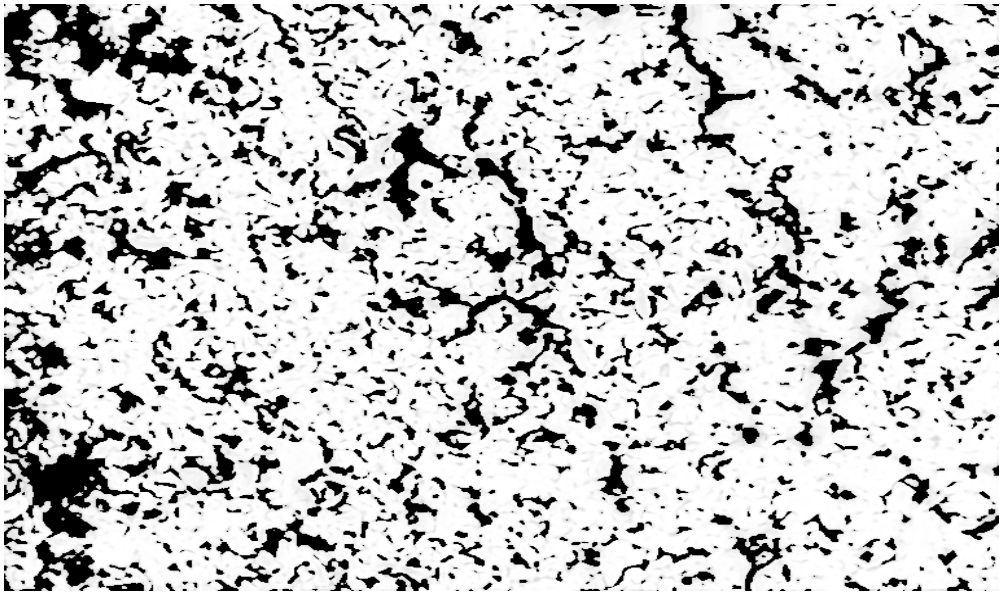

(B)

Figure 99:(A-B) 1 day and 35-day Grains binary Image (obtained through segmentation)

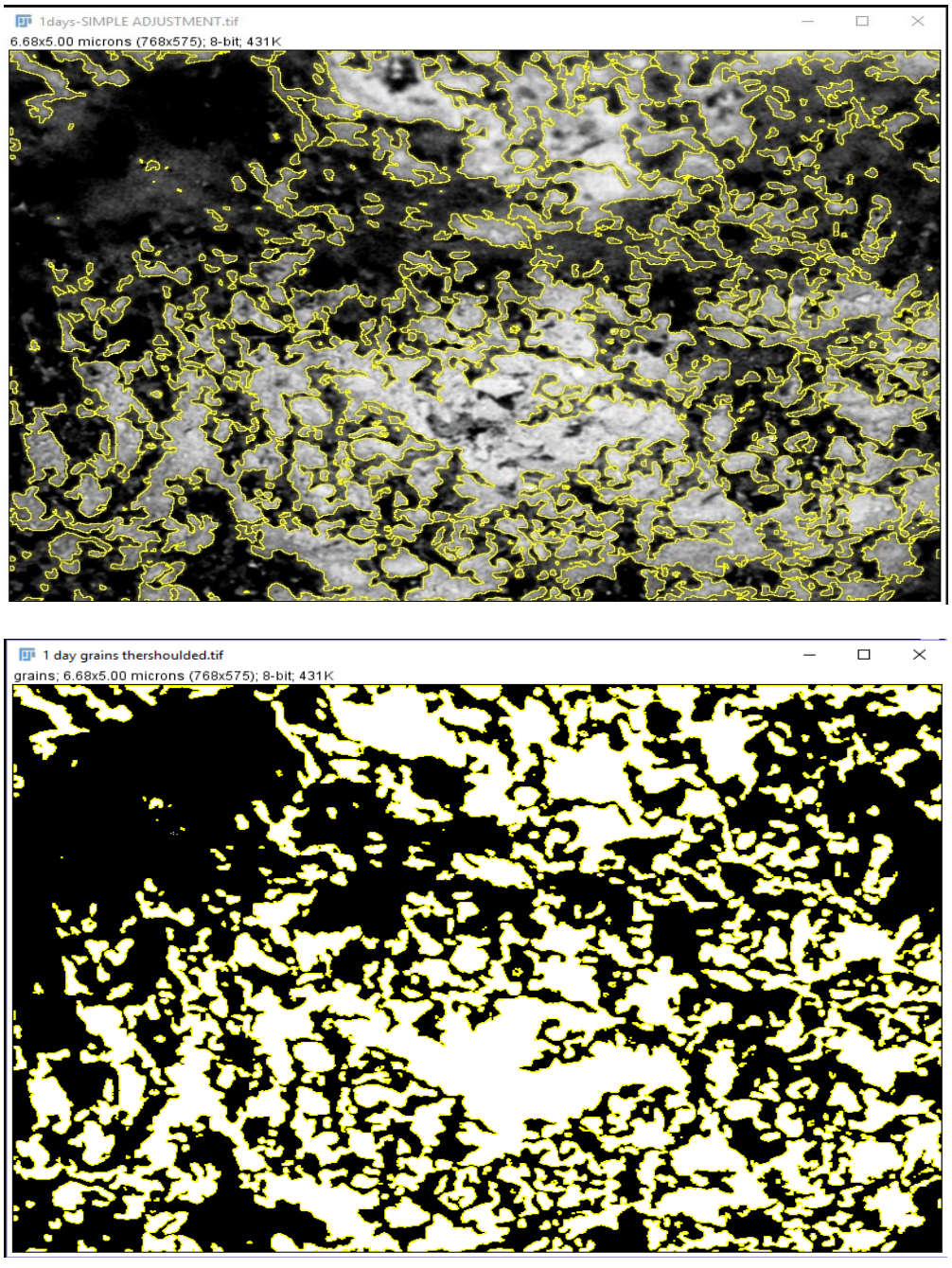

Figure 100: Imported binary data obtained without using watershed tool for 1-day 600ppm, SEM images double drainage

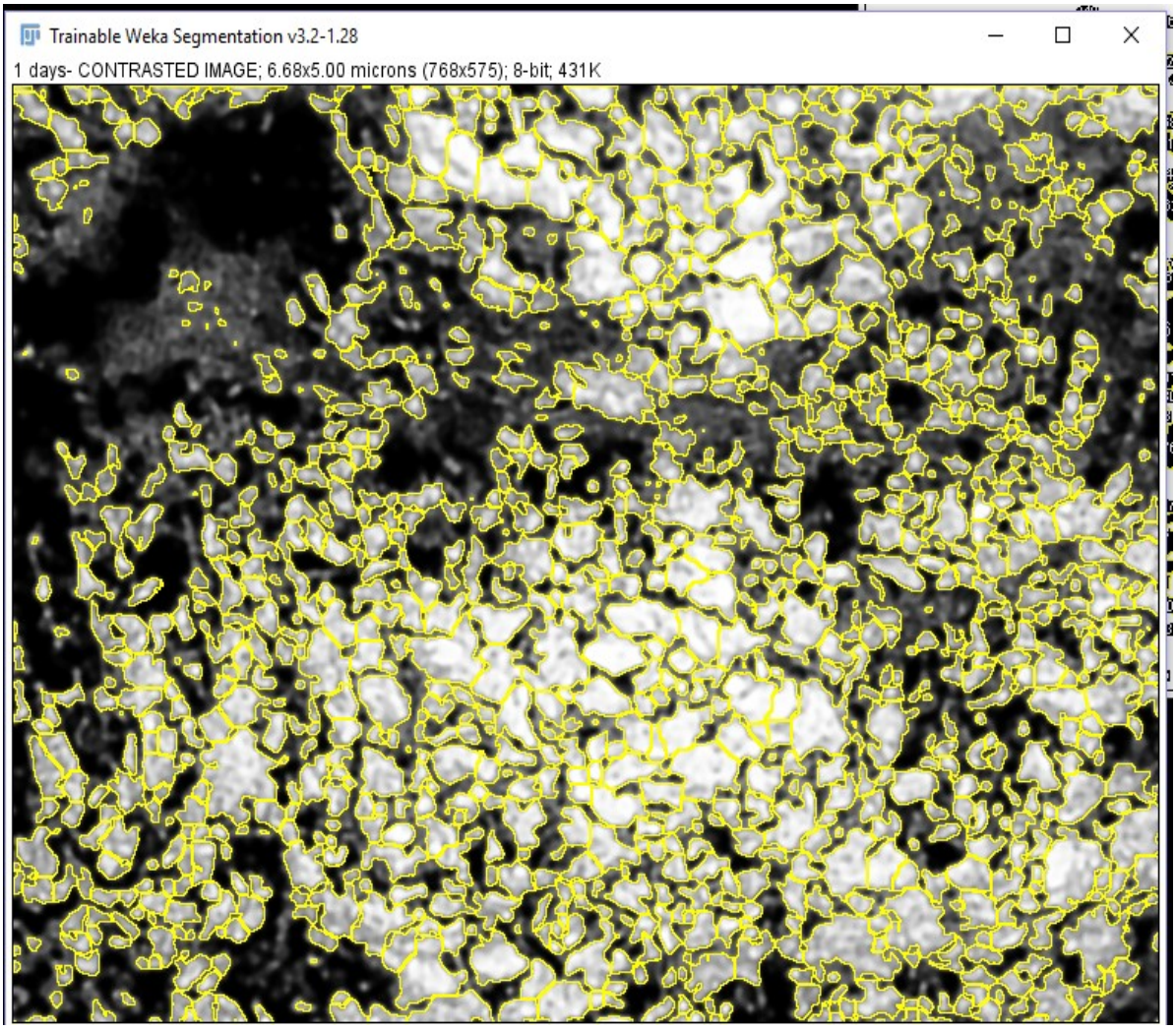

Figure 101: 1 Day SEM Grains binary imported image after using water shed tool

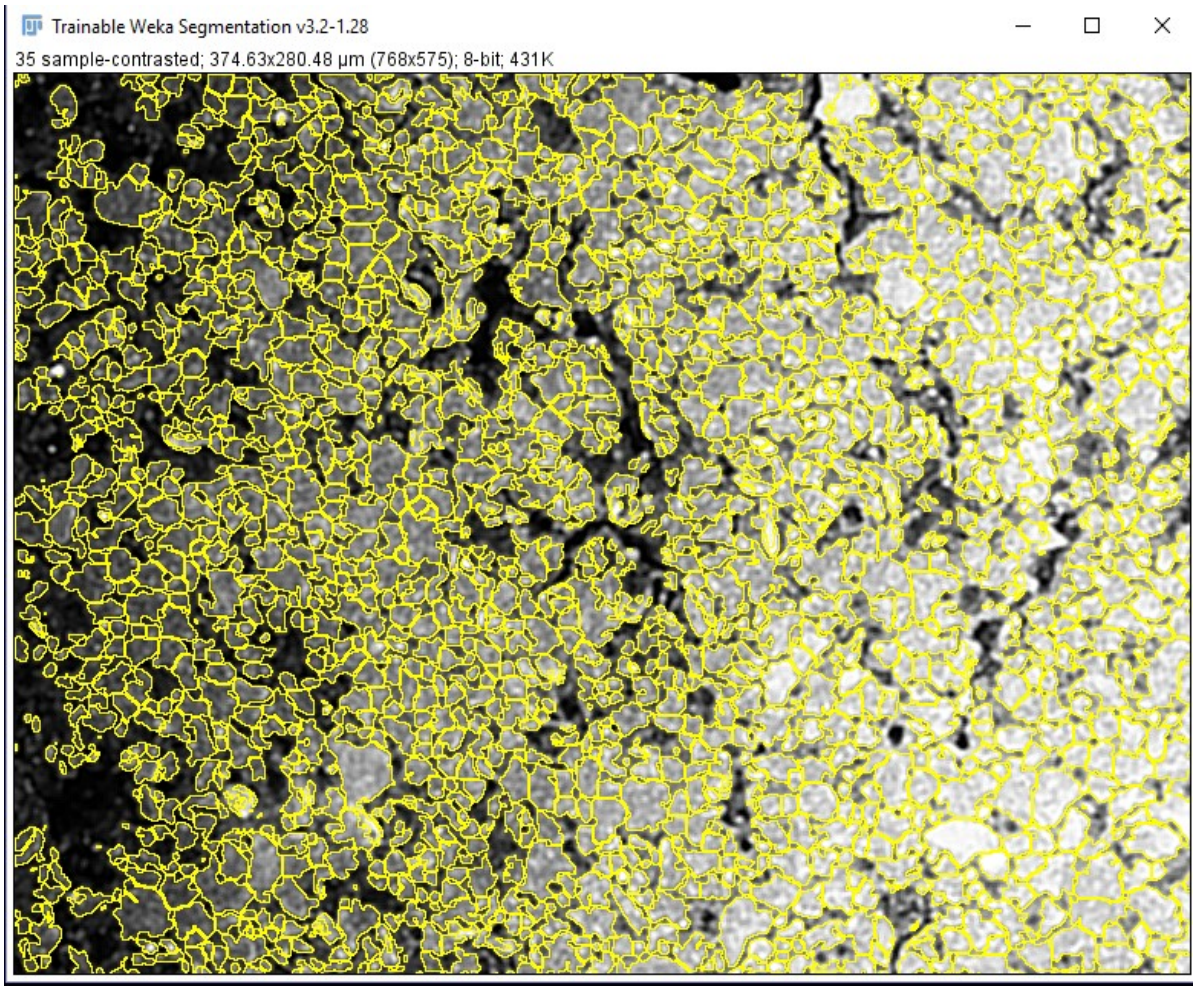

Figure 102: 35 day imported binary Grain images after using watershed tool breaking each grain into different segments,

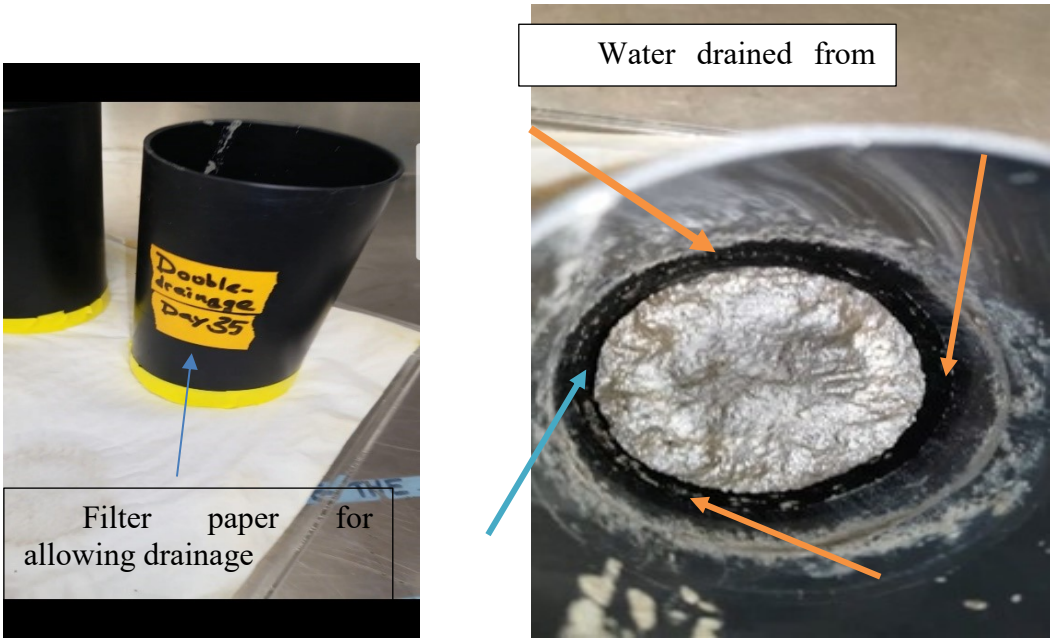

Figure 103: Physical Demonstration of Double drainage column after 35 days dosed with 600 ppm polymer double drainage. Modified from (Salam et al 2017)

5.3 Phase 3.5 Columns with 800 ppm dose tailings (Single Drainage columns)

Figure 104 A-E illustrates the images obtained from the columns dosed with 800 ppm polymer with Single drainage (no drainage). 3 different sets of images were processed to check the repeatability trend of the images and process. The image porosity of all three different sets of images showed a decrease with time, as shown in Figure 105. The image porosity decreased from 29-30% on Day 1 to 21-17% on Day 70. The real laboratory sample porosities as shown in Figure 107 showed a decreasing trend but not a much significant change was noted. The "0 days' (A couple of hours after mixing) lab sample porosity was calculated to be around 84% and after almost 77 days it dropped to 80%.

The total grains number calculation for 800 ppm single drainage images illustrated in Figure 108 showed some fluctuation, but it could be argued that no significant change in grain count exists. It can be concluded from these trends that 800ppm was slightly higher in grain frequency increase compared to 600ppm dose polymer.

Binary images data obtained were imported to the real images to check the agreeability of thresholding and segmentation. The imported binary images fitted the RAW SEM images shows the good output of the methodology developed for FFT SEM images as shown in Figure 110.

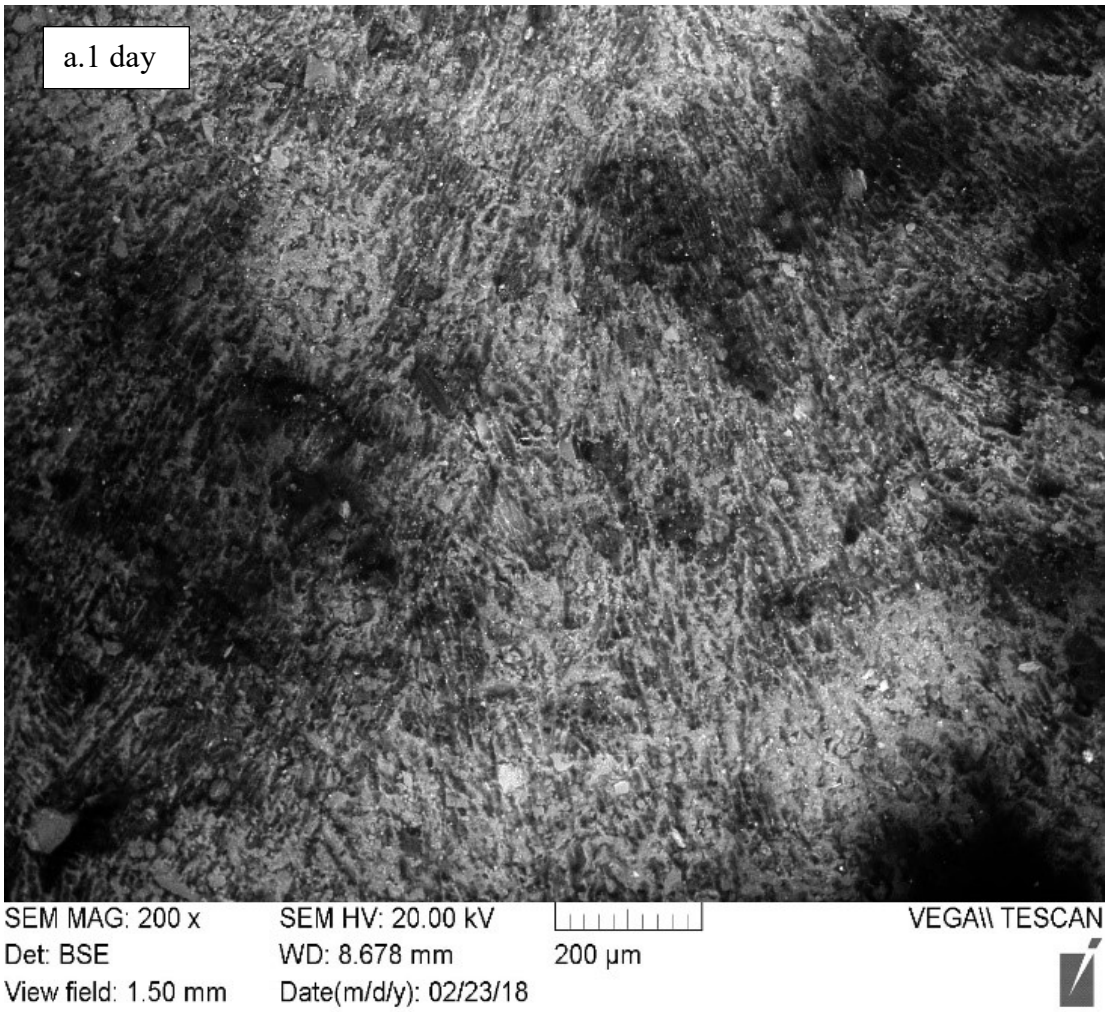
a.1 day
SEM MAG: 200 x
Det: BSE
View field: 1.50 mm
SEM HV: 20.00 kV
WD: 8.678 mm
Date(m/d/y): 02/23/18
200 µm
VEGA\\ TESCAN

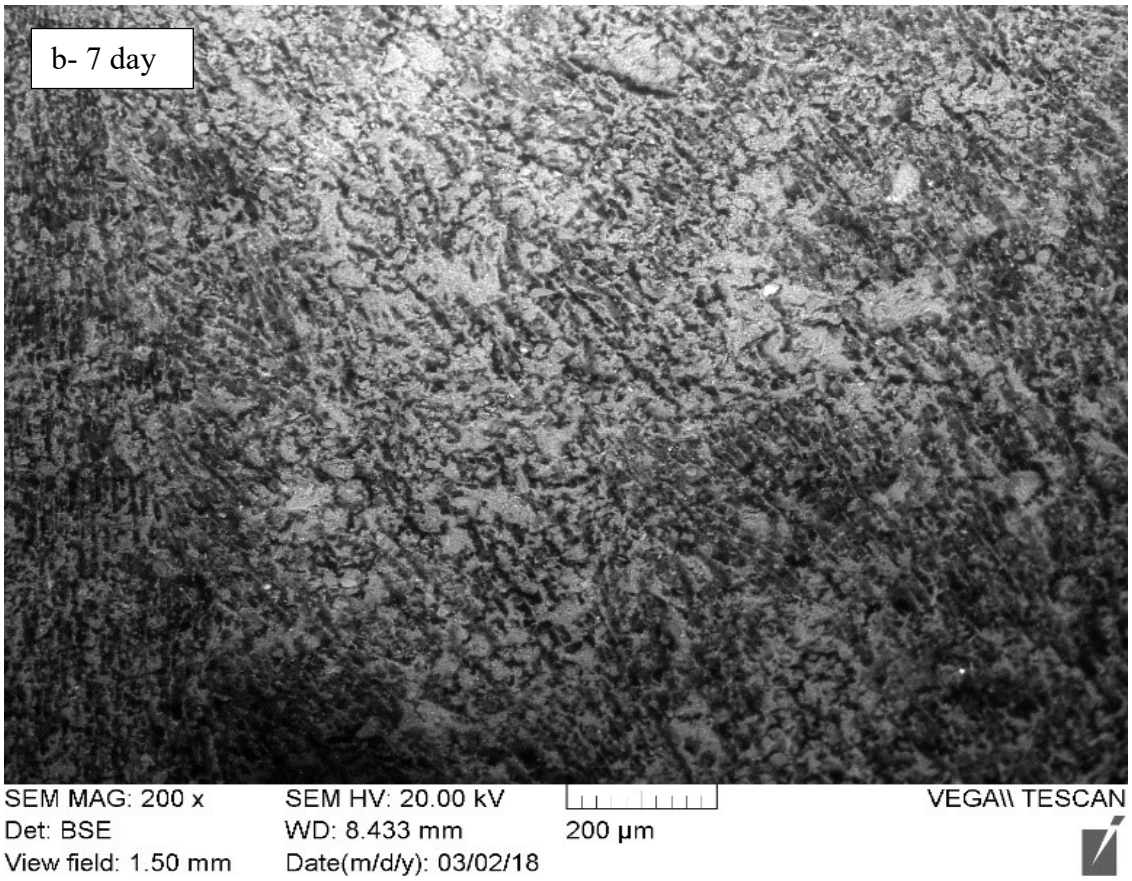
b- 7 day
SEM MAG: 200 x
Det: BSE
View field: 1.50 mm
SEM HV: 20.00 kV
WD: 8.433 mm
Date(m/d/y): 03/02/18
200 µm
VEGA\\ TESCAN

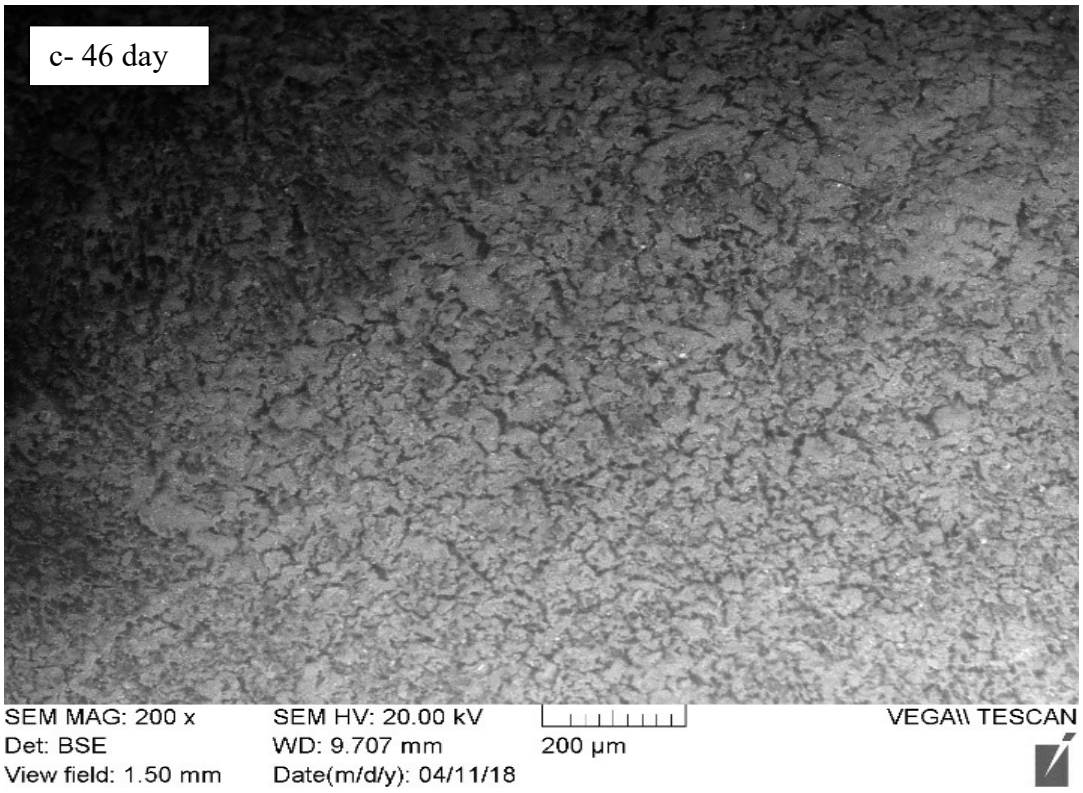
c- 46 day
SEM MAG: 200 x
Det: BSE
View field: 1.50 mm
SEM HV: 20.00 kV
WD: 9.707 mm
Date(m/d/y): 04/11/18
200 µm
VEGA\\ TESCAN

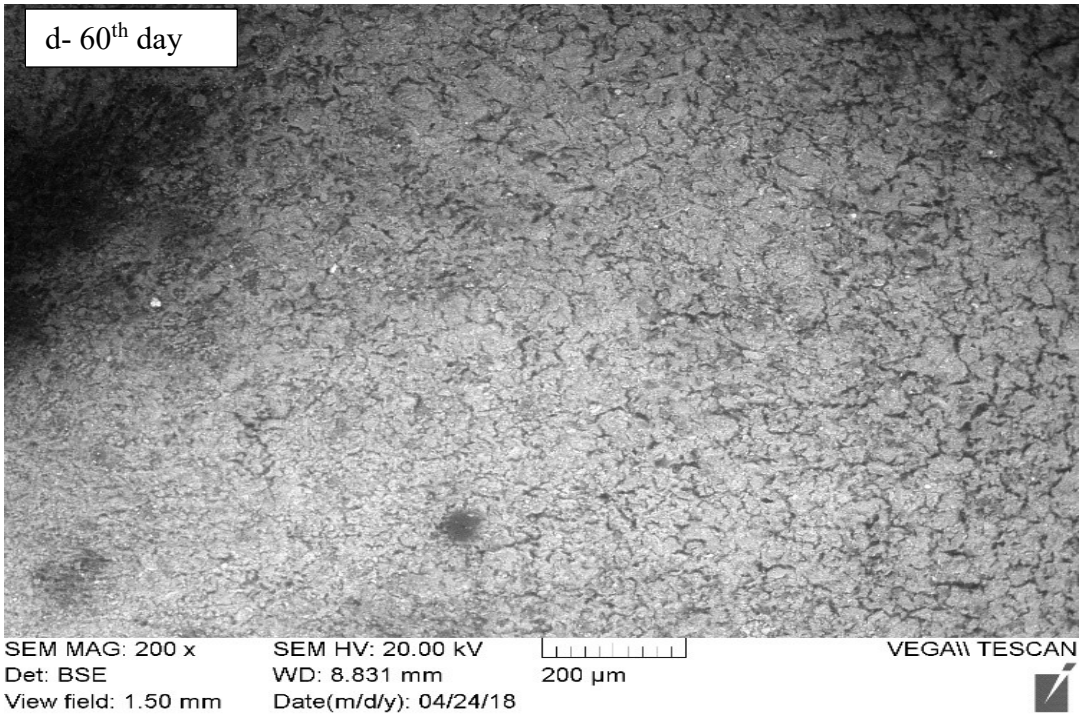
d- 60th day
SEM MAG: 200 x
Det: BSE
View field: 1.50 mm
SEM HV: 20.00 kV
WD: 8.831 mm
Date(m/d/y): 04/24/18
200 µm
VEGA\\ TESCAN

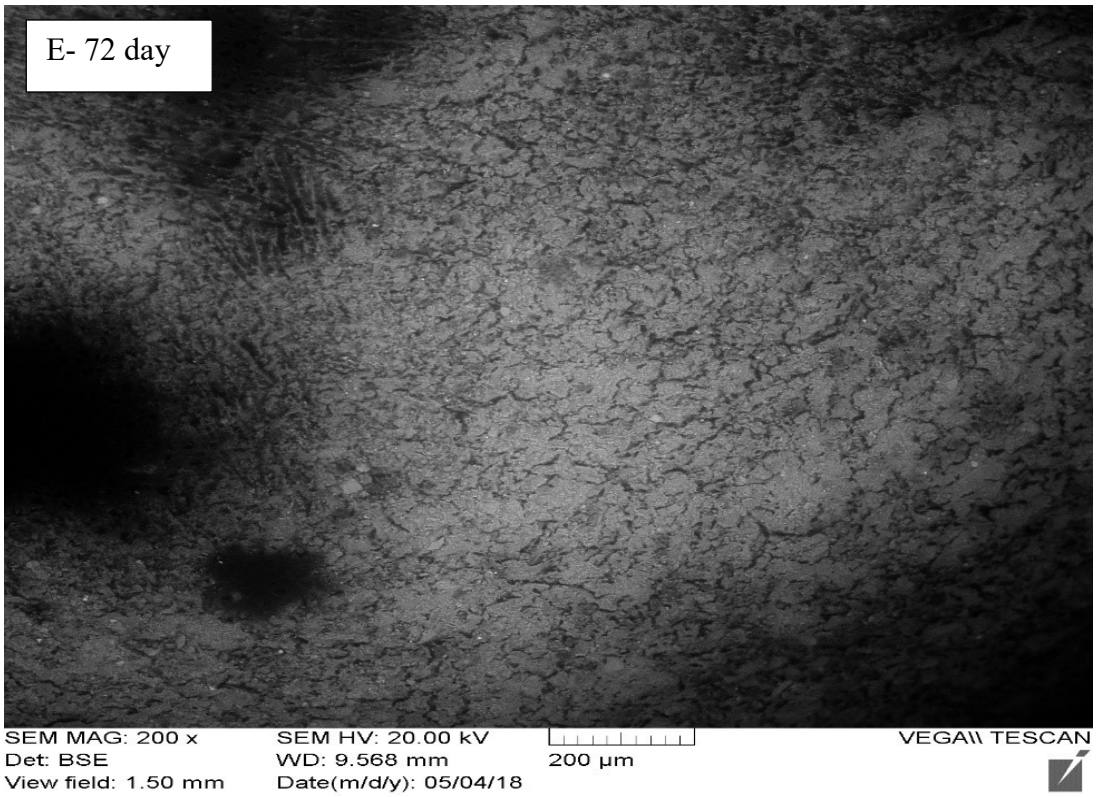

Figure 104: (A TO E) Scanning Electron Micrograph of polymer amended Oil sands tailings for dose of 800ppm, (After A , 1 day, b 7 day, c 47, d 60 days E, 70 days) – of Polymer Mixing, keeping Boundary Condition "No-drainage") Magnification 200x ,view field 750/

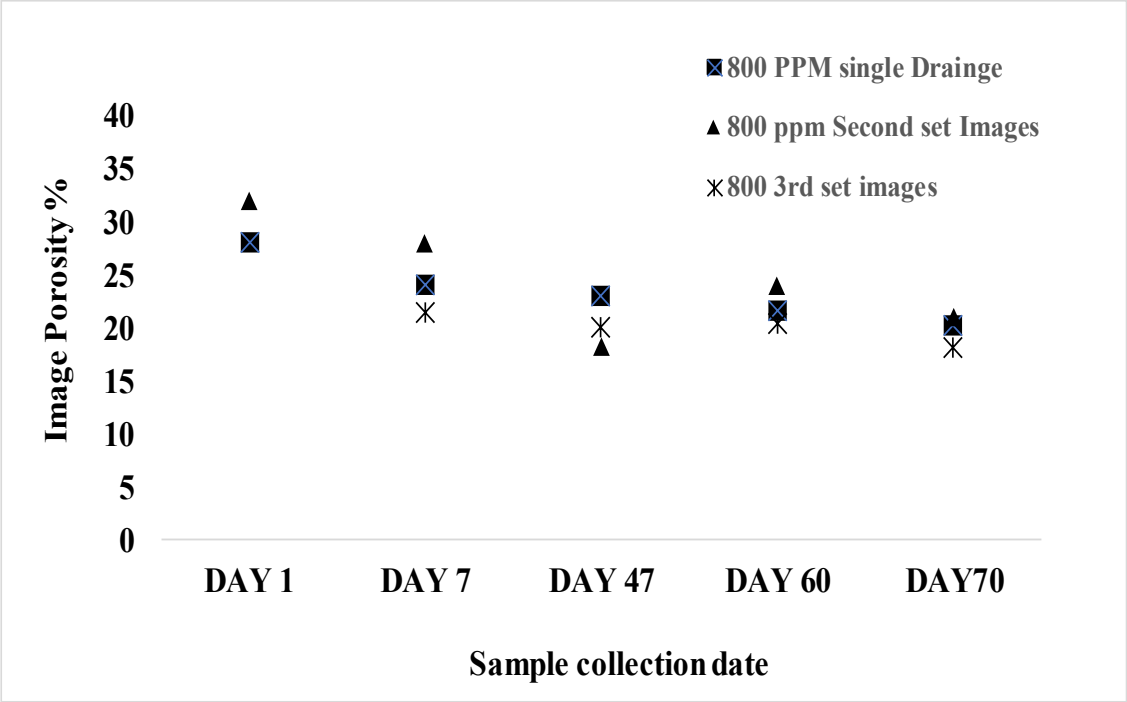

Figure 105: Porosity calculation for 3 different set of 800 ppm SEM images No-Drainage

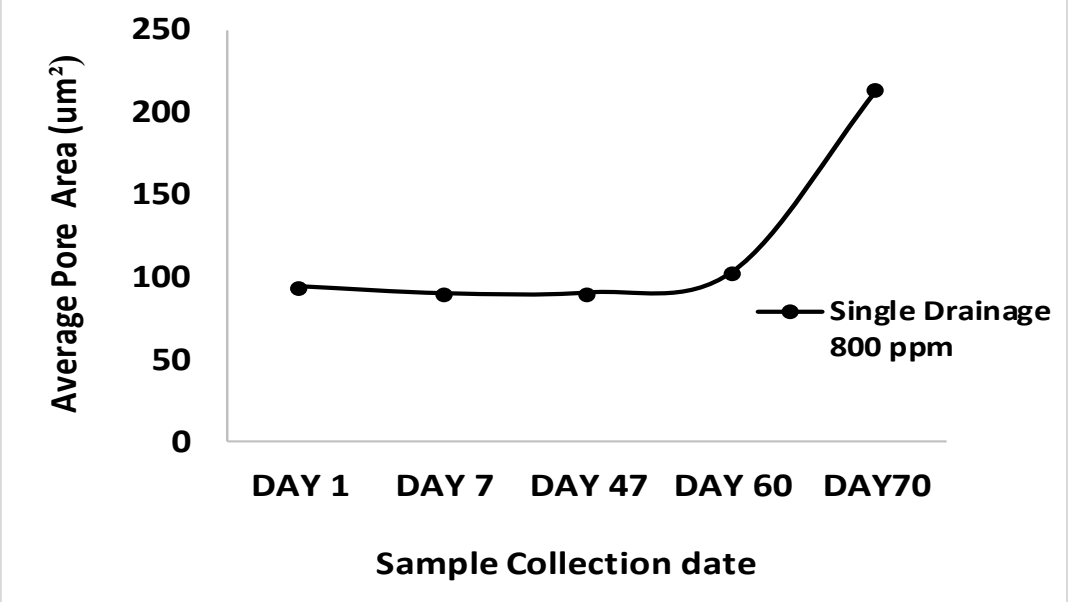

Figure 106: Average Pore Area from SEM Single drainage (800 ppm) Images

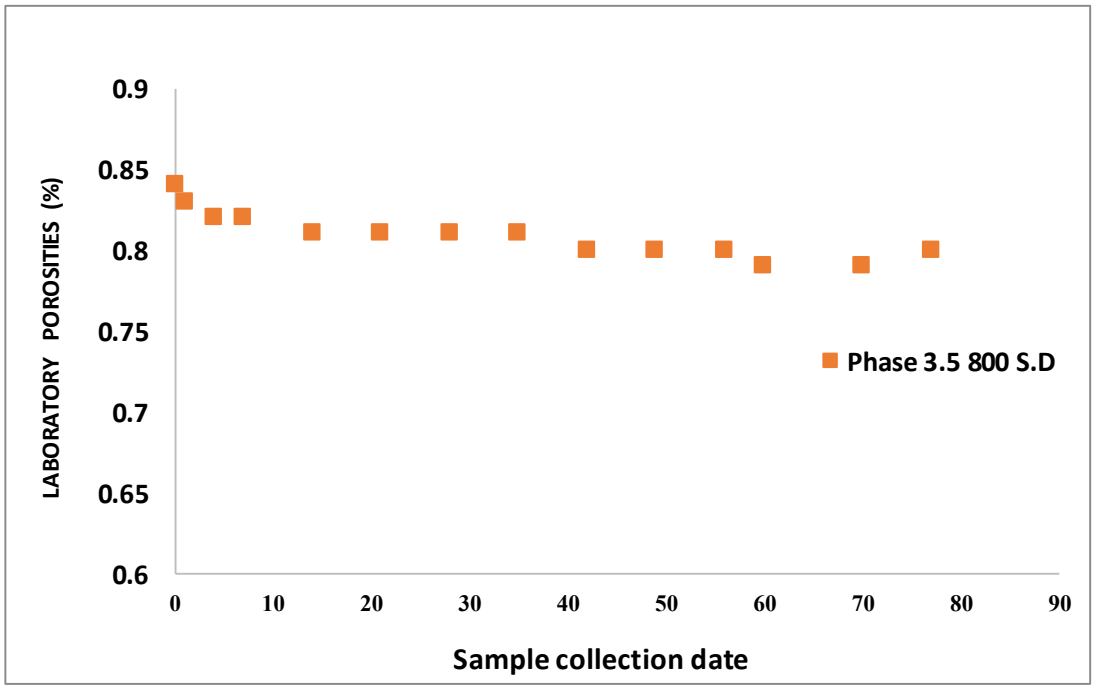

Figure 107: Laboratory Sample Porosity for 800 ppm single drainage (TOP of column) (Salam 2018)

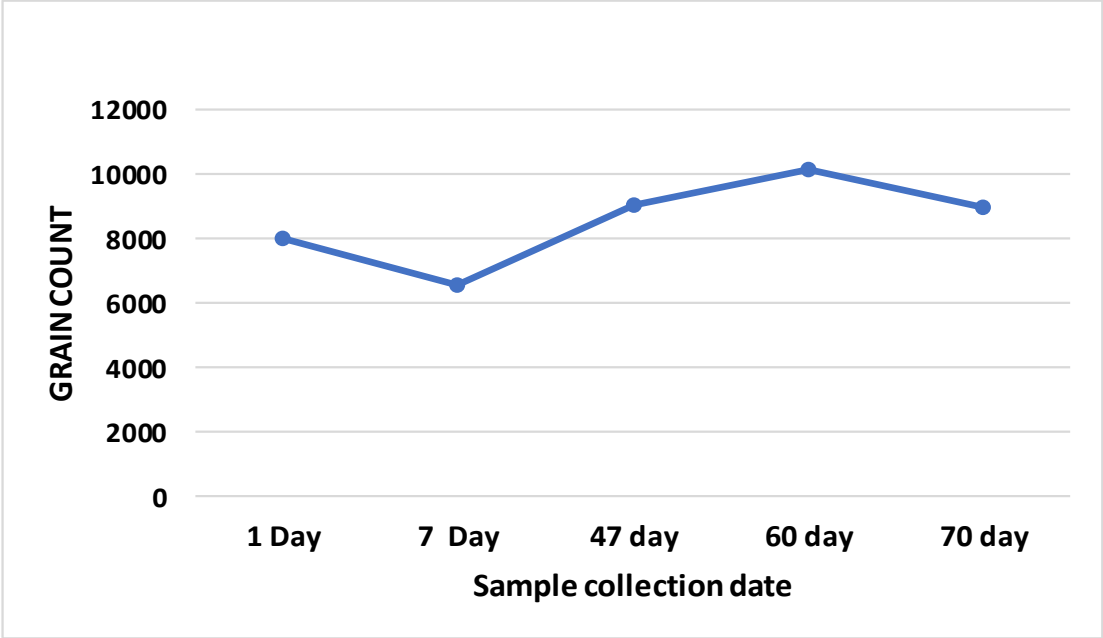

Figure 108: Total Number of Grains For 800ppm Single Drainage SEM images using water shed tool

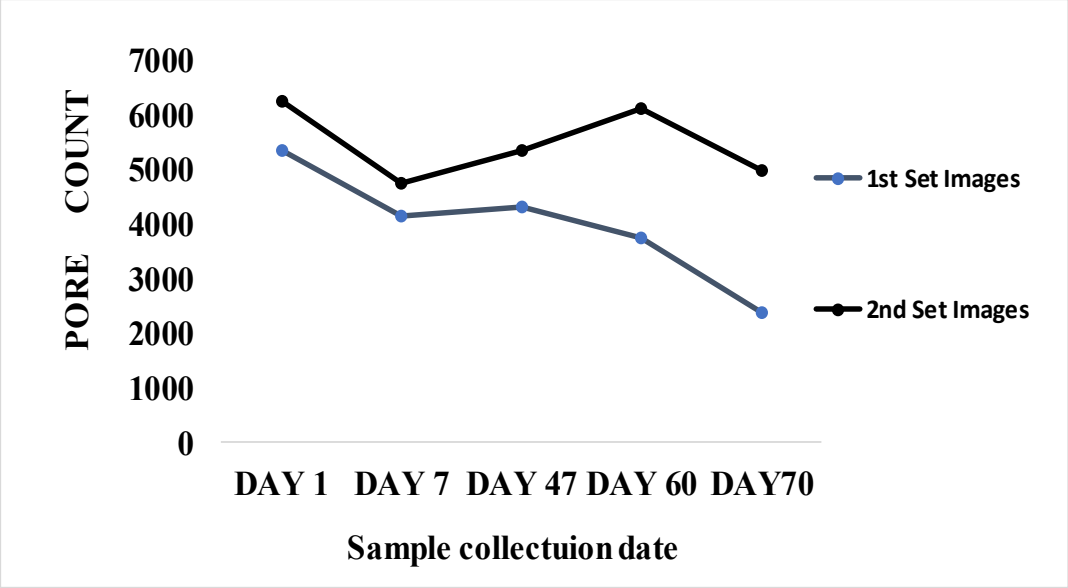

Figure 109: Total Pore Frequency for 2 different set of SEM images dosed with 800ppm

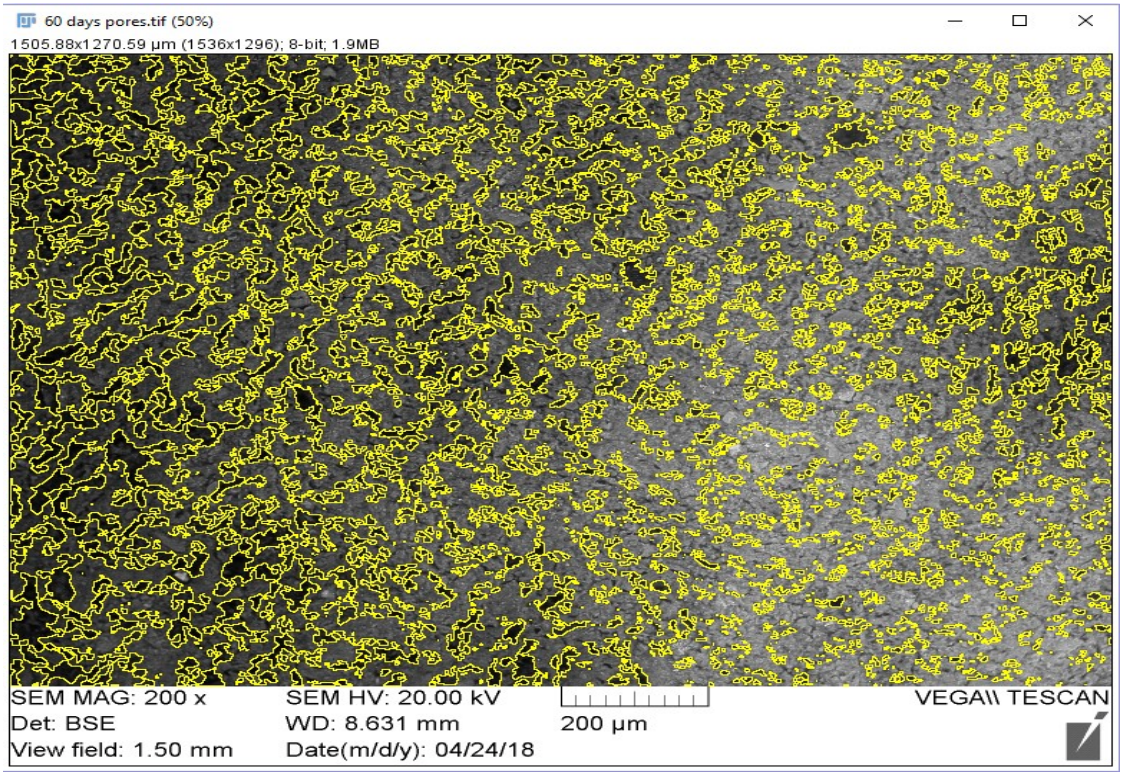

Figure 110; 60 days imported data of binary image to real pores on 800 SEM image as an example illustrated

5.1 General comparison of SEM Results for Phase 2, Phase 3 and Phase 3.5 images

The total pore count for all Phases is shown in Figure 111. It was noted that Phase 3.5 (Single drainage dosed with 800 ppm polymer) had a substantially higher pore count as compared to Phase 2 (600ppm Single drainage) and Phase 3 (double drainage 600ppm). It seems that the 800 ppm single drainage samples displayed a different kind of pore-size distribution, where many relatively small cracks like pores appear throughout the sample, as can be seen in Figure 104 above. 800 ppm samples do exhibit somewhat lower CST values than 600 ppm samples (Figure 117: Capillary suction test results for two different polymers), which is thought to imply better floc dewaterability. It can be seen in Figure 112, the image porosities, that the 800 ppm samples initially dewater faster than the 600 ppm samples for single drainage, but the 600 ppm samples achieve similar porosities by the end of the experiment.

Also, in Figure 112, the double drainage sample showed considerably more dewatering than the other three samples. This is in accordance with actual porosities measured in the laboratory experiments Figure 95, and can be noted in columns test Figure 103 above.

The different behavior is also seen in the average grain area (size) data as shown in Figure 113. Single drainage 600 ppm samples showed an increasing trend to a value between 350 um^2 to 370 um^2 by Day 28. The double drainage 600 ppm showed a higher initial already 260 um^2 on Day 1 however, a final value after 35 days was suddenly decreased

to (110-100 um^2).To examine why the grain size suddenly decreased by 35 days, the grain size histogram for day 21 and 35 is shown in Figure 114. This figure was generated from the quantitative data of 21- and 35-days images. High frequency of grains ranging between size 0-10 um diameter in the 35-day image were noted as compared to the 21-day image. Due to this high frequency of grains in 35 days image a fall in average grain area was noted in Figure 113 for phase 3(double drainage). However, it was eminent from Figure 114 that the maximum grain diameter calculated in 21 days image were between (280-290 um), While in 35 days sample there were some grains chunks between a size of (300-310 um) which illustrates an increase in grain size. This increase in grain size was also noted in the binary overlay images for both 21 and 35 days sample image as in, Figure 115 and Figure 116.

This leads us to conclude that more rapid dewatering initially due to the double drainage boundary condition favours increased flocculation (more flocculation occurs at lower water contents due to a proximity of dispersed particles), which in terms favors more sedimentation. Various results in Salam et al. (2017, 2018) suggest that the boundary condition affects the tailings in some fundamental way other than the shortening of the drainage path and that the influence of the boundary condition on dewatering is repeatable from sample to sample and over different doses.

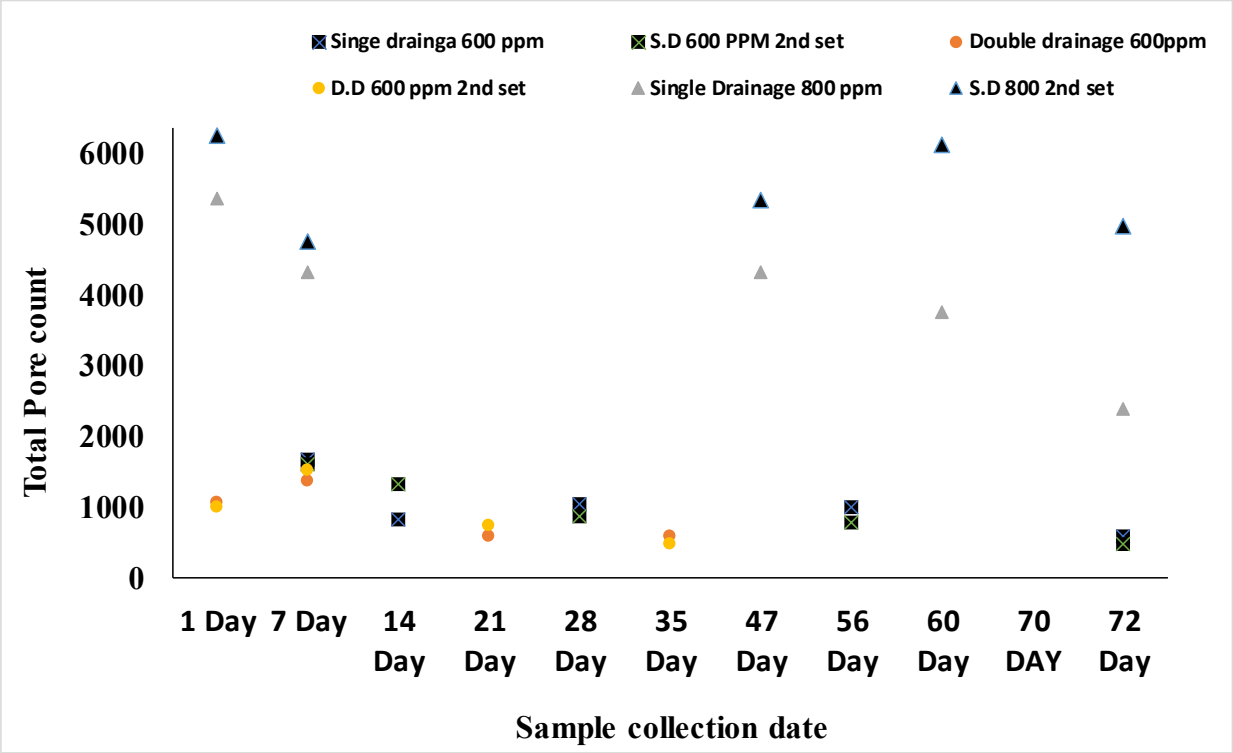

Figure 111: Comparison of Total Pore number Phase 2 (600 S.D), Phase 3 (600 D.D) and Phase 3.5 (800 S.D) for repeatable Images.

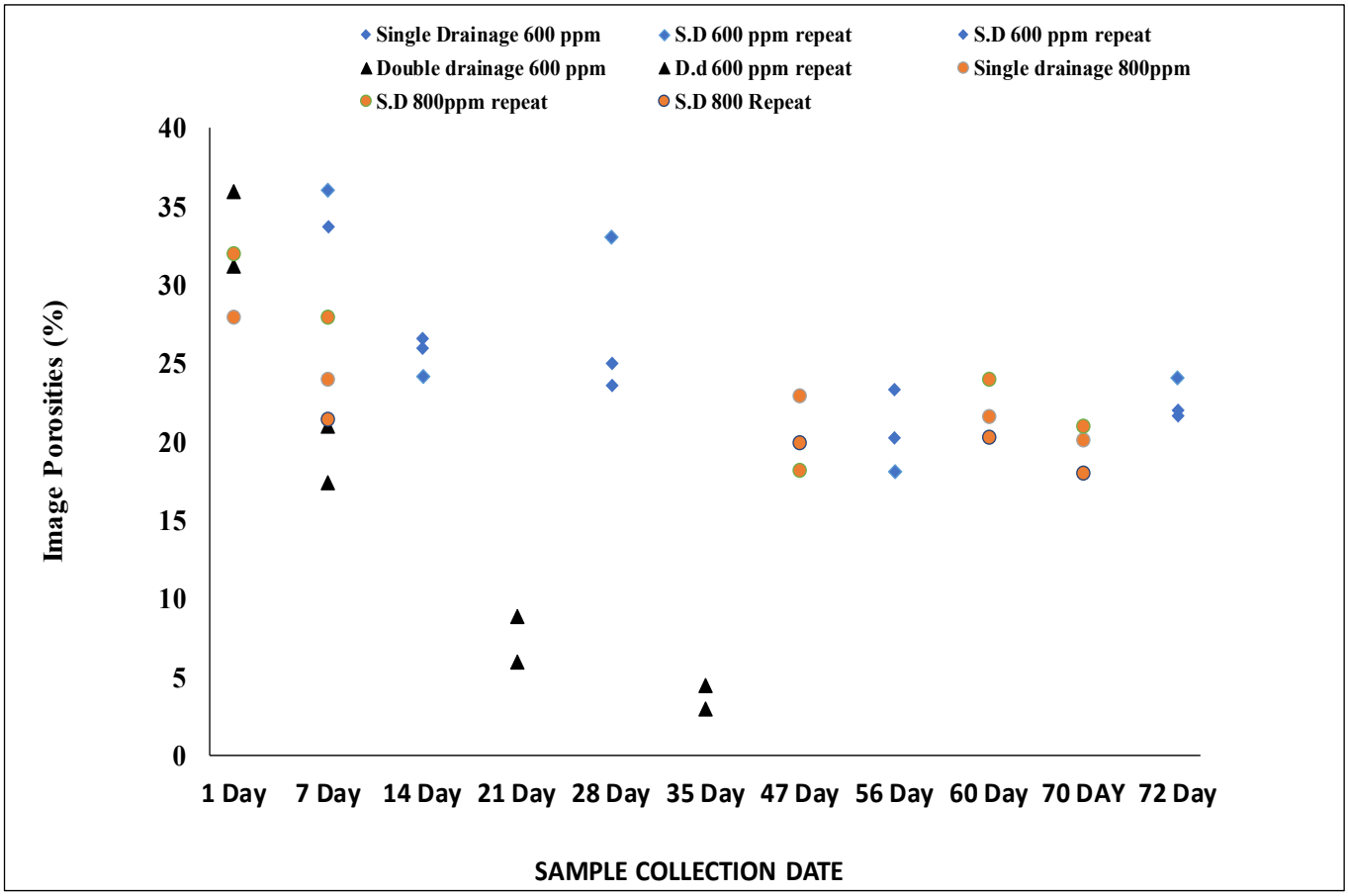

Figure 112: Comparison of Image Porosity for Phase 2 (600 S.D), Phase 3 (600 D.D) and Phase 3.5 (800 S.D) Images

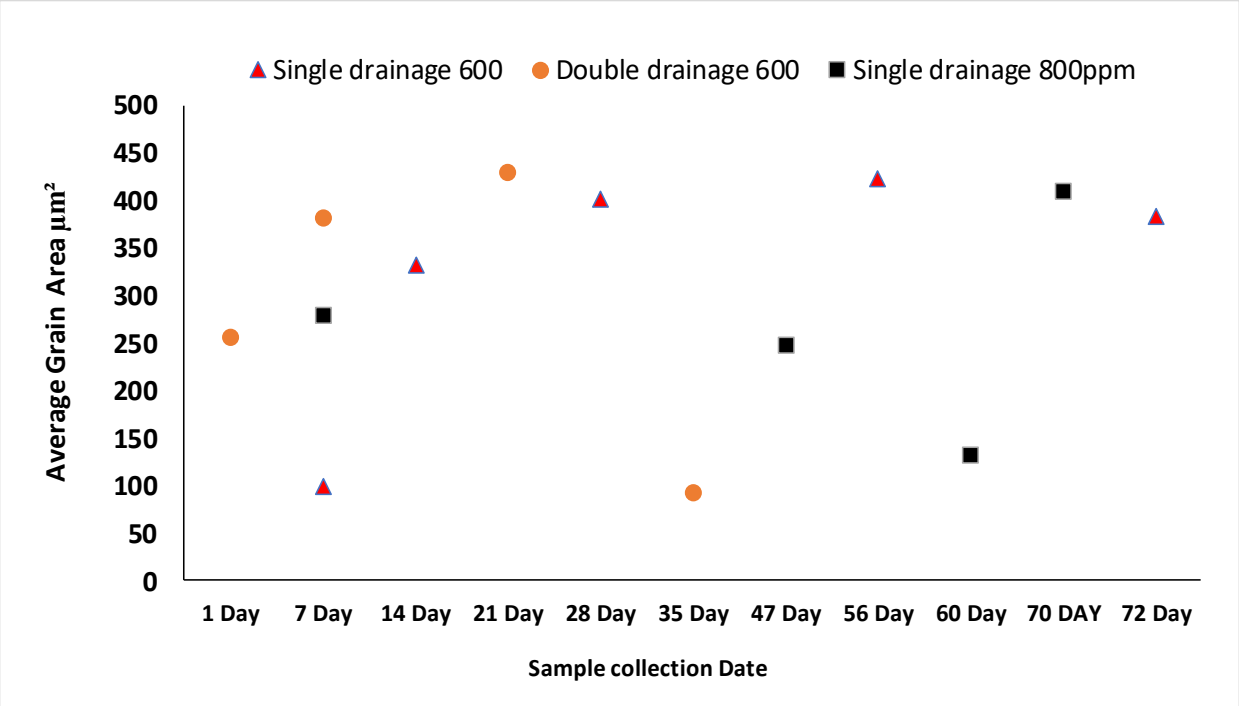

Figure 113: Average Grain Area (size), Phase 2 Single Drainage 600, Phase 3 Double drainage, and Single Drainage 800ppm.

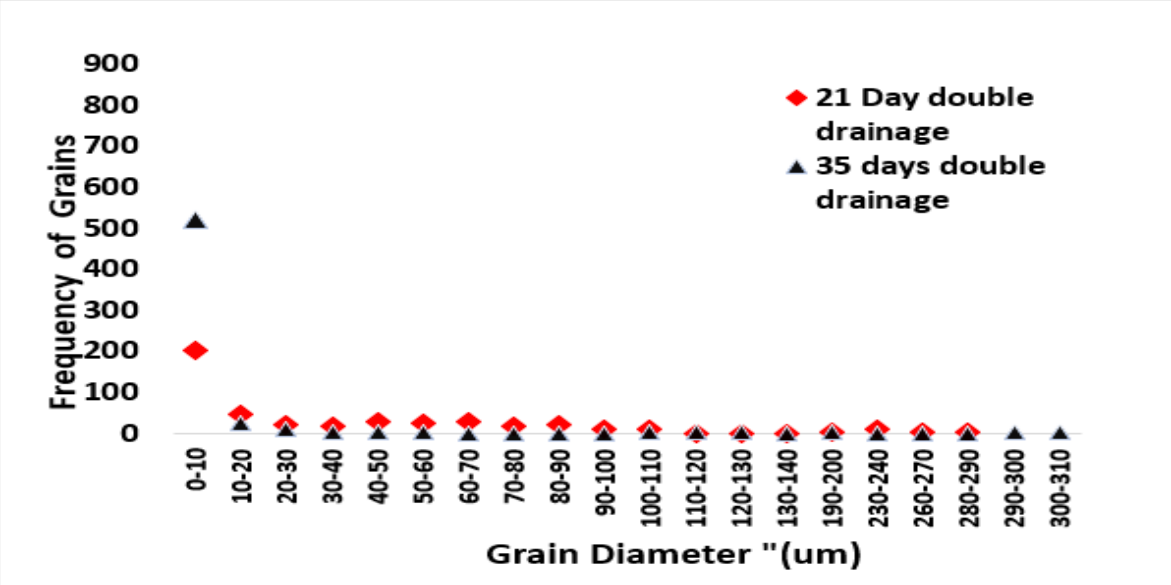

Figure 114: Grain diameter histogram for only Phase 3 (21 and 35 days) Images.

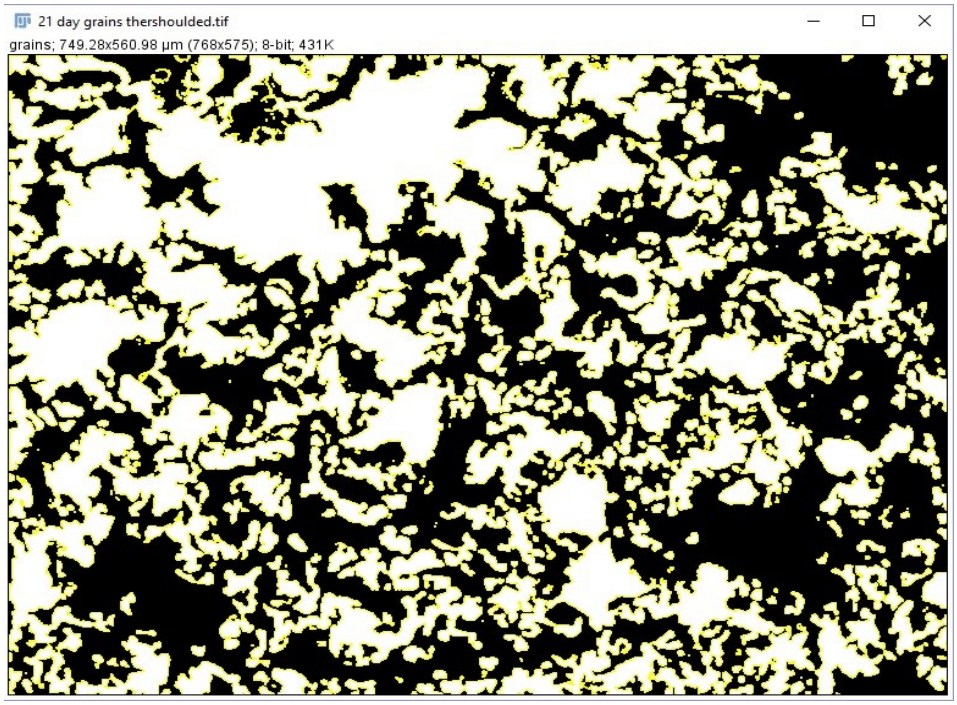

Figure 115: Imported binary image of 21 days Sample double drainage 600ppm

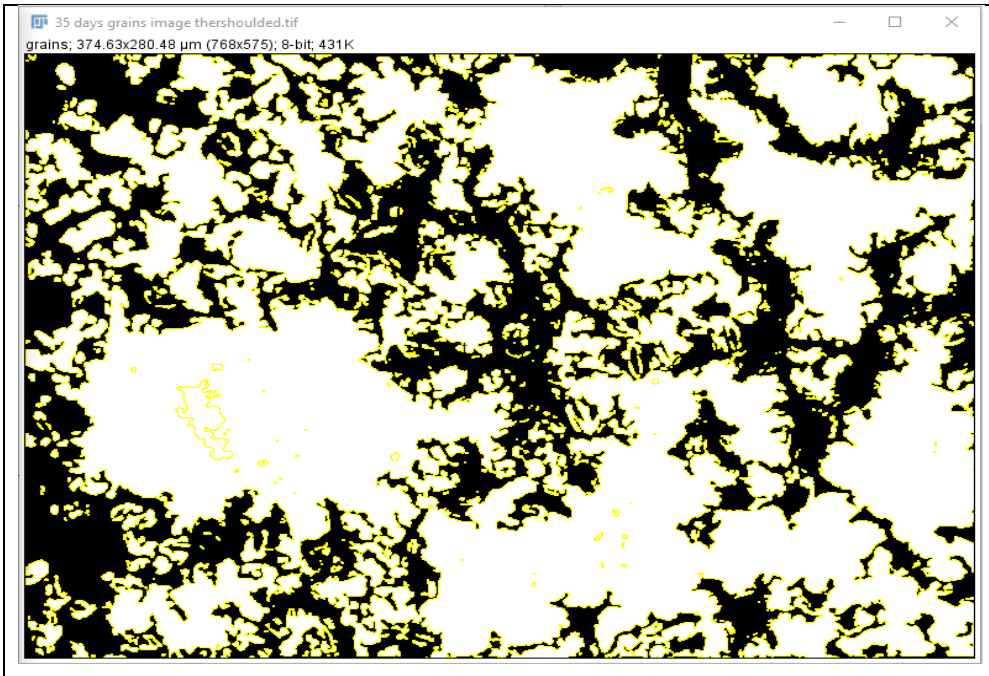

Figure 116: 35 day Imported binary Image (600 ppm double drainage)

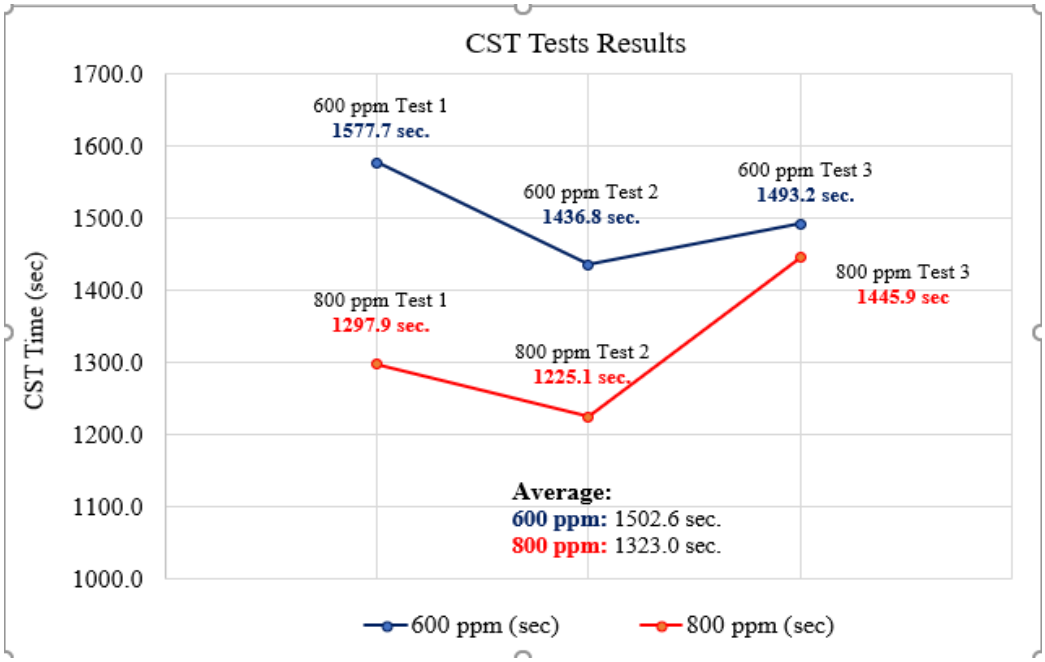

Figure 117: Capillary suction test results for two different polymers

5.2 Phase 4 optical microscope; 600 ppm

The total number of flocs and floc size distribution were analyzed over 48 hours in OM images. After this time usable images could not be obtained due to the opaqueness of the samples. Optical microscopic images from Figure 118(A to F) were digitally processed using ImageJ. In general, an increasing trend in average size can be detected. Additionally, the background space becomes clearer and the contrast between flocs and pore space improves over time. This is perhaps due to the association of small particles with large particles over time.

The floc size distribution for these images is presented in Figure 119 and

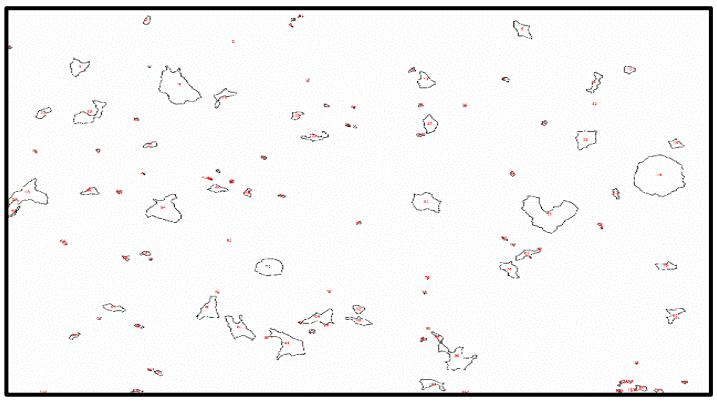

1 hour

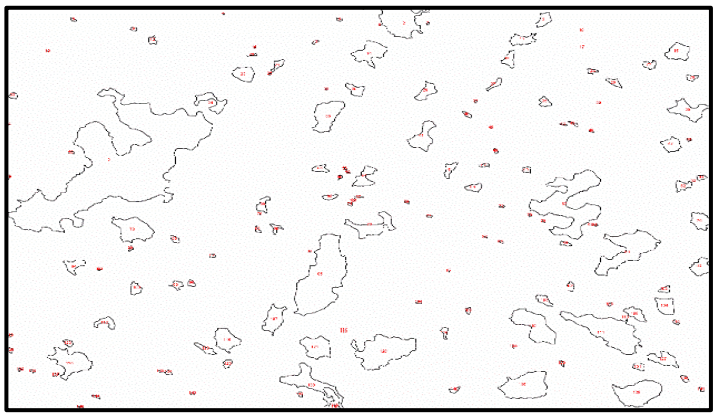

24 hours

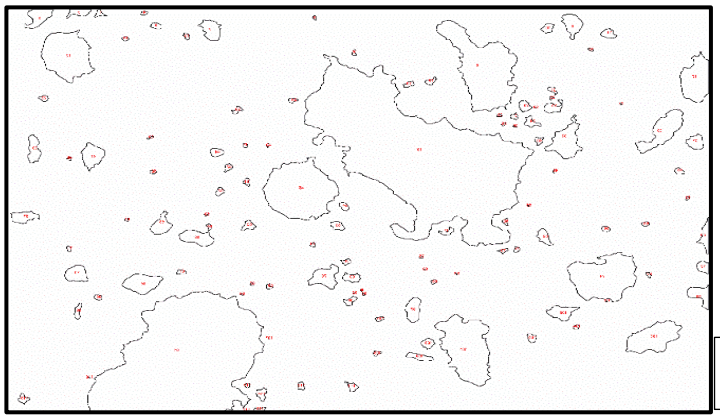

48hours

Figure 122: Floc size changes in optical microscope generated using Image J. (PHASE4 600PPM)

. There is a clear trend in the size of the largest flocs. At 1 hour after tailings were dosed with a polymer in Figure 119, the maximum size of flocs was between 70-110 micron. This maximum size of flocs was augmented for 48 hours to approximately 230-290 microns as shown in

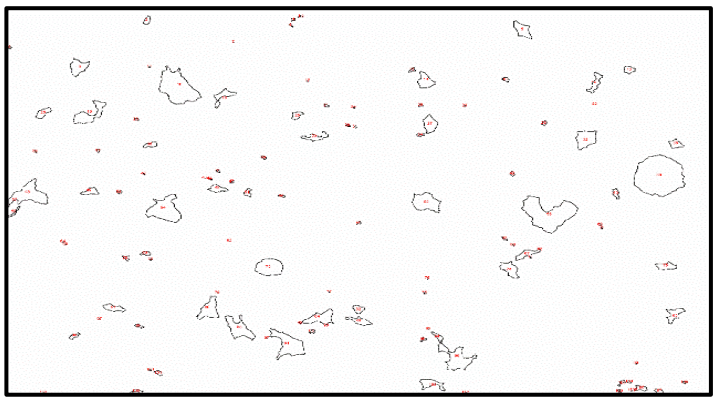

1 hour

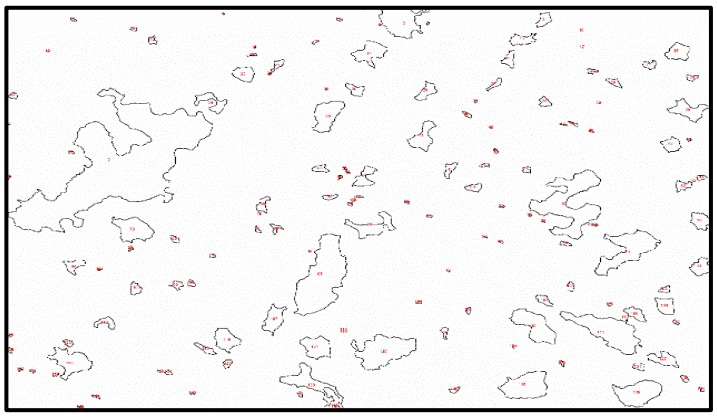

24 hours

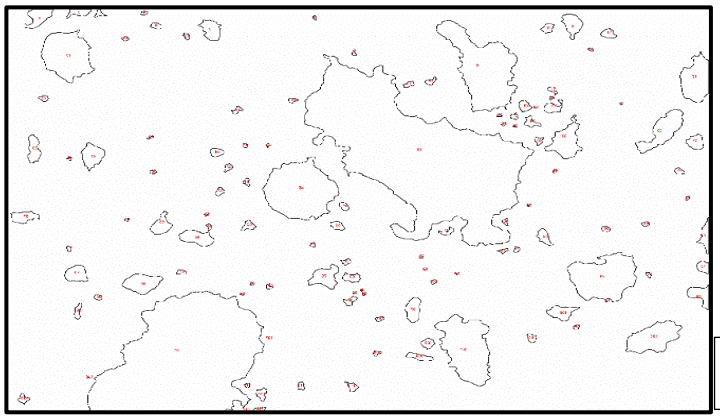

48hours

Figure 122: Floc size changes in optical microscope generated using Image J. (PHASE4 600PPM)

. The increase in the size of flocs is clearly seen in the binary images produced through image processing (e.g. Figure 122).

The total floc area (summing all areas found from each hour image) is shown in Figure 124, showing data for two images captured at each time and illustrates increasing trend with time. However, there are samples which show a decrease

in the total floc area between 8 to 24 hours. This may be due to settlement and segregation of the large flocs. The samples are obtained from the tailings water interface. Interestingly, in **Error! Reference source not found.**the size of flocs ranging between 0 -10 μm initially increases up to 24 hours, after then decreases to 48 hours. The decrease in count may be caused by ongoing flocculation, as smaller flocs in 0-10-micron range combine to form larger flocs, as can be seen in Figure 122 and Figure 123. The first increase in the count in the 0-10 μm range may be caused by small non-detectable particles combining to form clear flocs. However, the variability from replicate to replicate is highest in the 0-10 microns range (For example,

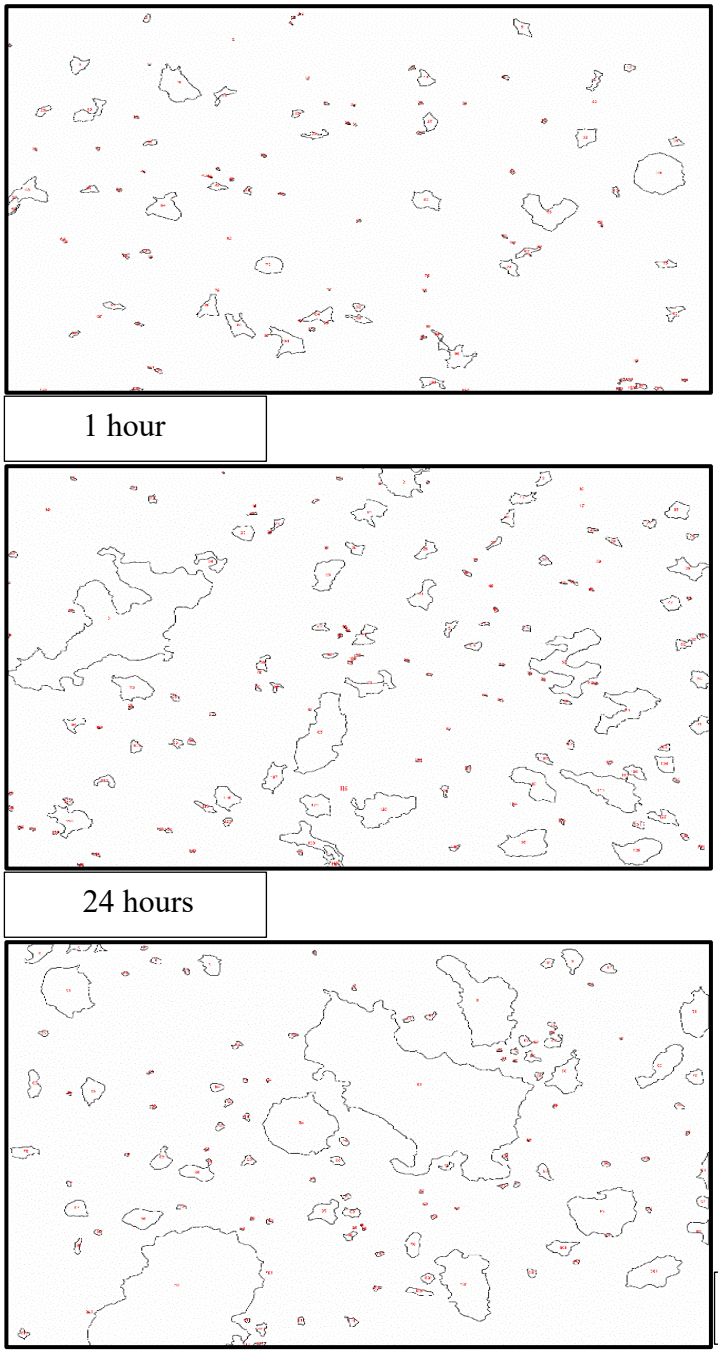

).

Figure 122: Floc size changes in optical microscope generated using Image J. (PHASE4 600PPM)

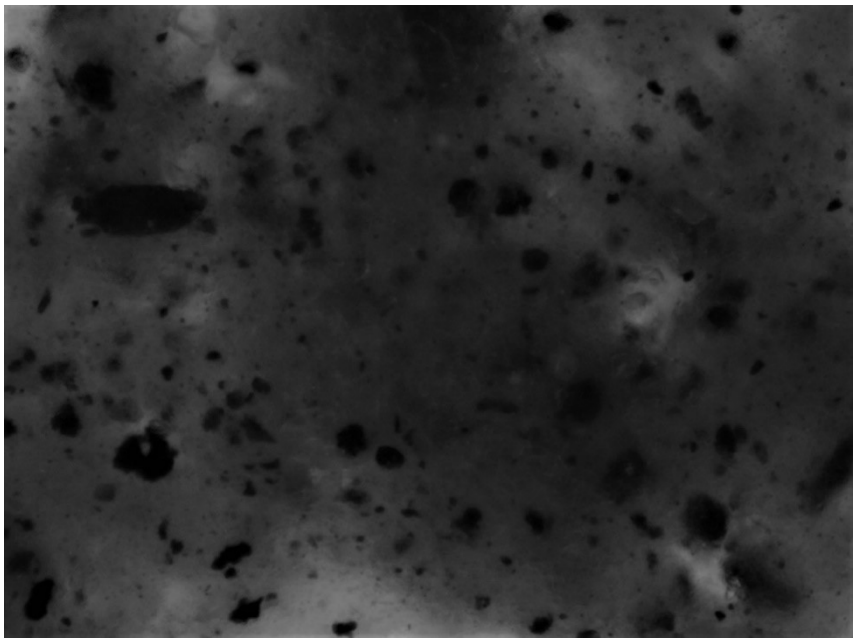

1-hour Sample

A.

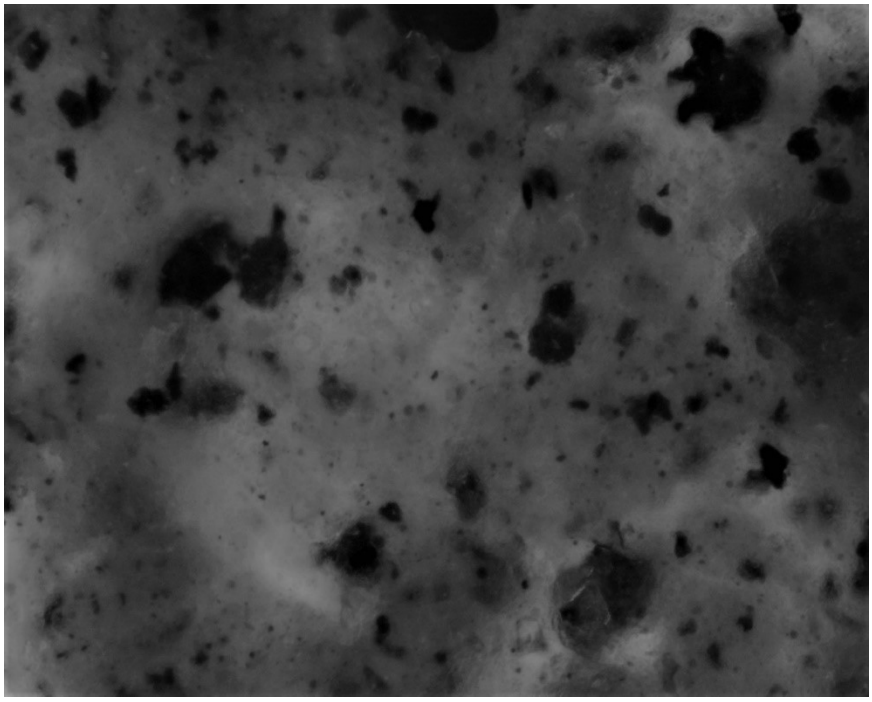

2-hour Sample

B.

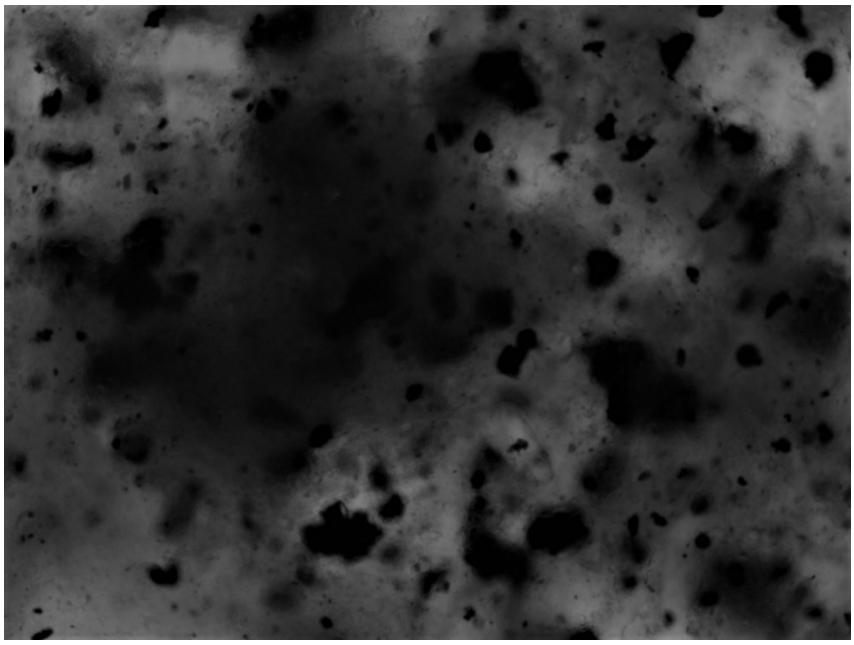

4-hour Sample

C.

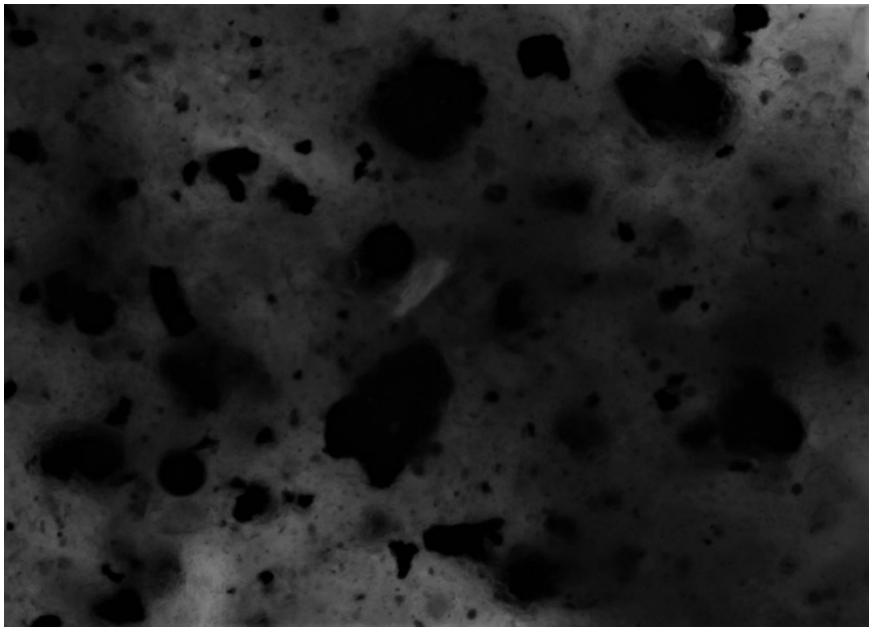

8-hour Sample

D.

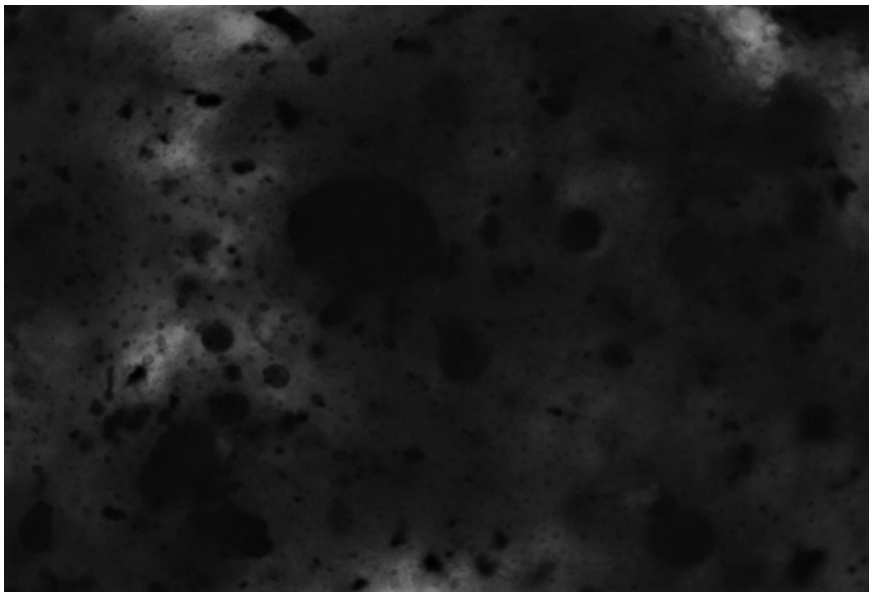

24-hour Sample

E.

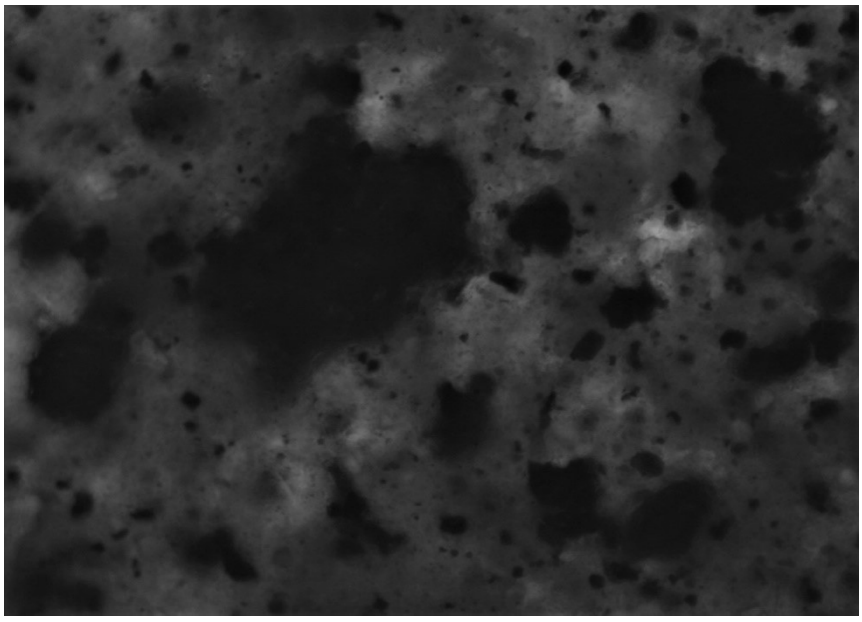

48-hour Sample

F.

Figure 118: Optical microscopy of polymer amended Oil sands tailings for dose of 600ppm, (A-1hour to F. 48 hour – of Polymer Mixing, Boundary Condition "Single drainage") Magnification 200x, view field 650/ micron wide)

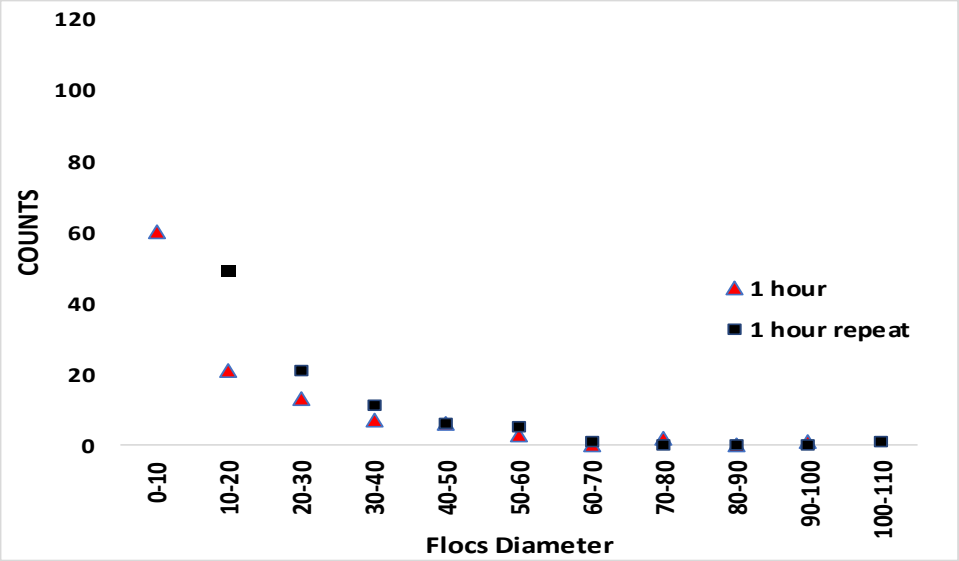

Figure 119: Optical microscope 1-hour Quantitative analysis of flocs size change (2 set of images)

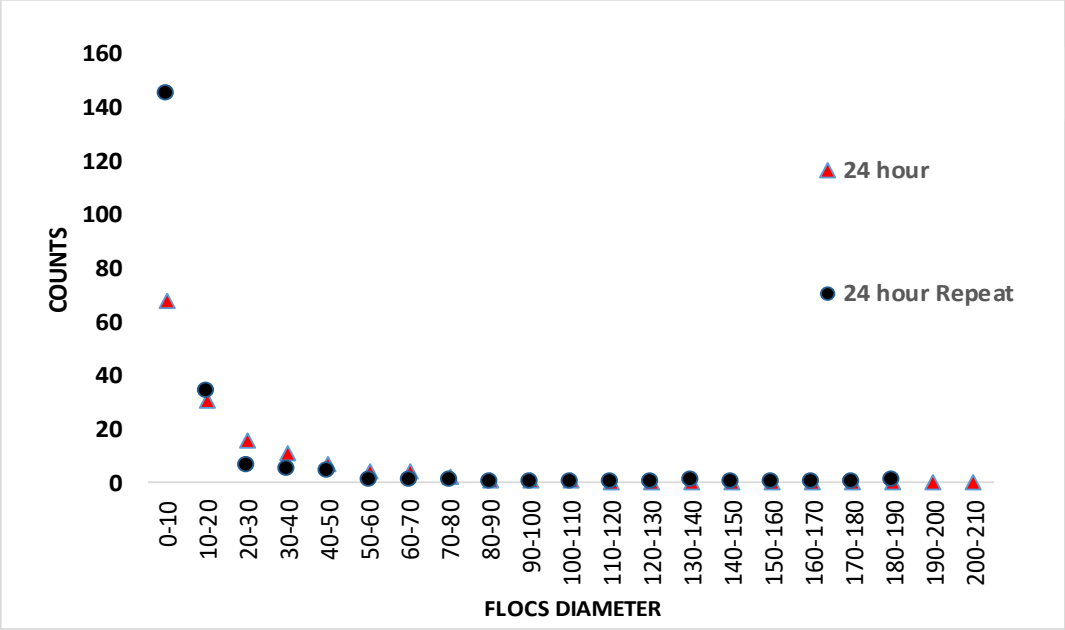

Figure 120: Optical microscope 24-hour quantitative analysis of flocs size (µm) change (2 set of images)

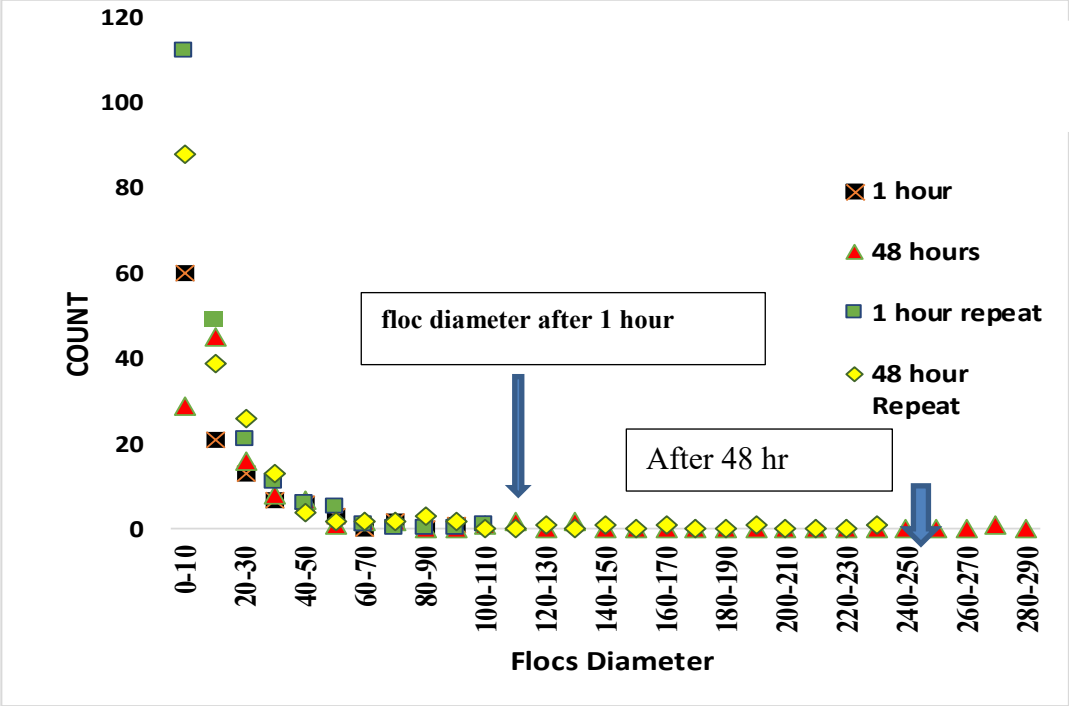

Figure 121: Repetitive Phase 3 Optical Microscopy Flocs diameter (µm) change results for 600ppm polymer dosed after 48 hour

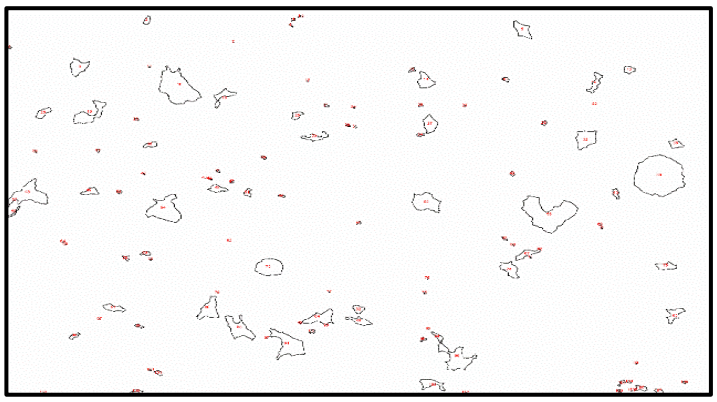

1 hour

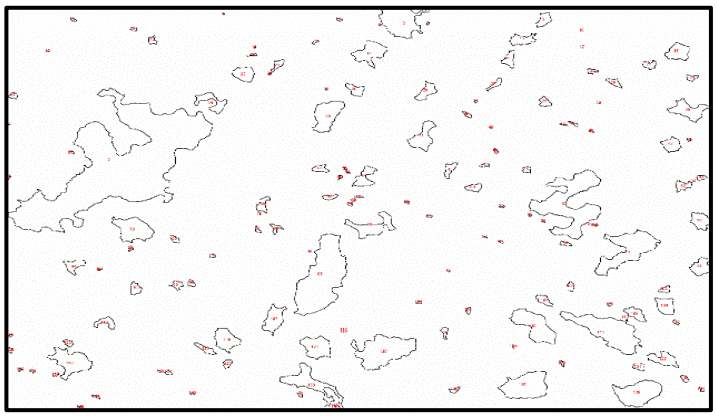

24 hours

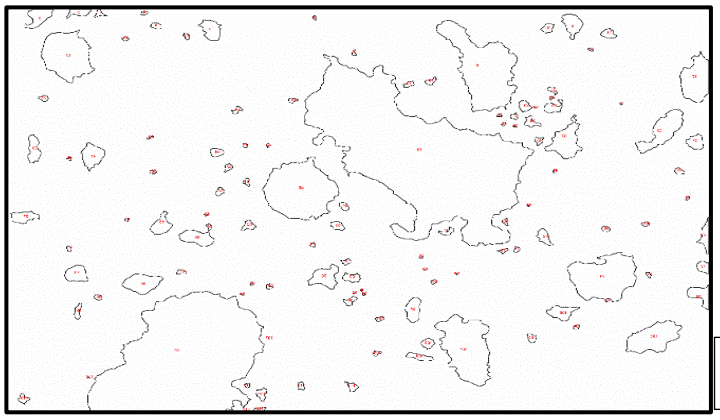

48hours

Figure 122: Floc size changes in optical microscope generated using Image J. (PHASE4 600PPM)

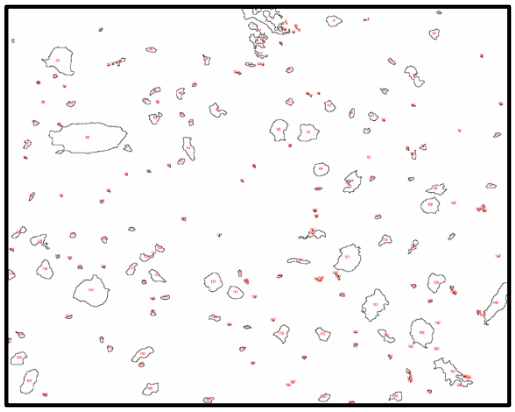

1 hour

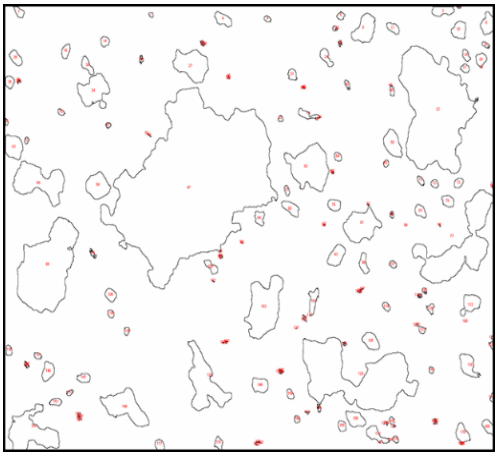

48 hours

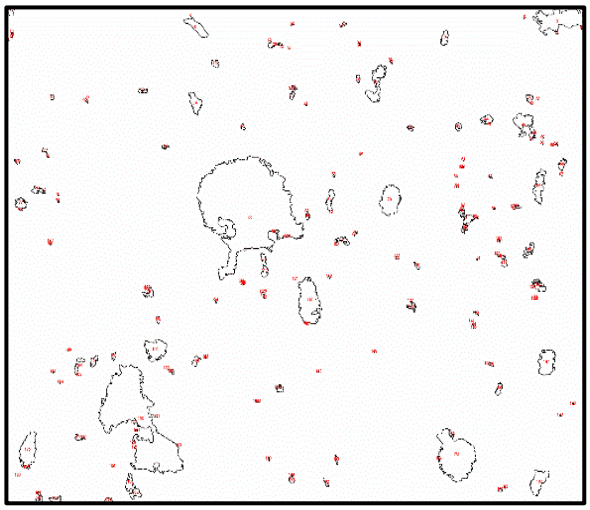

24 hours

Figure 123: Flocs size change in 2nd set of binary images for 600ppm.

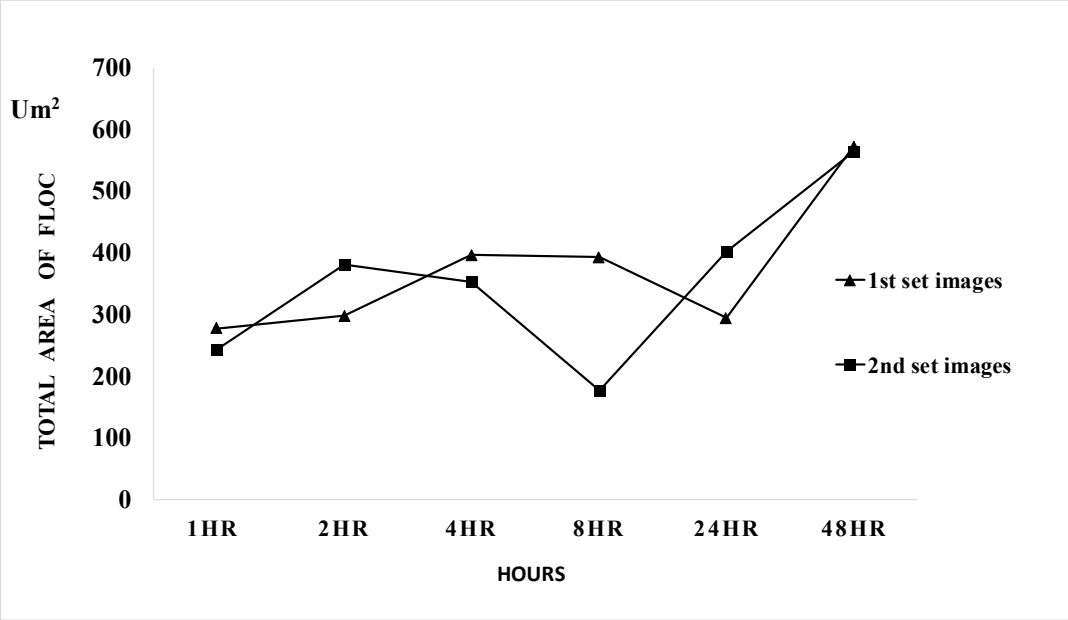

Figure 124: Total Area of flocs with time for 600 ppm single drainage from Optical Microscopy

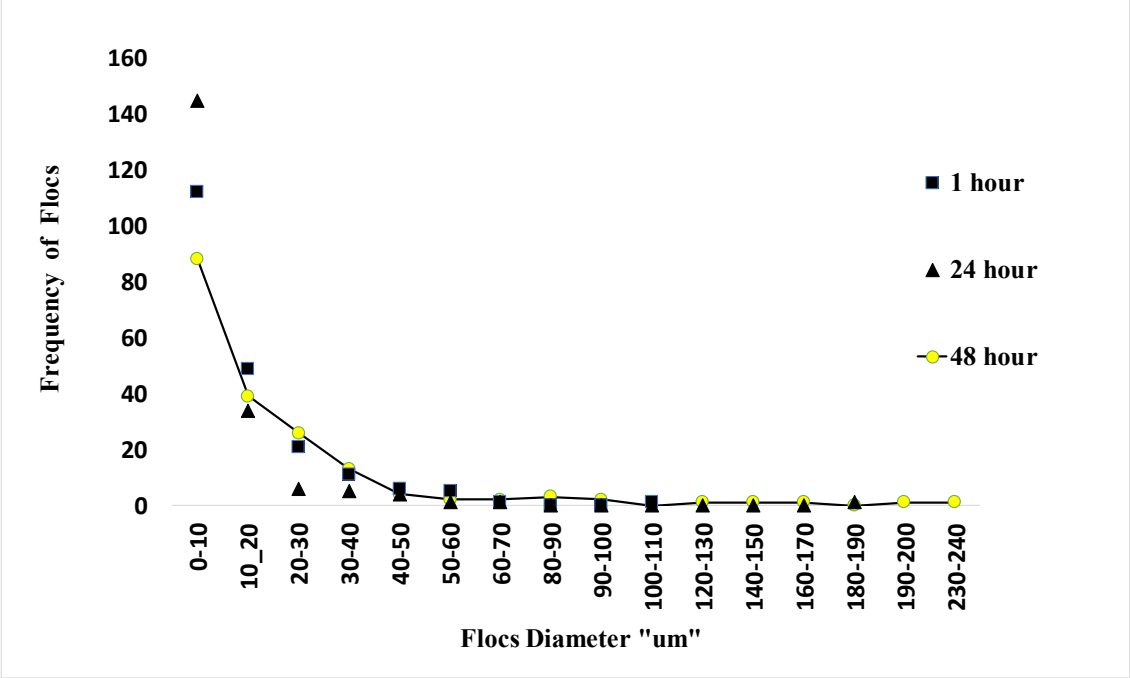

Figure 125: Flocs Count, Distribution Histogram for different date optical microscopic images

5.3 Phase 4 optical microscopy results (800ppm) single drainage

A repeatable increase in maximum floc size was also detected in the 800-ppm sample. Replicates for 1 hour, 12 hours, and 24 hours are shown in Figure 127 to Figure 129. Repeatability seems to be greater with respect to the 600-ppm sample, especially at the lower size ranges. The overall changes over 48 hours are shown in Figure 130, which compares size histograms at 1 hour and 48 hours.

In Figure 130 the maximum size of flocs in the 1-hour sample was found to be between 110-120 um. However, after 48 hours flocs size were dramatically increased reaching approximately to 290-300μm size. The second test results followed the same trend as the first set with only a 2 to 3 % increase or decrease in the size of flocs.

To give further credibility to these results, the results of the segmentation and thresholding binarized data was overlaid onto the real sample images as in Figure 131: Imported binary images to real images to check thresholding and binarization results It was found that segmented particles seem to fit to the outline of the real flocs quite well, which supports the methodology developed for FFT optical image processing.

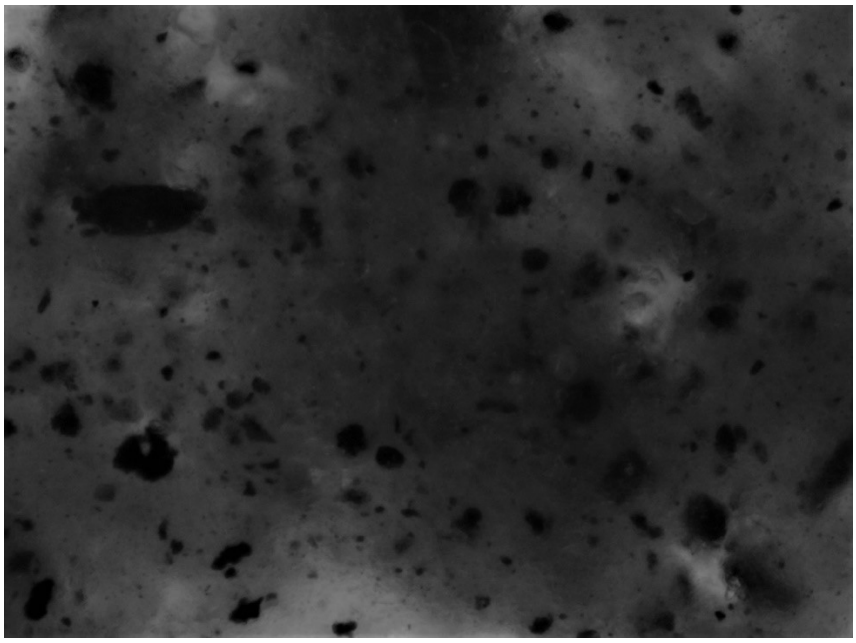

1-hour Sample

A.

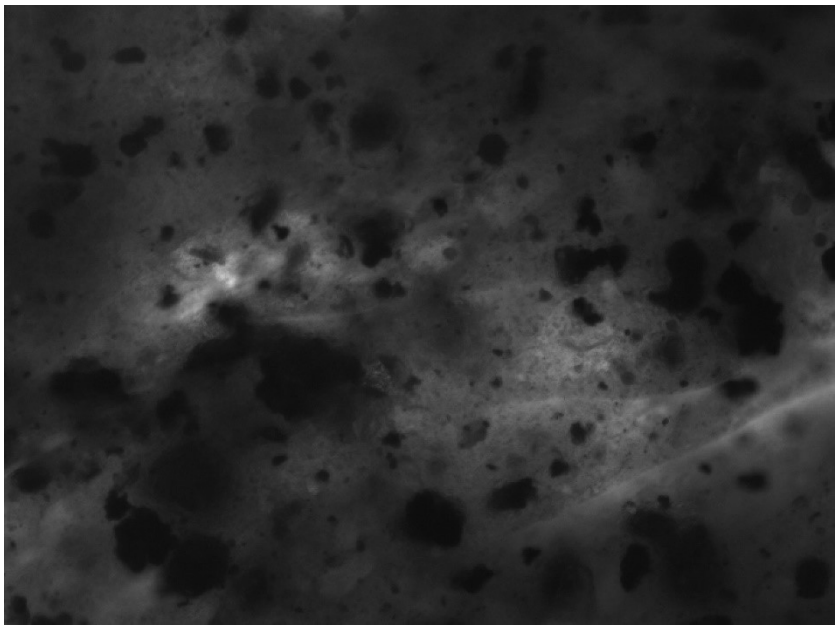

12-hour Sample

B

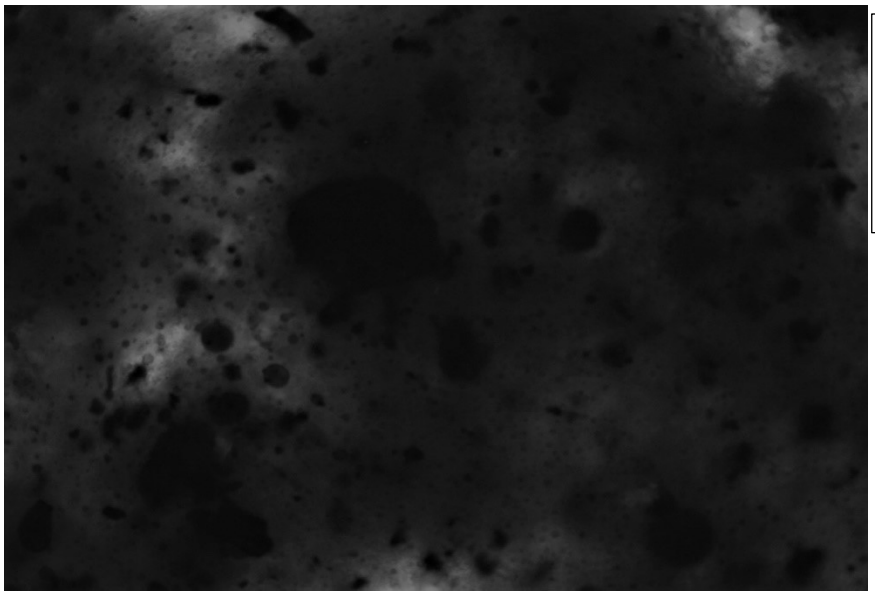

24-hour Sample

C

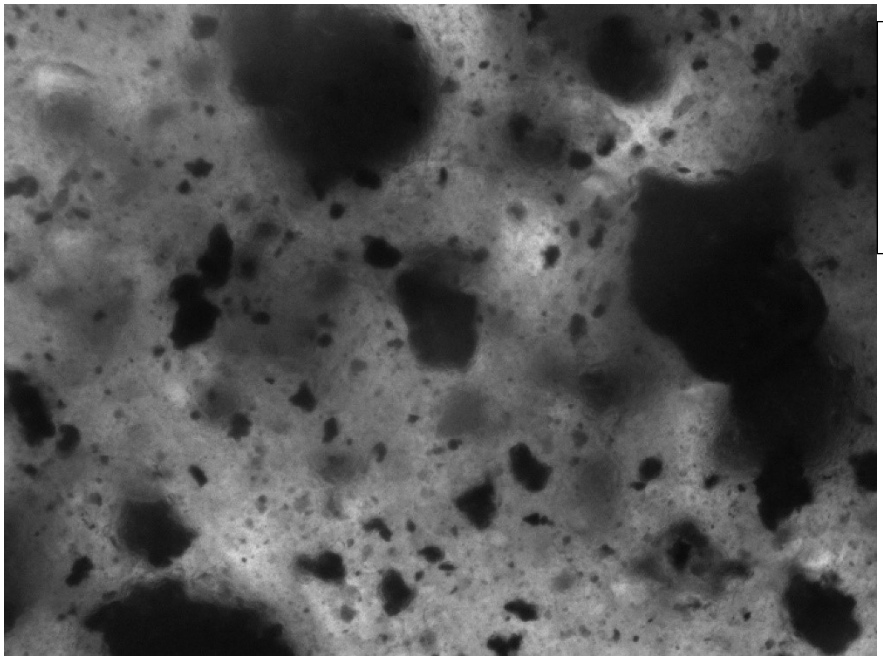

48-hour Sample

D

Figure 126: A-D Optical microscopy of polymer amended Oil sands tailings for dose of 800ppm, (1hour- and 48 hour – of Polymer Mixing, Boundary Condition "Single drainage") Magnification 200x, view field 650/ micron wide).

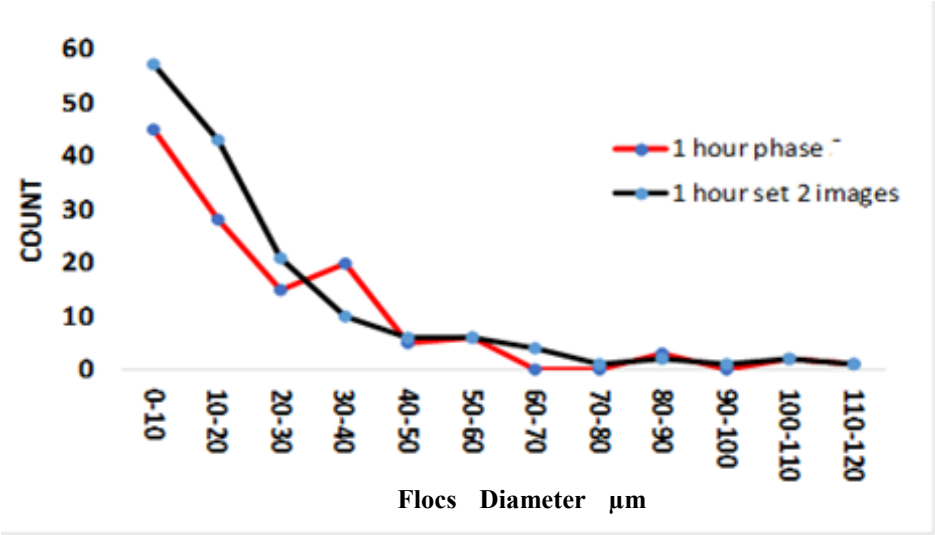

Figure 127 Repetitive Quantitative analysis results for 1-hour Optical microscope 800 ppm dose.

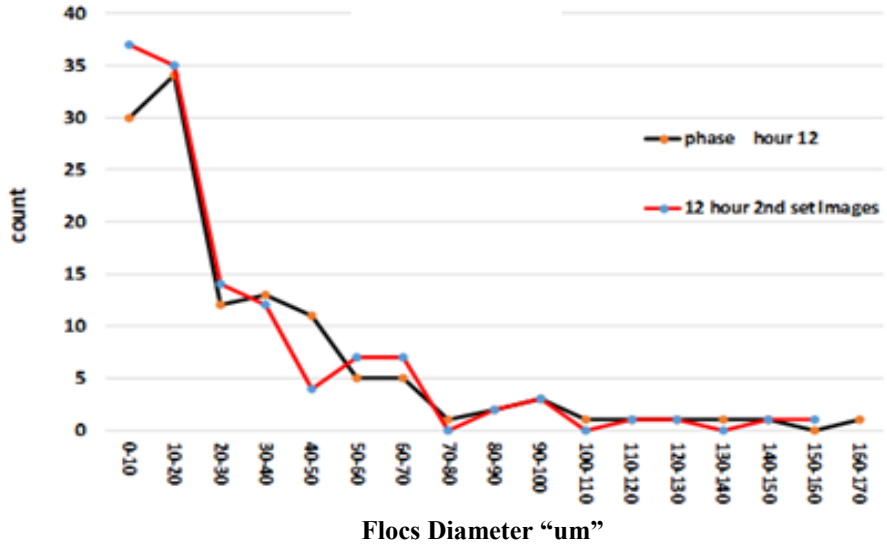

Figure 128: Repetitive Quantitative analysis results for 12-hour Optical microscope 800 ppm dose.

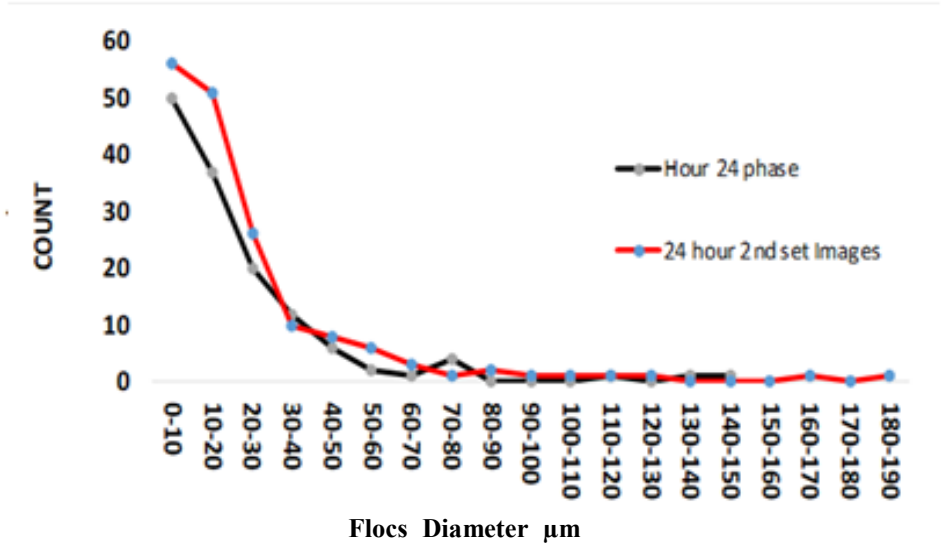

Figure 129: Repetitive Quantitative analysis results for 24-hour Optical microscope 800 ppm dose.

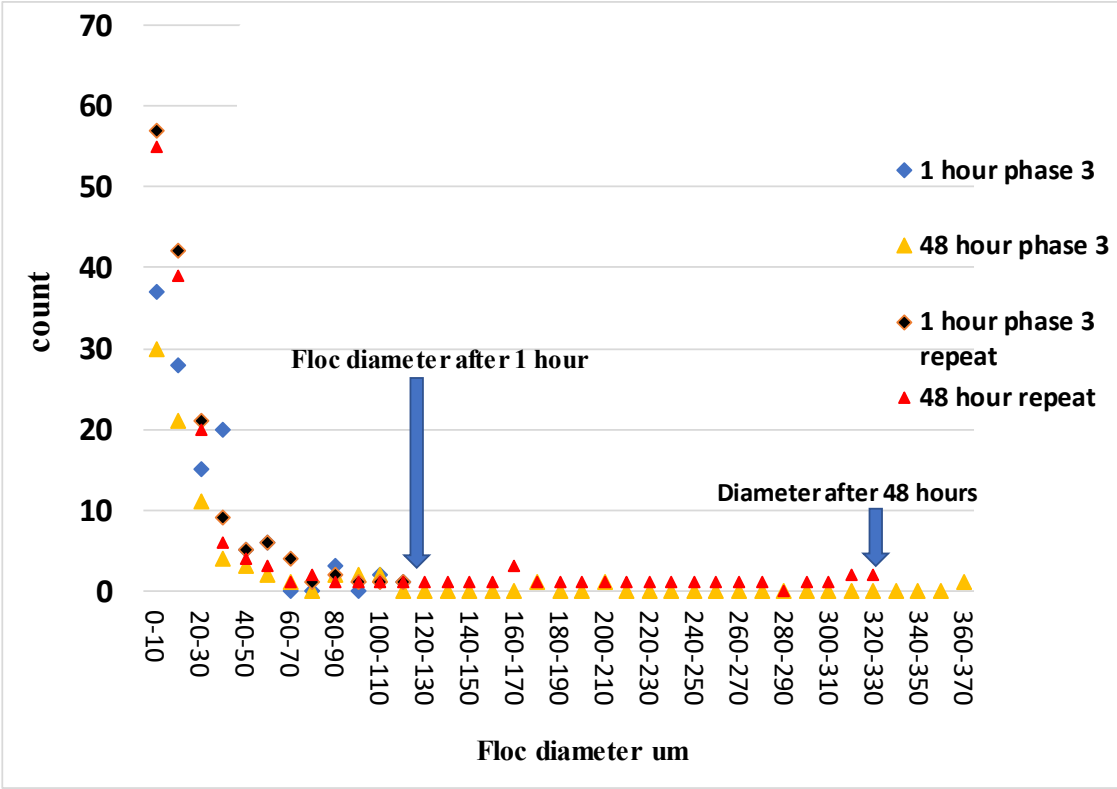

Figure 130: Repetitive Quantitative analysis and change in floc diameter results for 1 hour and 48-hour Optical microscope dosed with 800 ppm.

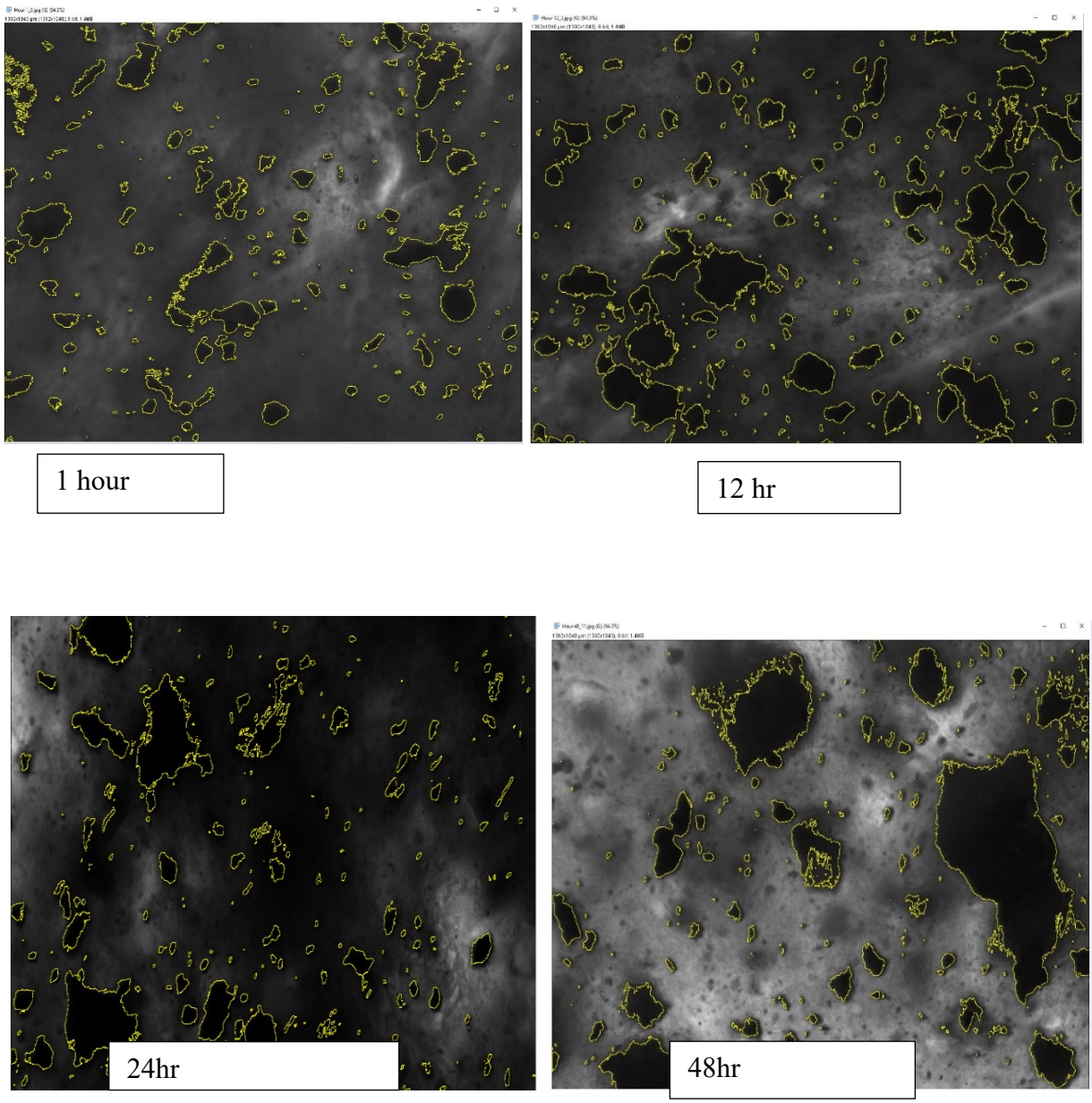

Figure 131: Imported binary images to real images to check thresholding and binarization results

5.4 Comparison Phase 3, and Phase 4 optical microscope results.

During the comparison of the two phases charts, it was found that flocs size has somewhat increased in the 800 ppm samples compared to 600 ppm samples. At 1 hour, the maximum size over two replicates was 70-100 microns for 600 ppm but was 100-120 microns for 800 ppm. Histograms for two of the replicates are shown in Figure 132. Furthermore, after 24 hours, the difference increased, with the 800 ppm samples showing maximum floc sizes up to 230 microns, while the 600 ppm samples showed an increase only up to 150 microns (Figure 133). However, as shown in Figure 134, by 48 hours the maximum floc size of 600 ppm and 800 ppm samples had increased up to 330 and 370 microns respectively.

Similar behavior is shown in the total area of flocs (Figure 135). The total area of flocs in every single image was added up to see the cumulative change in solids mass with time. The change in total solids mass in each area of image can be due to two factors, I) decrease in water content, and ii) increase in mass detectable through flocculation of very small and invisible particles into visible flocs or those small particles becoming part of visible flocs. It was found that during initial stages i.e. 1 hour, 8 hours, the increase in solids was faster in the 800-ppm sample. However, after 48 hours the total area after 48 hours for both 800 ppm and 600 ppm samples was approximately the same. This behavior was also noted in the real columns test, where the settlement of the tailings after 24 hours was largest for the 800 ppm sample (Figure 136), but after 7 days of no

detectable difference in the height of the tailings-water interface could be detected between the 600 ppm and 800 ppm samples (Figure 137).

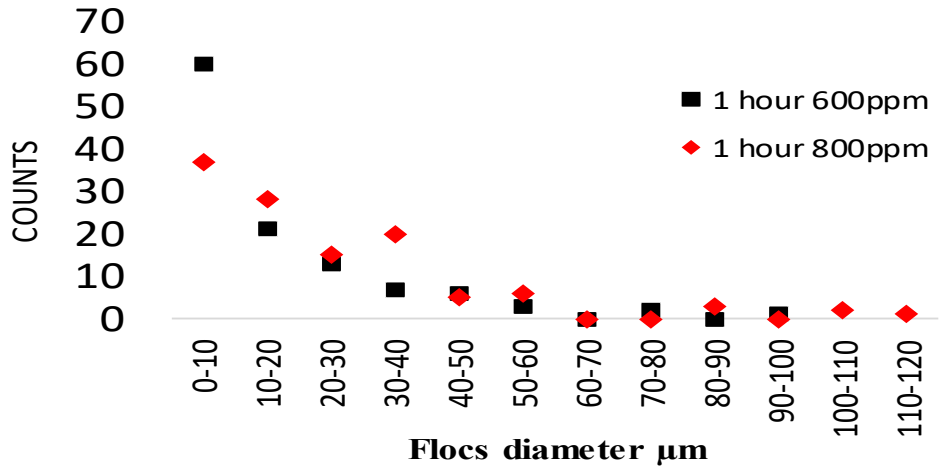

Figure 132: Flocs diameter comparison for 600 ppm and 800ppm, after 1-hour.

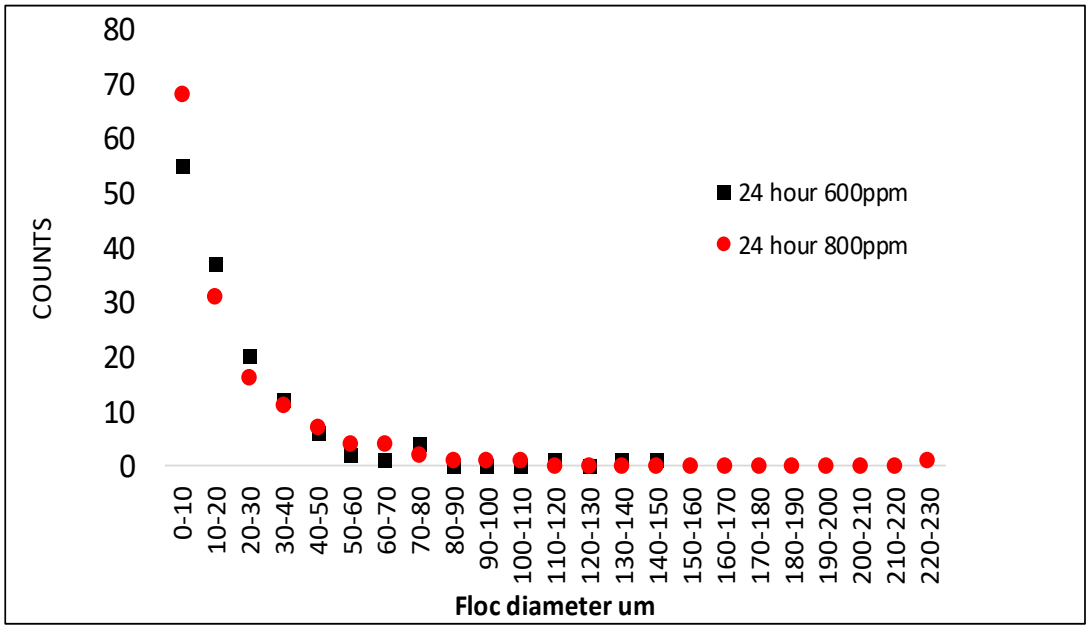

Figure 133: Flocs diameter comparison for 600 ppm and 800 ppm, after 24-hours

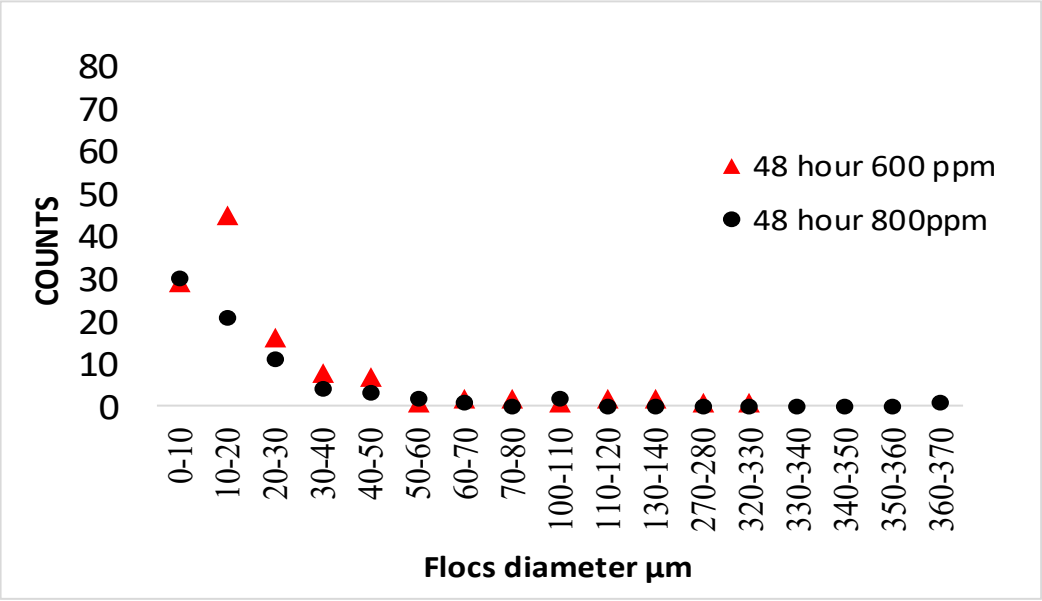

Figure 134: Floc diameter comparison for 600 ppm and 800pm after 48-hours

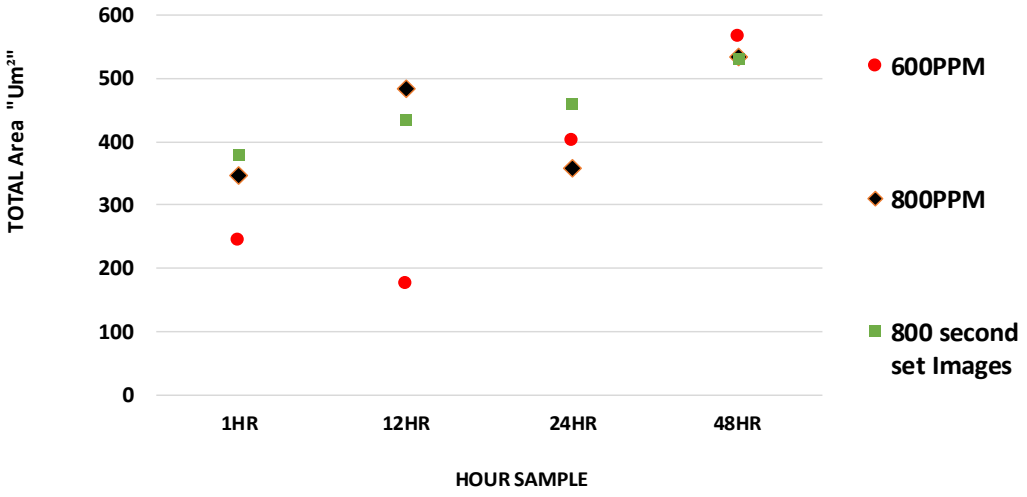

Figure 135: Total Area of flocs in each image on hourly basis calculated for 600ppm and 800ppm

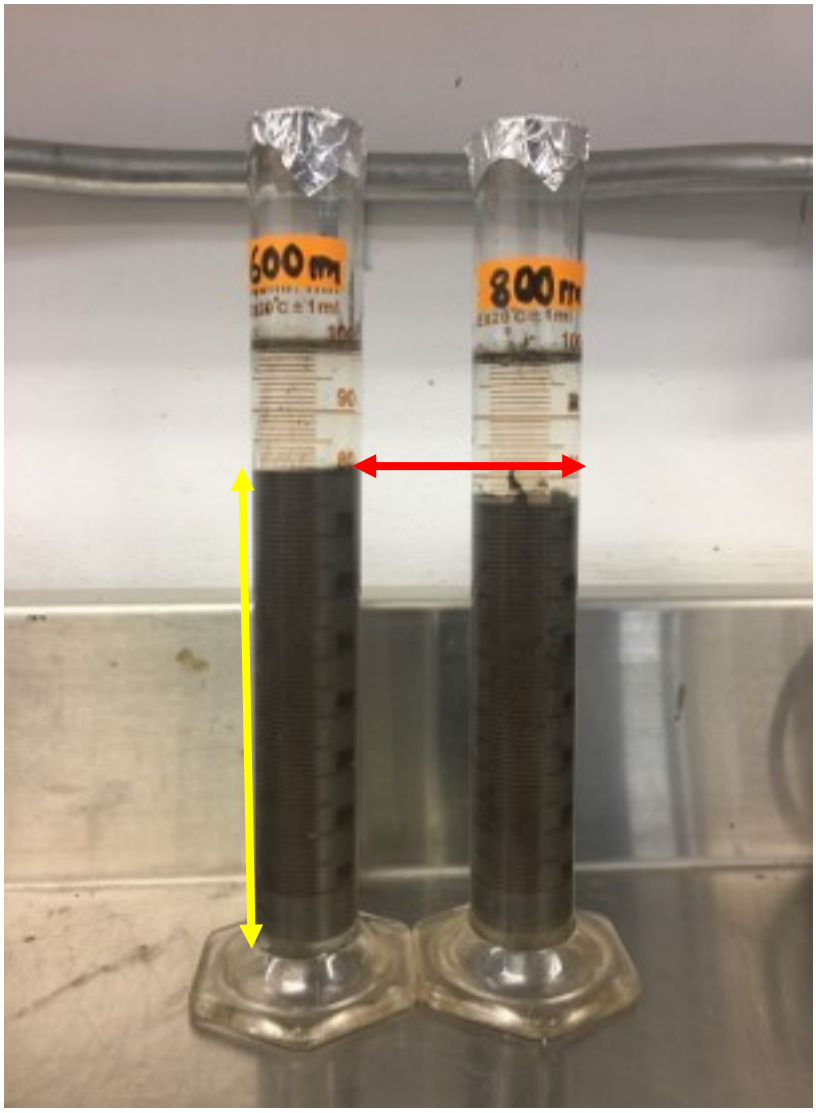

Figure 136: Settlement and height of tailings in columns after 24 hours for (left)600ppm and (right)800 ppm dosage different dosage.

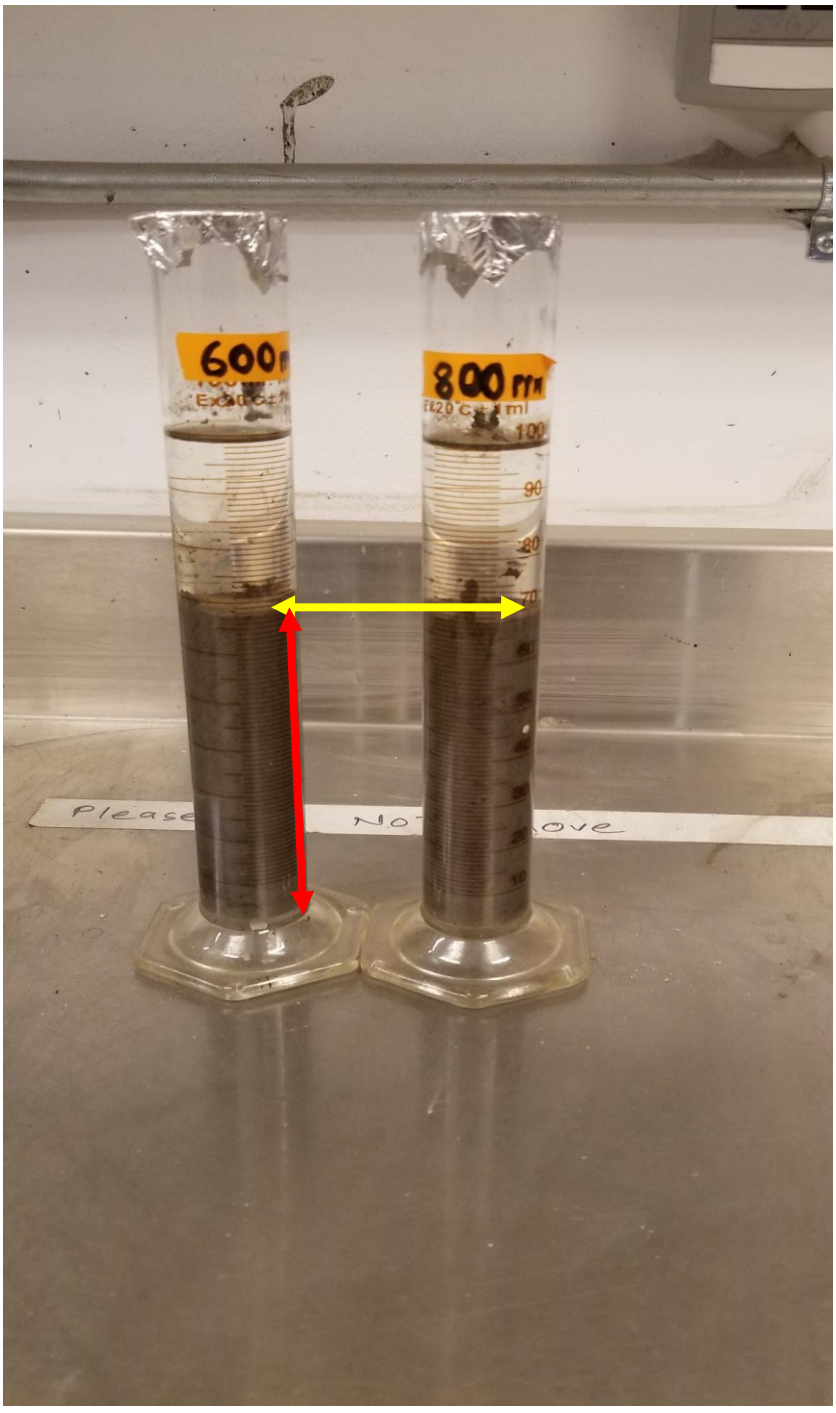

Figure 137: Settlement of same columns for different dosage after 7 days.

6 Chapter: **Conclusion & Recommendations**

This work studied the evolution of fabric in oil sands flocculated fluid fine tailings using SEM and OM images processed and interpreted using the Image J software and other image processing tools. Two polymer doses and two different boundary conditions (single and double drainage) were applied to initially 10 cm tall 15 cm diameter columns prepared at initial solids contents of 32-33%. The goal of the fabric analysis was to see if time-dependent changes in fabric occurred that were independent of consolidation.

6.1 Conclusions

- Repeatable trends in grain size and pore size distribution were obtainable for all types of experiments using the image processing methods developed in this work. For example, analysis of 3 images gave results with 3-4% difference from each other in terms of area porosity.
- The reported area porosity of the 2D images correlated with real porosity in the experiments. For example, double drainage showed lower porosity in images and in the experiments than single drainage.
- Analysis of both optical and SEM images suggest fabric changes over both short and long-time scales in the studied tailings. The optical microscopy shows quite clearly an increase in floc size over the 48 hours after sample preparation. The SEM images also suggest some ongoing fabric changes over days to weeks. This information will support conceptual model development related to observed changes in compressibility.

- The SEM results showed fabric differences between all three data sets examined. The sample with the best dewatering performance was the 600-ppm dose sample with double drainage. This sample showed larger average and maximum grain sizes and pore sizes than the other two samples. The grain sizes at Day 1 was substantially larger than for either of the single drainage tests.
- The 800-ppm optical microscope image analysis showed initially larger maximum floc sizes compared to 600 ppm dosed images. However, after 48 hours the difference in the maximum size substantially decreased. Therefore, while a short-term (<24 hour) evaluation of dewatering potential might suggest that 800 ppm would be the optimal choice, 600 Analysis of both optical and SEM images suggest fabric changes over both short and long-time scales in the studied tailings ppm eventually produces flocs of at least the same size as the 800 ppm tailings.
- The expected rate of sedimentation was increased as results of progressive flocculation till 48 hours, this resulted an increase in size of flocs leading to effective settlement in tailings columns.
- In general, the clarity of SEM images improves with lower water contents, while OM images have a minimum water content past which the technique is not usable.

.

6.2 Recommendation:

- There are many 2-D SEM images published in oil sands field to study the microstructure behavior of fluid fine tailings. 3-d images should be generated from fluid fine tailings the 3-D space will give new dimensions to visual and conceptual understanding as well as it will be a new inclusion in the oil sands field.
- Instead of using Greyscale Images, RGB images should be investigated, which may give more in-depth knowledge about other materials i.e. (bitumen, oil composition) in FFT samples by assigning proper pixel color to different intensities and defining each intensity i.e. red pore, blue grain, green bitumen or any other composition.
- The optical microscope technique is a powerful tool that allows for imaging of wet samples without requiring sample preparation by dehydration or rapid freezing, as in SEM. Some effort to extend the technique to lower water contents to allow for its use beyond 48 hours would be worthwhile

References:

Agarwal, S., Gupta, R. K., & Doraiswamy, D. (2009). A model for the collision efficiency of shear-induced agglomeration involving polymer bridging. Colloids and Surfaces A: Physicochemical and Engineering Aspects, 345(1-3), 224-230.

Ahmed, S., Lovell, C. W., & Diamond, S. (1974). Pore sizes and strength of a compacted clay.

Alberta energy regulatory board 2005. http://www.aer.ca/about-aer.

Arganda-Carreras, I., Kaynig, V., Rueden, C., Eliceiri, K. W., Schindelin, J., Cardona, A., & Sebastian Seung, H. (2017). Trainable Weka Segmentation: a machine learning tool for microscopy pixel classification. Bioinformatics, 33(15), 2424-2426.

BGC Engineering Inc., 2010. Oil Sands Tailings Technology Review. Oil Sands Research and Information Network, University of Alberta, School of Energy and the Environment, Edmonton, Alberta. OSRIN Report No. TR-1. 136 pp.

Beier, Nicholas, Ward Wilson, Adedeji Dunmola, and David Sego. (2013). Impact of Flocculation-Based Dewatering on the Shear Strength of Oil. NRC Research Press 1007 (July 2012): 1001–1007.

Beier, N. A. (2015). Development of a Tailings Management Simulation and Technology Evaluation Tool (Doctoral dissertation, University of Alberta).

Been, K. (1980). Stress strain behavior of a cohesive soil deposited under water (Doctoral dissertation, University of Oxford)..

Binet, J. L., & Mathé, G. (1962). Optical and electron microscope studies of the immunologically competent cells during the reaction of graft against the host. Annals of the New York Academy of Sciences, 99(3), 426-431.

Bothe, R., Dennis, J., Errington, J., Fahner, L., and Straker, J. 2010. Shell proposed Jack Mine expansion and Pierre River Mine projects, environmental impact assessment and application review, Fort McKay Industry Relations Corporation, Alberta.

Bajwa, T.M. (2015). Microstructure and macroscopic behavior of polymer amended oil sands mature fine tailings. (Doctoral dissertation, Carleton University, Ottawa, Canada).

Bullock, P., & Murphy, C. P. (1980). Towards the quantification of soil structure. Journal of Microscopy, 120(3), 317-328.

Bovi, R. C., Boschi, R. S., de Carvalho, C. C., & Cooper, M. (2016). Analysis of the soil sand fraction and recent sediments deposits: an approach based on two-dimensional image analysis. Soil Science, 181(11/12), 513-519.

COSIA. (2015). Tailings Projects. Retrieved March 2018, from Canada's Oil Sands Innovation Alliance http://www.cosia.ca/initiatives/tailings/tailings-projects.

Coulter, H. B. (1954). U.S. Patent No. 2,678,730. Washington, DC: U.S. Patent and Trademark Office.

Canadian association of petroleum producers (https://www.capp.ca/publications-and-statistics/crude-oil-forecast)

Clark, K.A., 1944. Hot water separation of Alberta bituminous sands. Can. Inst. Mining Metallurgy Trans., 47: 257.

Clark, K.A., and Pasternack, D.S. (1932). Hot water separation of bitumen from Alberta bituminous sand. Industrial & Engineering Chemistry, 24(12): 1410–1416.

Chalaturnyk, R.J., Scott, J.D., and O¨ zu¨m, B. 2002. Management of oil sands tailings. Petrol. Sci. Technol. 20(9–10): 1025–1046. doi:10.1081/LFT-120003695

Cymerman, G. K. (1999). Thickening and Disposal of Fine tails from oil sand processing. The 3rd UBC-McGill Int. Sym. Fund. of Mineral Processing. Quebec City: CIM

Carrier, W. D., Bromwell, L.G, and Somogyi, F. 1983. "Design Capacity of Slurred Mineral Waste Ponds". Journal of Geotechnical Engineering. 109 (5): 699-716.

Cássaro, F. A. M., Borkowski, A. K., Pires, L. F., Rosa, J. A., & da Costa Saab, S. (2011). Characterization of a Brazilian clayey soil submitted to conventional and no-tillage management practices using pore size distribution analysis. Soil and Tillage Research, 111(2), 175-179.

Cui, L., Li, L., Zhang, A., Pan, G., Bao, D., & Chang, A. (2011). Biochar amendment greatly reduces rice Cd uptake in a contaminated paddy soil: a two-year field experiment. BioResources, 6(3), 2605-2618.

Cooper, M., Boschi, R. S., Silva, V. B. D., & Silva, L. F. S. D. (2016). Software for micro morphometric characterization of soil pores obtained from 2-D image analysis. Scientia Agricola, 73(4), 388-393.

Danilaos, D.G. 1993. Introduction to the ESEM instrument. Microscopy Research and Technology, 25: 354 – 371.

Dawson, R. F., Sego, D. C., & Pollock, G. W. (1999). Freeze-thaw dewatering of oil sands fine tails. Canadian geotechnical journal, 36(4), 587-598..

Devenny, D., & Nelson, R. (2009). Economic screening of tailings options for oil sands plants. Tailings and Mine Waste. Banff, Alberta: University of Alberta, Department of Civil & Environmental Engineering, Edmonton, Alberta.

Devenny, D.W., (2010). A screening study of oil sands tailings technologies and practices. Prepared for Alberta Energy Research Institute, Edmonton, Alberta.

Elliot, T. R., & Heck, R. J. (2007). A comparison of optical and X-ray CT technique for void analysis in soil thin section. Geoderma, 141(1-2), 60-70.

Egerton, R. F. (2005) Physical principles of electron microscopy: an introduction to TEM, SEM, and AEM. Springer, 202.

Fair, A. (2008). The past, present and future of tailings at Syncrude. International Oil Sands Tailings Conference. Edmonton, Alberta, Canada.

Fard, M. A.H. 2011. Characterization of clay minerals in the Athabasca oil sands in water extraction and nonaqueous solvent extraction processes Ph.D. thesis. Department of Chemical and Materials Engineering, The University of Alberta, Edmonton, Alberta

Fox, P., & Berles, J. (1997). CS2: A piecewise-linear model for large strain consolidation. International Journal for Numerical and Analytical Methods in Geomechanics, 21(7), 453 - 475.

Ferreira, T., and Rasband, W. (2012). Image J/Fiji 1.46 User Guide, available from (http://imagej.nih.gov/ij/docs/guide/user-guide.pdf)

FTFC. (1995). Clark hot water extraction for fine tailings. In Advances in oil sands tailings research. Fine Tailings Fundamentals Consortium (FTFC), Oil Sands and Research Division, Alberta Department of Energy, Edmonton, Alberta. 1:79–84

Griffiths, F.J., and Joshi, R.C. 1989. Change in pore size distribution due to consolidation of clays. Geotechnique, 39(1): 159 -167.

Gardner, C. M., Laryea, K. B., & Unger, P. W. (1999). Soil physical constraints to plant growth and crop production. Land and Water Development Division, Food and Agriculture Organization.

Goldstein, J. (2003) Scanning electron microscopy and x-ray microanalysis. Kluwer Adacemic/Plenum Pulbishers, 689 p

Gonzales R. C. and Woods R. E. (1992) Digital Image Processing. Addison-Wesley Publishing Company.

Gagné, F., Douville, M., André, C., Debenest, T., Talbot, A., Sherry, J., & Bickerton, G. (2012). Differential changes in gene expression in rainbow trout hepatocytes exposed to extracts of oil sands process-affected water and the Athabasca River. Comparative Biochemistry and Physiology Part C: Toxicology & Pharmacology, 155(4), 551-559.

Gibson, R. E., England, G. L. and Hussey, M.J.L. 1967. "The Theory of One-Dimensional Consolidation of Saturated Clays". Géotechnique. 17 (3): 261-273.

Hamza, H. A., Stanonik, D. J., & Kessick, M. A. (1996). Flocculation of lime-treated oil sands tailings. Fuel, 75(3), 280-284

Holowenko, F.M., MacKinnon, M.D., and Fedorak, P.M. 2000. Methanogens and sulfate-reducing bacteria in oil sands fine tailings wastes. Can. J. Microbiol. 46: 927–937.

Herman, B., & Lemasters, J. J. (Eds.). (2012). Optical microscopy: emerging methods and applications. Elsevier.

Jeeravipoolvarn, S. 2005 Compression behavior of thixotropic oil sands tailings. M.A.Sc. thesis, Department of Civil and Environmental Engineering, The University of Alberta, Edmonton, Alberta.

Jeeravilpoolvarn, S., Miller, W., and Scott, J.D. (2014). Modelling effect of bitumen extraction processes on oil sands tailings ponds. 67th Canadian Geotechnical Conference Regina, SK.

Jury, W. A., Gardner, W. R., & Gardner, W. H. (1991). Soil physics. John Wiley & Sons, New York. Soil physics. John Wiley & Sons, New York.

Kaye B. H. (1989) A Random Walk Through Fractals, VCH Publishers.

Kaur, D., & Kaur, Y. (2014). Various image segmentation techniques: a review. International Journal of Computer Science and Mobile Computing, 3(5), 809-814.

Kynch, G. J. (1952). A theory of sedimentation. Transactions of Faraday Society, 48, 166-176.

Latief, F. D. E. (2016, August). Analysis and Visualization of 2D and 3D Grain and Pore Size ofFontainebleau Sandstone Using Digital Rock Physics. In Journal of Physics: Conference Series (Vol. 739, No. 1, p. 012047). IOP Publishing..

Lyn, D. A., Stamou, A. I., & Rodi, W. (1992). Density currents and shear-induced flocculation in sedimentation tanks. Journal of hydraulic Engineering, 118(6), 849-867.

Liang J, Guo Z, Deng L, Liu Y (2015). Mature fine tailings consolidation through microbial induced calcium carbonate precipitation. Can J Civ Eng 42:1–4

Lipiec, J., Tarkiewicz, S., & Kossowski, J. (1991). Soil physical properties and growth of spring barley as related to the degree of compactness of two soils. Soil and Tillage Research, 19(2-3), 307-317.

Latief, F. D. E. 2016, August. Analysis and Visualization of 2D and 3D Grain and Pore Size of Fontainebleau Sandstone Using Digital Rock Physics. In Journal of Physics: Conference Series (Vol. 739, No. 1, p. 012047). IOP Publishing.

Morgenstern, N.R., Fair, A.E., and McRoberts, E.C. 1988. Geotechnical engineering beyond soil mechanics — a case study. Canadian Geotechnical Journal, 25: 637–661

Matthews, J. G., Dhadli, N., House, P., & Simms, P. (2011, April). Field trials of thin-lift deposition of amended mature fine tailings at the Muskeg River Mine in Northern Alberta. In Proceedings of the 14th International Seminar on Paste and Thickened tailings (pp. 271-280). Australian Centre for Geomechanics.

Miller, W. G. (2010). Comparison of geoenvironmental properties of caustic and noncaustic oil sand fine tailings. University of Alberta.

Morgenstern, N.R., and Scott, J.D. 1995. Geo technique of fine tailings management. In the Proceedings of the ASCE Specialty Conference on Geo environment, New Orleans, Louisiana, 24 - 26 February 2000, Geotechnical Special Publication, 46(2): 1663- 1683.

Miller, Warren (2010) “Comparison of Geoenvironmental Properties of Caustic and Noncaustic Oil Sand Fine Tailings” Phd Thesis, University of Alberta Civil and Environmental Engineering, Alberta, Canada

Mikula, R.J. (2012). Advances in oil sands tailings handling: building the base for reclamation, In Restoration and Reclamation of Boreal Ecosystems: Attaining Sustainable Development, D.H. Vitt and J.H. Bhatti, editors (Cambridge University Press, 2012).

Masliyah, J., Zhou, Z., Xu, Z., Czarnecki, J., and Hamza, H. 2004. Understanding water based bitumen extraction from Athabasca Oil Sands. The Canadian Journal of Chemical Engineering, 82 : 628 – 654.

Mizani, S., (2016). Experimental study and surface deposition modelling of amended oil sands tailings products". PhD thesis, Carleton University, Ottawa, Canada

Masliya, J., Zhou, Z., Xu, Z., Czarnecki, J., and Hamza, H. 2004. Understanding water-based bitumen extraction from Athabasca Oil Sands. The Canadian Journal of Chemical Engineering, 82: 628 – 654

McKenna, G. (2009, November). Techniques for creating mining landforms with natural appearance. In Proceedings of the tailings and mine waste conference, Banff, Alberta (pp. 1-4).

Mackinnon, M.D., Matthews, W.H., and Shah, W.H., and Cuddy, R.G. 2001. Water quality issues associated with composite tailings (CT) technology for managing oil 317

Mackinnon, M.D., and Boerger, H. 1986. Description of two treatment methods for detoxifying oil sands tailings pond water. Water pollution Research Journal of Canada, 21: 496 – 512

Mizani, S., Soleimani, S., & Simms, P. (2013, June). Effects of polymer dosage on dewaterability, rheology, and spreadability of polymer-amended mature fine tailings. In Proceedings of the 16th international seminar on paste and thickened tailings, InfoMine, Vancouver (pp. 117-131).

Monroy, R., Zdravkovic, L., and Ridley, A. 2010. Evolution of microstructure in compacted London clay during wetting and loading. Geotechnique, 60(2): 105 -119

Mitchell, J.K., and Soga, K. 2005. Fundamentals of soil behavior. John Wiley & Sons Inc., Hoboken, New Jersey

Mikula, R.J., and Munoz, V.A. 2000. Characterization of emulsions and suspensions in the petroleum industry using Cryo-SEM and CLSM: colloids and surfaces: Physicochemical and Engineering Aspects, 174: 23–36

Marcelino, V., Cnudde, V., Vansteelandt, S., & Caro, F. (2007). An evaluation of 2D-image analysis techniques for measuring soil Microporosity. European Journal of Soil Science, 58(1), 133-140.

Macedo, A., Vaz, C. M. P., Naime, J. M., Cruvinel, P. E., & Crestana, S. (1999). X-ray microtomography to characterize the physical properties of soil and particulate systems. Powder technology, 101(2), 178-182.

Moore C. A. and Donaldson C. F. (1993) Quantifying Soil Microstructure Using Fractals. Geotechnique, Vol. 45 No.1, 105-116 Murthy Macedo A, Vaz C. M. P., Nairne 1. M., Cruvinel P. E. and Crestana S. (1999) X-Ray Microtomography To

Characterize The Physical Properties Of Soil And Particulate Systems. Powder Technology, Vol. 101, 178-182.

Masliyah, J., Zhou, Z., Xu, Z., Czarnecki, J., and Hamza, H. (2004). Understanding water-based bitumen extraction from Athabasca Oil Sands. The Canadian Journal of Chemical Engineering, 82: 628 – 654.

Nix, P.G., and Martin, R.W. 2006. Detoxification and reclamations of Suncor's oil sands tailing ponds. Environmental Toxicology and Water Quality, 7(2): 171 – 188 Kasperski, K. (1992). AOSTRA Journal of Research, 8, 11-53

Novoselov, K. S., Jiang, D., Schedin, F., Booth, T. J., Khotkevich, V. V., Morozov, S. V., & Geim, A. K. (2005). Two-dimensional atomic crystals. Proceedings of the National Academy of Sciences, 102(30), 10451-10453.

Nielsen, B.D. 2004. Non-destructive soil testing using x-ray computed tomography. M.A.Sc. thesis, Department of Civil Engineering, Montana State University Bozeman, Montana.

Naphade, M. R., Yeung, M. M., & Yeo, B. L. (1999, December). Novel scheme for fast and efficent video sequence matching using compact signatures. In Storage and Retrieval for Media Databases 2000 (Vol. 3972, pp. 564-573). International Society for Optics and Photonics.

Owolagba, J., and Azam, S. 2013. Unsaturated soil properties of centrifuged oil sand fine tailings. In Proceedings of the 66th Canadian Geotechnical Conference on Geoscience for sustainability, Montreal, Quebec, 29 September – 03 October 2013.

Oladipo omostoso treatment of fluid tailings in PIT lakes “technology solution for oil sands tailings management” Presentation at COSIA 2018 innovation summit.

Price, 2008. 11 million liters a day: The tar sands leaking Legacy, Environmental Defense 2008.

Pane, V., & Schiffman, R. L. (1997). The permeability of clay suspensions. Geotechnique, 47(2), 273-288.

Passoni, S., Borges, F. D. S., Pires, L. F., Saab, S. D. C., & Cooper, M. (2014). Software Image J to study soil pore distribution. Ciência e Agrotecnologia, 38(2), 122-128.

Pires, L. F., Reichardt, K., Cooper, M., Cássaro, F. A., Dias, N. M., & Bacchi, O. O. (2009). Pore system changes of damaged Brazilian oxisols and nitosols induced by wet-dry cycles as seen in 2-D micromorphologic image analysis. Anais da Academia Brasileira de Ciências, 81(1), 151-161..

Pires, L. F., Cooper, M., Cássaro, F. A. M., Reichardt, K., Bacchi, O. O. S., & Dias, N. M. P. (2008). Micromorphological analysis to characterize structure modifications of soil samples submitted to wetting and drying cycles. Catena, 72(2), 297-304.

Pane, V., and Schiffman, R. L. 1985. "A note on sedimentation and consolidation".Géotechnique. 35 (1): 69-72.

Passoni, S., Borges, F. D. S., Pires, L. F., Saab, S. D. C., & Cooper, M. (2014). Software Image J to study soil pore distribution. Ciência e Agrotecnologia, 38(2), 122-128.

Pollock, G. (1988). Large Strain Consolidation of Oil Sand Tailings Sludge, MS. c. Thesis, University of Alberta, Edmonton, Canada.

Qiu, Yunxin. 2000. “Optimum deposition for sub-aerial tailings disposal”. Thesis (Ph.D.) - University of Alberta, 2000.

Qi, S., Simms, P., & Vanapalli, S. (2017). Piecewise-Linear Formulation of Coupled Large-Strain Consolidation and Unsaturated Flow. I: Model Development and Implementation. Journal of Geotechnical and Geoenvironmental Engineering, 143(7), 04017018

Rogers, V.V., Wickström, M., Liber, K., and Mackinnon, M.D. 2001. Acute and sub chronic mammalian toxicity of naphthenic acids from oil sands tailings. Toxicological Sciences, 66(27): 341 – 355

Reimer, L. (2013). Scanning electron microscopy: physics of image formation and microanalysis (Vol. 45). Springer.

Roshani, A., Fall, M., and Kennedy, K. (2017). "Drying Behavior of Mature Fine Tailings Pre-Dewatered with Super-Absorbent Polymer (SAP): Column Experiments,” Geotechnical Testing Journal, Vol. 40, No. 2, 2017, pp. 210-220.

Romero E., and Simms, P. H. 2008. Microstructure investigation in unsaturated soil: A review with special attention to contribution of mercury intrusion porosimetry and environmental scanning electron microscopy. Geotech. Geo. Engg., 26: 705 – 727

Ringrose-Voase, A. J., & Bullock, P. (1984). The automatic recognition and measurement of soil pore types by image analysis and computer programs. Journal of Soil Science, 35(4), 673-684.

Russ J. C. (1994) The Image Processing Handbook, CRC Press.

Salam, A. M., Simms, P. H. and Örmeci, B. 2018. Structuration in polymer amended oil sands fine tailings. Submitted to the 71st Canadian Geotechnical Conference. Edmonton, Alberta, Canada

Salam, A. M., Simms, P. H. and Örmeci, B. 2017. Investigation of creep in polymer amended oil sands tailings. Proceedings of the 70th Canadian Geotechnical Conference. Ottawa, Ontario, Canada.

Scott, J.D., Jeeravipoolvarn, S., Kabwe, L., Wilson G.W. (2013). Properties Which Affect the Consolidation Behaviour of Mature Fine Tailings. In Proceedings of the 17th International conference on Tailings and Mine Waste, Banff, Alberta.

Schiffman, R. L., Chen, A.T.F., and Jordan, J. C. 1969. "An analysis of consolidation theories". Journal of the Soil Mechanics and Foundation division, Proceedings of the American Society of Civil Engineers, 95 (SM1): 285-312.

Schiffman, R.L., Vick, S.G. and Gibson, R.E. 1988. "Behavior and properties of hydraulic fills". In Hydraulic Fill Structures, American Society of Civil Engineers, Colorado State University. Van Zyl, D.J. and Vick, S.G. (eds): 166-202.

Sobkowicz, J.C. (2012). Oil Sands Tailings Technology Deployment Roadmap Project Report – Volume 1, Component Results.

Safe drinking water foundation (https://www.safewater.org/)

Soane, D. W. (2010). Oil Sands Tailings Treatment Via Surface Modification of Solids with Polymers. 2nd International Oil Sands Tailings Conference, 135-140

Simms, P.H. and Yanful, E.K. 2001. Measurement and estimation of soil–pore shrinkage in a clayey till during soil-water characteristic curve tests. Canadian Geotechnical Journal, 38(4): 741 - 754.

Taina, I. A., Heck, R. J., & Elliot, T. R. (2008). Application of X-ray computed tomography to soil science: A literature review. Canadian Journal of Soil Science, 88(1), 1-19

Tang, J., Biggar, K.W., Scott, J.D. and Sego, D.C. 1997. Examination of mature fine tailings using a scanning electron microscope, Canadian Geotechnical Conference, Ottawa, Ontario, 746-754

Umme Salma Rima (2013), Characterization and Centrifuge Dewatering of Oil Sands Fine Tailings, MAsc, University of Regina, Regina, Saskatchewan, Canada

Wells, P. S., & Caldwell, J. (2009, November). Vertical “wick” drains and accelerated dewatering of fine tailings in oil sands. In Tailings and Mine Waste Conference (Vol. 9)

Wells, P.S., Revington, A., and Omotoso, O. (2011). Mature fine tailings drying – technology update. In Proceedings of Paste 2011. Edited by R.J. Jewel and A.B. Fourie,5–7 April 2011. Australia Centre for Geomechanics, Perth, Australia. pp. 155–166.

Wells, P. S. (2011). Long term in-situ behavior of oil sands fine tailings in Suncor's Pond 1A. Proceeding of the Conference on Tailings and Mine Waste 2011.Vancouver, BC.

Xu, Y., and Dabros T. 2011. Alternatives to tailings ponds for oil sands tailings disposal. Natural Resources Canada. Virginia, USA.

Xu, Y., and Hamza, H. (2003) Thickening and disposal of oil sand tailings. Mining Engineering, 55(11): 19 – 25

Young, I. T., Gerbrands, J. J., & Van Vliet, L. J. (1998). Fundamentals of image processing (p. 113). Delft: Delft University of Technology.

Yao, Y. (2016). Dewatering Behaviour of Fine Oil Sands Tailings: An Experimental Study DOI: 10.4233/uuid:1ac8f35b-0738-42b4-8ae2-5a5f68941814

Yuan, S. (2009). Thickened tailings (paste) technology and its applicability in oil sand tailings management. Tailings and Mine Waste. Banff, Alberta: University of Alberta, Department of Civil & Environmental Engineering, Edmonton, Alberta.

Yiediboe, B., Lin, H. E., Jian, Y., Cong, L., & Zhenliang, W. The Relationship between the Physical Properties of Soil and Shape Factors of its Fragmented Aggregates: A Two-Dimensional Digital Image Processing and Analysis Approach.

Zbik, M. S., Smart, R. S. C., & Morris, G. E. (2008). Kaolinite flocculation structure. Journal of Colloid and Interface Science, 328(1), 73-80.

Appendices

Appendix A

A.1 Phase 2 SEM Contrasted results:

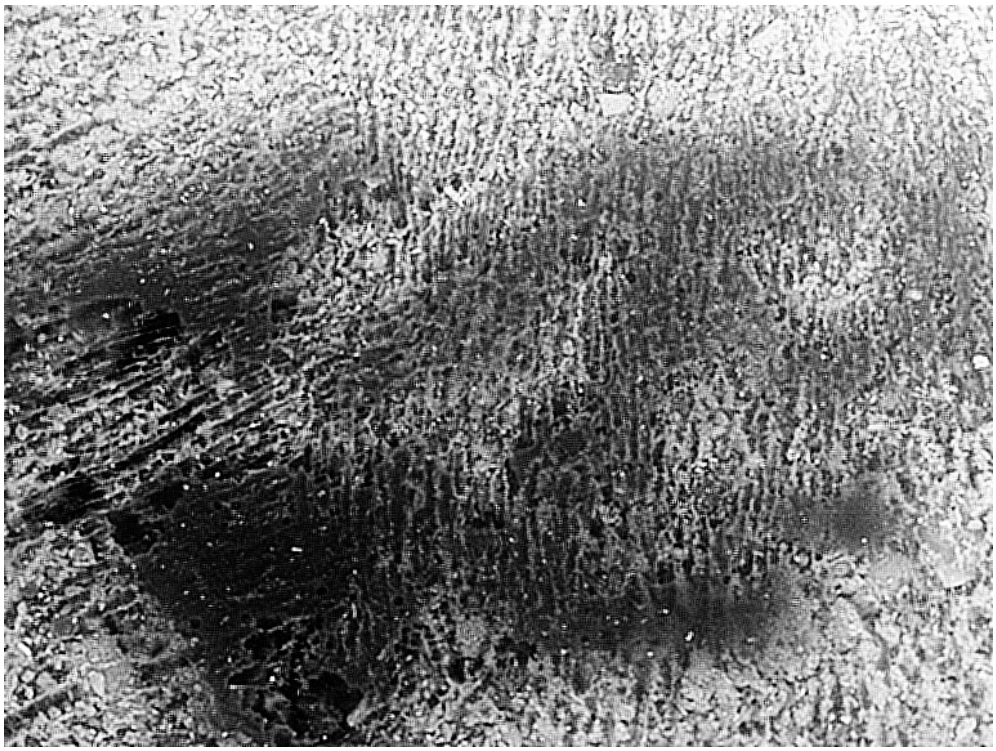

7 DAY Pixel Improved Pixel Results

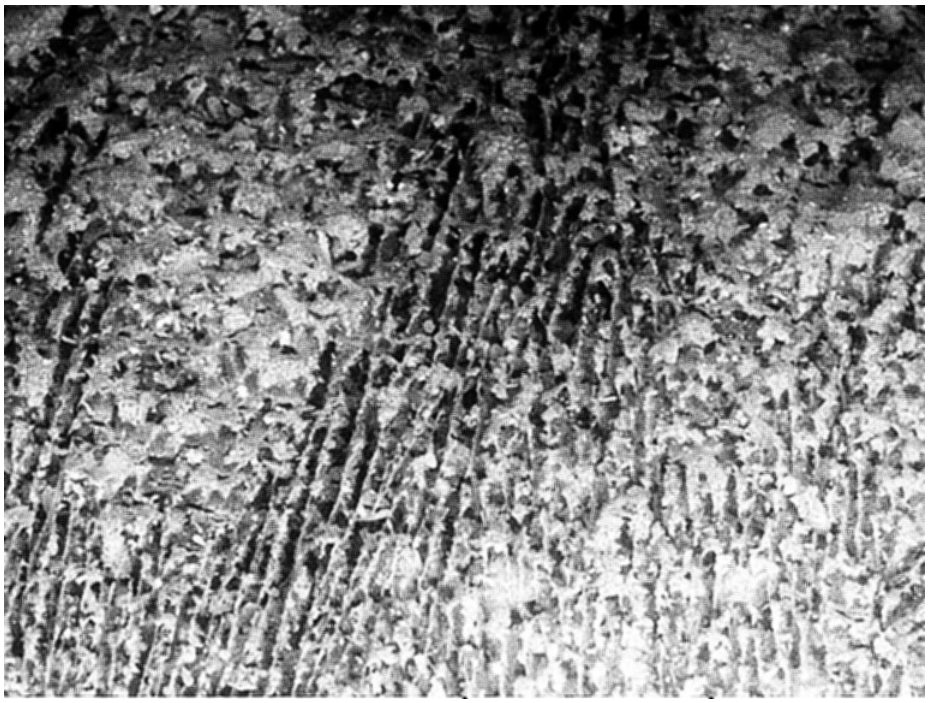

57 DAY, Improved Pixel results

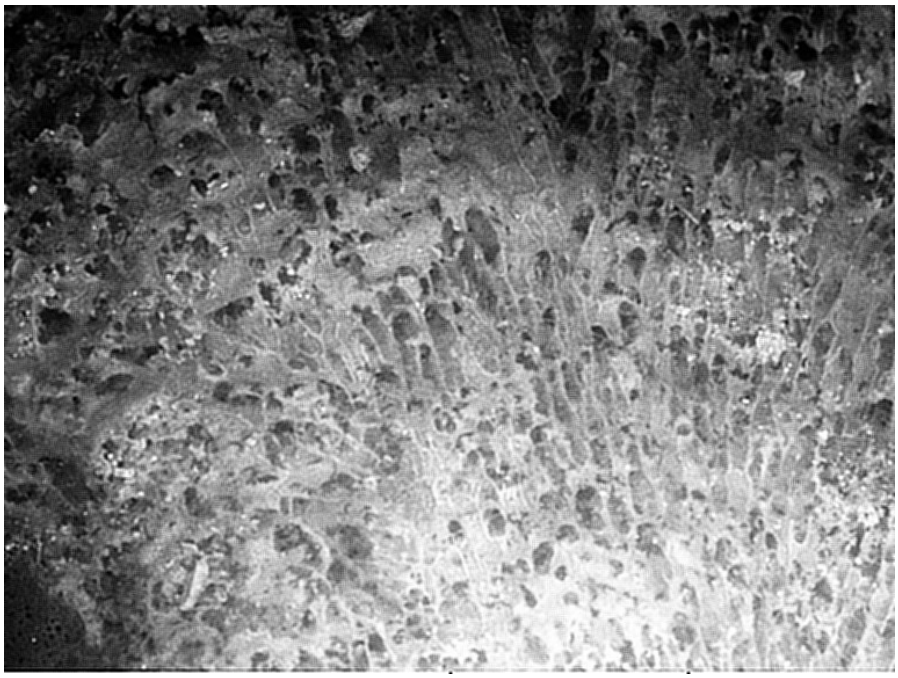

72 day

A.2 Thresholded images

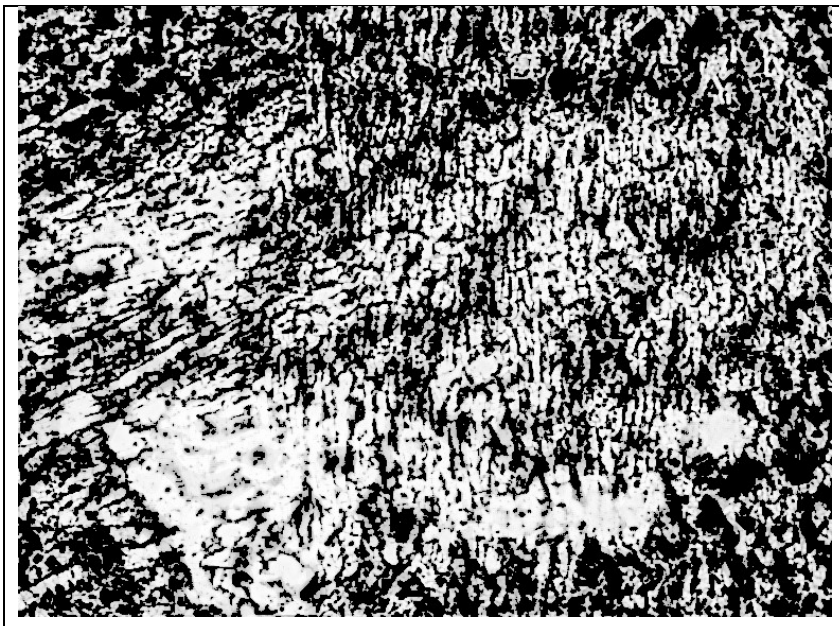

7 day thresholded image

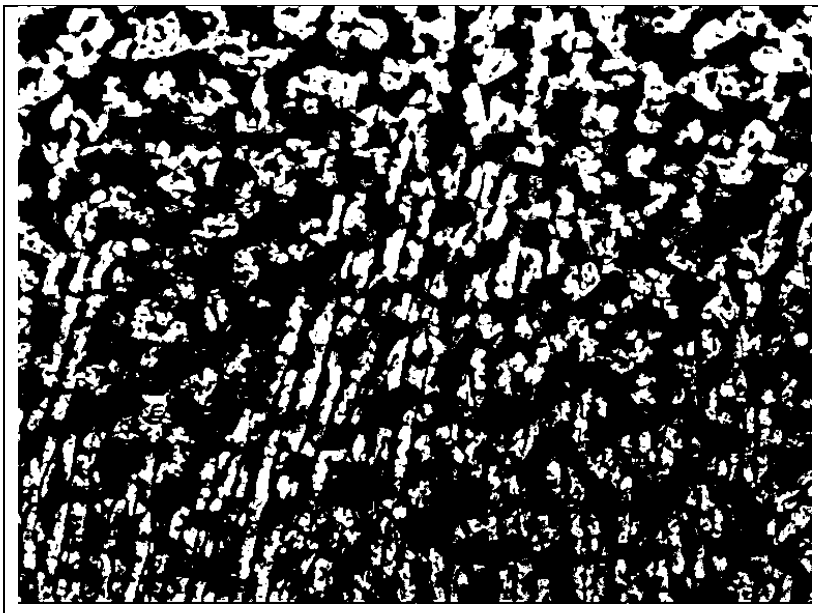

57 day thresholding image

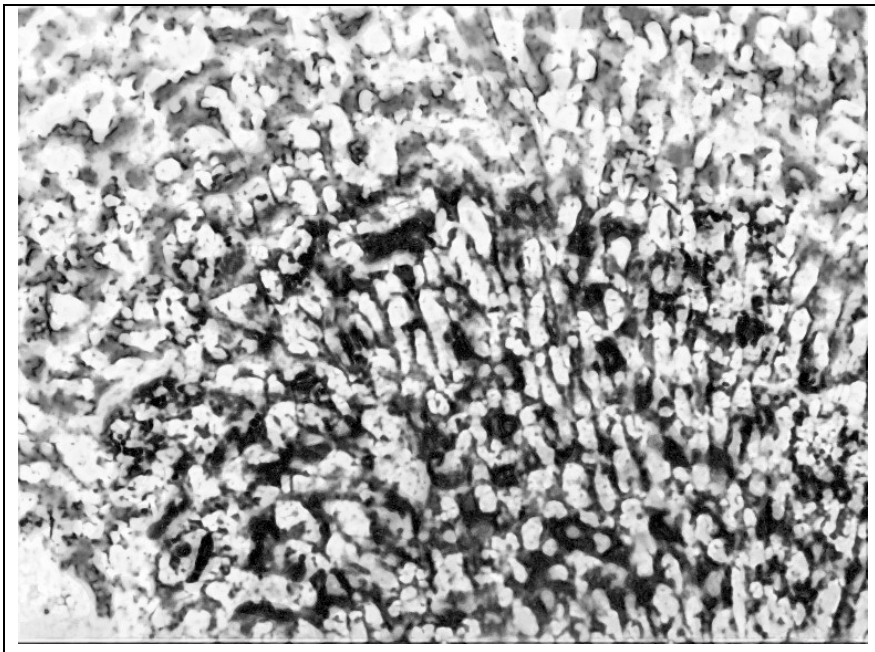

72 days thresholded image

A.3 Phase 2 SEM images Binary Images pores

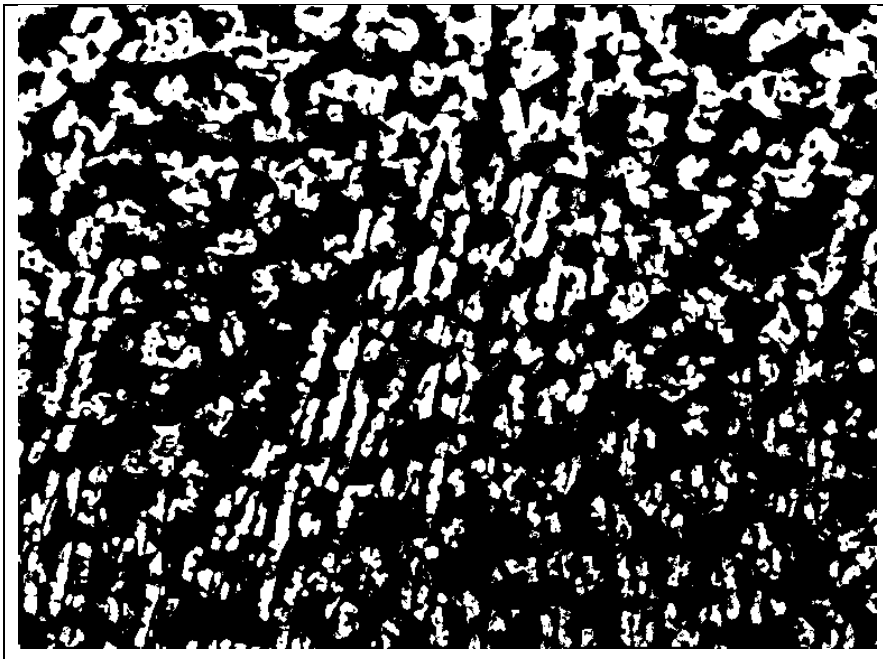

14 days

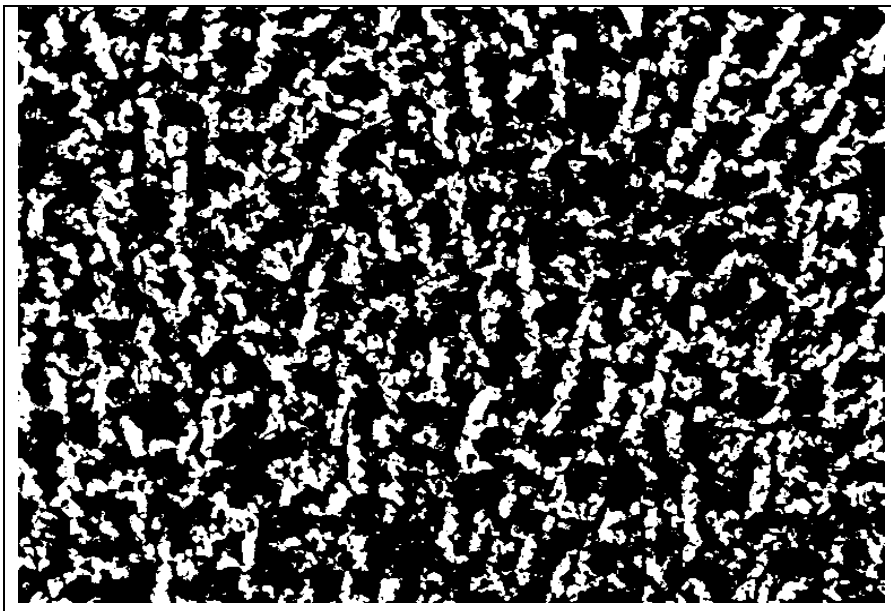

28 days

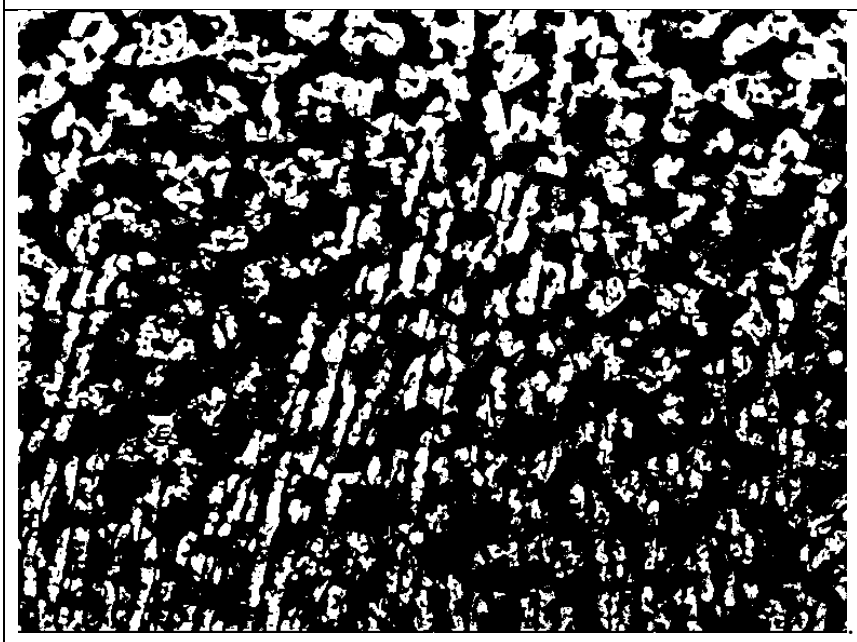

57 day

Appendix B

B.1 Phase 3 thresholded images 600ppm

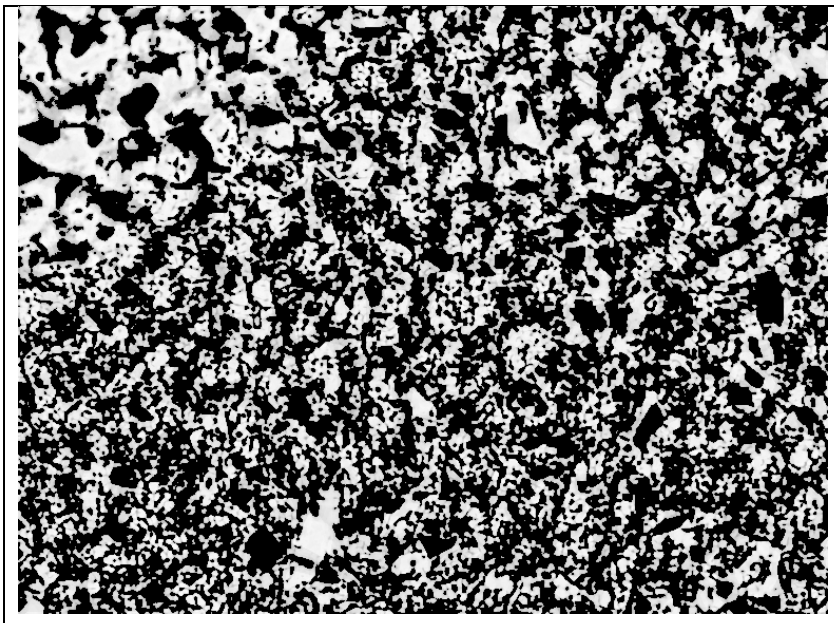

7 days pores

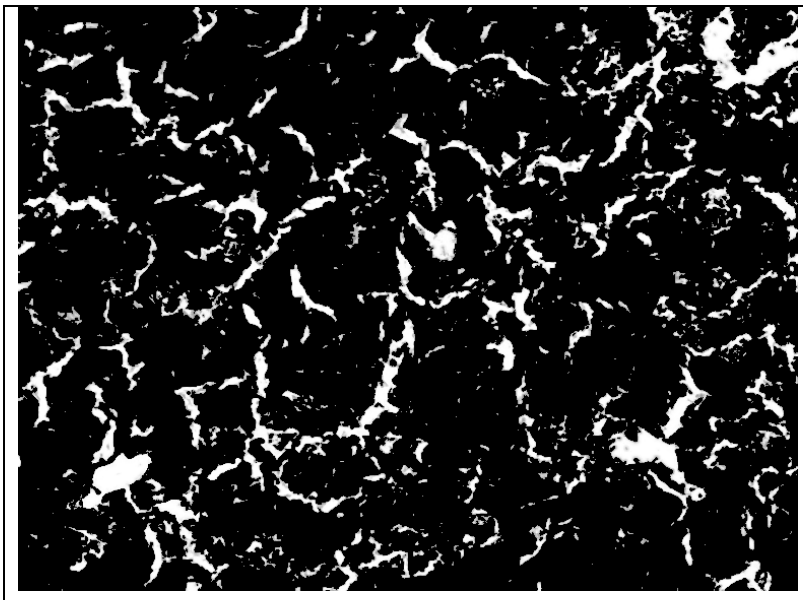

21 day pore thresholded image

B.2 Phase 3 SEM Images classifier used in analysis.

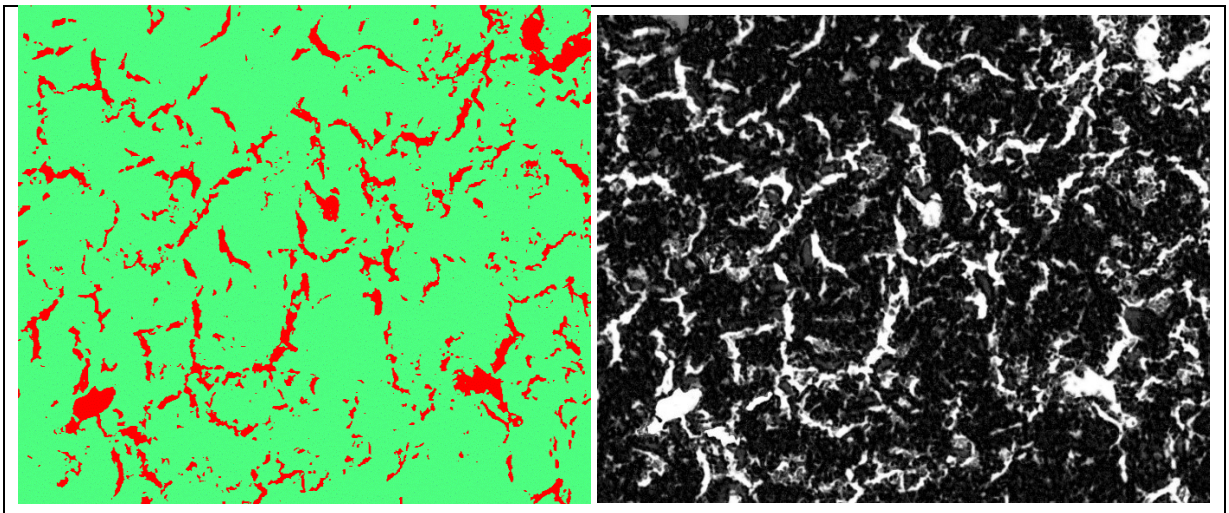

21 days, trainable weka segmentation done for 21-day image, and Binary pore image 21 day image after thresholding.

B.3 Phase 3.5: 800 ppm Single drainage Binary images of pores section

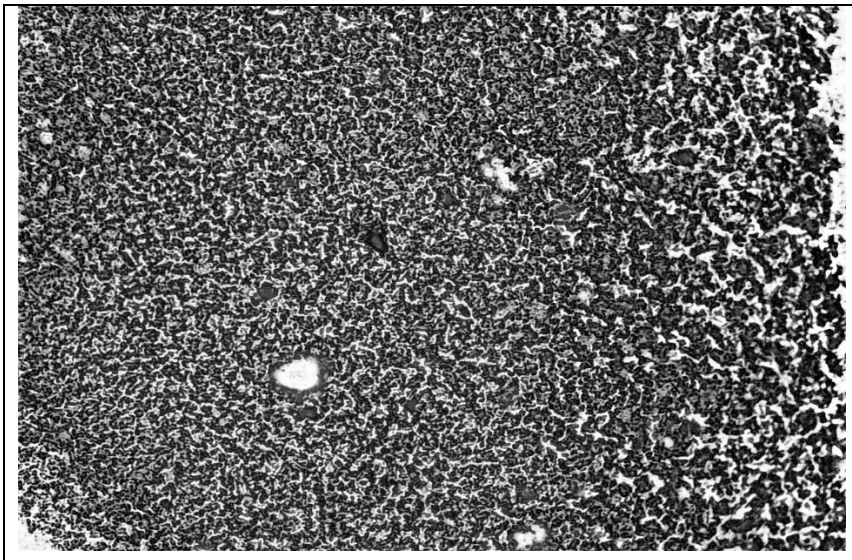

7 days pores

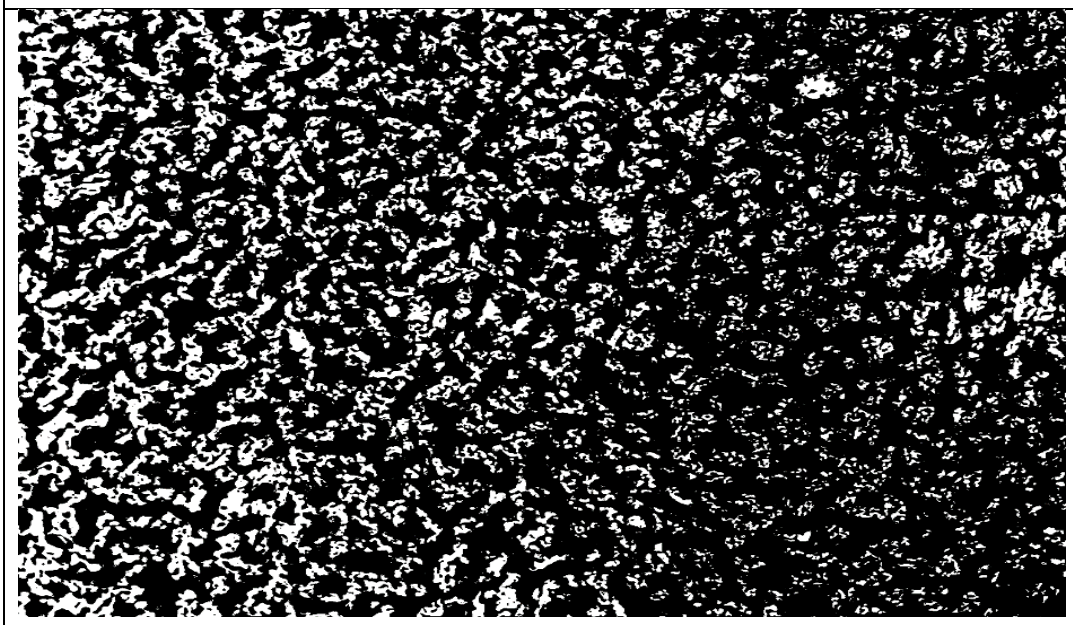

47 day

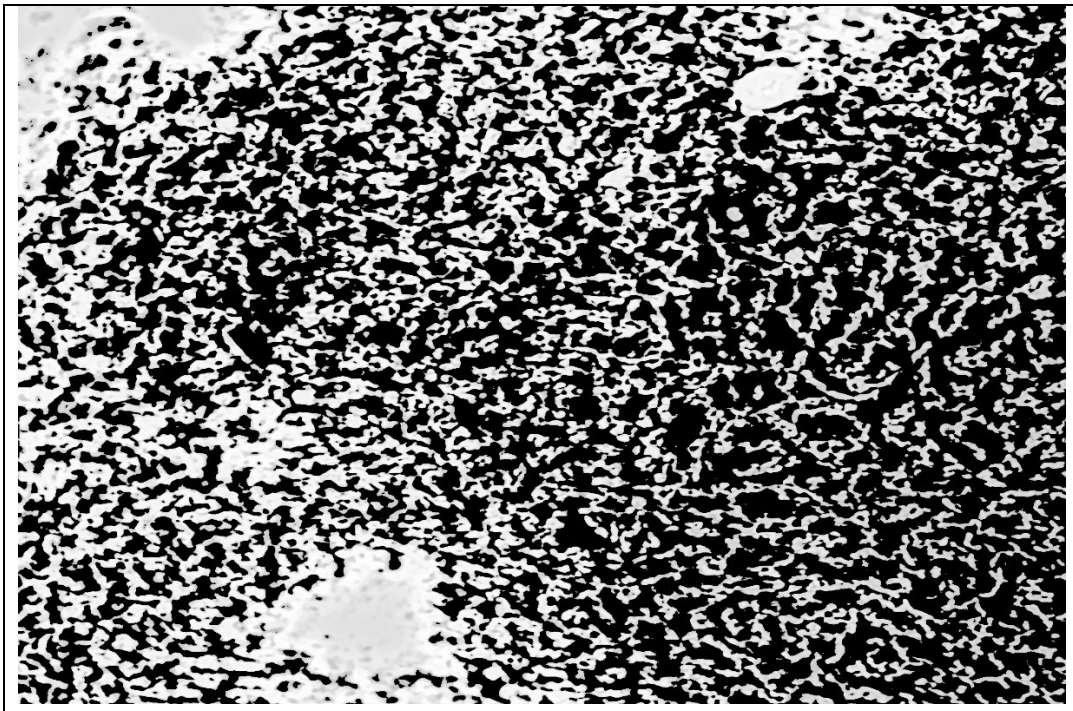

70 day

Appendix C

C.1 Phase 4 optical microscope 600ppm thresholded images 1 till 48 hours

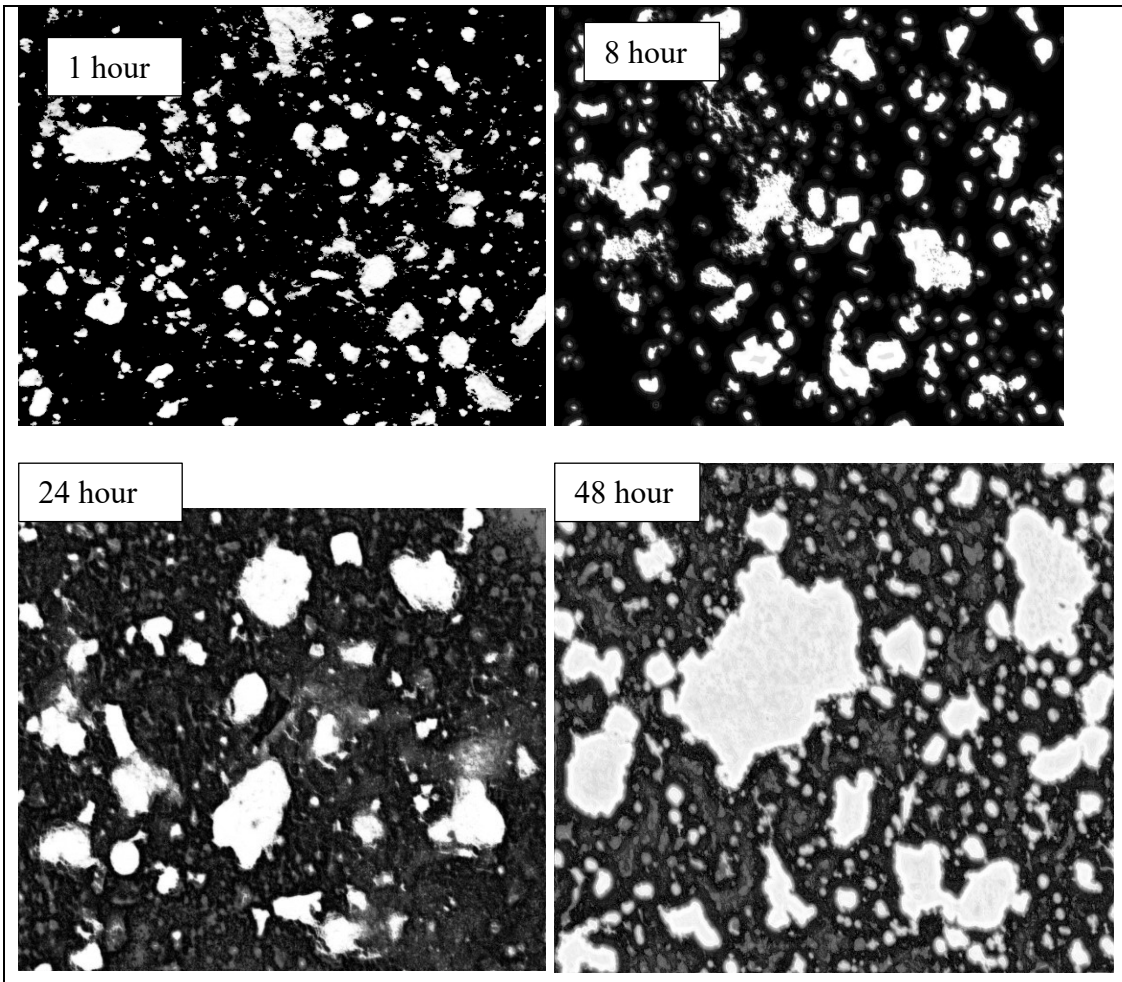

Thresholded images for different hours.

C.2 Phase 4 optical microscope 800ppm binary image 1 to 48 hours 2nd set results

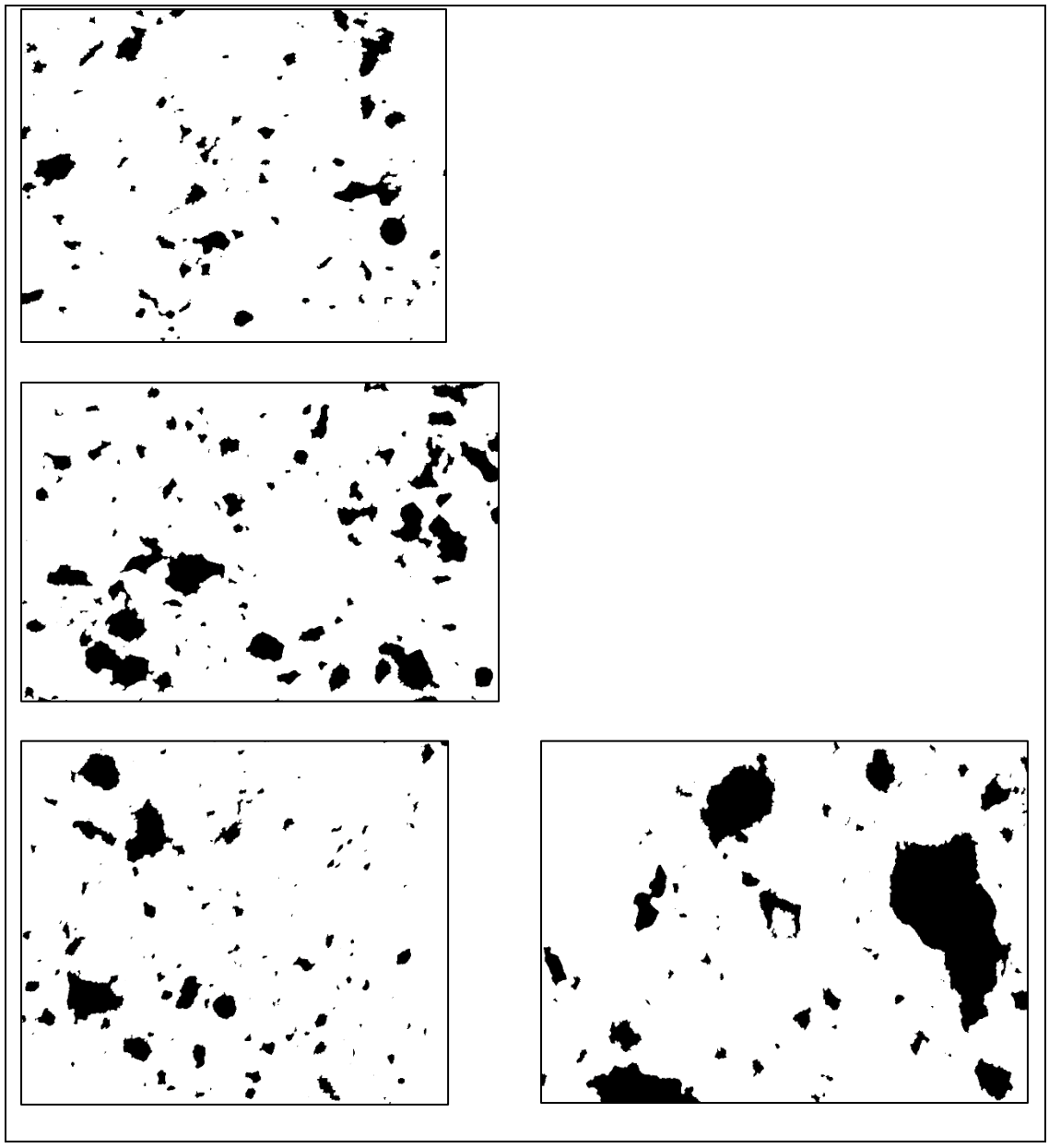

Polymer dose	Boundary condition	Raw FFT water content (%)	Water content just after mixing (%)	Water content at 24 hours (%)	Water content at 48 hours (%)
600 ppm	Single-drainage	208.07	224.97	222.26	N/A

800 ppm	Single-drainage	222.51	246.08	242.11	204.69